Biochimica et Biophysica Acta 1822 (2012) 1114–1124

Contents lists available at SciVerse ScienceDirect

Biochimica et Biophysica Acta

journal homepage: www.elsevier.com/locate/bbadis

Adaptation of respiratory chain biogenesis to cytochrome *c* oxidase deficiency caused by *SURF1* gene mutations

Nikola Kovářová [a], Alena Čížková Vrbacká [a,b], Petr Pecina [a], Viktor Stránecký [b], Ewa Pronicka [c], Stanislav Kmoch [b], Josef Houštěk [a,*]

[a] Institute of Physiology, Academy of Science of the Czech Republic, v.v.i., Prague, Czech Republic
[b] Institute for Inherited Metabolic Disorders, First Faculty of Medicine, Charles University in Prague, Prague, Czech Republic
[c] Department of Metabolic Diseases, Endocrinology and Diabetology, Children's Memorial Health Institute, Warsaw, Poland

ARTICLE INFO

Article history:
Received 11 November 2011
Received in revised form 9 March 2012
Accepted 12 March 2012
Available online 20 March 2012

Keywords:
Mitochondrial disorder
SURF1 gene
Leigh syndrome
Gene expression
Oxidative phosphorylation
Cytochrome *c* oxidase

ABSTRACT

The loss of Surf1 protein leads to a severe COX deficiency manifested as a fatal neurodegenerative disorder, the Leigh syndrome (LS^{COX}). Surf1 appears to be involved in the early step of COX assembly but its function remains unknown. The aim of the study was to find out how *SURF1* gene mutations influence expression of OXPHOS and other pro-mitochondrial genes and to further characterize the altered COX assembly. Analysis of fibroblast cell lines from 9 patients with *SURF1* mutations revealed a 70% decrease of the COX complex content to be associated with 32–54% upregulation of respiratory chain complexes I, III and V and accumulation of Cox5a subunit. Whole genome expression profiling showed a general decrease of transcriptional activity in LS^{COX} cells and indicated that the adaptive changes in OXPHOS complexes are due to a posttranscriptional compensatory mechanism. Electrophoretic and WB analysis showed that in mitochondria of LS^{COX} cells compared to controls, the assembled COX is present entirely in a supercomplex form, as $I–III_2–IV$ supercomplex but not as larger supercomplexes. The lack of COX also caused an accumulation of $I–III_2$ supercomplex. The accumulated Cox5a was mainly present as a free subunit. We have found out that the major COX assembly subcomplexes accumulated due to *SURF1* mutations range in size between approximately 85–140 kDa. In addition to the originally proposed S2 intermediate they might also represent Cox1-containing complexes lacking other COX subunits. Unlike the assembled COX, subcomplexes are unable to associate with complexes I and III.

1. Introduction

The eukaryotic cytochrome *c* oxidase (COX) (E.C.1.9.3.1), the complex IV (cIV) of the mitochondrial respiratory chain, is a multimeric enzyme of dual genetic origin, whose assembly is a complicated and highly regulated process.

The COX monomer of 205 kDa consists of 13 subunits. The three largest subunits Cox1, Cox2 and Cox3 are highly hydrophobic transmembrane proteins encoded by mitochondrial DNA and form the catalytic core. The ten small subunits (Cox4, Cox5a, Cox5b, Cox6a, Cox6b, Cox6c, Cox7a, Cox7b, Cox7c and Cox8) surrounding the core of the enzyme are encoded in the nuclear genome. They are necessary for the regulation of the COX functioning [1,2], the assembly/stability of the holoenzyme and for COX dimerization. Nijtmans et al. proposed a model showing four assembly intermediates (S1–S4) that accumulate during COX assembly [3]. Cox1 represents the first intermediate S1 which proceeds to Cox1–Cox4–Cox5a subassembly by insertion of Cox4–Cox5a heterodimer. The Cox2 then supposedly joins this S2 intermediate. The process continues by the formation of the third proposed intermediate S3 by the addition of most of the remaining subunits. Finally, Cox6a and Cox7a/b are added to complete the holoenzyme [3–5]. The incorporation of small, nuclear encoded subunits in the late stages of COX assembly has been addressed by recent studies [6,7] that indicate the existence of additional assembly intermediates as well as possible incorporation of some of these subunits into already preexisting holoenzyme, similarly as found in complex I biogenesis [8].

The COX assembly is a multistep progression through discrete short-lived intermediates requiring more than 30 diverse assistant factors. Of them, Surf1 is most likely involved in an early step of assembly during the association of Cox2 subunit with Cox1–Cox4–Cox5a subassembly. There is also evidence that Surf1 may act in the formation of heme a_3-Cu_B center [9]. Other known assembly proteins such as Sco1, Sco2, Cox11 and Cox17 are necessary for the copper insertion into COX. Proteins encoded by genes *COX10* and *COX15* are involved in the heme *a* biosynthesis [5,10].

COX deficiencies are mainly COX assembly defects. There are two main groups of COX defects that are caused by mutations either in

Abbreviations: OXPHOS, oxidative phosphorylation; COX, cytochrome *c* oxidase; LS^{COX}, Leigh syndrome on the basis of cytochrome *c* oxidase deficiency; cI, cII, cIII, cIV, respiratory chain complexes I–IV; cV, mitochondrial ATP synthase

* Corresponding author. Tel.: +420 2 4106 2434; fax: +420 2 4106 2149.
E-mail address: houstek@biomed.cas.cz (J. Houštěk).

0925-4439/$ – see front matter © 2012 Elsevier B.V. All rights reserved.
doi:10.1016/j.bbadis.2012.03.007

mtDNA genes encoding structural components of the COX or in nuclear genes encoding assembly factors. Recently, the first mutation in a nuclear-encoded structural subunit Cox6b1 was reported which causes a mitochondrial encephalomyopathy [11].

Up to now, pathogenic mutations in several assembly factors have been described. Quite common are mutations in *SCO1*, *SCO2* [12], *COX10* [13] and *COX15* [14] but the most frequent are mutations in *SURF1* gene [10]. Human Surf1 is a 30 kDa transmembrane protein localized in the inner mitochondrial membrane [4,9]. The loss of the human Surf1 function is associated with Leigh syndrome, a fatal neurodegenerative disorder caused by severe COX deficiency (LS^{COX}). Leigh syndrome is frequent, although genetically heterogeneous, mitochondrial disorder [15,16]. It manifests as a progressive encephalopathy, mainly characterized by bilateral necrotic lesions in the basal ganglia and brainstem [17,18]. The first symptoms usually appear before two years of age and consist of optic atrophy, ophthalmoparesis, hypotonia, ataxia and dystonia. Most patients die a few years after the onset of symptoms [19,20].

In this work we focused on a further characterization of the isolated COX deficiency due to mutations in *SURF1* gene. The exact function of this protein is still unknown but it was suggested that human Surf1 promotes the association of Cox2 with the assembly intermediate composed of Cox1, Cox4 and Cox5a. The aim of the present study was to find out how mutations in *SURF1* gene influence protein and/or transcript level of OXPHOS and other pro-mitochondrial genes and to further characterize the altered COX assembly. In the experiments we used fibroblasts from 9 patients carrying different mutations in *SURF1* gene (Table 1) and 5 control fibroblast cell lines.

Our results indicate that *SURF1* gene mutations induce a pronounced, but variable decrease in the protein content of COX subunits apparent as relative enrichments in Cox5a subunit, but also a compensatory increase in respiratory complexes I, III and V, not mirrored by any changes in transcript levels for subunits of OXPHOS complexes and related mitochondrial biogenesis factors. A detailed analysis of COX assembly process shows that the patient fibroblasts accumulate the Cox5a subunit and assembly intermediates between ~85 and 140 kDa containing dominant portion of Cox1 but only substoichiometric amounts of Cox4-1, Cox5a or Cox2, and that assembled COX in LS^{COX} fibroblasts is exclusively present in a supercomplex form.

2. Material and methods

2.1. Patients

Fibroblast cell lines from 9 patients with *SURF1* mutations and COX deficiency were used in this study. All the patients showed major clinical symptoms associated with mitochondrial disease due to COX specific defect. For relevant clinical, biochemical and molecular data on individual patients see [20,21] and Table 1. Importantly, Western blot experiments confirmed the absence of Surf1 protein in all patient cell lines used in this study [20,21]. Selected 5 control fibroblast cell lines were used repeatedly in previous diagnostic biochemical tests and showed no signs of any mitochondrial or other metabolic defect.

Table 1
SURF1 mutations in LS^{COX} fibroblasts used in the study.

Patient	Exon	Mutations	Mutation type
P1	9/7	845 del CT/T704 > C	Frameshift: stop codon 870–872/ Met235 > Thr
P2	9/9	845 del CT/845 del CT	Frameshift: stop codon 870–872
P3	9/?	845 del CT/?	Frameshift: stop codon 870–872/?
P4	9/8	845 del CT/A821 > G	Frameshift: stop codon 870–872/ Tyr274 > Cys
P5	9/9	845 del CT/845 del CT	Frameshift: stop codon 870–872
P6	9/?	845 del CT/?	Frameshift: stop codon 870–872/?
P7	6/9	C574 > T/845 del CT	Arg192 > Trp/Frameshift: stop codon 870–872
P8	4/8–9	312 insATdel10/821 del18	Frameshift: stop codon 316–318/exon 8 removal
P9	7/7	C688 > T/C688 > T	Arg230 > stop

The project was approved by the ethics committees of all collaborating institutions. Informed consent was obtained from the parents of the patients according to the Declaration of Helsinki of the World Medical Association.

2.2. Cell cultures

Human skin fibroblasts were cultured at 37 °C in 5% CO_2 atmosphere in the DMEM medium (with L-glutamine, sodium pyruvate and high glucose concentration 4.5 g/l) supplemented with 10% fetal bovine serum, 20 mM HEPES pH 7.5 and in the presence of penicillin (10 U/ml) and streptomycin (10 μg/ml). Cells were harvested using 0.05% trypsin and 0.02% EDTA and washed twice in phosphate-buffered saline (PBS, 140 mM NaCl, 5 mM KCl, 8 mM Na_2HPO_4, 1.5 mM KH_2PO_4, pH 7.2).

2.3. Isolation of mitochondria

Isolation utilizing hypotonic disruption of cells was carried out according to [22] with slight modifications to increase the yield. Weighed cell pellet was suspended in ten times the amount of 10 mM Tris-buffer supplemented with protease inhibitor cocktail (PIC, Sigma, 1:500). Cells were homogenized using Teflon/glass homogenizer (8 strokes, 600 rpm) and immediately 1/5 volume of 1.5 M sucrose was added. Homogenate was centrifuged at 600 *g*, 10 min at 4 °C and supernatant was saved. The pellet was suspended in the original volume of SEKTP (250 mM sucrose, 40 mM KCl, 20 mM Tris, 2 mM EGTA, pH 7.6, PIC 1:500), rehomogenized and centrifuged again at 600 *g*. Pooled supernatants were centrifuged at 10 000 *g*, 10 min at 4 °C min and pelleted mitochondria were washed by centrifugation and suspended in SEKTP. Protein concentration was measured by Bradford method (BioRad).

2.4. Isolation of membranes

For native electrophoresis, mitochondria-enriched membrane fraction was prepared from 20 mg wet weight aliquots of sedimented cells as described [23]. Briefly, cells were homogenized (30 strokes, 500 rpm) in 0.5 ml of 83 mM sucrose, 6.6 mM Imidazole pH 7, PIC 1:500, and centrifuged at 20 000 *g*, 10 min at 4 °C. Samples were frozen and stored at −80 °C.

2.5. Electrophoretic techniques and immunoblotting

Samples of mitochondria or pelleted cell membranes were solubilized for 15 min at 0 °C using indicated concentrations of dodecyl maltoside or digitonin and centrifuged for 20 min at 20 000 *g*. Proteins in supernatants were analyzed by BN-PAGE and hrCN3-PAGE [23,24] on 6–15% separating gel using the Mini-Protean apparatus (BioRad). For two-dimensional electrophoresis, gel slices from the 1st dimension were incubated in 1% SDS and 1% mercaptoethanol for 1 h and then subjected to SDS-PAGE on 10% slab gels [25].

Proteins were transferred from gels to PVDF-membranes (Immobilon-P, Millipore) using semidry electrotransfer. The membranes were blocked with 10% non-fat dried milk in TBS (150 mM NaCl, 10 mM Tris, pH 7.5) for 1 h and incubated for 2 h with the specific primary antibodies diluted in TBST (TBS with 0.1% Tween-20). Monoclonal antibodies to NDUFB6, Core1, Rieske protein, Cox1, Cox2, Cox4-isoform 1, Cox5a, d subunit of cV and Blue Native OXPHOS Complexes Detection Kit (containing monoclonal antibodies to NDUFA9, SDH 70, Core2, Cox4, α-subunit of complex V) were obtained from Mitosciences; goat polyclonal antibody to Cox3 was from Santa Cruz Biotechnology; rabbit

polyclonal antibody to subunit F_o-a [26], rabbit polyclonal antiserum to mGPDH was custom prepared against the C-terminal of the protein [27]; and rabbit antibody to porin (VDAC1) was a kind gift from Prof. Vito De Pinto, University of Catania. Membranes were then incubated for 1 h with corresponding secondary fluorescent antibodies — IRDye 680- or 800-conjugated donkey anti-goat IgG or goat anti-mouse IgG (Molecular Probes) or goat anti-rabbit IgG (Rockland). Detection of proteins was performed using Odyssey fluorescence scanner at the excitation of 680 nm and emission of 700 nm or 800 nm. The quantification of signals was carried out in Aida Image Analyzer program version 3.21. For presentation, the data from individual control and patient cell lines were averaged and subgroups were statistically evaluated using Student's t-test.

2.6. In-gel activity staining of complex IV

Activity staining of complex IV in native gels was performed according to a modified protocol originally described in [28]. Gel slices were stained using solution of 50 mM sodium phosphate buffer (pH 7.4), 0.5 mM DAB (3,3′-diaminobenzidine tetrahydrochloride) and 1.1 mM oxidized cytochrome *c* overnight. For better visibility of reddish bends indicating complex IV activity in contrast to the Coomassie stain background, gels were scanned through blue filter.

2.7. RNA preparation, cDNA labeling and hybridization

Total RNA was isolated from patient and control cultured cells using the TRIZOL solution (Invitrogen). As a common reference RNA for gene expression studies, total RNA from cultured HeLa cells was used. RNA concentration was determined spectrophotometrically at 260 nm by NanoDrop (NanoDrop Technologies) and its quality was checked on Agilent 2100 bioanalyzer (Agilent Technologies). Aliquots of isolated RNA were stored at −80 °C until the analysis.

Isolated RNA (500 ng) was reverse transcribed, labeled and hybridized onto Agilent 44 k human genome microarray using Two-color Microarray Based Gene Expression Analysis Kit (Agilent Technologies). All 9 patient and 5 control samples (Cy5-labeled) were hybridized against common reference RNA (Cy3-labeled).

The hybridized slides were scanned with GenePix 4200A scanner (Axon Instruments) with PMT gains adjusted to obtain unsaturated images of the highest intensity. Agilent Feature Extraction software was used for image analysis of the TIFF files, generated by the scanner.

2.8. Experimental setup and microarray data normalization

Comparative analysis was performed according to MIAME guidelines [29]. Normalization was performed in R statistical environment (http://www.r-project.org) using the Limma package [30] which is part of the Bioconductor project (http://www.bioconductor.org). Raw data from individual arrays were processed using Loess normalization and normexp background correction. The quantile function was used for normalization between arrays. Linear model was fitted for each gene given a series of arrays using lmFit function. The empirical Bayes method was used to rank differential expression of genes using eBayes function. Multiple testing corrections were performed using Benjamini and Hochberg method [31].

Data accession — gene expression data reported in this study are stored and available in Gene Expression Omnibus repository (GEO ID: GSE26322) and (GEO ID: GPL 4133).

2.9. Statistical analysis

Gene expression was assessed as described previously [32] and gene expression signals were background corrected, log2 transformed and normalized using the quantile normalization method. Significant gene expression changes between control and patient subgroups were identified using t-test in R statistical environment (http://www.r-project.org/). Applied parameters are provided in corresponding result sections.

3. Results

3.1. Compensatory upregulation of OXPHOS complexes

The first aim of the study was to investigate whether the content of respiratory chain complexes can be modified as a consequence of *SURF1* mutations. Our previous study [21] indicated an increased content of F_1-ATPase α subunit in LS^{COX} patients that pointed to a compensatory mechanism induced by impaired energy provision. Therefore, we used the whole cell homogenate and isolated mitochondria from fibroblasts of LS^{COX} patients and controls to quantify the content of OXPHOS protein complexes by Western blotting of the proteins separated by SDS-PAGE. For immunodetection we used the OXPHOS Complexes Detection Kit (Mitosciences) containing specific monoclonal antibodies to representative subunits of OXPHOS complexes — NDUFA9 subunit of complex I, 70 kDa subunit of complex II, Core2 subunit of complex III, Cox4 subunit of complex IV, and alpha subunit of complex V. Their signals were related to the signal of the mitochondrial marker porin. Fig. 1A shows that the low content of complex IV (cIV) was associated with a slight increase in the content of complex I (cI), III (cIII) and V (cV) in LS^{COX} whole cell lysates. This was even more apparent and significant when analyzing isolated mitochondria (Fig. 1B). Specifically, a 70% decrease in cIV resulted in a 48% increase in the content of cI, 54% increase of cIII and 32% increase of cV, indicative of compensatory changes triggered by COX dysfunction and impairment of mitochondrial energy provision. Similar statistically significant upregulation of OXPHOS complexes content in LS^{COX} cells was observed using individual antibodies against other subunits of complexes I, III, and V — NDUFB6 of cI was increased to 147% of control ($p<0.05$), Core1 and Rieske protein of cIII were increased to 149% and 170% of control, respectively ($p<0.01$ and $p<0.05$, respectively), d and a subunits of cV were upregulated to 118% and 126% of control, respectively ($p<0.05$ and $p<0.01$, respectively). In contrast, the amounts of other dehydrogenases of the respiratory chain, complex II (cII) and mitochondrial glycerol 3-phosphate dehydrogenase (mGPDH) were not changed.

3.2. Variable content of COX subunits

As COX deficiency due to the absence of Surf1 assembly factor is characterized by accumulation of incomplete COX assemblies, we also determined the amount of several COX subunits in LS^{COX} fibroblasts in order to uncover putative variations in subunit content reflecting the impaired assembly. Control and LS^{COX} samples were analyzed by SDS-PAGE and Western blotting using monoclonal antibodies to three mitochondrial encoded COX subunits — Cox1, Cox2 and Cox3, and to two nuclear encoded COX subunits — Cox4 and Cox5a, all of which are implicated in early stages of COX assembly. Their content was again related to the content of porin. Both in homogenates and isolated mitochondria, all tested COX subunits showed a pronounced, but variable decrease in LS^{COX} fibroblasts. The decrease of individual subunits was 40–78% in cell homogenates (Fig. 2A) and 39–86% in isolated mitochondria (Fig. 2B). In both cases, the least decreased of the five tested subunits was the subunit Cox5a, indicating its relative accumulation compared to other COX subunits.

3.3. Gene expression profile and its correlation with protein content

To find out how the isolated COX deficiency modulates the expression of genes in LS^{COX} fibroblasts at the transcriptional level, whole genome transcript levels were determined in LS^{COX} and control fibroblasts using the 44 k human cDNA Agilent microarray.

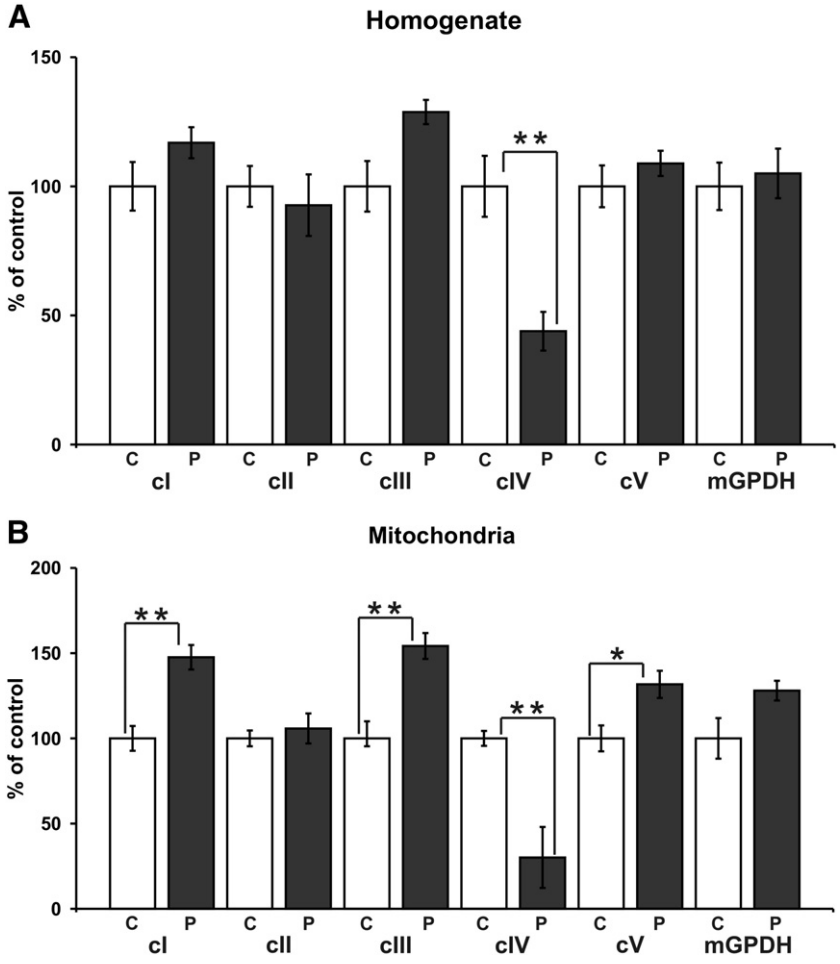

Fig. 1. Changes in the content of respiratory chain complexes in LS^{COX} fibroblasts. Western blot analysis of homogenates (A) and isolated mitochondria (B) from fibroblasts of patients (P) and controls (C) was performed using antibodies to subunits of cI (NDUFA9), cII (70 kDa subunit), cIII (Core2), cIV (Cox4-1), cV (alpha subunit), and mGPDH. Detected signals were quantified separately for individual control and patient cell line and related to the signal of mitochondrial porin detected from the same blots. All data of controls and patients were averaged and obtained value for patients was expressed as a percentage of controls value. Values are mean ± SE of 3 experiments, $p<0.05$ (*), $p<0.01$ (**).

The overall analysis comparing averaged data from control and patient subgroups indicated upregulation of 18501 genes (42%) and downregulation of 24832 genes (56%), but significant changes were shown only in a small number of genes (Table 2). Thus, 507 genes were differentially expressed at $p<0.05$ value and 95 genes at $p<0.01$. In case of genes encoding OXPHOS structural subunits, 20 were changed at $p<0.05$ (11 subunits of cI, 1 subunit of cIII, 2 subunit of cIV and 6 subunits of cV), but all of them were less expressed in LS^{COX} compared to controls, in contrast with the protein analysis. Of them, 3 genes have been 1.7–2 fold downregulated at $p<0.01$, namely cI subunits NDUFA4 and NDUFB6 and cV inhibitor protein IF_1. In addition, the expression of intramitochondrial superoxide dismutase (SOD1) was also decreased two-fold at $p<0.001$.

The increased content of respiratory chain cI, cIII and cV observed at the protein level was thus apparently not due to transcriptional upregulation of structural subunits genes. It is also important that no indication could be observed that the increase in these complexes could be ascribed to a significant upregulation of different regulatory genes. There was neither a significant change in the expression of genes encoding specific ancillary or assembly factors of the respiratory chain complexes, nor in mitochondrial biogenesis regulatory genes, such as *PGC1A*, *NRF1* or *TFAM*. The compensatory OXPHOS upregulation in LS^{COX} fibroblasts must therefore arise at later stages of protein expression.

Only the downregulation of mRNAs for two small, nuclear encoded COX subunits Cox7a2 and Cox6c (Table 3) seems to correspond to the decrease of COX complex. However, considering that the content of COX subunits is decreased due to the stalled assembly, the transcriptional downregulation of these two subunits may only be coincidental since they are incorporated into the COX complex at the late stage of the assembly process.

3.4. Modified COX assembly pattern in LS^{COX} fibroblasts

While it has long been established that Surf1 deficiency is associated with a pronounced COX deficiency and accumulation of its assembly intermediates, most studies to date have been using relatively strong detergent dodecyl maltoside to analyze the assembly pattern of cytochrome *c* oxidase by BN-PAGE. In order to identify COX assemblies under conditions closer to the in-situ state, we solubilized isolated membrane fractions from LS^{COX} and control fibroblasts with the mild detergent digitonin (4 and 8 g/g protein) and separated them using native electrophoretic techniques BN-PAGE and hrCN3-PAGE, which allow for detection of native OXPHOS supercomplexes.

In control fibroblasts, the signal from antibodies against Cox1, Cox4-1 and Cox5a (Fig. 3A–C) was distributed among the i) COX monomer, ii) COX dimer and heterodimers and iii) supercomplexes (relative content of i/ii/iii approximately 1:0.25:1 — see quantification or distribution profiles in Fig. 3). The supercomplexes' migration distance and parallel WB detection with antibodies raised against subunits of cI and cIII (NDUFB6 and Core1, respectively) (Fig. 3D), indicated that the detected supercomplexes represent the previously

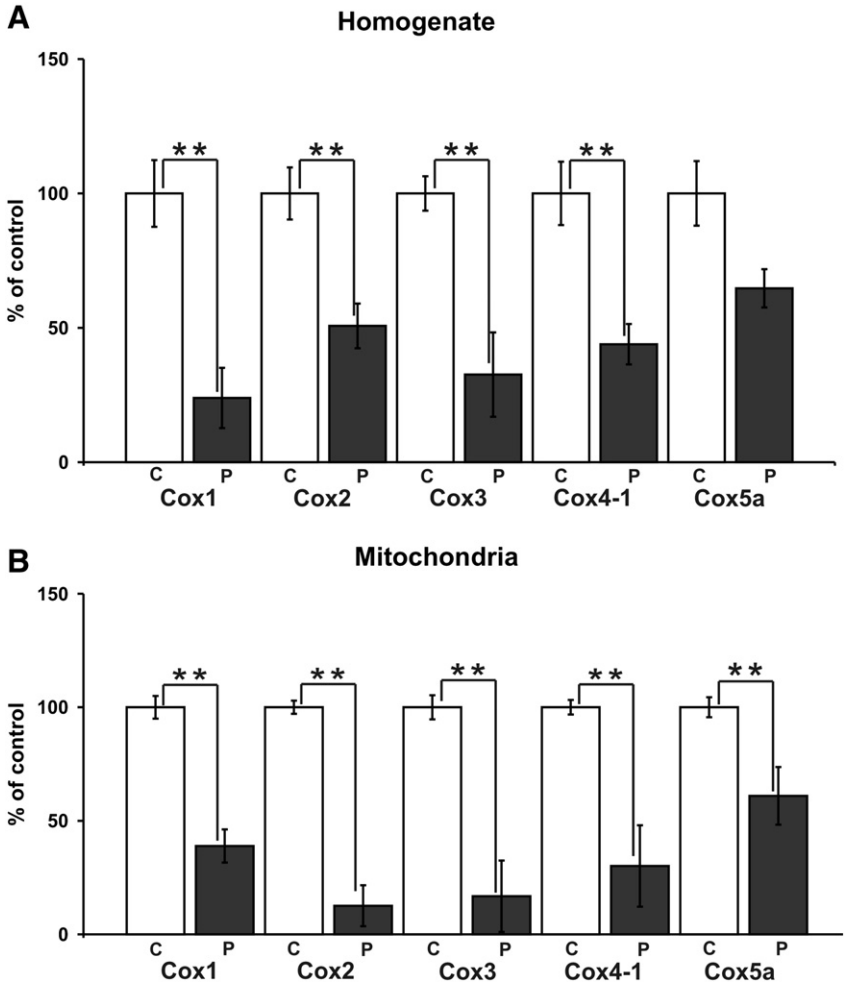

Fig. 2. Decreased content of COX subunits in LS^{COX} fibroblasts. Homogenates (A) and isolated mitochondria (B) from fibroblasts of patients (P) and controls (C) were analyzed by Western blots using antibodies to COX subunits 1, 2, 3, 4-1 and 5a. Signals were processed as described in Fig. 1. Values are mean ± SE of 3 experiment, $p<0.01$ (**).

characterized assemblies I_1–III_2–IV_1, I_1–III_2–IV_2, and I_1–III_2–IV_3 (supercomplexes consisting of one copy of complex I, dimer of complex III, and 1–3 copies of complex IV), the first one being the most abundant. Interestingly, the vast majority of the cI and cIII signals were found in supercomplexes, in contrast with cIV, which seems to reflect the excess capacity of COX. A strikingly different pattern was observed in LS^{COX} fibroblasts. Here, the signal from anti-COX antibodies was mainly distributed between an assembly intermediate of about 130 kDa and a single form of supercomplex. Very little of COX monomer and almost no dimer could be detected in patient cells (Fig. 3A–C) as apparent from the relative content of these assemblies (note that the three-fold amount of patient sample relative to control was used). Based on the comparison with the control lane, the single supercomplex in LS^{COX} represents the I_1–III_2–IV_1 species. The detection of the I_1–III_2 supercomplex and the dimer of cIII in patient fibroblasts (Fig. 3D) indicates that the low content of COX limits the supercomplex assembly. The absence of larger supercomplexes may indicate that the association of multiple copies of cIV is less stable than the "core" I_1–III_2–IV_1 species, and therefore requires more abundant pool of COX than in control fibroblasts. Alternatively, the assembly of COX in the absence of Surf1 may yield complexes with slightly modified structure preventing their multimerization.

An apparently identical migration distance of the I_1–III_2–IV_1 species in control and LS^{COX} cells as well as its detection with all of the used antibodies suggest that this supercomplex contains the fully assembled COX in patient fibroblasts. This was confirmed by COX in-gel activity staining, which detected active COX as a monomer and also in the supercomplex region in both control and patient sample (Fig. 3C). Indeed, in a parallel BN-PAGE experiment with dodecyl maltoside-solubilized membrane fractions, we observed dissociation of the COX-containing supercomplex with a simultaneous increase in the content of COX holoenzyme in both the control and LS^{COX} fibroblasts (Fig. 4). To provide further evidence, we performed two-dimensional BN/BN-PAGE analysis of the supercomplex composition (Fig. 5). While the BN-PAGE in the first dimension preserves the supercomplex associations in digitonin-solubilized samples, the presence of dodecyl maltoside in the cathode buffers of the second dimension BN-PAGE results in their dissociation into free complexes. Western blot detection with Cox1 and Cox4 antibodies revealed a dominant form of COX dissociating from the supercomplexes in both the control and patient cells with approximate size of 200 kDa, apparently representing the fully assembled COX holoenzyme (Fig. 5). The other, less dominant bands below the monomer recognized by both Cox1 and Cox4-1 antibodies represented dissociation products of COX likely

Table 2
Differentially expressed genes in LS^{COX} fibroblasts.

Genes	p value	Changed	Down	Up
All	0.05	507	347	160
	0.01	95	72	23
OXPHOS	0.05	20	20	0
	0.01	3	3	0

Table 3
Differential expression of OXPHOS genes in LS^{COX} fibroblasts at $p<0.05$.

Gene	Protein	M	Fold change	p value
SOD1	Superoxide dismutase 1	−1.03	2.00	0.001
NDUFA4	NADH dehydrogenase, 1 alpha subcomplex, subunit 4, 9 kDa	−0.97	2.00	0.002
NDUFB6	NADH dehydrogenase, 1 beta subcomplex, subunit 6, 17 kDa, t.v. 2	−0.80	1.70	0.008
ATPIF1	ATP synthase, inhibitory factor 1, t.v. 3	−0.73	1.66	0.01
ATP5H	ATP synthase, subunit d, t.v. 1	−0.71	1.60	0.02
COX6C	Cytochrome *c* oxidase, subunit 6c	−0.84	1.80	0.02
NDUFAF2	NADH dehydrogenase, 1 alpha subcomplex, assembly factor 2	−0.72	1.70	0.02
ATP5J2	ATP synthase, subunit F2, t.v. 1	−0.69	1.60	0.02
NDUFA12	NADH dehydrogenase, 1 alpha subcomplex, subunit 12, 13 kDa	−0.81	1.70	0.02
NDUFA1	NADH dehydrogenase, 1 alpha subcomplex, subunit 1, 7.5 kDa	−0.72	1.70	0.03
NDUFA2	NADH dehydrogenase, 1 alpha subcomplex, subunit 2, 8 kDa	−0.70	1.60	0.03
NDUFB3	NADH dehydrogenase, 1 beta subcomplex, subunit 3, 12 kDa	−0.65	1.60	0.03
ATP5J	ATP synthase, subunit F6	−0.70	1.60	0.03
ATP5C1	ATP synthase, gamma subunit, t.v. 2	−0.61	1.50	0.04
NDUFB10	NADH dehydrogenase, 1 beta subcomplex, subunit 10, 22 kDa	−0.59	1.50	0.04
COX7A2	Cytochrome *c* oxidase subunit 7a polypeptide 2 (liver)	−0.64	1.60	0.04
NDUFA8	NADH dehydrogenase, 1 alpha subcomplex, subunit 8, 19 kDa	−0.63	1.50	0.04
NDUFA6	NADH dehydrogenase, 1 alpha subcomplex, subunit 6, 14 kDa	−0.59	1.50	0.05
UQCRQ	Ubiquinol-cytochrome *c* reductase, subunit VII, 9.5 kDa	−0.60	1.50	0.05
ATP5E	ATP synthase, epsilon subunit	−0.66	1.60	0.05
NDUFS7	NADH dehydrogenase, Fe–S protein 7, 20 kDa	−0.56	1.50	0.05

t.v. — transcription variant.

appearing due to combination of two detergents during the 2D BN/BN experiment, as they migrate in direct vertical below the monomer.

3.5. Accumulation of non-canonical assembly intermediate in LS^{COX} fibroblasts

As expected, the analysis of COX subunits in Fig. 2 revealed a decreased content of several detected COX subunits in a LS^{COX} patient but it also suggested that Cox5a is much less affected in case of Surf1 defect compared with other subunits. To find out in which form this subunit accumulates we performed a detailed analysis of COX assembly intermediates and subcomplexes solubilized from mitochondrial membranes by mild detergent digitonin, using antibodies to Cox5a, Cox4-1, Cox2 and Cox1 subunits. When a two-dimensional BN/SDS-PAGE was performed to resolve well the low molecular weight region, a distinct distribution of COX subunits 1, 2, 4 and 5a was apparent (Fig. 6A). The second dimension yielded resolution superior to the BN gel that allowed for an easier identification of early assembly intermediates of subunits 4 and 5a. In the LS^{COX} cells, Cox5a was present mainly as a free subunit (band y), less in COX holoenzyme, Cox4–Cox5a complex (band x) or in supercomplexes. The Cox4 was also present in LS^{COX} cells in free form (band z) and as assembly subcomplexes, but most of Cox4 was detected in holoenzyme and supercomplexes. The Cox1 was present in LS^{COX} cells in supercomplex, COX monomer and dominantly in the detected subcomplex, together with Cox4 and Cox5a. This major subcomplex accumulating in patient fibroblast with *SURF1* mutations was repeatedly considered as the S2 assembly intermediate. However, its size detected in our immunodetection experiments (~130 kDa broad band ranging ~85–140 kDa) only marginally corresponds to the theoretical mass of the Cox1–Cox4–Cox5a complex (85 kDa). Although the mass determination may be misleading due to specific detergent micelles behavior, the migration range and shape of the band of the anti Cox1 antibody suggests at least two major entities being present (Fig. 6B), with the smaller aligning with a Cox1-containing subassembly present marginally also in the control cells. Furthermore, from the 2D Western blot images it became clearly apparent that Cox4 and Cox5a are present in substoichiometric amounts in this subcomplex (Fig. 6A). When the COX holoenzyme, with the assumed 1:1:1 ratio of the subunits, was used as a reference for relative quantification, the proportion of Cox1 appeared to be in pronounced excess over the Cox4 and Cox5a subunits. Parallel quantification directly from the first dimension BN gels yielded similar subunit ratios, although in this case the quantification is less reliable due to possible problems with antibody reactivity towards native proteins within detergent micelles. Both systems, however, indicated underrepresentation of the nuclear-encoded subunits in the putatively stoichiometric Cox1–Cox4–Cox5a subassembly. Therefore, we hypothesize that the detected band could represent a so far incompletely characterized complex, or rather comigrating complexes that may include the S2 intermediate as well as other protein factors involved in COX assembly. The signal of Cox2 was present in COX monomer and supercomplex but a small amount of Cox2 was also in the 130 kDa region, again strongly underrepresented with respect to Cox1.

To provide a comparison of our findings using digitonin solubilisates with previous studies where COX assembly was analyzed by 2D BN/SDS PAGE in samples solubilized by dodecyl maltoside, we performed a parallel experiment using this stronger detergent. As expected, the majority of signal found in the supercomplexes region shifted towards the COX monomer (Fig. 6C). The migration of the subcomplexes shifted towards lower molecular weights, creating pattern similar to studies that identified the S2 and S1 intermediates in the LS^{COX} cells (Fig. 6C, D). Whether the migration difference of assembly intermediates, solubilized by either digitonin or dodecyl maltoside, is solely due to different detergent micelles or rather due to partial dissociation of Cox1-containing subcomplex using stronger detergent could not be definitively judged in this experimental setup. Nevertheless, the underrepresentation of Cox4 and Cox5a versus Cox1 (relatively as compared to the antibody signal ratios in the holoenzyme) is retained in experiments using both detergents.

4. Discussion

Mitochondrial disorders due to impaired structure and function of the OXPHOS system can be associated with upregulation of mitochondrial biogenesis and increased mitochondrial content, or subcellular distribution such as in RRFs [33] or in myocardial tissue from failing heart [34]. The mechanism underlying these changes is, however, unclear.

In this study we investigated whether the frequent type of COX deficiency due to *SURF1* mutations can also be followed by compensatory changes in the OXPHOS system and found apparent upregulation of three respiratory chain complexes — cI, cIII and cV. Rather than direct consequence of the Surf1 protein absence, we hypothesize that the compensatory upregulation is triggered by secondary effects of the energy provision impairment due to COX deficiency. One of the triggers might be decreased mitochondrial membrane potential, which was previously reported in LS^{COX} by our group [35] and others [36]. Other signal towards OXPHOS upregulation might be the increased turnover of unassembled proteins by mitochondrial proteases [37] or the related increased level of mitochondrial autophagy. The comparison of Western blot data and mRNA expression profiling further indicated that posttranscriptional events rather than transcriptional upregulation of genes encoding subunits of these complexes are responsible for the changes observed.

To assess possible changes in gene expression we analyzed the whole genome expression pattern of LS^{COX} patient and control

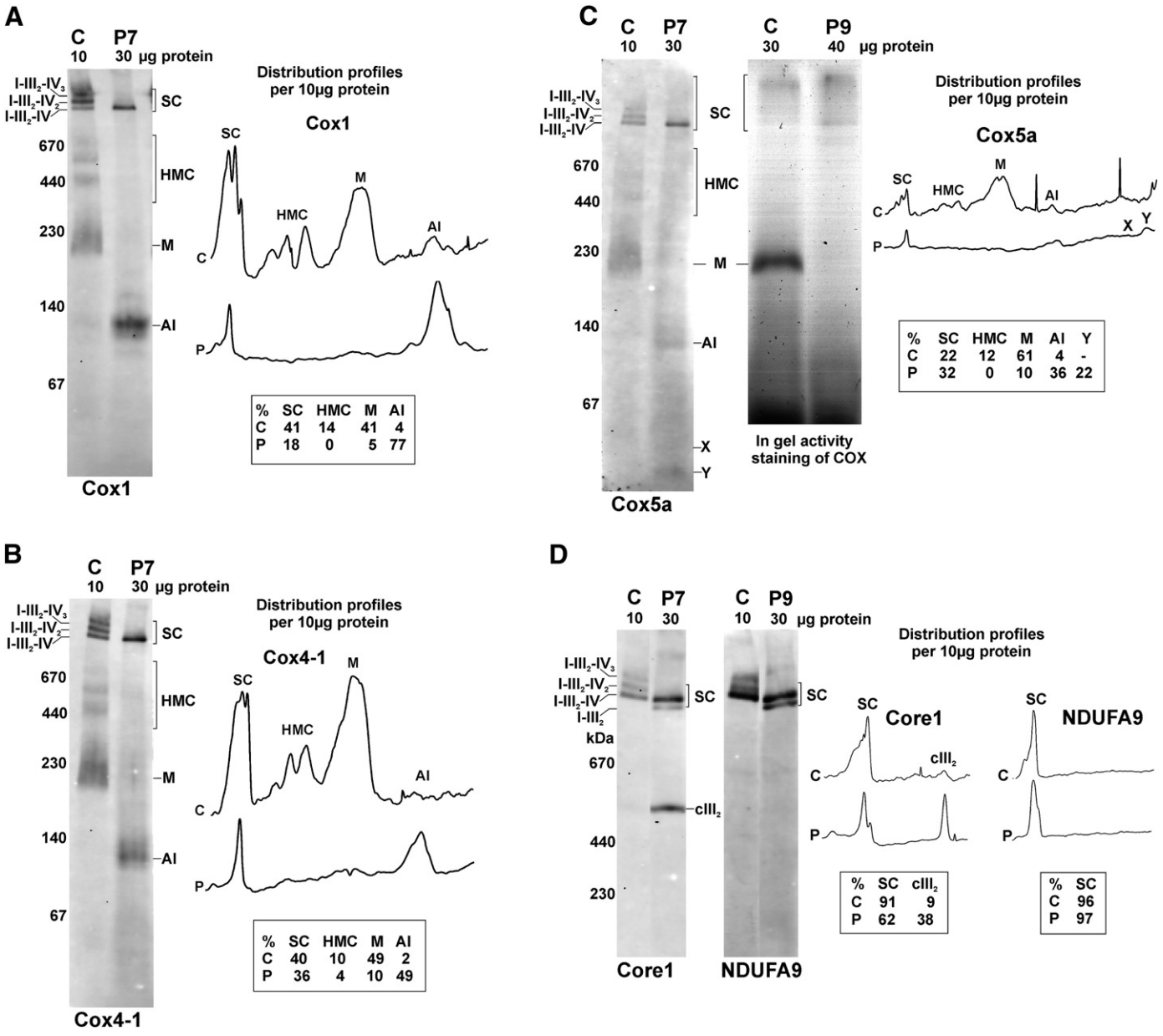

Fig. 3. Digitonin solubilized COX assembly intermediates and COX supercomplexes in LS^{COX} fibroblasts. Mitochondrial membrane proteins from fibroblasts were solubilized using 4 g detergent/g protein, indicated protein aliquots were resolved by BN-PAGE (patient — P7, 30 µg protein, control — C, 10 µg protein). For Western blot detection antibodies to Cox1 (A), Cox4-1 (B), Cox5a (C), Core1 and NDUFA9 (D) were used. COX supercomplexes (SC), high molecular complexes (HMC), monomer (M), assembly intermediates (AI), Cox4-5a heterodimer (X), free Cox5a subunit (Y) and dimer of complex III ($cIII_2$) are marked in blots and distribution profiles (detected signals in patient blots were re-counted to 10 µg protein). The presence of COX subunits in different COX forms as percentage is illustrated by tables inserted under the profiles. In gel activity staining of complex IV in control (C) and LS^{COX} patient (P9) mitochondria solubilized using digitonin (4 g detergent/g protein) is depicted in part C of the figure. Active monomer of cIV in control mitochondria and active cIV in supercomplexes (SC) in both control and LS^{COX} patient mitochondria were detected after scanning of the gel through blue filter.

fibroblasts using a 44 k human cDNA Agilent microarray to find out, whether the mutated *SURF1* gene caused changes in the expression of COX and other OXPHOS genes. Clearly, the downregulation of COX content was not associated with a significant and consistent change of transcripts for COX subunits, parallel to their low content or accumulation as in case of Cox5a. This may not be surprising when assuming that the low content of COX primarily results from a lack of an assembly factor but not from a lack of COX subunits. On the other hand, we did not find a transcriptional correlation with the compensatory increase of three respiratory chain complexes, the adaptive change that could result from a transcriptional activation of structural genes or specific assembly factors or pro-mitochondrial regulatory master genes such as *PGC1A*, *NRF1* and *TFAM*. None of those appeared to be the case.

The current view of the respiratory chain organization in the inner mitochondrial membrane has undergone a major paradigm shift during the last decade. The complexes are no longer considered as single entities with electron transfer occurring through mobile carriers coenzyme Q (CoQ) and cytochrome *c*, but rather as organized into respiratory supercomplexes, also known as respirasomes [38]. The supercomplexes are composed of cI, cIII, and cIV, and it has been recently demonstrated that they even contain cytochrome *c* and CoQ and are therefore capable of transferring electrons all the way from NADH to oxygen [38,39]. The absence of any of the three complexes inevitably results in disappearance of the supercomplexes [39]. In this regard, we were interested how would the selective decrease of cIV in LS^{COX} fibroblasts influence the supercomplex pattern. Indeed, we observed pronounced changes in the association of COX into

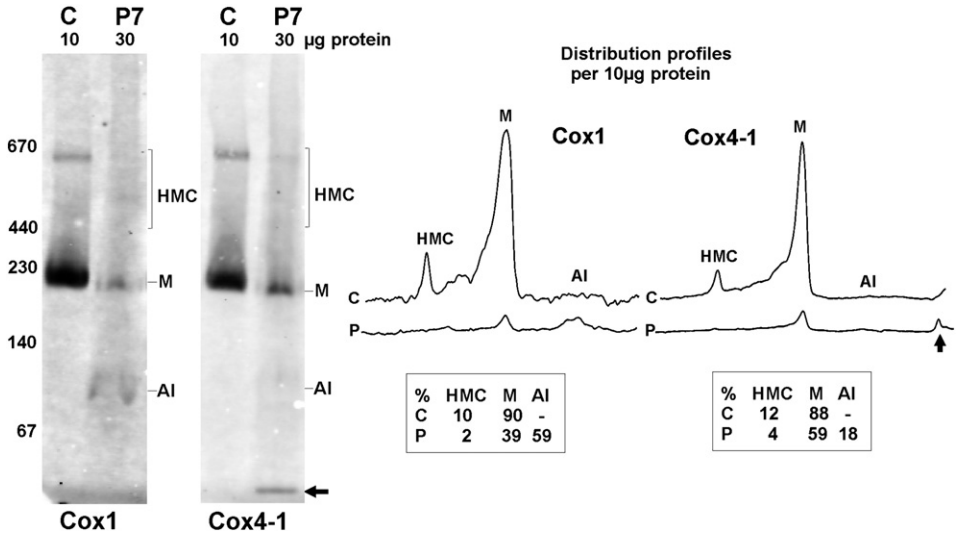

Fig. 4. Dodecyl maltoside-solubilized COX forms in LS^{COX} fibroblasts. Mitochondrial membrane proteins from fibroblasts were solubilized using 2 g detergent/g protein, indicated protein aliquots were resolved by BN-PAGE (patient — P7, 30 µg protein, control — C, 10 µg protein). For Western blot detection antibodies to Cox1 and Cox4-1 were used. COX in high molecular complexes (HMC), COX monomer (M) and assembly intermediate (AI) are marked in blots and distribution profiles (with re-counting signals representing patient to 10 µg protein), inserts give their quantification in percents. An arrow marks free Cox4-1 subunits in LS^{COX} patient fibroblasts.

supercomplexes between patient and control cells. Surprisingly, practically all of the fully assembled COX in LS^{COX} was found in the $I–III_2–IV_1$ supercomplex. In controls, the COX was distributed among the $I–III_2–IV_{1-3}$ supercomplexes, but also a significant portion of the enzyme remained in the form of monomer, dimer and smaller complexes. In control cells, the formation of supercomplexes seemed to be limited by the cI availability as its whole portion was associated in supercomplexes. The unassociated portion of COX perhaps represents the excess enzyme capacity often reported for this complex [40,41]. In LS^{COX} cells, on the other hand, the limiting component was COX, as evidenced by accumulation of the $I–III_2$ supercomplex or even free $cIII_2$. Our results suggest that upon its assembly into the holoenzyme, COX was preferentially associated with cI and cIII to form supercomplexes, likely to the advantage of improved efficiency of the electron transfer through substrate channeling [38]. We could speculate whether the changes of COX distribution might lead to functional alterations in respiratory chain. In our previous studies concerning LS^{COX} fibroblasts we reported unexpectedly high oxygen consumption that was only about 30–50% decreased compared to controls even though the COX content and activity reached only quarter of control values [10,35]. At the time, we interpreted this finding as an upregulated electron transport activity of incomplete COX assemblies. Looking at the pattern of COX-containing complexes as revealed by the present study, an alternative explanation comes to mind. If we assume that only the portion of COX associated in supercomplexes participates in electron transfer from substrates to oxygen, then this would explain the higher oxygen consumption per unit of COX in LS^{COX} fibroblasts compared to controls.

Another issue emanating from our BN-PAGE experiments is the relative underrepresentation of COX dimer and dimer-containing supercomplexes in LS^{COX} cells. This is apparently in contrast to a frequent opinion that dimer represents the active form of the complex [42]. This popular view is mostly based on the fact, that COX has been repeatedly crystallized in dimeric form [43]. Also, the isolated COX dimer shows cooperative kinetics in the binding of cytochrome *c* [44,45] suggesting a physiological role for the dimer. On the other hand, the pattern of supercomplexes that are usually present in multiple forms differing in the number of copies of COX, or indeed the predominance of the $I–III_2–IV_1$ supercomplex in patient cells strongly suggests that COX is acquired into supercomplexes in monomeric form and is able to perform its enzymatic activity as such. Nevertheless, we also cannot rule out the possibility that COX assembled in the absence of Surf1 is unable to dimerize. Similarly, HEK293 cells with subunit Cox5a knockdown presented with COX assembly defect that also resulted in decreased level of COX dimeric structures [6]. Whether the dimer underrepresentation is a specific result of an incomplete event during assembly or a mere consequence of generally decreased COX cannot be resolved at the moment.

Owing to the relatively low protein size resolution of 1D BN-PAGE, we employed 2D BN/BN-PAGE to precisely identify the COX complex that was associated in the supercomplex. In fact, the detection on the blots from one-dimensional gels using antibodies against subunits Cox1, Cox4, and Cox5a could not rule out the possibility that just the COX assembly intermediate is recruited into the supercomplexes. Indeed, studies dealing with COX assembly suggested, that supercomplexes could contain, in addition to COX holoenzyme, also some COX assembly subcomplexes [6,46]. Even more specifically, the study by Lazarou et al. concerning the assembly of COX nuclear-encoded subunits clearly showed that unlike controls, *SURF1* patient fibroblasts are able to efficiently incorporate all tested subunits into the supercomplex, including the early-assembled subunit Cox4 [7]. However, our experiments including activity staining in the 1D gel, and the second native dimension in the presence of dodecyl maltoside which dissociates the superassemblies revealed disintegration of the supercomplex into full size cI, cIII, and cIV, demonstrating that predominantly the fully assembled and active form of COX rather than its assembly intermediates interact with other OXPHOS complexes. Nevertheless, the finding by Lazarou et al. is very intriguing as it indicates a possible mechanism for COX nuclear subunit recycling of the full-size complex (within the respiratory supercomplex) specific for cells lacking Surf1 protein. In this way, it could substitute the role of a Surf1 protein-containing complex involved in repair/maintenance of COX as suggested by Reinhold et al. [47].

The precise identity of the major COX subcomplex accumulated in LS^{COX} cells is clearly the most puzzling issue of the present study. While it is generally agreed that cells harboring *SURF1* mutations accumulate the S2 COX assembly intermediate (composed of subunits 1, 4, and 5a) [17,48,49], several lines of evidence suggest that we may be looking at a different complex. First of all, the size of the detected subcomplex – 130 kDa – is much larger than the predicted mass of S2 intermediate of 85 kDa. As the mass calculations from BN-PAGE may be incorrect, we further examined the composition of this subcomplex in the second dimension using SDS-PAGE and found that it contained at least subunits Cox1, 2, 4, and 5a.

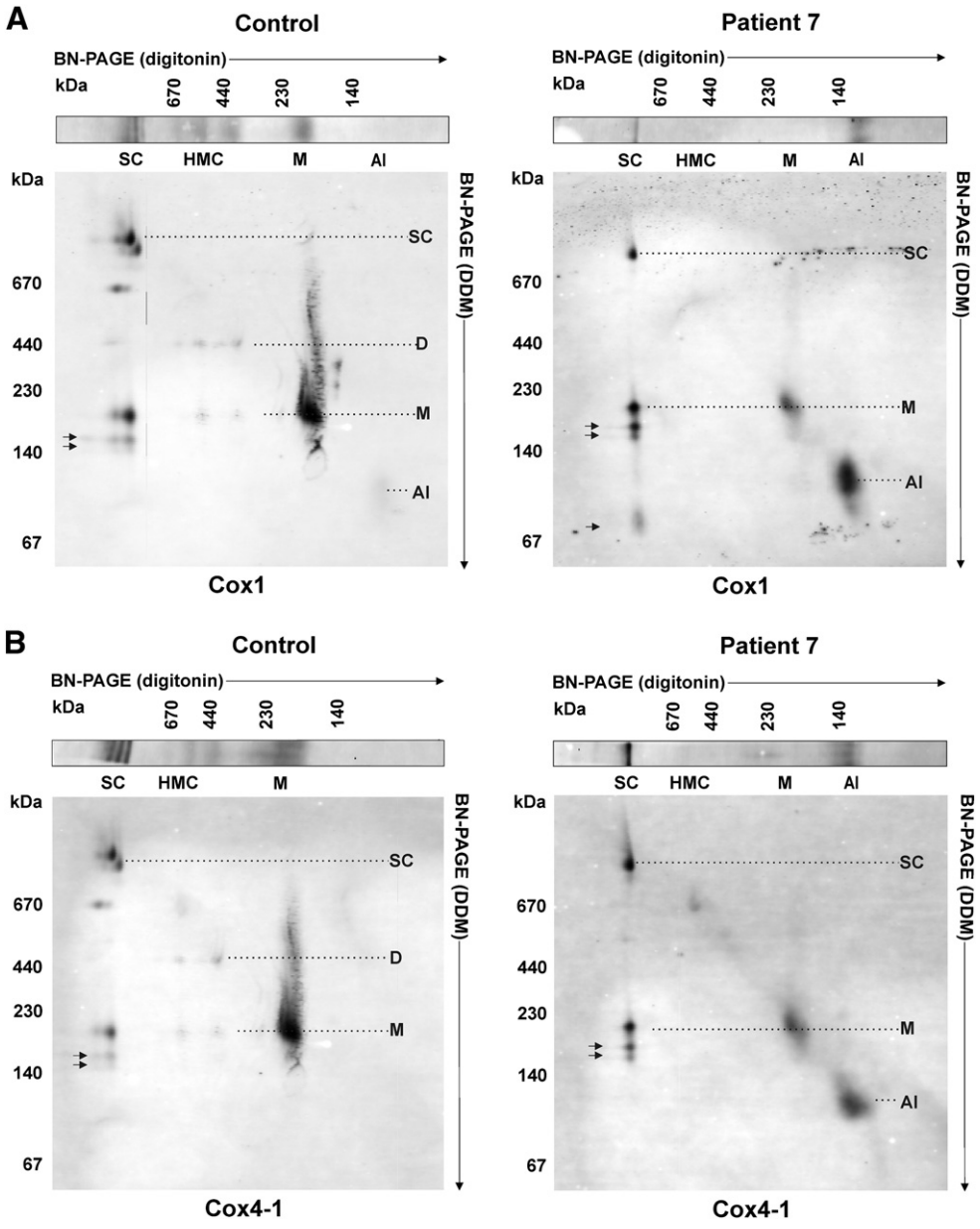

Fig. 5. Two-dimensional BN/BN-PAGE analysis of COX forms in LS^{COX} fibroblasts. Digitonin-solubilized (4 g/g protein) mitochondrial proteins from control (40 μg protein) and patient 7 (60 μg protein) fibroblasts were resolved by BN-PAGE in the first dimension. In the second dimension 0.02% dodecyl maltoside (DDM) was used in cathode buffers. COX supercomplexes (SC), dimer (D), monomer (M) and assembly intermediate (AI) were detected using Cox1 (A) and Cox4-1 (B) antibodies. Arrows mark the putative degradation products of COX.

Importantly, relative quantification revealed that Cox1 was likely present in excess over the other two subunits, perhaps by as much as one order of magnitude. We assume that this finding can only be explained by the presence of several comigrating complexes with approximate size close to 130 kDa. One of them might be a canonical COX assembly intermediate consisting of subunits 1, 2, 4, and 5a in stoichiometric amount. In addition, Cox1 would be associated in different types of complex(es) lacking any other COX subunit. These assemblies could represent not yet described complexes that could function in maturation of the subunit, insertion of its prosthetic groups, its posttranslational import into the inner membrane, or even repair/maintenance of the complex. The precise assignment of the identity/function of this intermediate would be greatly alleviated if we knew the function of Surf1. The studies performed in bacteria suggest that Surf1 serves as a heme-binding chaperone for heme a_3 insertion into the Cox1 subunit [50,51]. In the eukaryotic yeast model, Surf1 ortholog Shy1 is associated within a COX protein assembly complex of ~450 kDa along with early-assembled subunits and other assembly factors such as Coa1, Coa3, Cox14, where it functions as a factor coupling Cox1 translational regulation to assembly by relieving the sequestered Cox1 translational activator Mss51 [46,52–54]. In addition, Shy1 is probably also involved in Cox1 maturation–insertion of heme cofactors similar to bacteria [55,56]. Importantly, the multiple roles seem to be retained in the mammalian (human) Surf1, as the protein was found to associate in three distinct complexes in HEK293 cells [47]. The authors demonstrate that one of these complexes, of an approximate size of 200 kDa, represents a *bona fide* COX assembly intermediate as its formation is dependent on mitochondrial translation. We can therefore hypothesize, that the accumulated COX subcomplexes in LS^{COX} fibroblasts likely represent the entity identical to the Surf1-containing complex identified by Reinhold et al., of course smaller by 30 kDa due to Suf1 absence. The smaller portion of the broad ~85–140 kDa band, with dominant Cox1 signal in relation to other subunits, would represent associations involved in Cox1 maturation

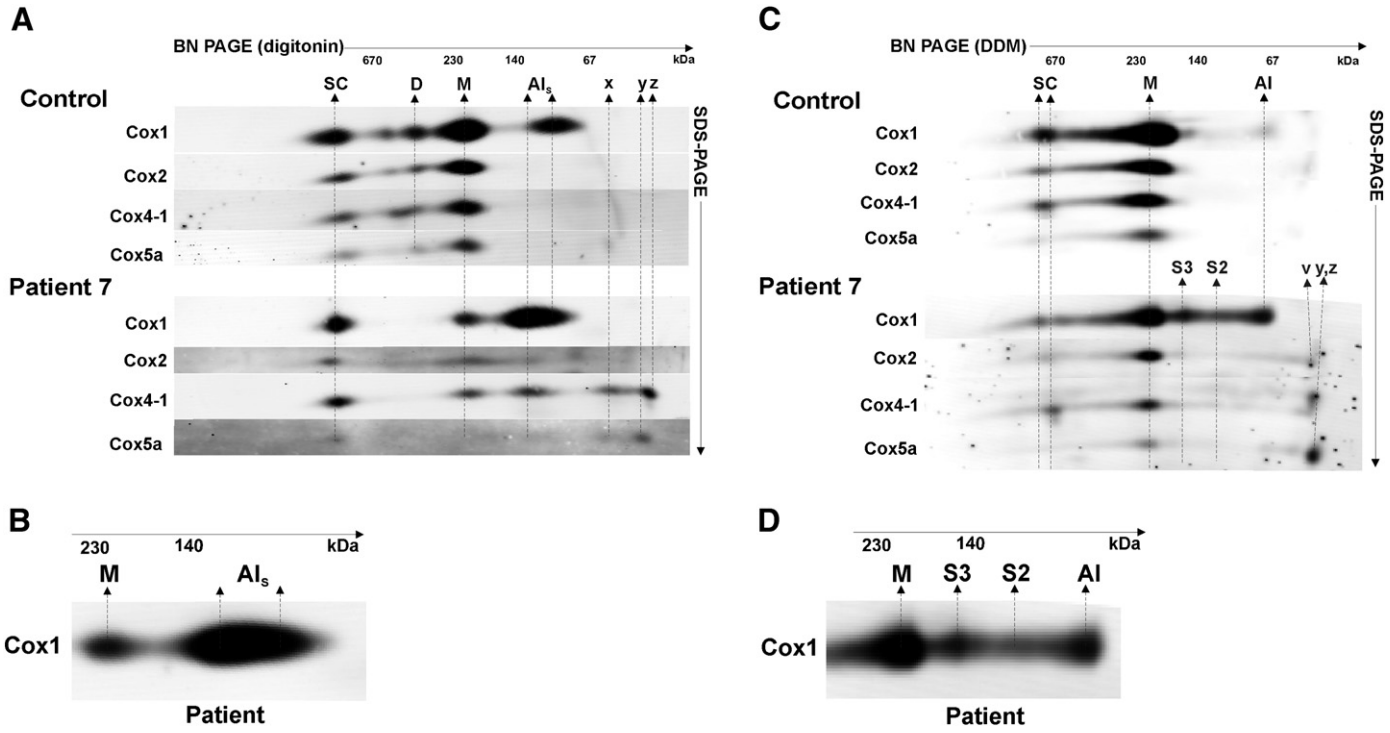

Fig. 6. Two-dimensional BN/SDS-PAGE analysis of COX forms in LS^{COX} fibroblasts. For 2D analysis digitonin-solubilized (4 g/g protein) mitochondrial proteins from control and patient 7 fibroblasts (50 μg protein aliquots) (A) and DDM solubilized (2 g/g protein) mitochondrial proteins from control and patient 7 fibroblasts (50 μg and 70 μg protein aliquots) (C) were used. Cox subunits 1, 2, 4-1 and 5a were detected after Western blotting with specific antibodies. Signals of these subunits in COX supercomplexes (SC), dimer (D), monomer (M), assembly intermediates (AIs, S2, S3), Cox4-5a heterodimer (x), free Cox2 (v), free Cox5a (y) and free Cox4-1 (z) subunits are marked. Differences between separation/migration of COX assembly intermediates after solubilization of membranes with digitonin (B) and DDM (D) in LS^{COX} patients are depicted in more detail.

or translation-assembly coupling. Possible interacting partners would recruit from a group of proteins fulfilling roles similar to yeast proteins Mss51, Coa1, Coa2, Coa3, or Cox14. Although mammalian orthologs of these were not identified, phylogenetically unrelated proteins may have taken up the vacant niche, such as the recently identified factor C12orf62 that links Cox1 translation and assembly [57]. The larger portion of the accumulated subcomplex, on the other hand, would represent COX assembly intermediate identified as S2, likely stalled in the phase of Cox2 association with the Cox1–Cox4–Cox5a complex, as all of these subunits were found comigrating in this region. Further understanding could be achieved by mass-spectroscopic analysis of the accumulated subcomplexes, and pulse-chase labeling experiments should indicate the position of these intermediates within the time frame of COX assembly.

Acknowledgements

This work was supported by grants from the Grant Agency of the Ministry of Health of the Czech Republic (NS9759, NT12370-5), the Grant Agency of the Czech Republic (305/08/H037), and institutional support provided by Ministry of Education, Youth and Sports of the Czech Republic (projects AVOZ 50110509, RVO: 67985823, and MSM0021620806).

References

[1] B. Beauvoit, O. Bunoust, B. Guerin, M. Rigoulet, ATP-regulation of cytochrome oxidase in yeast mitochondria: role of subunit VIa, Eur. J. Biochem. 263 (1999) 118–127.
[2] L.A. Allen, X.J. Zhao, W. Caughey, R.O. Poyton, Isoforms of yeast cytochrome *c* oxidase subunit V affect the binuclear reaction center and alter the kinetics of interaction with the isoforms of yeast cytochrome *c*, J. Biol. Chem. 270 (1995) 110–118.
[3] L.G. Nijtmans, J.W. Taanman, A.O. Muijsers, D. Speijer, C. Van den Bogert, Assembly of cytochrome-*c* oxidase in cultured human cells, Eur. J. Biochem. 254 (1998) 389–394.
[4] V. Tiranti, C. Galimberti, L. Nijtmans, S. Bovolenta, M.P. Perini, M. Zeviani, Characterization of SURF-1 expression and Surf-1p function in normal and disease conditions, Hum. Mol. Genet. 8 (1999) 2533–2540.
[5] L. Stiburek, H. Hansikova, M. Tesarova, L. Cerna, J. Zeman, Biogenesis of eukaryotic cytochrome *c* oxidase, Physiol. Res. 55 (Suppl. 2) (2006) S27–S41.
[6] D. Fornuskova, L. Stiburek, L. Wenchich, K. Vinsova, H. Hansikova, J. Zeman, Novel insights into the assembly and function of human nuclear-encoded cytochrome *c* oxidase subunits 4, 5a, 6a, 7a and 7b, Biochem. J. 428 (2010) 363–374.
[7] M. Lazarou, S.M. Smith, D.R. Thorburn, M.T. Ryan, M. McKenzie, Assembly of nuclear DNA-encoded subunits into mitochondrial complex IV, and their preferential integration into supercomplex forms in patient mitochondria, FEBS J. 276 (2009) 6701–6713.
[8] M. Lazarou, M. McKenzie, A. Ohtake, D.R. Thorburn, M.T. Ryan, Analysis of the assembly profiles for mitochondrial- and nuclear-DNA-encoded subunits into complex I, Mol. Cell. Biol. 27 (2007) 4228–4237.
[9] J. Yao, E.A. Shoubridge, Expression and functional analysis of SURF1 in Leigh syndrome patients with cytochrome *c* oxidase deficiency, Hum. Mol. Genet. 8 (1999) 2541–2549.
[10] P. Pecina, H. Houstkova, H. Hansikova, J. Zeman, J. Houstek, Genetic defects of cytochrome *c* oxidase assembly, Physiol. Res. 53 (Suppl. 1) (2004) S213–S223.
[11] V. Massa, E. Fernandez-Vizarra, S. Alshahwan, E. Bakhsh, P. Goffrini, I. Ferrero, P. Mereghetti, P. D'Adamo, P. Gasparini, M. Zeviani, Severe infantile encephalomyopathy caused by a mutation in COX6B1, a nucleus-encoded subunit of cytochrome *c* oxidase, Am. J. Hum. Genet. 82 (2008) 1281–1289.
[12] E.A. Shoubridge, Cytochrome *c* oxidase deficiency, Am. J. Med. Genet. 106 (2001) 46–52.
[13] M.J. Coenen, L.P. van den Heuvel, C. Ugalde, M. Ten Brinke, L.G. Nijtmans, F.J. Trijbels, S. Beblo, E.M. Maier, A.C. Muntau, J.A. Smeitink, Cytochrome *c* oxidase biogenesis in a patient with a mutation in COX10 gene, Ann. Neurol. 56 (2004) 560–564.
[14] M. Bugiani, V. Tiranti, L. Farina, G. Uziel, M. Zeviani, Novel mutations in COX15 in a long surviving Leigh syndrome patient with cytochrome *c* oxidase deficiency, J. Med. Genet. 42 (2005) e28.
[15] D. Leigh, Subacute necrotizing encephalomyelopathy in an infant, J. Neurol. Neurosurg. Psychiatry 14 (1951) 216–221.
[16] M.O. Pequignot, R. Dey, M. Zeviani, V. Tiranti, C. Godinot, A. Poyau, C. Sue, S. Di Mauro, M. Abitbol, C. Marsac, Mutations in the SURF1 gene associated with Leigh syndrome and cytochrome *c* oxidase deficiency, Hum. Mutat. 17 (2001) 374–381.
[17] V. Tiranti, K. Hoertnagel, R. Carrozzo, C. Galimberti, M. Munaro, M. Granatiero, L. Zelante, P. Gasparini, R. Marzella, M. Rocchi, M.P. Bayona-Bafaluy, J.A. Enriquez, G. Uziel, E. Bertini, C. Dionisi-Vici, B. Franco, T. Meitinger, M. Zeviani, Mutations of SURF-1 in Leigh disease associated with cytochrome *c* oxidase deficiency, Am. J. Hum. Genet. 63 (1998) 1609–1621.

[18] Z. Zhu, J. Yao, T. Johns, K. Fu, I. De Bie, C. Macmillan, A.P. Cuthbert, R.F. Newbold, J. Wang, M. Chevrette, G.K. Brown, R.M. Brown, E.A. Shoubridge, SURF1, encoding a factor involved in the biogenesis of cytochrome *c* oxidase, is mutated in Leigh syndrome, Nat. Genet. 20 (1998) 337–343.
[19] J. Smeitink, L. van den Heuvel, S. DiMauro, The genetics and pathology of oxidative phosphorylation, Nat. Rev. Genet. 2 (2001) 342–352.
[20] D. Piekutowska-Abramczuk, M. Magner, E. Popowska, M. Pronicki, E. Karczmarewicz, J. Sykut-Cegielska, T. Kmiec, E. Jurkiewicz, T. Szymanska-Debinska, L. Bielecka, M. Krajewska-Walasek, K. Vesela, J. Zeman, E. Pronicka, SURF1 missense mutations promote a mild Leigh phenotype, Clin. Genet. 76 (2009) 195–204.
[21] P. Pecina, M. Capkova, S.K. Chowdhury, Z. Drahota, A. Dubot, A. Vojtiskova, H. Hansikova, H. Houst'kova, J. Zeman, C. Godinot, J. Houstek, Functional alteration of cytochrome *c* oxidase by SURF1 mutations in Leigh syndrome, Biochim. Biophys. Acta 1639 (2003) 53–63.
[22] H.A. Bentlage, U. Wendel, H. Schagger, H.J. ter Laak, A.J. Janssen, J.M. Trijbels, Lethal infantile mitochondrial disease with isolated complex I deficiency in fibroblasts but with combined complex I and IV deficiencies in muscle, Neurology 47 (1996) 243–248.
[23] I. Wittig, H.P. Braun, H. Schagger, Blue native PAGE, Nat. Protoc. 1 (2006) 418–428.
[24] I. Wittig, M. Karas, H. Schagger, High resolution clear native electrophoresis for in-gel functional assays and fluorescence studies of membrane protein complexes, Mol. Cell. Proteomics 6 (2007) 1215–1225.
[25] H. Schagger, G. von Jagow, Tricine-sodium dodecyl sulfate-polyacrylamide gel electrophoresis for the separation of proteins in the range from 1 to 100 kDa, Anal. Biochem. 166 (1987) 368–379.
[26] A. Dubot, C. Godinot, V. Dumur, B. Sablonniere, T. Stojkovic, J.M. Cuisset, A. Vojtiskova, P. Pecina, P. Jesina, J. Houstek, GUG is an efficient initiation codon to translate the human mitochondrial ATP6 gene, Biochem. Biophys. Res. Commun. 313 (2004) 687–693.
[27] T. Honzik, Z. Drahota, M. Bohm, P. Jesina, T. Mracek, J. Paul, J. Zeman, J. Houstek, Specific properties of heavy fraction of mitochondria from human-term placenta — glycerophosphate-dependent hydrogen peroxide production, Placenta 27 (2006) 348–356.
[28] E. Zerbetto, L. Vergani, F. Dabbeni-Sala, Quantification of muscle mitochondrial oxidative phosphorylation enzymes via histochemical staining of blue native polyacrylamide gels, Electrophoresis 18 (1997) 2059–2064.
[29] A. Brazma, P. Hingamp, J. Quackenbush, G. Sherlock, P. Spellman, C. Stoeckert, J. Aach, W. Ansorge, C.A. Ball, H.C. Causton, T. Gaasterland, P. Glenisson, F.C. Holstege, I.F. Kim, V. Markowitz, J.C. Matese, H. Parkinson, A. Robinson, U. Sarkans, S. Schulze-Kremer, J. Stewart, R. Taylor, J. Vilo, M. Vingron, Minimum information about a microarray experiment (MIAME)-toward standards for microarray data, Nat. Genet. 29 (2001) 365–371.
[30] G.K. Smyth, Limma: linear models for microarray data, Bioinformatics and Computational Biology Solutions using R and Bioconductor, Springer, New York, 2005, pp. 397–420.
[31] Y. Benjamini, Y. Hochberg, Controlling the false discovery rate: a practical and powerful approach to multiple testing, J. R. Stat. Soc. (1995) 289–300.
[32] A. Cizkova, V. Stranecky, R. Ivanek, H. Hartmannova, L. Noskova, L. Piherova, M. Tesarova, H. Hansikova, T. Honzik, J. Zeman, P. Divina, A. Potocka, J. Paul, W. Sperl, J.A. Mayr, S. Seneca, J. Houstek, S. Kmoch, Development of a human mitochondrial oligonucleotide microarray (h-MitoArray) and gene expression analysis of fibroblast cell lines from 13 patients with isolated F1Fo ATP synthase deficiency, BMC Genomics 9 (2008) 38.
[33] F. Sasarman, G. Karpati, E.A. Shoubridge, Nuclear genetic control of mitochondrial translation in skeletal muscle revealed in patients with mitochondrial myopathy, Hum. Mol. Genet. 11 (2002) 1669–1681.
[34] M. Sebastiani, C. Giordano, C. Nediani, C. Travaglini, E. Borchi, M. Zani, M. Feccia, M. Mancini, V. Petrozza, A. Cossarizza, P. Gallo, R.W. Taylor, G. d'Amati, Induction of mitochondrial biogenesis is a maladaptive mechanism in mitochondrial cardiomyopathies, J. Am. Coll. Cardiol. 50 (2007) 1362–1369.
[35] P. Pecina, M. Capkova, S.K. Chowdhury, Z. Drahota, A. Dubot, A. Vojtiskova, H. Hansikova, H. Houst'kova, J. Zeman, C. Godinot, J. Houstek, Functional alteration of cytochrome *c* oxidase by SURF1 mutations in Leigh syndrome, Biochim. Biophys. Acta 1639 (2003) 53–63.
[36] M. Wasniewska, E. Karczmarewicz, M. Pronicki, D. Piekutowska-Abramczuk, K. Zablocki, E. Popowska, E. Pronicka, J. Duszynski, Abnormal calcium homeostasis in fibroblasts from patients with Leigh disease, Biochem. Biophys. Res. Commun. 283 (2001) 687–693.
[37] L. Stiburek, J. Zeman, Assembly factors and ATP-dependent proteases in cytochrome *c* oxidase biogenesis, Biochim. Biophys. Acta 1797 (2010) 1149–1158.
[38] G. Lenaz, M.L. Genova, Structural and functional organization of the mitochondrial respiratory chain: a dynamic super-assembly, Int. J. Biochem. Cell Biol. 41 (2009) 1750–1772.
[39] R. Acin-Perez, P. Fernandez-Silva, M.L. Peleato, A. Perez-Martos, J.A. Enriquez, Respiratory active mitochondrial supercomplexes, Mol. Cell 32 (2008) 529–539.
[40] E. Gnaiger, Oxygen conformance of cellular respiration. A perspective of mitochondrial physiology, Adv. Exp. Med. Biol. 543 (2003) 39–55.
[41] A. Kudin, S. Vielhaber, C.E. Elger, W.S. Kunz, Differences in flux control and reserve capacity of cytochrome *c* oxidase (COX) in human skeletal muscle and brain suggest different metabolic effects of mild COX deficiencies, Mol. Biol. Rep. 29 (2002) 89–92.
[42] F. Fontanesi, I.C. Soto, D. Horn, A. Barrientos, Assembly of mitochondrial cytochrome *c*-oxidase, a complicated and highly regulated cellular process, Am. J. Physiol. Cell Physiol. 291 (2006) C1129–C1147.
[43] T. Tsukihara, H. Aoyama, E. Yamashita, T. Tomizaki, H. Yamaguchi, K. Shinzawa-Itoh, R. Nakashima, R. Yaono, S. Yoshikawa, The whole structure of the 13-subunit oxidized cytochrome *c* oxidase at 2.8 A [see comments], Science 272 (1996) 1136–1144.
[44] S. Arnold, B. Kadenbach, The intramitochondrial ATP/ADP-ratio controls cytochrome *c* oxidase activity allosterically, FEBS Lett. 443 (1999) 105–108.
[45] I. Lee, A.R. Salomon, S. Ficarro, I. Mathes, F. Lottspeich, L.I. Grossman, M. Huttemann, cAMP-dependent tyrosine phosphorylation of subunit I inhibits cytochrome *c* oxidase activity, J. Biol. Chem. 280 (2005) 6094–6100.
[46] D.U. Mick, K. Wagner, M. van der Laan, A.E. Frazier, I. Perschil, M. Pawlas, H.E. Meyer, B. Warscheid, P. Rehling, Shy1 couples Cox1 translational regulation to cytochrome *c* oxidase assembly, EMBO J. 26 (2007) 4347–4358.
[47] R. Reinhold, B. Bareth, M. Balleininger, M. Wissel, P. Rehling, D.U. Mick, Mimicking a SURF1 allele reveals uncoupling of cytochrome *c* oxidase assembly from translational regulation in yeast, Hum. Mol. Genet. 20 (2011) 2379–2393.
[48] L. Stiburek, K. Vesela, H. Hansikova, P. Pecina, M. Tesarova, L. Cerna, J. Houstek, J. Zeman, Tissue-specific cytochrome *c* oxidase assembly defects due to mutations in SCO2 and SURF1, Biochem. J. 392 (2005) 625–632.
[49] J.W. Taanman, S.L. Williams, Assembly of cytochrome *c* oxidase: what can we learn from patients with cytochrome *c* oxidase deficiency? Biochem. Soc. Trans. 29 (2001) 446–451.
[50] A. Hannappel, F.A. Bundschuh, B. Ludwig, Characterization of heme-binding properties of *Paracoccus denitrificans* Surf1 proteins, FEBS J. 278 (2011) 1769–1778.
[51] F.A. Bundschuh, A. Hannappel, O. Anderka, B. Ludwig, Surf1, associated with Leigh syndrome in humans, is a heme-binding protein in bacterial oxidase biogenesis, J. Biol. Chem. 284 (2009) 25735–25741.
[52] A. Barrientos, D. Korr, A. Tzagoloff, Shy1p is necessary for full expression of mitochondrial COX1 in the yeast model of Leigh's syndrome, EMBO J. 21 (2002) 43–52.
[53] A. Barrientos, A. Zambrano, A. Tzagoloff, Mss51p and Cox14p jointly regulate mitochondrial Cox1p expression in *Saccharomyces cerevisiae*, EMBO J. 23 (2004) 3472–3482.
[54] I.C. Soto, F. Fontanesi, J. Liu, A. Barrientos, Biogenesis and assembly of eukaryotic cytochrome *c* oxidase catalytic core, Biochim. Biophys. Acta (2011), doi: 10.1016/j.bbabio.2011.09.005.
[55] O. Khalimonchuk, M. Bestwick, B. Meunier, T.C. Watts, D.R. Winge, Formation of the redox cofactor centers during Cox1 maturation in yeast cytochrome oxidase, Mol. Cell. Biol. 30 (2010) 1004–1017.
[56] F. Pierrel, M.L. Bestwick, P.A. Cobine, O. Khalimonchuk, J.A. Cricco, D.R. Winge, Coa1 links the Mss51 post-translational function to Cox1 cofactor insertion in cytochrome *c* oxidase assembly, EMBO J. 26 (2007) 4335–4346.
[57] W. Weraarpachai, F. Sasarman, T. Nishimura, H. Antonicka, K. Aure, A. Rotig, A. Lombes, E.A. Shoubridge, Mutations in C12orf62, a factor that couples COX I synthesis with cytochrome *c* oxidase assembly, cause fatal neonatal lactic acidosis, Am. J. Hum. Genet. 90 (2012) 142–151.

Biochimica et Biophysica Acta 1862 (2016) 705–715

Contents lists available at ScienceDirect

Biochimica et Biophysica Acta

journal homepage: www.elsevier.com/locate/bbadis

Tissue- and species-specific differences in cytochrome *c* oxidase assembly induced by *SURF1* defects

Nikola Kovářová [a], Petr Pecina [a], Hana Nůsková [a], Marek Vrbacký [a], Massimo Zeviani [b,c], Tomáš Mráček [a], Carlo Viscomi [c], Josef Houštěk [a,*]

[a] Institute of Physiology of the Czech Academy of Sciences, Vídeňská 1083, Prague, Czech Republic
[b] Molecular Neurogenetics Unit, Instituto Neurologico "C. Besta", via Temolo 4, 20126 Milan, Italy
[c] MRC-Mitochondrial Biology Unit, Wellcome Trust MRC Bldg, Addenbrookes Hospital Hills Rd, Cambridge CB2 0XY, UK

ARTICLE INFO

Article history:
Received 23 June 2015
Received in revised form 8 December 2015
Accepted 8 January 2016
Available online 13 January 2016

Keywords:
Cytochrome *c* oxidase
Respiratory supercomplexes
Leigh syndrome
SURF1$^{-/-}$ mouse knockout
Doxycycline
Pulse-chase

ABSTRACT

Mitochondrial protein SURF1 is a specific assembly factor of cytochrome *c* oxidase (COX), but its function is poorly understood. *SURF1* gene mutations cause a severe COX deficiency manifesting as the Leigh syndrome in humans, whereas in mice *SURF1*$^{-/-}$ knockout leads only to a mild COX defect. We used *SURF1*$^{-/-}$ mouse model for detailed analysis of disturbed COX assembly and COX ability to incorporate into respiratory supercomplexes (SCs) in different tissues and fibroblasts. Furthermore, we compared fibroblasts from *SURF1*$^{-/-}$ mouse and *SURF1* patients to reveal interspecies differences in kinetics of COX biogenesis using 2D electrophoresis, immunodetection, arrest of mitochondrial proteosynthesis and pulse-chase metabolic labeling.

The crucial differences observed are an accumulation of abundant COX1 assembly intermediates, low content of COX monomer and preferential recruitment of COX into I–III_2–IV_n SCs in *SURF1* patient fibroblasts, whereas *SURF1*$^{-/-}$ mouse fibroblasts were characterized by low content of COX1 assembly intermediates and milder decrease in COX monomer, which appeared more stable. This pattern was even less pronounced in *SURF1*$^{-/-}$ mouse liver and brain. Both the control and *SURF1*$^{-/-}$ mice revealed only negligible formation of the I–III_2–IV_n SCs and marked tissue differences in the contents of COX dimer and III_2–IV SCs, also less noticeable in liver and brain than in heart and muscle. Our studies support the view that COX assembly is much more dependent on SURF1 in humans than in mice. We also demonstrate markedly lower ability of mouse COX to form I–III_2–IV_n supercomplexes, pointing to tissue-specific and species-specific differences in COX biogenesis.

1. Introduction

Mammalian oxidative phosphorylation system (OXPHOS) consists of five multisubunit protein complexes and two mobile electron carriers — ubiquinone and cytochrome *c*. Electron transporting complexes I–IV (cI–cIV) form the respiratory chain (RC), where transfer of electrons from reducing equivalents to molecular oxygen leads to proton pumping across the inner mitochondrial membrane (IMM), resulting in mitochondrial proton gradient formation. ATP synthase, complex V (cV), then uses electrochemical potential of the proton gradient as a driving force for ATP synthesis. Organization of RC complexes in the IMM appears to be rather dynamic and individual RC complexes coexists with respiratory supercomplexes (SCs) composed of cI, cIII and cIV [2]. As proposed by the "plasticity model" of the RC organization, SCs differ in various tissues and cell types and their composition could be regulated according to actual energetics demands and substrate availabilities [1].

Complex IV - cytochrome *c* oxidase (COX, cIV), the terminal enzyme of the RC transfers electrons from reduced cytochrome *c* to oxygen molecule embedded in its structure. In mammals, COX can be detected as a monomer, dimer or as a part of several SCs. COX is formed by 14 different subunits. Three largest subunits COX1, COX2 and COX3 are coded for by mitochondrial DNA (mtDNA) and represent the catalytic core of the enzyme. Ten subunits (COX4, COX5a, COX5b, COX6c, COX7b, COX7c, COX8, COX7a, COX6b, COX6a) encoded by nuclear genes are involved in COX regulation, assembly, stability and dimerization [20,26,58]. Recently, the NDUFA4, formerly described as complex I subunit was recognized as the 14th nuclear encoded subunit of COX [6]. NDUFA4 is loosely attached to the assembled COX complex and appears to be essential for enzyme biogenesis [48]. COX molecules also contain several metal cofactors in two copper sites (Cu_A, Cu_B) and two heme moieties (heme *a* and a_3). Mammalian COX assembly pathway proceeds via four/five step-by-step assembly intermediates S1–S2–S3–S4*–S4, where S4 represents a fully assembled COX monomer [20]. COX biosynthesis

Abbreviations: COX, Cytochrome *c* oxidase; OXPHOS, oxidative phosphorylation system; IMM, inner mitochondrial membrane; RC, respiratory chain; cI–cV, RC complexes I–V; CL, cardiolipin; SCs, respiratory supercomplexes; LS, Leigh syndrome; mtDNA, mitochondrial DNA; DOX, doxycycline.

* Corresponding author.
E-mail address: houstek@biomed.cas.cz (J. Houštěk).

http://dx.doi.org/10.1016/j.bbadis.2016.01.007

and assembly of individual subunits is a highly regulated process, depending on many ancillary/assembly proteins. They are essential for different steps of COX biogenesis, from regulation of expression of catalytic core subunits (LRPPRC, TACO1, hCOA3, COX14) [15,64,65,68], through copper metabolism and insertion (COX17, SCO1, SCO2, COX11, COX19, COA6, COX20) [10,22,31–34,43], heme *a* biosynthesis and insertion (COX10, COX15, FDX2) [3,4,51], to membrane insertion and processing of catalytic core subunits (OXA1l, COX18) [60]. A few other COX assembly proteins have been identified; they participate in early (SURF1, COA5) [24,60] or intermediate stages (PET100) [36] of COX biogenesis, but their precise function is as of yet unknown.

SURF1 is a 30 kDa hydrophobic protein localized in the IMM, encoded by a *SURF1* nuclear gene, which is part of a highly conserved housekeeping gene cluster, the surfeit locus [19,60,62,69]. Up to now, SURF1 is supposed to be involved in a formation of S2 assembly intermediate, most likely in association of COX2 subunit with COX1–COX4–COX5a subassembly [59,66]. However, its function might be more redundant, because studies on yeast homolog Shy1 indicate, that Shy1/SURF1 might play a role in heme *a* transfer/insertion into COX1 subunit [7,57]. Tissue-dependent copper deficiency was found in patients harboring *SURF1* gene mutations, which points to a possible function of SURF1 in maintaining of proper cellular copper homeostasis [58]. Moreover, a recently identified MITRAC12 protein [38] was found to interact with SURF1 and COX1 in a mitochondrial translation regulation assembly intermediate of COX1, which further extends possible roles of the SURF1 in COX biogenesis.

Mutations in the human *SURF1* gene result in a severe reduction of fully assembled, active COX and accumulation of COX assembly intermediates in patients' cells and tissues. *SURF1* mutations manifest usually several months after birth as a fatal neurodegenerative mitochondrial disorder, Leigh syndrome (LS) [52,70]. In recent studies 74 known *SURF1* gene mutations have been summarized and linked to LS and atypical LS [35], but without genotype–phenotype correlation [5,12,46,47,61,63]. To better understand SURF1 function, *SURF1* knockout mouse (*SURF1*$^{-/-}$ mouse) model was generated [18]. *SURF1*$^{-/-}$ mice were smaller at birth, had mild reduction in motor skills at adult age and COX activity was found to be mildly reduced in all tissues examined. Interestingly, *SURF1*$^{-/-}$ mice showed prolonged lifespan compared to wild-type littermates that was later assigned to enhanced insulin sensitivity and increased mitochondrial biogenesis [17,49]. Animals were also protected from neuronal damage induced by kainic acid accompanied by reduced mitochondrial uptake of calcium ions [18]. In addition, recent study revealed that loss of *SURF1* initiates mitochondrial stress response pathways, including mitochondrial biogenesis, the UPR^{MT} and Nrf2 activation [49].

In the present study, we used the *SURF1*$^{-/-}$ mouse model for detailed analysis of disturbed COX assembly and COX ability to incorporate into respiratory SCs in different tissues and fibroblasts. Furthermore, we examined *SURF1*$^{-/-}$ mouse fibroblasts in comparison with human fibroblasts of patients with *SURF1* mutations to reveal interspecies differences in kinetics of COX biogenesis pathway, from assembly intermediates to SCs. We show an accumulation of abundant COX1 assembly intermediates and preferential recruitment of COX into I–III$_2$–IV$_n$ SCs in *SURF1* patient fibroblasts, whereas *SURF1*$^{-/-}$ mouse fibroblasts were characterized by much milder decrease in COX monomer, which was also more stable. Interestingly, murine COX, both in the wild type and in *SURF1* knockout showed only limited preference towards the formation of SCs.

2. Material and methods

2.1. Experimental material

For experiments different tissues were obtained from 3-month-old *SURF1*$^{-/-}$ knockout B6D2F1 mice [18], generated by the insertion of a *loxP* sequence in exon 7 of the mouse *SURF1* gene, leading to an aberrant, prematurely truncated and highly unstable protein, and from control wild type *SURF1*$^{+/+}$ mice. Immortalized skin fibroblasts from control and *SURF1*$^{-/-}$ mouse [18] were cultured at 37 °C in 5% atmosphere of CO_2 in a DMEM medium supplemented by 10% fetal bovine serum, 20 mM HEPES (pH 7.5) and geneticin (50 μg/ml). The same conditions were used for cultivation of human patients' skin fibroblasts lacking the SURF1 protein due to 845 del CT mutations of *SURF1* gene [44] and from controls, except that geneticin was replaced with penicillin (10 μg/ml) and streptomycin (10 μg/ml). The project was approved by the ethics committees of Institute of Physiology, CAS. Informed consent was obtained from the parents of the patients according to the Declaration of Helsinki of the World Medical Association.

2.2. Isolation of mitochondria

Muscle (hind leg) was minced in a K medium (150 mM KCl, 2 mM EDTA, 50 mM Tris, pH 7.4) supplemented with protease inhibitor cocktail (1:500, PIC from Sigma) and homogenized by ultra turrax IKA (2× for 15 s, level 4) and glass-teflon homogenizer (600 rpm, 5 strokes). 5% (*w*/*v*) homogenate was centrifuged 10 min at 600 g and postnuclear supernatant was centrifuged 10 min at 10,000 g. Pelleted mitochondria were washed once (10,000 g, 10 min) and resuspended in K medium.

Liver mitochondria were isolated from 10% homogenate prepared in STE medium (250 mM sucrose, 10 mM Tris, 2 mM EDTA, pH 7.2) supplemented with PIC (1:500) using glass-teflon homogenizer (600 rpm, 7 strokes). Postnuclear (800 g, 10 min) supernatant filtered through a gauze was centrifuged for 15 min at 5200 g, pelleted mitochondria were washed twice (13,000 g, 10 min) in STE with PIC and then resuspended in STE medium.

Heart mitochondria were isolated essentially as liver mitochondria, except that postnuclear supernatant was centrifuged for 10 min at 13,000 g.

Fibroblast mitochondria were isolated according to Bentlage et al. [9] with slight modifications. Cells harvested using 0.05% trypsin and 0.02% EDTA were sedimented (600 g, 5 min) and washed twice in phosphate-buffered saline (PBS — 140 mM NaCl, 5 mM KCl, 8 mM Na_2HPO_4, 1.5 mM KH_2PO_4, pH 7.2). Weighed cell pellet was suspended in ten times (*w*/*v*) the amount of 10 mM Tris-buffer with PIC (1:500) and homogenized by teflon-glass homogenizer (8 strokes, 600 rpm). Immediately afterwards 1/5 volume of 1.5 M sucrose was added. Homogenate was centrifuged at 600 g, 10 min and mitochondria containing supernatant was kept on ice. Pellet was suspended in original volume of SEKTP (250 mM sucrose, 40 mM KCl, 20 mM Tris, 2 mM EGTA, pH 7.6, PIC 1:500), rehomogenized (5 strokes, 800 rpm) and centrifuged at 600 g, 10 min. The supernatants were pooled and centrifuged 10,000 g, 10 min. Sedimented mitochondria were washed with SEKTP (10,000 g, 10 min) and suspended in SEKTP.

All isolations were performed at 4 °C and mitochondria were stored at −80 °C. Protein concentration was measured according to [11].

2.3. Protein analysis by Blue Native PAGE (BNE) and BNE/SDS PAGE

Mitochondrial pellets were suspended in MB2 buffer (1.5 M ε-aminocapronic acid, 150 mM Bis-tris, 0.5 mM EDTA, pH 7.0), solubilized with digitonin (8 g/g protein) for 15 min on ice and centrifuged for 20 min at 20,000 g, 4 °C. Samples for BNE were prepared from supernatants by adding 1/20 volume of 5% SBG dye (Serva Blue G 250) in 750 mM ε-aminocapronic acid and 1/10 volume of 50% (*v*/*v*) glycerol.

Frozen cell pellets were resuspended in sucrose buffer (83 mM sucrose, 6.6 mM imidazole/HCl, PIC 1:500, pH 7.0) [67] and sonicated for 10 s to obtain 10% (*w*/*v*) suspension. Cell membranes were sedimented for 30 min at 100,000 g, 4 °C, solubilized with digitonin (4 g/g protein) in an imidazole buffer (2 mM ε-aminocapronic acid, 1 mM EDTA, 50 mM NaCl, 50 mM imidazole, pH 7.0) for 10 min and centrifuged at 30,000 g, 20 min at 4 °C [67]. For BNE analysis supernatants

were mixed with 1/10 volume of 50% (*v*/v) glycerol and with 5% SBG dye in 750 mM ε-aminocapronic acid at a dye/digitonin ratio 1:8 (*w*/w).

Solubilized mitochondria were analyzed by Bis-tris BNE [56] on 5–12% polyacrylamide gradient gels, cell membranes were analyzed by imidazole BNE [67] on 5–16% polyacrylamide gradient gels using the Mini-Protean apparatus (BioRad).

For two-dimensional separation by BNE/SDS PAGE, the stripes of BNE gel were incubated in 1% SDS and 1% 2-mercaptoethanol for 1 h and then subjected to SDS PAGE on a 10% slab gel [55].

2.4. Western blot analysis

Proteins were transferred from the gels to PVDF membranes (Immobilon-P, Millipore) using semidry electroblotting. The membranes were blocked with 5% (*w*/*v*) non-fat dried milk in TBS (150 mM NaCl, 10 mM Tris, pH 7.5) for 1 h and incubated 2 h or overnight at 4 °C with primary antibodies diluted in TBS with 0.1% Tween-20. Monoclonal primary antibodies to the following enzymes of OXPHOS were used: SDHA (ab14715, Abcam), CORE1 (ab110252, Abcam), NDUFB6 (ab110244, Abcam), NDUFS3 (ab110246, Abcam), COX1 (ab14705, Abcam). The detection of the signals was performed with the secondary Alexa Fluor 680-labeled antibody (Life Technologies) using the Odyssey fluorescence scanner (LI-COR). Quantification of detected signals from BNE/SDS PAGE was carried out in Aida Image Analyzer program, version 3.21.

2.5. Spectrophotometric assays

COX, cII (succinate:cytochrome *c* oxidoreductase (SCCR)) and citrate synthase (CS) activities were measured as previously [44], cI (NADH:cytochrome c oxidoreductase (NCCR)) activity was measured as in [50].

2.6. Doxycycline treatment of the cells

Experiment was performed as described in [41]. Briefly, fibroblasts (grown to 70% confluence in DMEM medium) were treated with 15 μg/ml doxycycline (DOX) for 7 days and then washed 3 times with PBS to withdraw DOX. Subsequently, the cells were collected at different time points (0, 6, 16, 24, 48, 72 and 96 h) after DOX removal. Weighed pellets of cells were stored at −80 °C for analysis of solubilized cell membranes by 2D BNE/SDS-PAGE. Two independent experiments of DOX inhibition in human and mouse fibroblasts were performed. COX1 antibody signals from 2D Western blots were quantified using Aida Image Analyzer v. 3.21 (Raytest). The relative distribution of signal between individual COX forms (assembly intermediates, monomer, dimer, supercomplexes) was determined from 2D blots. The total COX1 signal for each given time point was calculated from 1D SDS PAGE (see Fig. 4 E–H in the Data in Brief appendix) and normalized to SDHA signal. COX1 signal was then divided by the relative quantities obtained in the first step. The resulting datasets from each experiment were resampled to [0, 100] interval and averaged values from two experiments plotted as comparative 2D maps.

2.7. Metabolic pulse-chase labeling of mtDNA encoded proteins

Proteins encoded by mtDNA were labeled using ^{35}S-Protein Labeling Mix (Met + Cys; Perkin Elmer NEG072) by procedure described in [37]. Briefly, cells were incubated for 16 h with chloramphenicol (40 μg/ml), washed twice in PBS, and after 15 min incubation in DMEM medium without methionine and cysteine (DMEM-Met-Cys) and 15 min incubation in DMEM-Met-Cys with cycloheximide (CHX; 0.1 mg/ml), ^{35}S-Protein Labeling Mix (350 μCi/150 mm dish) was added. Cells were incubated for 2 h, then 250 μM cold Met and Cys was added and after 15 min cells were washed with PBS + 250 μM cold Met and Cys and finally with PBS. Cells were grown in standard DMEM medium supplemented with 5% (*v*/v) fetal bovine serum and harvested at different times (0.5 h, 6 h, 16 h, 24 h). Pellets of labeled cells were mixed with the same *w*/w of unlabeled cells, cell membranes were isolated, solubilized with digitonin and analyzed by 2D BNE/SDS PAGE. Gels were stained in a Coomassie R 250 dye, dried and radioactivity was detected using Pharos FX™ Plus Molecular Imager (Bio-Rad). COX1 radioactive signals from 2D gels (Fig. 4 A, B, C, D) were quantified using Aida Image Analyzer v. 3.21 and relative quantities of individual COX forms (assembly intermediates, monomer, supercomplexes) were used to divide the respective COX1 signal for given chase-time from 1D SDS PAGE, normalized to overall radioactive signal in each time point. The resulting datasets from each experiment were resampled to [0, 100] interval and plotted as comparative 2D maps.

3. Results

3.1. Decreased COX activities in *SURF1*$^{-/-}$ mouse tissues and fibroblasts

Analysis of RC activities in isolated mitochondria from *SURF1*$^{-/-}$ mouse tissues and in fibroblasts whole cell lysates showed that COX activities related to activity of citrate synthase (CS) were decreased to 37–62% of control (heart 55%, liver 37%, brain 50%, muscle 48%, fibroblasts 62%) (Table 1), as previously described in [18]. Activities of other RC enzymes were not significantly changed in *SURF1*$^{-/-}$ mouse tissues/fibroblasts (not shown). The activity of CS was increased (22.7%) in *SURF1*$^{-/-}$ liver mitochondria but not in other tissues. This may suggest some compensatory upregulation of mitochondrial biogenesis, as observed previously in heart and skeletal muscle [49], or in *SURF1* patient cells [28]. In general, the COX defect in *SURF1*$^{-/-}$ mouse tissues and fibroblasts is less pronounced than in *SURF1* patients' fibroblasts and tissues, where COX activity was decreased to 10–30% of control values [44,59]. These results are in agreement with differences in phenotype severity between *SURF1*$^{-/-}$ mice and *SURF1* patients: while patients suffer from fatal Leigh syndrome, *SURF1*$^{-/-}$ mice show increased lifespan without considerable mitochondrial dysfunction [18,49].

Table 1
Changes in COX and CS activities in *SURF1*$^{-/-}$ mouse.

	SURF1$^{+/+}$			SURF1$^{-/-}$			SURF1$^{-/-}$/SURF1$^{+/+}$	
	COX	*CS*	*COX/CS*	*COX*	*CS*	*COX/CS*	*COX*	COX/CS
Heart	3385.9 ± 120.8	2047.9 ± 136.7	1.7	2228.5 ± 190.7	2433.7 ± 218.2	0.9	65.8**	55.4**
Muscle	2486.7 ± 39.5	451.5 ± 50.2	5.5	1110.7 ± 121.3	420.5 ± 27.8	2.6	44.7**	47.9**
Liver	1495.2 ± 63.4	253.7 ± 11.5*	5.9	675.9 ± 23.0	311.3 ± 14.2	2.2	45.2**	36.8**
Brain	1527.2 ± 97.1	627.9 ± 28.2	2.4	744.5 ± 17.7	609.9 ± 24.1	1.2	48.7**	50.2**
Fibroblasts	459.3 ± 33.6	333.7 ± 15.3	1.4	248.3 ± 49.3	280.3 ± 28.4	0.9	54.1**	62.3*

COX and CS enzyme activities (nmol/min/mg protein) were measured spectrophotometrically in *SURF1*$^{+/+}$ and *SURF1*$^{-/-}$ mouse tissues and fibroblasts, ratio between *SURF1*$^{-/-}$ and *SURF1*$^{+/+}$ values was expressed in %. The values are mean ± S.E. (n = 5–7).

* $p < 0.05$.

** $p < 0.01$.

3.2. Decreased content of assembled COX complexes and accumulation of COX assembly intermediates in SURF1$^{-/-}$ mouse tissues and fibroblasts

We performed 2D BNE/SDS PAGE analysis in combination with Western blot to detect and quantify various COX forms from assembly intermediates to supercomplexes in examined *SURF1*$^{+/+}$ and *SURF1*$^{-/-}$ mouse tissues and fibroblasts (Figs. 1, 2; Fig. 3 in the Data in Brief appendix). Generally, decreased COX activities in various *SURF1*$^{-/-}$ mouse tissues and fibroblasts corresponded to decreased total COX content on Western blots. The amount of fully assembled forms of COX (monomer, dimer and COX-containing SCs) was down-regulated in *SURF1*$^{-/-}$ mouse. In heart, liver and brain (Fig. 1 A, C, D; Fig. 3 in the Data in Brief appendix) it was in good agreement with measured COX activity (heart 53%, liver 39%, brain 64%), whereas in muscle it was somewhat higher (82%) and in fibroblasts lower (30%) (Fig. 1 B, E), than expected from activity measurements, possibly due to semi-quantitative character of WB immunodetection (antibody reactivity in different tissues, large differences in amounts of different COX forms).

Relative distribution of individual COX forms varied considerably between the studied control mouse tissues. Monomer represented the dominant form in all tissues, with relative amount ranging from 50% in heart to as much as 85–95% of total COX in brain and liver. Significant content of COX dimers (18–27%) and III_2–IV SC (13–15%) was detected in heart and muscle (Fig. 1 A, B; Fig. 2 A, B; Fig. 3 in the Data in Brief appendix), whereas in liver and brain we found only negligible amount of these COX forms (Fig. 1 C, D; Fig. 2 C, D; Fig. 3 in the Data in Brief appendix). Weak signals of COX were also detected above 1 MDa. These SCs were larger than I–III_2 SC (detected by strong cI and cIII signals) and therefore presumably represent the I–III_2–IV_n SCs.

In *SURF1*$^{-/-}$ mouse tissues, the amount of assembled COX forms was lower compared to *SURF1*$^{+/+}$, but the COX monomer was still the dominant form. COX dimer still represented 10–20% of total COX in heart and muscle but it almost disappeared in liver and brain (Fig. 1 A–D; Fig. 2 A–D; Fig. 3 in the Data in Brief appendix). III_2–IV SC was preserved in small amount in all tissues, and weak COX signals of higher I–III_2–IV_n SCs were detected only in heart and muscle. In contrast to controls, we detected increased content of COX1 assembly intermediates (AI) in muscle and heart, representing approximately 10% of total COX signal. In liver and brain, the accumulation of AI was negligible (Fig. 1 A–D; Fig. 2 A–D).

In *SURF1*$^{+/+}$ mouse fibroblasts, the COX monomer represented more than 90% of total COX signal, the remainder being comprised of small contribution of COX dimer, III_2–IV and I–III_2–IV_n SCs (Fig. 1 E; Fig. 3 in the Data in Brief appendix). In *SURF1*$^{-/-}$ mouse fibroblasts, the COX defect was more accentuated than in other mouse tissues — we detected reduced signal of COX monomer, negligible content of I–

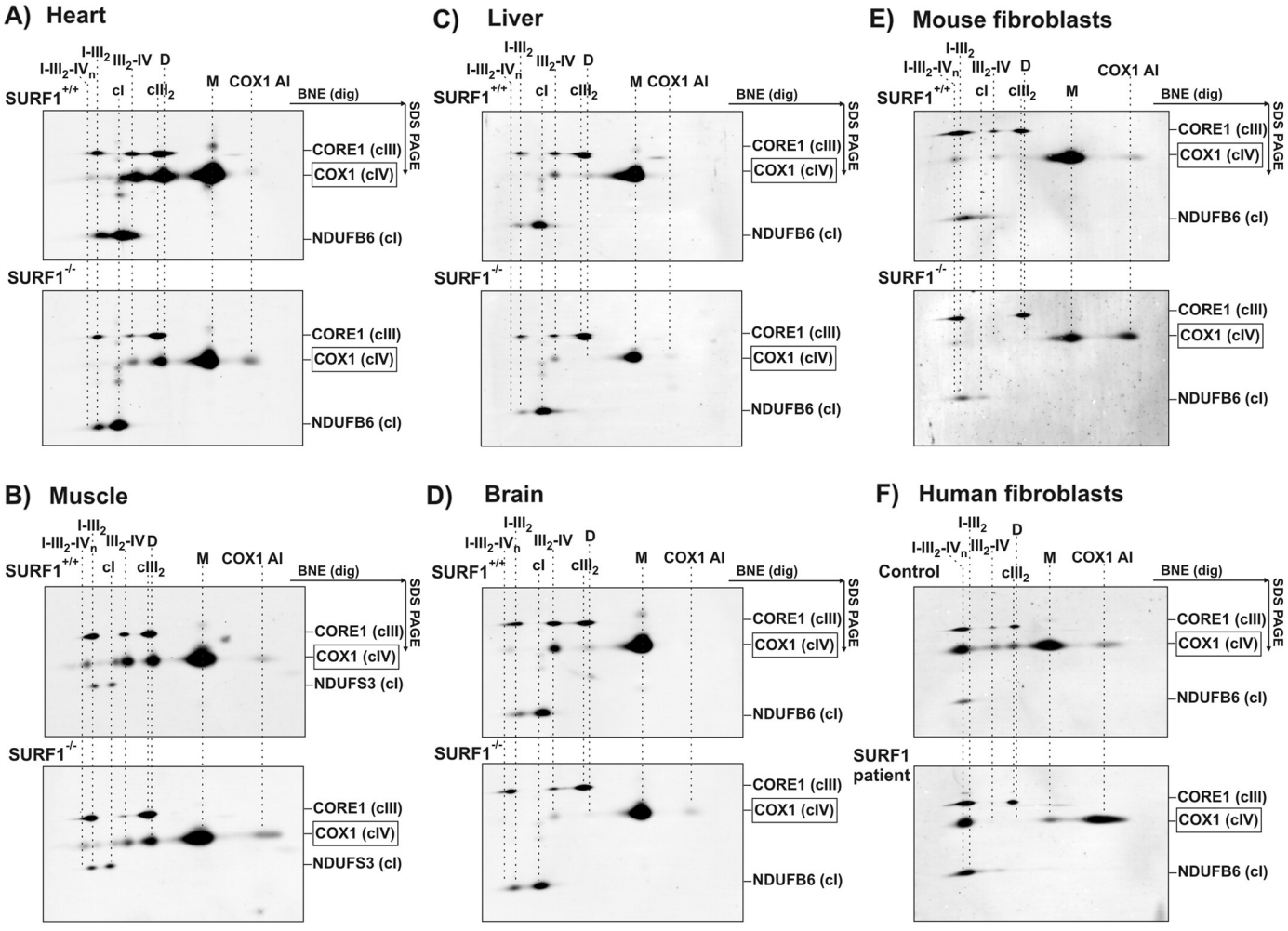

Fig. 1. Two-dimensional electrophoretic analysis of different COX forms present in *SURF1*$^{-/-}$ mouse tissues and fibroblasts and *SURF1* patient fibroblasts. Respiratory complexes and supercomplexes were solubilized using 8 g digitonin/g protein of isolated mitochondria, separated by BNE in the first dimension and SDS PAGE in the second dimension and detected by Western blots using specific antibodies to COX1 (cIV), CORE1 (cIII), NDUFB6 (cI) and NDUFS3 (cI). For analysis, heart (A), muscle (B), liver (C), brain (D) and fibroblast (E) of *SURF1*$^{+/+}$ and *SURF1*$^{-/-}$ mice as well as fibroblasts (F) of human control and *SURF1* patient were used. COX1 assembly intermediates (COX1 AI), COX monomer (M), COX dimer (D), III_2–IV SC (III_2–IV), I–III_2 SC (I–III_2), I–III_2–IV_n SCs (I–III_2–IV_n), complex III dimer ($cIII_2$), complex I (cI).

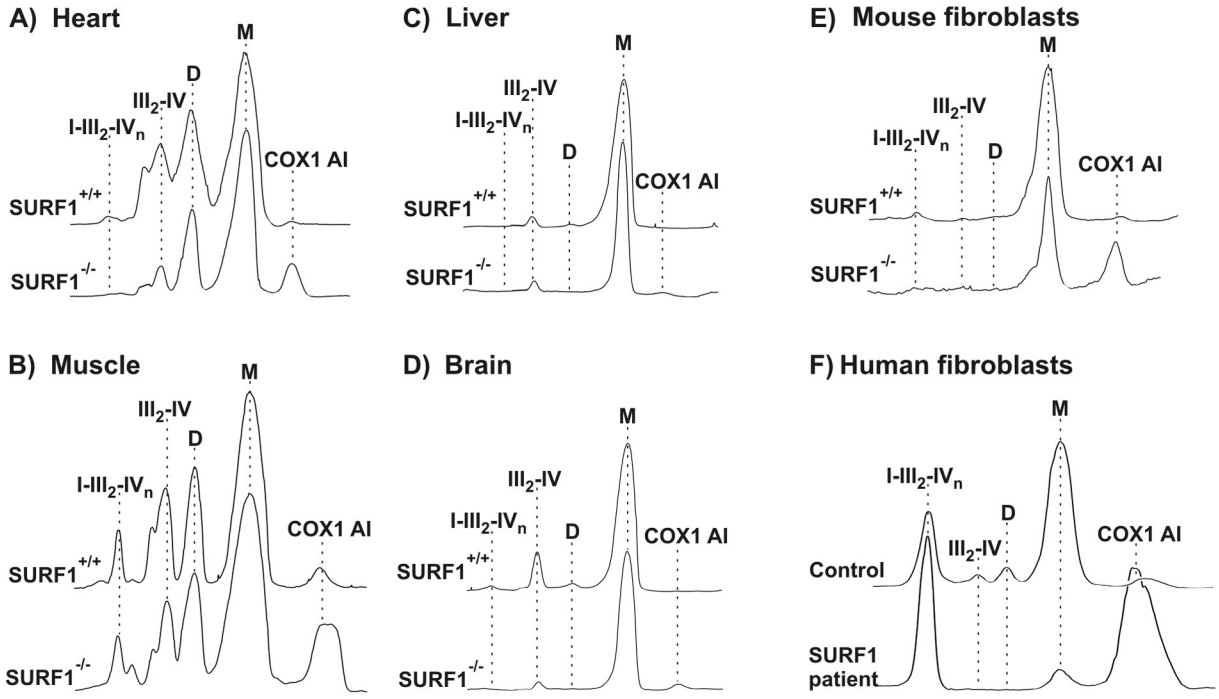

Fig. 2. Distribution profiles of the COX1 signal in different COX forms resolved by BNE/SDS PAGE analysis. COX1 signals from two-dimensional electrophoretic analysis in Fig. 1 were expressed as quantitative distribution profiles. *SURF1*$^{+/+}$ and *SURF1*$^{-/-}$ mice heart (A), muscle (B), liver (C), brain (D) and fibroblasts (E) and human control and *SURF1* patient fibroblasts (F). Individual COX forms are indicated: COX1 assembly intermediates (COX1 AI), COX monomer (M), COX dimer (D), III_2–IV SC (III_2–IV), I–III_2–IV_n SCs (I–III_2–IV_n).

III_2–IV_n SCs and markedly accumulated COX assembly intermediates, which represented 30% of total COX signal (Fig. 1 E; Fig. 3 in the Data in Brief appendix).

Other RC complexes (cI and cIII) were not affected by the COX defect in *SURF1*$^{-/-}$ mouse tissues and fibroblasts. As expected, the content of COX-containing III_2–IV SC was reduced (Fig. 1 A–E; Figs. 1, 2 in the Data in Brief appendix).

3.3. SURF1 patient fibroblasts preserve large I–III_2–IV_n supercomplexes

Given the marked differences in COX activities between *SURF1* patient and *SURF1*$^{-/-}$ mouse fibroblasts and respective controls, we also performed 2D BNE/SDS PAGE analysis on human control and *SURF1* patient fibroblasts to obtain interspecies comparison of the COX assembly defect consequences. In human control fibroblasts, COX was mainly found as a monomer and I–III_2–IV_n SCs (Fig. 1 F). There was also higher amount of COX dimer and III_2–IV SC in comparison to *SURF1*$^{+/+}$ mouse fibroblasts (Fig. 1 E, F; Fig. 3 in the Data in Brief appendix). In *SURF1* patient fibroblasts, two dominant COX forms were detected: the majority of fully assembled COX was detected in the I–III_2–IV_n SCs and as the large amount of COX1 assembly intermediates. In contrast the signal of COX monomer represented less than 10% of total COX, a pattern significantly different to *SURF1*$^{-/-}$ mouse fibroblasts (Fig. 1 E, F; Fig. 3 in the Data in Brief appendix). Taken together, we show that the COX defect due to lack of SURF1 caused by *SURF1* gene mutations/knockout exerts both tissue and species specificity.

3.4. COX supercomplexes assembly kinetics

Our present experiments indicate significant differences in COX association into III_2–IV and I–III_2–IV_n SCs between human and mouse, which can be observed both in control and SURF1-deficient fibroblasts. To explore the dynamics of COX incorporation into supercomplexes, we transiently treated cells with doxycycline (DOX), a reversible inhibitor of mitochondrial translation, to deplete the cells of mtDNA encoded OXPHOS subunits [41]. Human and mouse control and SURF1-deficient fibroblasts were cultured for 7 days in the presence of DOX and, after DOX removal, cells were collected at different time points (t0, t6, t16, t24, t48, t72, t96 h) to follow the assembly of newly synthesized mitochondrial-encoded subunits into RC complexes and subsequently into associated supercomplexes.

First we checked the amount of remaining COX in cell homogenates after DOX treatment. Using SDS PAGE and Western blot analysis (Fig. 4 in the Data in Brief appendix), we clearly showed lower levels of COX1 subunit in comparison with controls (DOX untreated cells) in all cell lines studied. COX1 antibody signals normalized to signals of SDHA were decreased to 30% and 34% in control and *SURF1* patient fibroblasts, and to 20% and 23% in *SURF1*$^{+/+}$ and *SURF1*$^{-/-}$ mouse fibroblasts, respectively. DOX treatment caused also slight decrease of cIII and cV levels, yet the greatest decrease was, unsurprisingly, observed in the content of cI, with its 7 mitochondrially encoded subunits.

Isolated membranes from fibroblasts were subsequently solubilized with digitonin (4 g/g protein) and analyzed by 2D BNE/SDS PAGE in combination with Western blot. In both human fibroblast lines, antibody detection of COX1 subunit signals revealed decrease in all COX forms at time point t0 (Fig. 3 A, B, E, F). Apparently, human cells preserved the reported stoichiometric distribution of COX (COX1) among COX assembly intermediates (AI), COX monomer, dimer and COX SCs (III_2–IV, I–III_2–VI_n) throughout the doxycycline treatment. The balance between COX AI and monomer was also maintained during the time course after DOX withdrawal. Specifically, in human control cells (Fig. 3 A, E), the longer the cells were cultured after DOX removal, the more COX monomer and SCs were synthesized and at time point t96 h COX1 signal reached the original steady state (DOX untreated cells). At all time points, the monomer was still the prevalent COX form. In *SURF1* patients' fibroblasts (Fig. 3 B, F) at t0 (after DOX removal), COX monomer was the main COX assembled form as its level decreased less than the content of COX associated into I–III_2–IV_n SCs. At t0 and all successive time points, signals of COX1 assembly intermediates represented the dominant form of COX and COX monomer

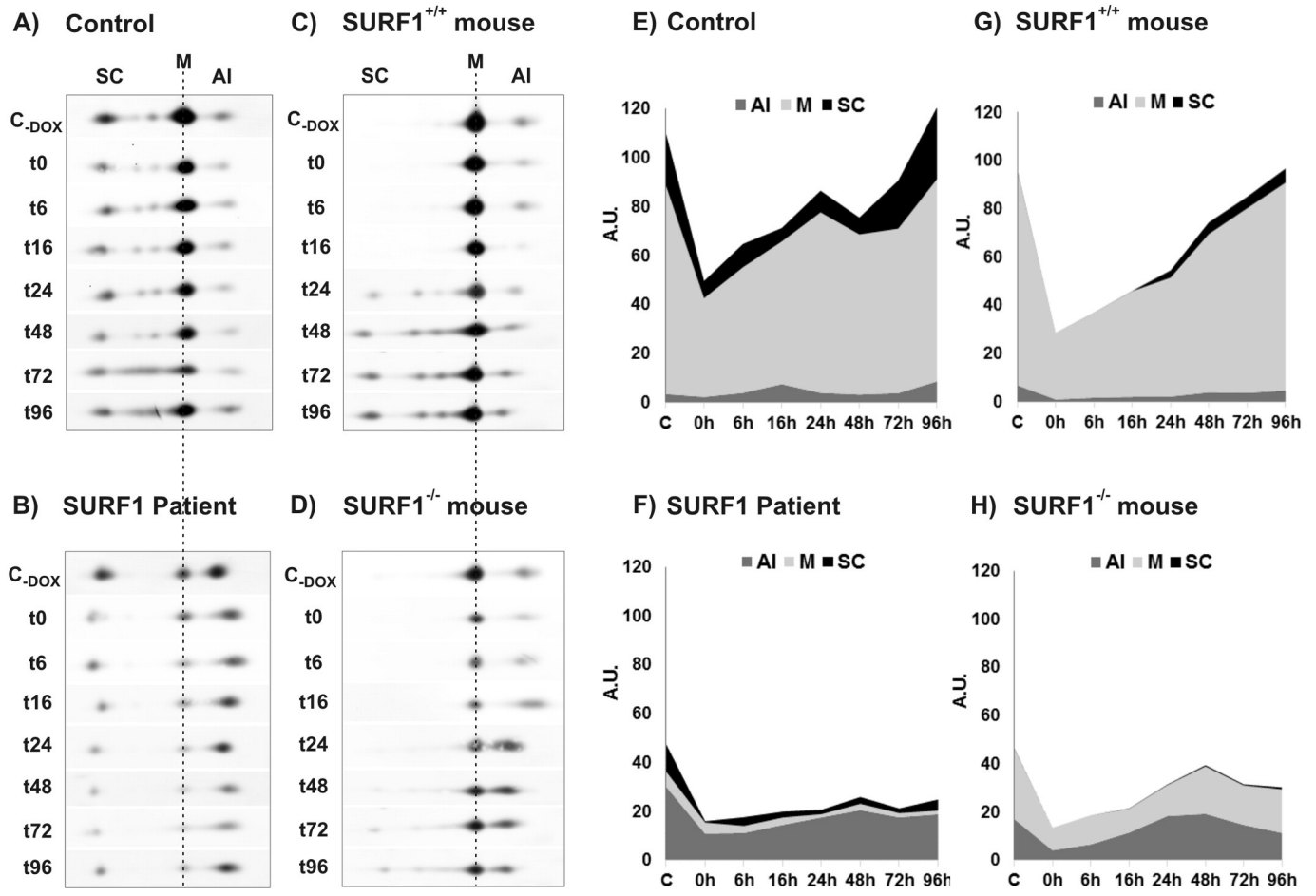

Fig. 3. Analysis of COX assembly in SURF1-deficient mouse and human fibroblasts following the release of doxycycline-arrested mitochondrial protein translation. BNE/SDS PAGE representative Western blot analysis using antibody to COX1 subunit performed in doxycycline treated (A) human control and (B) *SURF1* patient fibroblasts and (C) *SURF1*$^{+/+}$ and (D) *SURF1*$^{-/-}$ mouse fibroblasts. For BNE analysis, cell membranes were isolated and solubilized by digitonin (4 g dig/g protein). COX1 assembly intermediates (AI), COX monomer (M), COX supercomplexes (SC) are marked. Control cells without DOX (C_{-DOX}), times t0–t96 represent time points in hours after DOX removal, when the cells were harvested. Two independent DOX experiments for each cell line were performed to generate 2D maps showing distribution of COX1 forms along the DOX experiments at time points t0–t96 h (0 h–96 h) in (E) human control and (F) *SURF1* patient fibroblasts and (G) *SURF1*$^{+/+}$ and (H) *SURF1*$^{-/-}$ mouse fibroblasts. Relative quantities of individual COX forms (assembly intermediates, monomer, dimer, supercomplexes) were used to divide the respective COX1 signal for given time point from 1D SDS PAGE (see Fig. 4 E–H in the Data in Brief appendix), normalized to SDHA signal. The resulting datasets from each experiment representing individual COX forms in human and mice cells were rescaled (minimum = 0, maximum = 100) and averaged to plot in comparative 2D maps. COX assembly intermediates (AI), COX monomer (M), COX supercomplexes (SC).

further decreased. Compared to control cells, COX1 signal in *SURF1* patient did not reach the steady state levels observed in cells without DOX treatment even at t96 h.

The shift in balance between COX monomer and AI towards the AI was also clearly observable in *SURF1*$^{-/-}$ mouse fibroblasts and was maintained throughout the time course as in *SURF1* patients' cells. However, in other aspects, mouse and human models differed. First, the incorporation of newly synthesized COX subunits into higher SCs was delayed in mouse fibroblasts and only started to appear at t16–24 h (Fig. 3 C, D, G, H). Also, the COX SCs represented only minor portion of COX, which was just barely detectable by COX1 antibody in mouse cells without DOX treatment both on *SURF1*$^{+/+}$ and *SURF1*$^{-/-}$ background. The COX monomer was the dominant COX form in all mouse cells; it increased significantly in *SURF1*$^{+/+}$ cells from t0 to t96 h, while in *SURF1*$^{-/-}$ cells AI represented up to 50% of COX1 signal, gradually accumulating at the respective time points.

The interspecies differences between mouse and human fibroblasts are clearly visualized in 2D maps of COX distribution into individual forms (Fig. 3 E–H). In human fibroblasts (Fig. 3 E, F), COX incorporation into SCs was much more prevalent than in mouse cells (Fig. 3 G, H), control human cells maintained stable proportion between COX monomer and SCs, whereas *SURF1* patient cells preferentially incorporated the assembled COX into SCs rather than into COX monomer. In *SURF1*$^{+/+}$ and *SURF1*$^{-/-}$ mouse cells (Fig. 3 G, H), COX SCs amount was negligible when compared to COX monomer. DOX experiment thus clearly showed COX assembly defect due to *SURF1* gene mutation/knock out. *SURF1* patients' cells accumulated more COX assembly intermediates and most of assembled COX incorporated into SCs, whereas *SURF1*$^{-/-}$ mouse cells accumulated less COX AI and were characterized by more stable COX monomer compared to *SURF1* patient.

3.5. Pulse-chase labeling of mitochondrially encoded COX subunits

As a follow up on the doxycycline experiments aimed at comparison of control and *SURF1* defective human and mouse fibroblasts, we analyzed the assembly kinetics of COX directly by pulse-chase ^{35}S labeling of mitochondrial translation products. Fibroblast cell lines pretreated with chloramphenicol (16 h/overnight) were washed and pulsed with ^{35}S labeled Met-Cys in the presence of cycloheximide (CHX). Cells were then chased with cold Met-Cys without CHX at time points 0.5 h, 6 h, 16 h, 24 h to follow the time course of newly synthesized COX1, COX2, and COX3 subunits incorporation into assembly intermediates, monomer and SCs of COX. Isolated cell membranes were analyzed by 2D BNE/SDS PAGE after solubilization with digitonin (4 g/g protein).

In control human fibroblasts we observed the major portion of COX1 incorporated in assembly intermediates, whereas a small part was

already present in the COX monomer and I–III_2–IV_n SCs at chase time 0.5 h (Fig. 4 A; Fig. 5 A). COX2 and COX3 subunits followed the same pattern but the migration distance and thus the identity of their respective assembly intermediates differed from COX1 (Fig. 4 A). At chase time 16 h, COX AI signal considerably decreased, accompanied by the increase of remaining forms, i.e. COX monomer, COX dimer and COX SCs. This pattern was consistent for signals from all three mtDNA encoded COX subunits. At the 24 h chase, COX monomer became the dominant form, and the COX1 assembly intermediates almost disappeared. In the case of *SURF1* patient cells (Fig. 4 B; Fig. 5 B), COX1 assembly intermediates clearly dominated at chase 0.5 h. Small portion of COX monomer and SCs were also present, but they are only distinguishable from the signals of COX2 and COX3 subunits (Fig. 4 B). At chase 16 h, COX1 assembly intermediates still represented the dominant COX form, with small portion of COX1 shifting to the monomer as well as into COX SCs. At the end of the chase periods at t24 h, the signals of COX subunits weakened in patient cells, but the amount of COX1 assembly intermediates still prevailed over the fully assembled COX forms.

When we analyzed the COX assembly kinetics in *SURF1*$^{+/+}$ mouse fibroblasts (Fig. 4 C; Fig. 5 C), we observed high amount of COX1 assembly intermediates, but also considerable signal of fully assembled new COX monomer and beginning of SCs formation at chase time 0.5 h. At longer chase periods COX1 assembly intermediates almost disappeared. We were able to detect COX monomer together with COX dimer, and COX-containing SCs, similar to the observation in DOX experiment using COX1 antibody from time point t24 h onwards. In *SURF1*$^{-/-}$ mouse fibroblasts at time points 0.5 h and 6 h, the formation of COX1 AI was prevailing over the signal of monomer (Fig. 4 D; Fig. 5 D), similar to human *SURF1* patient cells. However, at later time points COX1 assembly intermediates rapidly disappeared, whereas newly synthesized COX monomer appeared stable, and only its content was clearly decreased when compared to *SURF1*$^{+/+}$ mouse cells. As in *SURF1*$^{+/+}$ mouse cells, large I–III_2–IV_n SCs were clearly detected.

In both *SURF1*$^{-/-}$ and *SURF1* patient fibroblasts the amount of newly synthesized COX1 subunit during the pulse (t0.5 h) reaches approximately 70–80% of respective control levels. While an increase in COX1 translation could result in the apparent increase in the amount of COX monomer in *SURF1*$^{-/-}$ cells, this does not seem to be the case in our model.

Taken together, also when followed by pulse-chase, the COX assembly kinetics in mouse *SURF1*$^{+/+}$ and *SURF1*$^{-/-}$ fibroblasts showed significant differences from the respective human cells, particularly regarding COX assembly intermediates depletion/accumulation and stability of COX monomer. As can be seen from 2D maps in Fig. 5 A–D, control human cells became depleted of COX AI at later time point (chase t24 h) than *SURF1*$^{+/+}$ mouse cells (chase t16 h), which indicates possible slower COX1 biogenesis in humans. Also, *SURF1*$^{-/-}$ mouse fibroblasts coped better with SURF1 protein absence; they accumulated less COX AI and were able to synthesize more stable COX monomer when compared to *SURF1* patient cells, where the SURF1 seems to be crucial for effective COX1 biogenesis and its incorporation to COX monomer.

The assembly kinetics of mtDNA subunits for other OXPHOS complexes, e.g. cytochrome *b* of cIII or ATP6 and 8 of cV, was comparable

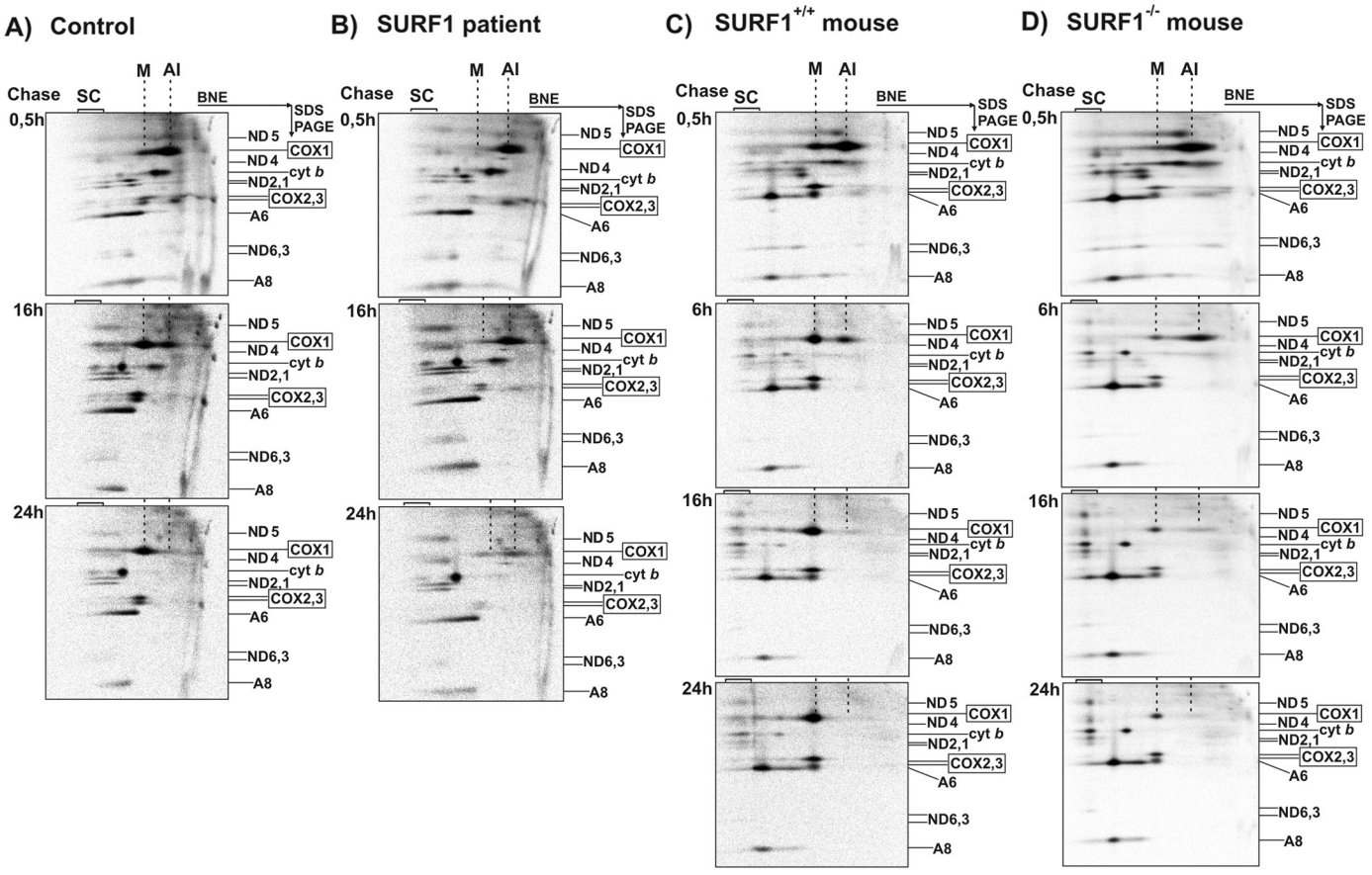

Fig. 4. Pulse-chase metabolic labeling of mitochondrially synthesized proteins in SURF1-deficient mouse and human fibroblasts. (A, B) Human control and *SURF1* patient fibroblasts, (C, D) *SURF1*$^{+/+}$ and *SURF1*$^{-/-}$ mouse fibroblasts. Mitochondrial translation products of mouse and human fibroblasts were labeled with [^{35}S] methionine + cysteine for 2 h in the presence of cycloheximide. After indicated time of chase (0.5 h, 6 h, 16 h, 24 h) with cold methionine and cysteine, cell membranes were isolated, solubilized by digitonin (4 g/g protein) and analyzed by BNE/SDS PAGE. Radioactivity was detected in stained dried gels. On the right side of each gel, individual mtDNA coded subunits are marked and mtDNA coded COX subunits COX1, COX2, COX3 are highlighted in frames. COX assembly intermediates (AI), COX monomer (M) are marked by dotted lines; COX SCs (SC).

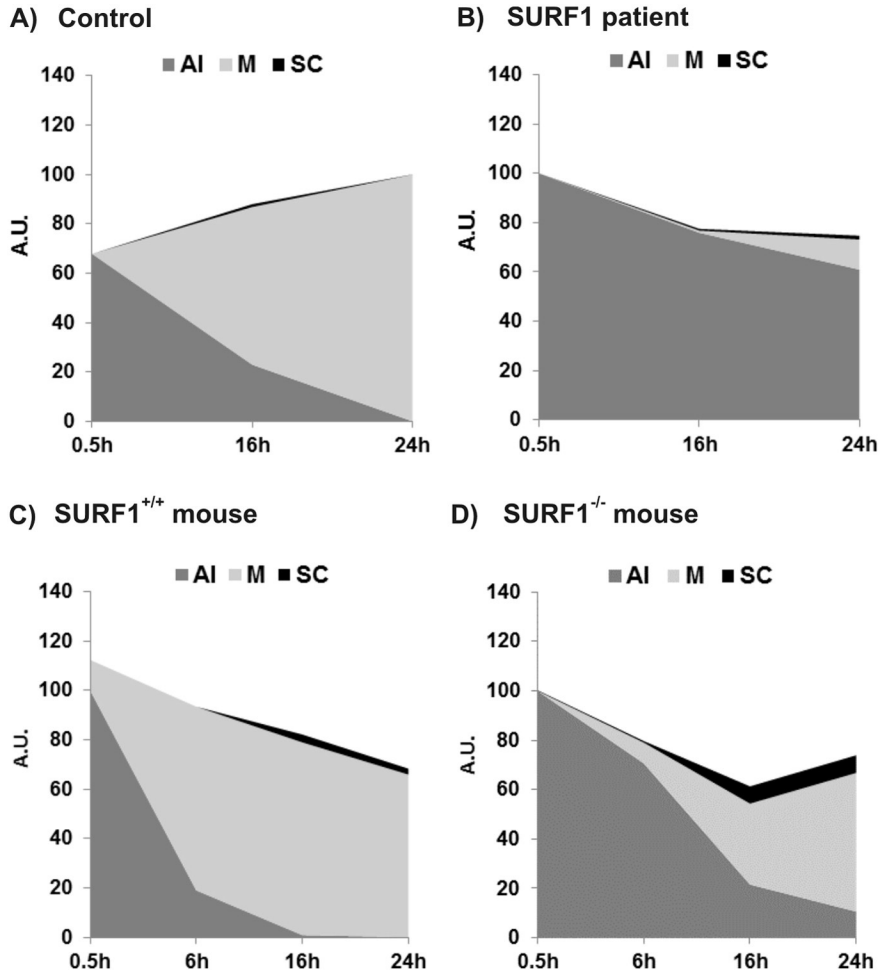

Fig. 5. 2D maps of pulse-chase metabolic labeling of mitochondrially synthesized COX1 subunit. (A) Human control and (B) *SURF1* patient fibroblasts, (C) *SURF1*$^{+/+}$ and (D) *SURF1*$^{-/-}$ mouse fibroblasts. 2D maps show biogenesis of COX1 subunit along the pulse-chase experiment at chase times t0.5, t6, t16 and t24 h (0.5 h–24 h). Relative quantities of individual COX forms (assembly intermediates, monomer, supercomplexes) were used to divide the respective COX1 signal for given time chase from 1D SDS PAGE, normalized to overall radioactive signal in each time chase. The resulting datasets from each experiment representing individual COX forms in human and mouse cells were rescaled (minimum = 0, maximum = 100) and plotted in comparative 2D maps. COX assembly intermediates (AI), COX monomer (M), COX supercomplexes (SC).

in human control and patient cells as well as in *SURF1*$^{+/+}$ and *SURF1*$^{-/-}$ mouse cells (Fig. 4 A–D), as can be expected for isolated COX defect.

4. Discussion

In the present study we analyzed the COX biogenesis from assembly intermediates (AI) to supercomplexes (SC) in tissues and fibroblasts from *SURF1*$^{-/-}$ mouse and *SURF1* patient fibroblasts to address the observed tissue and interspecies differences in phenotype severity. To characterize changes at steady state conditions as well as the dynamics of COX *de novo* synthesis, we combined enzyme activity measurements, 2D PAGE/immunodetection on doxycycline arrested cells and ^{35}S-labeling of mtDNA encoded proteins.

Numerous studies indicate that SURF1 protein (SURF1) promotes early stages of COX biogenesis, from COX1 translation regulation to its association with other COX subunits into COX AI [20,42,58,62]. Despite the absence of SURF1, 10–30% of control amount of active COX is assembled in *SURF1* patients' fibroblasts [44]. Thus, while improving its efficacy, SURF1 is not absolutely essential in the COX assembly process [52]. Decreased levels of COX holoenzyme and reduction of COX activity were found to be accompanied by decreased levels of COX subunits [44,69] and accumulation of specific COX AIs. In *SURF1* patients, COX subcomplexes were detected in primary fibroblasts, skeletal muscle and heart, while their amount was very low in liver and brain [59,60,62]. Likewise, we have also observed tissue variance in COX assembly process in *SURF1*$^{-/-}$ mouse tissues on Western blots, where we detected markedly variable amount of accumulated COX1-containing subcomplexes (Fig. 1 A–D). However, the severity of COX assembly defect in tissues from *SURF1*$^{-/-}$ mouse was not as pronounced as in *SURF1*$^{-/-}$ mouse fibroblasts possibly because the assembly defect better manifests in proliferating cell cultures than in largely post-mitotic tissues studied (Fig. 1 E, F).

4.1. COX subassemblies and formation of monomer

Observed COX1-containing subcomplexes can either be COX degradation products or more likely represent true AIs, as they are predominantly labeled already at the shortest chase times (t0.5 h, Fig. 4 A–D). Furthermore, AIs labeling gradually decreased during the chase, in contrast to the increase in the COX monomer signal. However, AI dynamics differed between human and murine models of SURF1 deficiency. In *SURF1* patient fibroblasts, COX1-subassemblies persisted throughout the chase without the progression into COX monomer. Contrariwise, *SURF1*$^{-/-}$ mouse fibroblasts had higher content of COX monomer from the beginning and its levels remained stable from t6 h onwards, while COX1 AIs gradually disappeared between t16–24 h, arguing for considerably faster turnover of COX1 AIs in mouse cells.

This is in line with our doxycycline (DOX) treatment experiments. COX1-subassemblies detected in lesser amount also in both types of control cells most likely reflect significant limiting step of COX

assembly, which proceeds at slower pace e.g. because of incorporation of catalytic components of the enzyme (hemes, Cu_B). Fittingly, in bacteria [13,23] and yeast the SURF1 homologs were linked with heme *a* incorporation into COX1. Shy1 — yeast homolog of SURF1 — forms early assembly intermediate with COX1 [39]. In this intermediate, both heme *a* cofactor sites are most likely formed in a stepwise process — heme *a* in a transition to the Shy1-containing complex and heme a_3 within Shy1 complex. Cu_B site was also suggested to be formed at this stage, since Shy1 was found to transiently interact with Cu_B metallochaperone COX11. Thus, formation of heterobimetallic Cu_B-heme a_3 site should occur in the Shy1 complex [27]. In addition, Shy1 was found also in association with COX15, heme *a* synthase, most likely cooperating on heme *a* transfer and insertion into early COX1 assembly intermediates [7]. While SURF1 can likely function analogously in the mammalian cells, this has yet to be experimentally proved. As in case of mammalian SURF1, Shy1 seems not to be absolutely required for COX1 maturation steps, because yeast strains lacking Shy1 have still residual fully assembled and active COX.

Interestingly, the assembly process seems to proceed faster in mouse than in human fibroblasts. Thus, at chase time point 16 h, all COX1 in mouse cells was assembled in holoenzyme while in human fibroblasts a significant portion of the subunit was still present in assembly intermediates. This could be due to a higher reservoir of COX1 AIs in control human cells and, along with faster decomposition of stalled AIs, may partially explain the milder phenotype of SURF1 absence in mouse. Faster assembly and rapid recycling of unincorporated subunits in mouse system would result in more frequent assembly "attempts" producing higher steady state COX content than in human patient cells.

On the contrary, translational activation of COX1 specifically in mouse cells may yield analogous outcome. In this respect, the phenotype of yeast Shy1 mutant was partially restored by the suppressor *MSS51* through increased translation of COX1 [8]. Mss51p is primarily specific translation factor for *COX1* mRNA, that acts on the 5′ untranslated region (UTR) of *COX1* mRNA to promote translation initiation [27]. However, mammalian mitochondrial mRNAs do not have significant 5′ UTRs [40] and this may be the reason why functional homolog of translation activator Mss51p has not been found yet. On the other hand, human homolog (LRPPRC) of the yeast translational activator Pet309 has been reported and, in addition, translational activator of COX1 TACO1 is necessary for efficient translation of COX1 [64]. These proteins, or other yet unidentified factor(s), may effectively act as species-specific suppressors of COX defects in *SURF1*$^{-/-}$ mouse cells. Larger pool of translated COX1 accessible for finishing of COX1 maturation without SURF1 may then lead to synthesis of higher amount of COX and thus be the cause of the milder COX defect in *SURF1*$^{-/-}$ mouse cells. However, our data do not support such possibility. As already mentioned the decrease in the amount of newly synthesized COX1 subunit was approximately equal in both mouse and human fibroblasts with *SURF1* defect without any indication of compensatory upregulation in mouse cells.

Impaired COX biogenesis due to SURF1 deficiency is characterized by accumulation of the S2 intermediate containing COX1–COX4–COX5a subunits [20,42]. S2 represents an important rate limiting step and can usually be detected even in control cells/tissues. Recently, MITRAC complexes (mitochondrial translation regulation assembly intermediates of COX) were described as part of COX biogenesis pathway [38]. Their suggested function lies in regulation of COX1 translation by coordinating the interaction of COX1 with specific assembly proteins before entering the further steps of COX assembly. This regulatory cycle should be actually considered as an alternative mechanism of COX1 biogenesis in mammals to that in yeast. SURF1 was also found to be part of MITRAC complexes together with hCOA3 (MITRAC12) [15] and other COX assembly proteins (COX15, COX16, C12orf62). However, it is possible that the S2 subassemblies merely co-migrate with MITRAC complexes on native gels. The presence of several types of complexes and/or their dynamics in recruitment and release of various assembly factors has been reflected in changes of migration patterns of COX1-containing assemblies in 2D gels. We propose that absence of SURF1 does not exclude formation of MITRAC complexes and their accumulation with S2 subassemblies. Indeed, we consistently detect complexes that may represent such associations in COX defective cells/tissues characterized by impaired efficiency of COX1 biogenesis and its delayed interaction with other COX subunits.

4.2. COX incorporation into supercomplexes

COX holoenzyme is known to interact with other RC complexes and form supercomplexes (SCs) [21,25,41,54]. However, in all mouse tissues examined in this study, COX monomer represented the dominant COX form. We also detected the presence of COX dimer and III_2–IV SC and these forms were decreased or even disappeared in *SURF1*$^{-/-}$ mouse. The signal of large I–III_2–IV_n SCs was quite weak in *SURF1*$^{+/+}$ mouse heart and muscle despite the fact that these SCs are usually observed in digitonin solubilizates [53,67]. Interestingly, several recent studies reported the absence of COX SCs (III_2–IV and I–III_2–IV_n) in liver and fibroblasts from C57Bl/6 J mouse strain, which served also as the parental strain for formation of *SURF1*$^{-/-}$ mouse [16,29]. This was associated with the presence of short isoform of COX7a2l (SCAFI) subunit in this strain, which may preclude SC formation.

The relative absence of SCs in mouse samples contrasted with our observations in human fibroblasts, where we found strong signal of I–III_2–IV_n SCs. Therefore, we used DOX to analyze species-specific differences of COX ability to interact into SCs in control and SURF1 deficient human/mouse fibroblasts. In control human fibroblasts the COX1 signal increased equally in all detectable COX forms (AI, M, SCs), indicating a stable balance in distribution of COX forms. Due to decreased amount/stability of COX monomer, the SURF1-deficient patient fibroblasts preferably incorporated COX into I–III_2–IV_n SCs for its stabilization [28,30]. On the other hand, in mouse fibroblasts assembly kinetics of COX proceeded mostly just to the level of COX monomer. COX SCs formation was delayed, and although their content even exceeded the levels in untreated cells, these higher forms of COX represented just a small portion of the total COX quantity. This is the most important difference between *SURF1*$^{-/-}$ mouse and *SURF1* patient fibroblasts we uncovered. The preference towards SCs incorporation is not unique to *SURF1* human patients. Recent study on cybrid clones carrying the heteroplasmic cytochrome *b* m.15579 A > G mutation demonstrated that its deleterious effects were attenuated when cIII was assembled into I–III_2–IV_n SCs [14].

There is only limited amount of information available about COX assembly kinetics after DOX mediated inhibition. The most comprehensive study was performed in control cybrids (143B cells) and DOX caused strong decrease of overall COX signal and disappearance of COX SCs. Gradual incorporation of the COX into SCs was observed at 6 h after DOX removal and COX1 appeared in SCs even later [41]. In our human fibroblasts, about 30% of various COX assemblies remained after DOX treatment and also COX SCs were partially preserved. Similarly, mouse fibroblasts started to synthesize COX SCs a few hours after DOX removal, but in the end favored COX monomer as a main functional COX form. Control human and mouse fibroblasts resembled cybrid cells [41,45] as the amount of COX totally recovered 96 h after DOX treatment. Milder COX defect in *SURF1*$^{-/-}$ mouse fibroblasts also allowed the cells to reach the steady state after 96 h period, but *SURF1* patient cells were delayed in COX recovery, again pointing towards slower and more affected COX biogenesis.

In conclusion, our present study shows that COX in tissues or cells from the *SURF1*$^{+/+}$ and *SURF1*$^{-/-}$ mice exerts lower preference to be incorporated into SCs. On the other hand, I–III_2–IV_n SCs represented an important functional forms of COX in human cells, and even more so in *SURF1* patient fibroblasts. Another reason why the defect caused by SURF1 absence in mice is less dramatic when compared to *SURF1* patients is that COX monomer seems to be more stable in *SURF1*$^{-/-}$ mice

and at the same time the turnover of accumulated COX assembly intermediates is faster.

Transparency document

The Transparency document associated with this article can be found, in online version.

Acknowledgments

This work was supported by the Grant Agency of the Czech Republic (14-36804G), Ministry of Education, Youth and Sports of the Czech Republic (ERC CZ: LL1204, RVO:67985823), the Grant Agency of the Ministry of Health of the Czech Republic (NT12370-5) and ERC Advanced Grant FP7-322424.

Appendix A. Supplementary data

Supplementary data to this article can be found online at http://dx.doi.org/10.1016/j.bbadis.2016.01.007.

References

[1] R. Acin-Perez, J.A. Enriquez, The function of the respiratory supercomplexes: the plasticity model, Biochim. Biophys. Acta 1837 (4) (2014) 444–450.
[2] R. Acin-Perez, P. Fernandez-Silva, M.L. Peleato, A. Perez-Martos, J.A. Enriquez, Respiratory active mitochondrial supercomplexes, Mol. Cell 32 (4) (2008) 529–539.
[3] H. Antonicka, S.C. Leary, G.H. Guercin, J.N. Agar, R. Horvath, N.G. Kennaway, C.O. Harding, M. Jaksch, E.A. Shoubridge, Mutations in COX10 result in a defect in mitochondrial heme A biosynthesis and account for multiple, early-onset clinical phenotypes associated with isolated COX deficiency, Hum. Mol. Genet. 12 (20) (2003) 2693–2702.
[4] H. Antonicka, A. Mattman, C.G. Carlson, D.M. Glerum, K.C. Hoffbuhr, S.C. Leary, N.G. Kennaway, E.A. Shoubridge, Mutations in COX15 produce a defect in the mitochondrial heme biosynthetic pathway, causing early-onset fatal hypertrophic cardiomyopathy, Am. J. Hum. Genet. 72 (1) (2003) 101–114.
[5] W. Aulbert, K. Weigt-Usinger, C. Thiels, C. Kohler, M. Vorgerd, A. Schreiner, S. Hoffjan, T. Rothoeft, S.B. Wortmann, C.M. Heyer, T. Podskarbi, T. Lucke, Long survival in Leigh syndrome: new cases and review of literature, Neuropediatrics (2014).
[6] E. Balsa, R. Marco, E. Perales-Clemente, R. Szklarczyk, E. Calvo, M.O. Landazuri, J.A. Enriquez, NDUFA4 is a subunit of complex IV of the mammalian electron transport chain, Cell Metab. 16 (3) (2012) 378–386.
[7] B. Bareth, S. Dennerlein, D.U. Mick, M. Nikolov, H. Urlaub, P. Rehling, The heme a synthase Cox15 associates with cytochrome c oxidase assembly intermediates during Cox1 maturation, Mol. Cell. Biol. 33 (20) (2013) 4128–4137.
[8] A. Barrientos, D. Korr, A. Tzagoloff, Shy1p is necessary for full expression of mitochondrial COX1 in the yeast model of Leigh's syndrome, EMBO J 21 (1–2) (2002) 43–52.
[9] H.A. Bentlage, U. Wendel, H. Schagger, H.J. ter Laak, A.J. Janssen, J.M. Trijbels, Lethal infantile mitochondrial disease with isolated complex I deficiency in fibroblasts but with combined complex I and IV deficiencies in muscle, Neurology 47 (1) (1996) 243–248.
[10] M. Bourens, A. Boulet, S.C. Leary, A. Barrientos, Human COX20 cooperates with SCO1 and SCO2 to mature COX2 and promote the assembly of cytochrome c oxidase, Hum. Mol. Genet. 23 (11) (2014) 2901–2913.
[11] M.M. Bradford, A rapid and sensitive method for the quantitation of microgram quantities of protein utilizing the principle of protein–dye binding, Anal. Biochem. 72 (1976) 248–254.
[12] C. Bruno, R. Biancheri, B. Garavaglia, C. Biedi, A. Rossi, L.D. Lamba, M. Bado, M. Greco, M. Zeviani, C. Minetti, A novel mutation in the SURF1 gene in a child with Leigh disease, peripheral neuropathy, and cytochrome-c oxidase deficiency, J. Child Neurol. 17 (3) (2002) 233–236.
[13] F.A. Bundschuh, A. Hannappel, O. Anderka, B. Ludwig, Surf1, associated with Leigh syndrome in humans, is a heme-binding protein in bacterial oxidase biogenesis, J. Biolumin. Chemilumin. 284 (38) (2009) 25735–25741.
[14] L. Caporali, A.M. Ghelli, L. Iommarini, A. Maresca, M.L. Valentino, C. La Morgia, R. Liguori, C. Zanna, P. Barboni, V. De Nardo, A. Martinuzzi, G. Rizzo, C. Tonon, R. Lodi, M.A. Calvaruso, M. Cappelletti, A.M. Porcelli, A. Achilli, M. Pala, A. Torroni, V. Carelli, Cybrid studies establish the causal link between the mtDNA m.3890G > A/MT-ND1 mutation and optic atrophy with bilateral brainstem lesions, Biochim. Biophys. Acta 1832 (3) (2013) 445–452.
[15] P. Clemente, S. Peralta, A. Cruz-Bermudez, L. Echevarria, F. Fontanesi, A. Barrientos, M.A. Fernandez-Moreno, R. Garesse, hCOA3 stabilizes cytochrome c oxidase 1 (COX1) and promotes cytochrome c oxidase assembly in human mitochondria, J. Biolumin. Chemilumin. 288 (12) (2013) 8321–8331.
[16] M. Davoudi, H. Kotarsky, E. Hansson, V. Fellman, Complex I function and supercomplex formation are preserved in liver mitochondria despite progressive complex III deficiency, PLoS One 9 (1) (2014), e86767.
[17] S.S. Deepa, D. Pulliam, S. Hill, Y. Shi, M.E. Walsh, A. Salmon, L. Sloane, N. Zhang, M. Zeviani, C. Viscomi, N. Musi, H. Van Remmen, Improved insulin sensitivity associated with reduced mitochondrial complex IV assembly and activity, FASEB J. 27 (4) (2013) 1371–1380.
[18] C. Dell'Agnello, S. Leo, A. Agostino, G. Szabadkai, C. Tiveron, A. Zulian, A. Prelle, P. Roubertoux, R. Rizzuto, M. Zeviani, Increased longevity and refractoriness to Ca(2+)-dependent neurodegeneration in Surf1 knockout mice, Hum. Mol. Genet. 16 (4) (2007) 431–444.
[19] T. Duhig, C. Ruhrberg, O. Mor, M. Fried, The human Surfeit locus, Genomics 52 (1) (1998) 72–78.
[20] D. Fornuskova, L. Stiburek, L. Wenchich, K. Vinsova, H. Hansikova, J. Zeman, Novel insights into the assembly and function of human nuclear-encoded cytochrome c oxidase subunits 4, 5a, 6a, 7a and 7b, Biochem. J. 428 (3) (2010) 363–374.
[21] M.L. Genova, G. Lenaz, Functional role of mitochondrial respiratory supercomplexes, Biochim. Biophys. Acta 1837 (4) (2014) 427–443.
[22] A. Ghosh, P.P. Trivedi, S.A. Timbalia, A.T. Griffin, J.J. Rahn, S.S. Chan, V.M. Gohil, Copper supplementation restores cytochrome c oxidase assembly defect in a mitochondrial disease model of COA6 deficiency, Hum. Mol. Genet. 23 (13) (2014) 3596–3606.
[23] A. Hannappel, F.A. Bundschuh, B. Ludwig, Role of Surf1 in heme recruitment for bacterial COX biogenesis, Biochim. Biophys. Acta 1817 (6) (2012) 928–937.
[24] M. Huigsloot, L.G. Nijtmans, R. Szklarczyk, M.J. Baars, M.A. van den Brand, M.G. Hendriksfranssen, L.P. van den Heuvel, J.A. Smeitink, M.A. Huynen, R.J. Rodenburg, A mutation in C2orf64 causes impaired cytochrome c oxidase assembly and mitochondrial cardiomyopathy, Am. J. Hum. Genet. 88 (4) (2011) 488–493.
[25] Y. Chaban, E.J. Boekema, N.V. Dudkina, Structures of mitochondrial oxidative phosphorylation supercomplexes and mechanisms for their stabilisation, Biochim. Biophys. Acta 1837 (4) (2014) 418–426.
[26] B. Kadenbach, M. Huttemann, S. Arnold, I. Lee, E. Bender, Mitochondrial energy metabolism is regulated via nuclear-coded subunits of cytochrome c oxidase, Free Radic. Biol. Med. 29 (3–4) (2000) 211–221.
[27] O. Khalimonchuk, M. Bestwick, B. Meunier, T.C. Watts, D.R. Winge, Formation of the redox cofactor centers during Cox1 maturation in yeast cytochrome oxidase, Mol. Cell. Biol. 30 (4) (2010) 1004–1017.
[28] N. Kovarova, A. Cizkova Vrbacka, P. Pecina, V. Stranecky, E. Pronicka, S. Kmoch, J. Houstek, Adaptation of respiratory chain biogenesis to cytochrome c oxidase deficiency caused by SURF1 gene mutations, Biochim. Biophys. Acta 1822 (7) (2012) 1114–1124.
[29] E. Lapuente-Brun, R. Moreno-Loshuertos, R. Acin-Perez, A. Latorre-Pellicer, C. Colas, E. Balsa, E. Perales-Clemente, P.M. Quiros, E. Calvo, M.A. Rodriguez-Hernandez, P. Navas, R. Cruz, A. Carracedo, C. Lopez-Otin, A. Perez-Martos, P. Fernandez-Silva, E. Fernandez-Vizarra, J.A. Enriquez, Supercomplex assembly determines electron flux in the mitochondrial electron transport chain, Science 340 (6140) (2013) 1567–1570.
[30] M. Lazarou, S.M. Smith, D.R. Thorburn, M.T. Ryan, M. McKenzie, Assembly of nuclear DNA-encoded subunits into mitochondrial complex IV, and their preferential integration into supercomplex forms in patient mitochondria, FEBS J 276 (22) (2009) 6701–6713.
[31] S.C. Leary, Redox regulation of SCO protein function: controlling copper at a mitochondrial crossroad, Antioxid. Redox Signal. 13 (9) (2010) 1403–1416.
[32] S.C. Leary, P.A. Cobine, T. Nishimura, R.M. Verdijk, R. de Krijger, R. de Coo, M.A. Tarnopolsky, D.R. Winge, E.A. Shoubridge, COX19 mediates the transduction of a mitochondrial redox signal from SCO1 that regulates ATP7A-mediated cellular copper efflux, Mol. Biol. Cell 24 (6) (2013) 683–691.
[33] S.C. Leary, B.A. Kaufman, G. Pellecchia, G.H. Guercin, A. Mattman, M. Jaksch, E.A. Shoubridge, Human SCO1 and SCO2 have independent, cooperative functions in copper delivery to cytochrome c oxidase, Hum. Mol. Genet. 13 (17) (2004) 1839–1848.
[34] S.C. Leary, F. Sasarman, T. Nishimura, E.A. Shoubridge, Human SCO2 is required for the synthesis of CO II and as a thiol-disulphide oxidoreductase for SCO1, Hum. Mol. Genet. 18 (12) (2009) 2230–2240.
[35] I.C. Lee, A.W. El-Hattab, J. Wang, F.Y. Li, S.W. Weng, W.J. Craigen, L.J. Wong, SURF1-associated Leigh syndrome: a case series and novel mutations, Hum. Mutat. 33 (8) (2012) 1192–1200.
[36] S.C. Lim, K.R. Smith, D.A. Stroud, A.G. Compton, E.J. Tucker, A. Dasvarma, L.C. Gandolfo, J.E. Marum, M. McKenzie, H.L. Peters, D. Mowat, P.G. Procopis, B. Wilcken, J. Christodoulou, G.K. Brown, M.T. Ryan, M. Bahlo, D.R. Thorburn, A founder mutation in PET100 causes isolated complex IV deficiency in Lebanese individuals with Leigh syndrome, Am. J. Hum. Genet. 94 (2) (2014) 209–222.
[37] M. McKenzie, M. Lazarou, M.T. Ryan, Chapter 18 analysis of respiratory chain complex assembly with radiolabeled nuclear- and mitochondrial-encoded subunits, Methods Enzymol. 456 (2009) 321–339.
[38] D.U. Mick, S. Dennerlein, H. Wiese, R. Reinhold, D. Pacheu-Grau, I. Lorenzi, F. Sasarman, W. Weraarpachai, E.A. Shoubridge, B. Warscheid, P. Rehling, MITRAC links mitochondrial protein translocation to respiratory-chain assembly and translational regulation, Cell 151 (7) (2012) 1528–1541.
[39] D.U. Mick, K. Wagner, M. van der Laan, A.E. Frazier, I. Perschil, M. Pawlas, H.E. Meyer, B. Warscheid, P. Rehling, Shy1 couples Cox1 translational regulation to cytochrome c oxidase assembly, EMBO J 26 (20) (2007) 4347–4358.
[40] J. Montoya, D. Ojala, G. Attardi, Distinctive features of the 5′-terminal sequences of the human mitochondrial mRNAs, Nature 290 (5806) (1981) 465–470.
[41] D. Moreno-Lastres, F. Fontanesi, I. Garcia-Consuegra, M.A. Martin, J. Arenas, A. Barrientos, C. Ugalde, Mitochondrial complex I plays an essential role in human respirasome assembly, Cell Metab. 15 (3) (2012) 324–335.
[42] L.G. Nijtmans, J.W. Taanman, A.O. Muijsers, D. Speijer, C. Van den Bogert, Assembly of cytochrome-c oxidase in cultured human cells, Eur. J. Biochem. 254 (2) (1998) 389–394.

[43] C. Oswald, U. Krause-Buchholz, G. Rodel, Knockdown of human COX17 affects assembly and supramolecular organization of cytochrome c oxidase, J. Mol. Biol. 389 (3) (2009) 470–479.
[44] P. Pecina, M. Capkova, S.K. Chowdhury, Z. Drahota, A. Dubot, A. Vojtiskova, H. Hansikova, H. Houst'kova, J. Zeman, C. Godinot, J. Houstek, Functional alteration of cytochrome c oxidase by SURF1 mutations in Leigh syndrome, Biochim. Biophys. Acta 1639 (1) (2003) 53–63.
[45] R. Pello, M.A. Martin, V. Carelli, L.G. Nijtmans, A. Achilli, M. Pala, A. Torroni, A. Gomez-Duran, E. Ruiz-Pesini, A. Martinuzzi, J.A. Smeitink, J. Arenas, C. Ugalde, Mitochondrial DNA background modulates the assembly kinetics of OXPHOS complexes in a cellular model of mitochondrial disease, Hum. Mol. Genet. 17 (24) (2008) 4001–4011.
[46] D. Piekutowska-Abramczuk, M. Magner, E. Popowska, M. Pronicki, E. Karczmarewicz, J. Sykut-Cegielska, T. Kmiec, E. Jurkiewicz, T. Szymanska-Debinska, L. Bielecka, M. Krajewska-Walasek, K. Vesela, J. Zeman, E. Pronicka, SURF1 missense mutations promote a mild Leigh phenotype, Clin. Genet. 76 (2) (2009) 195–204.
[47] D. Piekutowska-Abramczuk, E. Popowska, M. Pronicki, E. Karczmarewicz, D. Tylek-Lemanska, J. Sykut-Cegielska, T. Szymanska-Dembinska, L. Bielecka, M. Krajewska-Walasek, E. Pronicka, High prevalence of SURF1 c.845_846delCT mutation in Polish Leigh patients, Eur. J. Paediatr. Neurol. 13 (2) (2009) 146–153.
[48] Pitceathly, R. D., S. Rahman, Y. Wedatilake, J. M. Polke, S. Cirak, A. R. Foley, A. Sailer, M. E. Hurles, J. Stalker, I. Hargreaves, C. E. Woodward, M. G. Sweeney, F. Muntoni, H. Houlden, J. W. Taanman, M. G. Hanna and U. K. Consortium, NDUFA4 mutations underlie dysfunction of a cytochrome c oxidase subunit linked to human neurological disease, Cell Rep. 3 (6) (2013) 1795–1805.
[49] D.A. Pulliam, S.S. Deepa, Y. Liu, S. Hill, A.L. Lin, A. Bhattacharya, Y. Shi, L. Sloane, C. Viscomi, M. Zeviani, H. Van Remmen, Complex IV-deficient Surf1(−/−) mice initiate mitochondrial stress responses, Biochem. J. 462 (2) (2014) 359–371.
[50] P. Rustin, D. Chretien, T. Bourgeron, B. Gerard, A. Rotig, J.M. Saudubray, A. Munnich, Biochemical and molecular investigations in respiratory chain deficiencies, Clin. Chim. Acta 228 (1) (1994) 35–51.
[51] A.D. Sheftel, O. Stehling, A.J. Pierik, H.P. Elsasser, U. Muhlenhoff, H. Webert, A. Hobler, F. Hannemann, R. Bernhardt, R. Lill, Humans possess two mitochondrial ferredoxins, Fdx1 and Fdx2, with distinct roles in steroidogenesis, heme, and Fe/S cluster biosynthesis, Proc. Natl. Acad. Sci. U. S. A. 107 (26) (2010) 11775–11780.
[52] E.A. Shoubridge, Cytochrome c oxidase deficiency, Am. J. Med. Genet. 106 (1) (2001) 46–52.
[53] H. Schagger, Respiratory chain supercomplexes of mitochondria and bacteria, Biochim. Biophys. Acta 1555 (1–3) (2002) 154–159.
[54] H. Schagger, K. Pfeiffer, Supercomplexes in the respiratory chains of yeast and mammalian mitochondria, EMBO J 19 (8) (2000) 1777–1783.
[55] H. Schagger, G. von Jagow, Tricine-sodium dodecyl sulfate-polyacrylamide gel electrophoresis for the separation of proteins in the range from 1 to 100 kDa, Anal. Biochem. 166 (2) (1987) 368–379.
[56] H. Schagger, G. von Jagow, Blue native electrophoresis for isolation of membrane protein complexes in enzymatically active form, Anal. Biochem. 199 (2) (1991) 223–231.
[57] D. Smith, J. Gray, L. Mitchell, W.E. Antholine, J.P. Hosler, Assembly of cytochrome-c oxidase in the absence of assembly protein Surf1p leads to loss of the active site heme, J. Biolumin. Chemilumin. 280 (18) (2005) 17652–17656.
[58] L. Stiburek, H. Hansikova, M. Tesarova, L. Cerna, J. Zeman, Biogenesis of eukaryotic cytochrome c oxidase, Physiol. Res. 55 (Suppl. 2) (2006) S27–S41.
[59] L. Stiburek, K. Vesela, H. Hansikova, P. Pecina, M. Tesarova, L. Cerna, J. Houstek, J. Zeman, Tissue-specific cytochrome c oxidase assembly defects due to mutations in SCO2 and SURF1, Biochem. J. 392 (Pt 3) (2005) 625–632.
[60] L. Stiburek, J. Zeman, Assembly factors and ATP-dependent proteases in cytochrome c oxidase biogenesis, Biochim. Biophys. Acta 1797 (6–7) (2010) 1149–1158.
[61] J. Tanigawa, K. Kaneko, M. Honda, H. Harashima, K. Murayama, T. Wada, K. Takano, M. Iai, S. Yamashita, H. Shimbo, N. Aida, A. Ohtake, H. Osaka, Two Japanese patients with Leigh syndrome caused by novel SURF1 mutations, Brain Dev. 34 (10) (2012) 861–865.
[62] V. Tiranti, C. Galimberti, L. Nijtmans, S. Bovolenta, M.P. Perini, M. Zeviani, Characterization of SURF-1 expression and Surf-1p function in normal and disease conditions, Hum. Mol. Genet. 8 (13) (1999) 2533–2540.
[63] A.K. van Riesen, H. Antonicka, A. Ohlenbusch, E.A. Shoubridge, E.K. Wilichowski, Maternal segmental disomy in Leigh syndrome with cytochrome c oxidase deficiency caused by homozygous SURF1 mutation, Neuropediatrics 37 (2) (2006) 88–94.
[64] W. Weraarpachai, H. Antonicka, F. Sasarman, J. Seeger, B. Schrank, J.E. Kolesar, H. Lochmuller, M. Chevrette, B.A. Kaufman, R. Horvath, E.A. Shoubridge, Mutation in TACO1, encoding a translational activator of COX I, results in cytochrome c oxidase deficiency and late-onset Leigh syndrome, Nat. Genet. 41 (7) (2009) 833–837.
[65] W. Weraarpachai, F. Sasarman, T. Nishimura, H. Antonicka, K. Aure, A. Rotig, A. Lombes, E.A. Shoubridge, Mutations in C12orf62, a factor that couples COX I synthesis with cytochrome c oxidase assembly, cause fatal neonatal lactic acidosis, Am. J. Hum. Genet. 90 (1) (2012) 142–151.
[66] S.L. Williams, I. Valnot, P. Rustin, J.W. Taanman, Cytochrome c oxidase subassemblies in fibroblast cultures from patients carrying mutations in COX10, SCO1, or SURF1, J. Biolumin. Chemilumin. 279 (9) (2004) 7462–7469.
[67] I. Wittig, H.P. Braun, H. Schagger, Blue native PAGE, Nat. Protoc. 1 (1) (2006) 418–428.
[68] F. Xu, J.B. Addis, J.M. Cameron, B.H. Robinson, LRPPRC mutation suppresses cytochrome oxidase activity by altering mitochondrial RNA transcript stability in a mouse model, Biochem. J. 441 (1) (2012) 275–283.
[69] J. Yao, E.A. Shoubridge, Expression and functional analysis of SURF1 in Leigh syndrome patients with cytochrome c oxidase deficiency, Hum. Mol. Genet. 8 (13) (1999) 2541–2549.
[70] Z. Zhu, J. Yao, T. Johns, K. Fu, I. De Bie, C. Macmillan, A.P. Cuthbert, R.F. Newbold, J. Wang, M. Chevrette, G.K. Brown, R.M. Brown, E.A. Shoubridge, SURF1, encoding a factor involved in the biogenesis of cytochrome c oxidase, is mutated in Leigh syndrome, Nat. Genet. 20 (4) (1998) 337–343.

Data in Brief Appendix

(Supplementary material)

Title

Data on cytochrome *c* oxidase assembly in mice and human fibroblasts or tissues induced by *SURF1* defect.

Authors:

Nikola Kovářová[a], Petr Pecina[a], Hana Nůsková[a], Marek Vrbacký[a], Massimo Zeviani[b,c], Tomáš Mráček[a], Carlo Viscomi[c], Josef Houštěk[a*]

Affiliations:

[a]Institute of Physiology of the Czech Academy of Sciences, Vídeňská 1083, Prague, Czech Republic; [b]Molecular Neurogenetics Unit, Instituto Neurologico "C. Besta", via Temolo 4, 20126 Milan, Italy; [c]MRC-Mitochondrial Biology Unit, Wellcome Trust MRC Bldg, Addenbrookes Hospital Hills Rd, Cambridge CB2 0XY, U.K.

[*] corresponding author

E-mail address: houstek@biomed.cas.cz Tel.: +420 24106 2434

Key words:

Cytochrome *c* oxidase, respiratory chain, SURF1, knockout, doxycycline

Abbreviations:

Cytochrome *c* oxidase (COX); doxycycline (DOX)

Abstract

This paper describes data related to a research article entitled “Tissue- and species-specific differences in cytochrome *c* oxidase assembly induced by *SURF1* defects” [1]. This paper includes data of the quantitative analysis of individual forms of respiratory chain complexes I, III and IV present in *SURF1* knockout (*SURF1*$^{-/-}$) and control (*SURF1*$^{+/+}$) mouse fibroblasts and tissues and in fibroblasts of human control and patients with *SURF1* gene mutation. It also includes data demonstrating response of complex IV, cytochrome *c* oxidase (COX), to reversible inhibition of mitochondrial translation in *SURF1*$^{-/-}$ mouse and *SURF1* patient fibroblast cell lines.

Specifications Table

Subject area	Biochemistry
More specific subject area	Mitochondria, COX assembly, SURF1 protein
Type of data	Figures
How data was acquired	Western blots of SDS and BNE/SDS PAGE, antibody signals quantification, values expressed in percent of controls.
Data format	Analyzed, presented in text
Experimental factors	*SURF1* mouse knockout, human *SURF1* mutations, doxycycline inhibition of mitochondrial DNA translation
Experimental features	Digitonin solubilisation of mitochondrial proteins, immunodetection of respiratory chain complexes
Data source location	Department of Bioenergetics, Institute of Physiology, Czech Academy of Sciences, Czech Republic, Prague
Data accessibility	Data are provided in this article

Value of the data

- Different proportions and native forms of respiratory chain complexes detected by 2D PAGE and WB in mammalian tissues or cells.
- Tissue- and species-specificity of COX biogenesis at normal and pathological conditions.
- Reversible mitochondrial translation arrest for analysis of newly synthesized COX in mouse/human fibroblasts.
- Approach to study different assembly defects of respiratory chain complexes containing mtDNA-encoded subunits.

1. Data

In the present work, we show differences in amounts of individual forms of respiratory chain complexes I, III and IV quantified from western blots of 2D BNE/SDS PAGE analysis, as determined in mitochondria of *SURF1*$^{+/+}$ and *SURF1*$^{-/-}$ mouse fibroblasts and tissues (heart, muscle, brain, liver) and also in mitochondria of human control and SURF1 deficient fibroblasts (Fig. 1, 2, 3).

Then we show data (Fig. 4) from analysis of fibroblast cell lines from *SURF1*$^{-/-}$ mouse, *SURF1* patient and controls, in which translation of mitochondrial DNA encoded proteins was reversibly inhibited with doxycycline (DOX). After DOX removal, the formation of newly synthetized COX in time (0-96 hours) was assessed by SDS PAGE and western blot analysis.

2. Experimental Design, Materials and Methods

See research article “Tissue- and species-specific differences in cytochrome *c* oxidase assembly induced by *SURF1* defects”.

Acknowledgements

This work was supported by the Grant Agency of the Czech Republic (14-36804G), Ministry of Education, Youth and Sports of the Czech Republic (ERC CZ: LL1204, RVO:67985823), the Grant Agency of the Ministry of Health of the Czech Republic (NT12370-5) and ERC Advanced Grant FP7-322424.

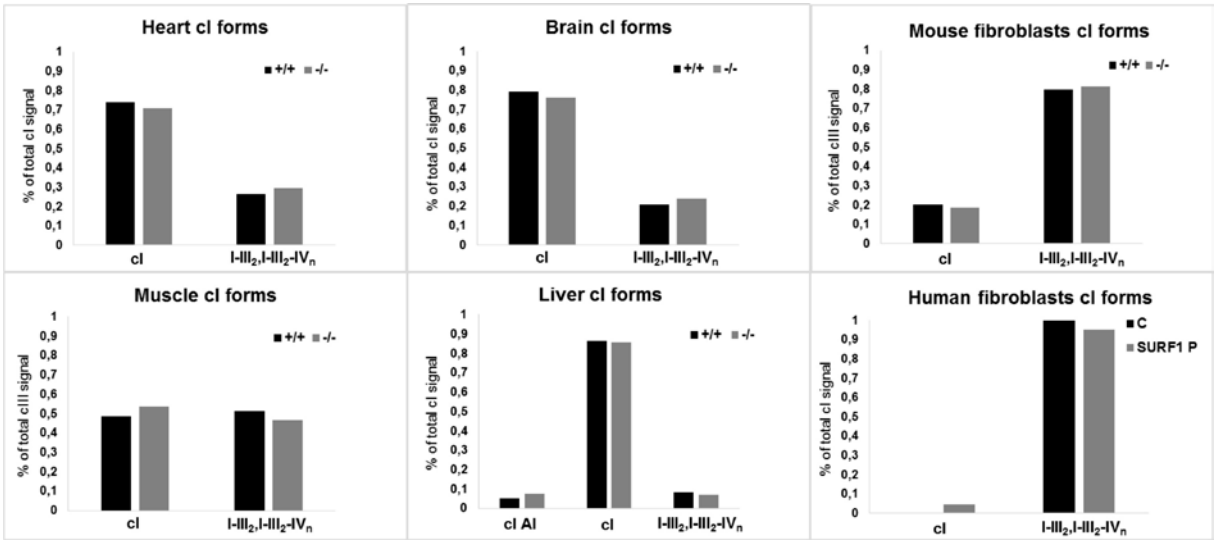

Figure 1. Complex I (cI) forms present in *SURF1*$^{-/-}$ mouse tissues and fibroblasts and *SURF1* patient fibroblasts. For analysis, *SURF1*$^{+/+}$ mouse (+/+), *SURF1*$^{-/-}$ mouse (-/-), human control (C) and *SURF1* patient (SURF1 P) data from BNE/SDS PAGE western blots (see Fig. 1 in [1]) were used. Signals of NDUFB6 (NDUFS3 in muscle) subunit were quantified and expressed as percentage of overall NDUFB6 (NDUFS3) signal of each tissue/cell western blot. cI assembly intermediates (cI AI); supercomplexes I-III$_2$ and I-III$_2$-IV$_n$ (I-III$_2$, I-III$_2$-IV$_n$).

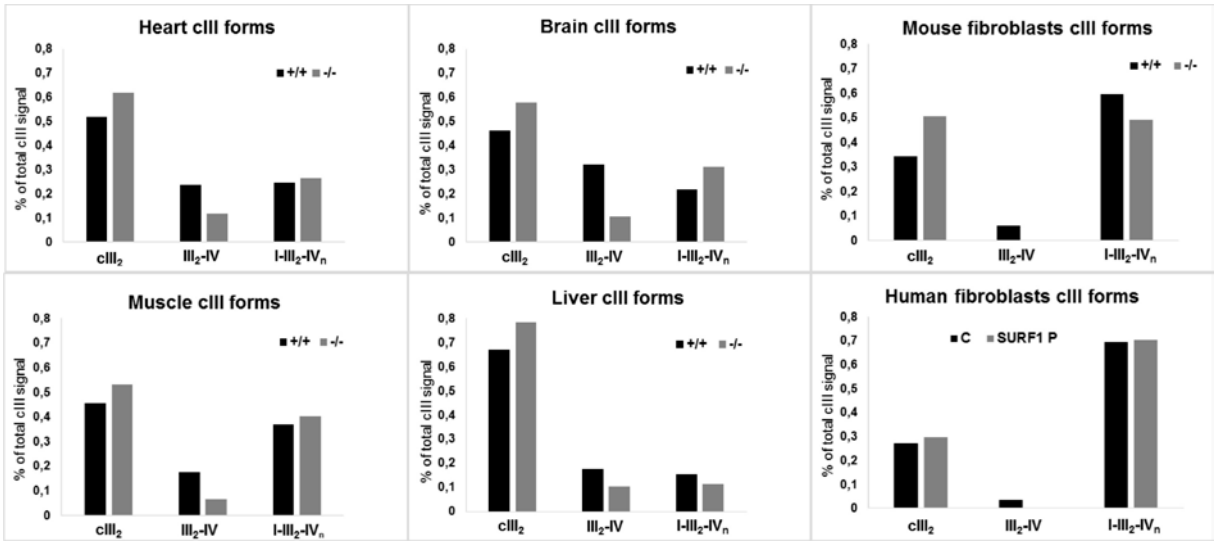

Figure 2. Complex III (cIII) forms present in *SURF1*$^{-/-}$ mouse tissues and fibroblasts and *SURF1* patient fibroblasts. For analysis, *SURF1*$^{+/+}$ mouse (+/+), *SURF1*$^{-/-}$ mouse (-/-), human control (C) and *SURF1* patient (SURF1 P) data from BNE/SDS PAGE western blots (see Fig. 1

in [1]) were used. Signals of CORE1 subunit were quantified and expressed as percentage of overall CORE1 signal of each tissue/cell western blot. cIII dimer ($cIII_2$); supercomplexes III_2-IV, I-III_2 and I-III_2-IV_n (III_2-IV, I-III_2, I-III_2-IV_n).

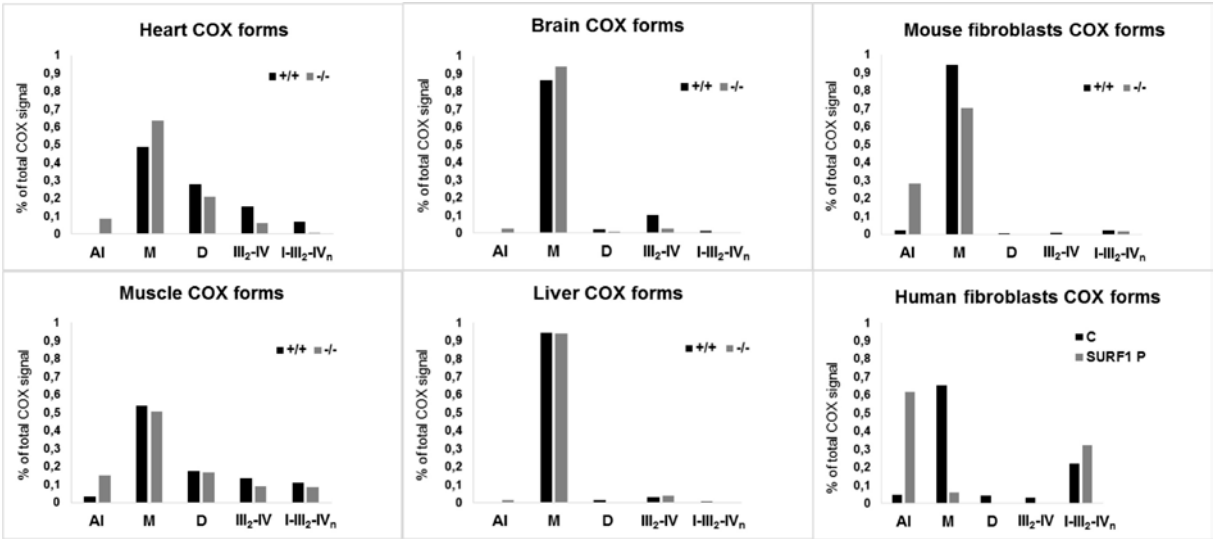

Figure 3. COX forms present in *SURF1*$^{-/-}$ mouse tissues and fibroblasts and *SURF1* patient fibroblasts. For analysis, *SURF1*$^{+/+}$ mouse (+/+), *SURF1*$^{-/-}$ mouse (-/-), human control (C) and *SURF1* patient (SURF1 P) data from BNE/SDS PAGE western blots (see Fig. 1 in [1]) were used. Signals of COX1 were quantified and expressed as percentage of overall COX1 signal in each tissue/cell western blot. COX assembly intermediates (AI), COX monomer (M), COX dimer (D), supercomplexes III_2-IV and I-III_2-IV_n (III_2-IV, I-III_2-IV_n).

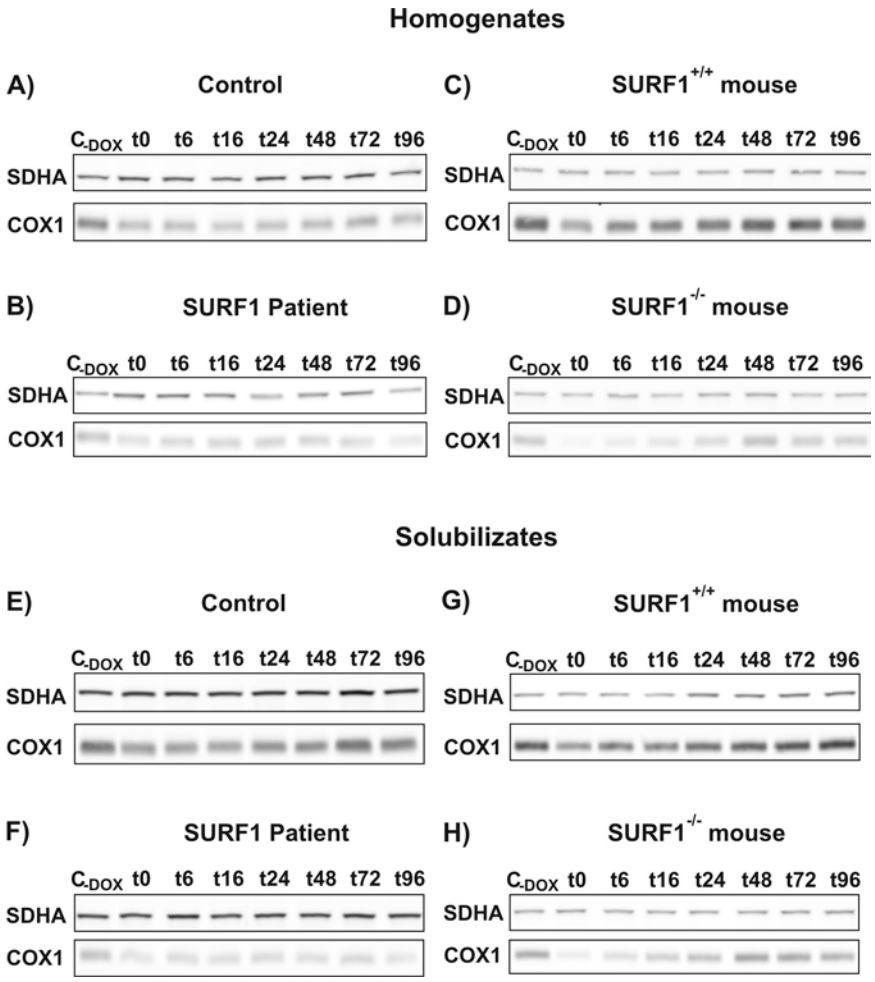

Figure 4. Decreased COX1 amount after DOX treatment. Homogenates from DOX treated human control and *SURF1* patient fibroblasts (**A, B**), *SURF1*$^{+/+}$ and *SURF1*$^{-/-}$ mouse fibroblasts (**C, D**) and digitonin solubilizates from DOX treated human control and *SURF1* patient fibroblasts (**E, F**), *SURF1*$^{+/+}$ and *SURF1*$^{-/-}$ mouse fibroblasts (**G, H**) were analyzed on SDS PAGE in combination with western blot to obtain overall COX1 signal at different time points (t0 - t96 hours) after DOX treatment. Signal of SDHA was used as reference. Control cells without DOX treatment (C_{-DOX}).

References

[1] N. Kovářová, P. Pecina, H. Nůsková, M. Vrbacký, M. Zeviani, T. Mráček, C. Viscomi, J. Houštěk

Tissue- and species-specific differences in cytochrome c oxidase assembly induced by SURF1 defects

Biochim Biophys Acta, 1862(4) (2016), pp. 705-715

[2] C. Dell'Agnello, S. Leo, A. Agostino, G. Szabadkai, C. Tiveron, A. Zulian, A. Prelle, P. Roubertoux, R. Rizzuto, M. Zeviani
Increased longevity and refractoriness to Ca(2+)-dependent neurodegeneration in Surf1 knockout mice
Hum Mol Genet, 16(4) (2007), pp. 431-44

[3] P. Pecina, M. Čapková, S. K. Chowdhury, Z. Drahota, A. Dubot, A. Vojtíšková, H. Hansíková, H. Houšťková, J. Zeman, C. Godinot, J. Houštěk
Functional alteration of cytochrome c oxidase by SURF1 mutations in Leigh syndrome
Biochim Biophys Acta, 1639(1) (2003), pp. 53-63

[4] H. A. Bentlage, U. Wendel, H. Schägger, H. J. ter Laak, A. J. Janssen, J. M. Trijbels
Lethal infantile mitochondrial disease with isolated complex I deficiency in fibroblasts but with combined complex I and IV deficiencies in muscle
Neurology, 47(1) (1996), pp. 243-8

[5] I. Wittig, H.P. Braun, H. Schägger
Blue native PAGE
Nat Protoc, 1(1) (2006), pp. 418-28

[6] M. M. Bradford
A rapid and sensitive method for the quantitation of microgram quantities of protein utilizing the principle of protein-dye binding
Anal Biochem, 72 (1976), pp. 248-54

[7] H. Schägger, G. von Jagow
Blue native electrophoresis for isolation of membrane protein complexes in enzymatically active form
Anal Biochem, 199(2) (1991), pp. 223-31

[8] H. Schägger, G. von Jagow

Tricine-sodium dodecyl sulfate-polyacrylamide gel electrophoresis for the separation of proteins in the range from 1 to 100 kDa
Anal Biochem, 166(2) (1987), pp. 368-79

[9] D. Moreno-Lastres, F. Fontanesi, I. García-Consuegra, M. A. Martín, J. Arenas, A. Barrientos, C.
Ugalde, Mitochondrial complex I plays an essential role in human respirasome assembly
Cell Metab, 15(3) (2012), pp. 324-35

Biochem. J. (2015) **466**, 601–611 (Printed in Great Britain) doi:10.1042/BJ20141462

Alteration of structure and function of ATP synthase and cytochrome *c* oxidase by lack of F_o-a and Cox3 subunits caused by mitochondrial DNA 9205delTA mutation

Kateřina Hejzlarová*, Vilma Kaplanová*, Hana Nůsková*, Nikola Kovářová*, Pavel Ješina*, Zdeněk Drahota*, Tomáš Mráček*, Sara Seneca† and Josef Houštěk*[1]

*Institute of Physiology Academy of Sciences of the Czech Republic v.v.i., Vídeňská 1083, 14220 Prague 4, Czech Republic
†Center for Medical Genetics, UZ Brussel, Vrije Universiteit Brussel, Laarbeeklaan 101, 1090 Brussels, Belgium

Mutations in the *MT-ATP6* gene are frequent causes of severe mitochondrial disorders. Typically, these are missense mutations, but another type is represented by the 9205delTA microdeletion, which removes the stop codon of the *MT-ATP6* gene and affects the cleavage site in the *MT-ATP8/MT-ATP6/MT-CO3* polycistronic transcript. This interferes with the processing of mRNAs for the Atp6 (F_o-a) subunit of ATP synthase and the Cox3 subunit of cytochrome *c* oxidase (COX). Two cases described so far presented with strikingly different clinical phenotypes – mild transient lactic acidosis or fatal encephalopathy. To gain more insight into the pathogenic mechanism, we prepared 9205delTA cybrids with mutation load ranging between 52 and 99 % and investigated changes in the structure and function of ATP synthase and the COX. We found that 9205delTA mutation strongly reduces the levels of both F_o-a and Cox3 proteins. Lack of F_o-a alters the structure but not the content of ATP synthase, which assembles into a labile, ∼60 kDa smaller, complex retaining ATP hydrolytic activity but which is unable to synthesize ATP. In contrast, lack of Cox3 limits the biosynthesis of COX but does not alter the structure of the enzyme. Consequently, the diminished mitochondrial content of COX and non-functional ATP synthase prevent most mitochondrial ATP production. The biochemical effects caused by the 9205delTA microdeletion displayed a pronounced threshold effect above ∼90 % mutation heteroplasmy. We observed a linear relationship between the decrease in subunit F_o-a or Cox3 content and the functional presentation of the defect. Therefore we conclude that the threshold effect originated from a gene–protein level.

Key words: ATP synthase, cytochrome *c* oxidase, mitochondrial diseases, mtDNA *MT-ATP6* mutation, oxidative phosphorylation, threshold effect.

INTRODUCTION

Mitochondrial diseases due to disorders of the oxidative phosphorylation system (OXPHOS) are frequently caused by mitochondrial DNA (mtDNA) point mutations in protein-coding genes [1]. They alter the amino acid composition or (less frequently) lead to the formation of truncated protein if a premature stop codon has been formed. Up to now, over 200 point mutations of mtDNA have been reported. By their nature, they can be either homoplasmic and/or heteroplasmic and affect different mitochondrially synthesized subunits (www.mitomap.org [2]). In 1996, Seneca et al. [3] found a new type of mtDNA mutation that affects the *MT-ATP6* and *MT-CO3* genes by microdeletion of two bases, TA, in mtDNA at positions 9205–9206 (9205delTA). This mutation removes the stop codon of the *MT-ATP6* gene and alters the splicing site for processing of the polycistronic *MT-ATP8/MT-ATP6/MT-CO3* transcript. The 9205delTA mutation can be expected to alter the levels of *MT-ATP6* and *MT-CO3* transcripts and thus the synthesis of the F_o-a (Atp6) subunit of ATP synthase and the Cox3 subunit of cytochrome *c* oxidase (COX), which could limit the biogenesis of these two respiratory chain complexes.

The first case with the 9205delTA mutation presented with a relatively mild phenotype – seizures with several episodes of transient lactic acidosis [3]. Analysis of patient fibroblasts with the reported homoplasmic mutation revealed no changes in *MT-ATP6* and *MT-CO3* mRNA processing, a significant increase in deadenylation of *MT-ATP8/MT-ATP6* bicistron [4], and relatively insignificant biochemical changes [5]. The second case of the 9205delTA mutation was a child with severe encephalopathy and hyperlactacidaemia [6]. In correspondence with the fatal clinical course, the patient fibroblasts showed a pronounced alteration of ATP synthase structure and a low activity and protein content of COX resulting in a ∼70 % decrease in mitochondrial ATP synthesis [7]. There was a marked and specific decrease in *MT-ATP8/MT-ATP6/MT-CO3* primary transcript processing. F_o-a subunit content and its *de novo* synthesis were reduced 10-fold when compared with the other ATP synthase subunits. Both cases were reported to be homoplasmic and therefore we speculated that an additional nuclear-encoded mitochondrial factor might be involved in processing of the *MT-ATP8/MT-ATP6/MT-CO3* transcript and modulate the deleterious effects of the 9205delTA mutation [7]. It was of interest to compare the cells from both cases. While both cases were supposedly homoplasmic,

Abbreviations: BNE, blue native electrophoresis; COX, cytochrome *c* oxidase; DDM, *n*-dodecyl-β-D-maltoside; DMEM, Dulbecco's modified Eagle's medium; FCCP, carbonyl cyanide *p*-trifluoromethoxyphenylhydrazone; hrCNE1, high-resolution clear native electrophoresis; LLS, Leigh-like syndrome; LS, Leigh syndrome; MILS, maternally inherited LS; NARP, neurogenic muscle weakness, ataxia and retinitis pigmentosa; OSCP, oligomycin-sensitivity conferral protein; OXPHOS, oxidative phosphorylation system; TMPD, *N,N,N′,N′*-tetramethyl-*p*-phenylenediamine; TPP^+, tetraphenylphosphonium; WB, Western blot.

[1] To whom correspondence should be addressed (email houstek@biomed.cas.cz).

methodological limitations mean that they can only be claimed to have a mutation load >98 %. Later we identified heteroplasmy of the 9205delTA mutation in the fibroblasts of high passage from the first patient, indicating that negative segregation of the mutation occurred during the prolonged cultivation and unmasked the mutation heteroplasmy. The phenotypic differences between the two patients may therefore be caused by a threshold effect with a very steep dependence close to homoplasmy [8] and tissue-specific differences in heteroplasmy.

To gain more insight into the pathogenic mechanism of the 9205delTA mutation, we prepared cybrid cell lines with a varying load of the mtDNA 9205delTA mutation and investigated changes in the structure and function of ATP synthase and COX. We found that the 9205delTA mutation strongly reduces the levels of both F_o-a and Cox3 proteins, alters the structure of ATP synthase, decreases the content of COX, and prevents most of the mitochondrial ATP synthesis. All of the biochemical effects exerted a pronounced threshold effect above 90 % heteroplasmy. In addition, we found that a slightly smaller ATP synthase complex devoid of the F_o-a subunit is formed but it is rather labile and unable to synthesize ATP.

MATERIALS AND METHODS

Chemicals

Unless otherwise indicated, chemicals of the highest purity were obtained from Sigma–Aldrich.

Preparation of cybrids and isolation of mitochondria

Transmitochondrial cybrids were prepared according to [9]. Fibroblasts from the two patients P1 [3] and P2 [7] harbouring the 9205delTA mutation and from controls were enucleated by centrifugation in Dulbecco's modified Eagle's medium (DMEM, BioTech) containing 10 μg/ml cytochalasin B and then fused with mtDNA-less (ρ^0) 143B TK$^-$ osteosarcoma cells by adding a 50 % (w/v) solution of PEG with 10 % (v/v) DMSO. Cells were selected for 3 weeks in DMEM containing 5 % (v/v) fetal bovine serum, 0.1 mg/ml 5-bromodeoxyuridine and lacking uridine. The ring-cloned and subcloned cybrid cells were grown to ~90 % confluence, harvested using 0.05 % (w/v) trypsin and 0.02 % (w/v) EDTA, and washed twice in PBS before use.

Mitochondria from cybrid or fibroblast cells were isolated at 4 °C by a hypo-osmotic shock method [10]. The freshly harvested cells were disrupted in 10 mM Tris/HCl, pH 7.4, homogenized in a Teflon/glass homogenizer (10 % homogenate, w/v) and then sucrose was added to a final concentration of 0.25 M. Mitochondria were sedimented from the 600 ***g*** postnuclear supernatant by 10 min centrifugation at 10000 ***g***, washed, and resuspended in 0.25 M sucrose, 2 mM EGTA, 40 mM KCl and 20 mM Tris/HCl, pH 7.4.

In some experiments we also used the membrane fraction obtained by 10 min centrifugation of cell homogenate (10 % (w/v) in 83 mM sucrose and 6.6 mM imidazole, pH 7.0) at 15000 ***g*** [11]. Samples were stored at − 80 °C.

PCR and restriction analysis

To determine the amount of 9205delTA mtDNA, the isolated DNA was amplified by PCR using mismatch primers (bold) 5′-CCT CTA CCT GCA CGA CAA T**GC** A-3′ (forward) and 5′-CGT TAT G**C**A **T**TG GAA GTG AAA TCA C-3′ (reverse), corresponding to nt 9183–9329 (147 bp) [5]. Mismatch primers generated two *Nsi*I restriction sites in the case of wild-type mtDNA (fragments 116 + 22 + 9 bp) and one *Nsi*I restriction site in the case of mutated mtDNA (138 + 9 bp). PCR products were digested with *Nsi*I (Roche) for 3 h at 37 °C, the enzyme was inactivated for 15 min at 65 °C, and DNA fragments were separated on 1.5 % (w/v) agarose in TBE buffer (0.09 M Tris/HCl, 0.09 M H_3BO_3 and 2 mM sodium EDTA, pH 8.0). Ethidium bromide-stained gels were visualized on the transiluminator BioDocAnalyze (Biometra) and the signal was quantified using Aida 3.21 Image Analyzer. Heteroplasmy was expressed as a percentage of mutated mtDNA relative to the total signal of amplified mtDNA.

Electrophoresis, Western blot analysis, in-gel ATPase activity

SDS-PAGE [12] was performed on 10 % (w/v) polyacrylamide slab minigels (MiniProtean System, Bio-Rad Laboratories) at room temperature. Samples of whole cells or isolated mitochondria were heated for 20 min at 40 °C in a sample lysis buffer (2 % (v/v) 2-mercaptoethanol (Fluka), 4 % (w/v) SDS (Serva), 50 mM Tris/HCl (pH 7.0) and 10 % (v/v) glycerol).

Separation of native OXPHOS complexes by blue native (BNE) [11,13] or high-resolution clear native electrophoresis (hrCNE1 system) [14] was performed on polyacrylamide gradient (6–15 % for COX analysis, 4–13 % for ATP synthase analysis) minigels at 7 °C. Mitochondrial or membrane fraction proteins were solubilized with *n*-dodecyl-β-D-maltoside (DDM) or digitonin at the indicated detergent/protein ratio for 15 min on ice. The samples were centrifuged for 20 min at 4 °C and 30000 ***g***, and either Coomassie Brilliant Blue G dye (Serva Blue G-250, 0.125 g/g detergent) or Ponceau Red dye (0.005 %) and 5 % glycerol were added to the supernatants before electrophoresis. For two-dimensional (2D) analysis, strips of the first dimension native gels were incubated for 1 h in 1 % (w/v) SDS and 1 % (v/v) 2-mercaptoethanol at room temperature, washed in water and subjected to SDS-PAGE for separation in the second dimension.

Gels were blotted onto PVDF membrane (Millipore) by semi-dry electrotransfer (1 h at 0.8 mA/cm^2) and the membrane was blocked in 5 % defatted milk (Promil) in TBS (150 mM NaCl and 10 mM Tris/HCl, pH 7.5). The membranes were washed twice in TBST (TBS with 0.1 % (v/v) Tween-20) and immunodecorated with the following primary antibodies diluted in TBST: rabbit polyclonal antibodies to subunits F_o-c (1:1000) and F_o-a (1:500) [7], mouse monoclonal antibodies from Abcam to subunits F_1-α (1:1000, ab110273), F_1-β (1:2000, ab14730), F_o-d (1:700, ab110275), OSCP (oligomycin-sensitivity conferral protein) (1:250, ab110276), Cox1 (1:1000, ab14705), Cox2 (1:1000, ab110258), Cox4 (1:1000, ab110261), Cox5a (1:500, ab110262), Cox6c (1:500, ab110267), Core2 subunit (1:1000, ab14745) and pyruvate dehydrogenase (PDH, 1:1000, ab110334). Goat polyclonal antibody to Cox3 (1:200 in TBST with 3 % (w/v) BSA) was from Santa Cruz Biotechnology (sc-23986), rabbit polyclonal antibody to porin (1:1000) was a gift from Professor Vito de Pinto (Dipartimento di Scienze Chimiche - Università di Catania, Catania, Italy). For a quantitative detection, the following infra-red fluorescent secondary antibodies (Alexa Fluor 680, Life Technologies; IRDye 800, Rockland Immunochemicals) diluted in TBST were used: goat anti-mouse IgG (1:3000, A21058), goat anti-rabbit IgG (1:3000, A21109), donkey anti-rabbit IgG (1:3000, 611-732-127), and donkey anti-goat IgG (1:3000, A21084). The fluorescence was detected using ODYSSEY infra-red imaging system (LI-COR Biosciences) and the signal was quantified using Aida 3.21 Image Analyzer software.

ATPase hydrolytic activity was detected on native gels immediately after electrophoresis according to [15]. Briefly, gels were incubated for 1 h in 35 mM Tris/HCl, 270 mM glycine, 14 mM $MgSO_4$, 0.2 % (w/v) $Pb(NO_3)_2$ and 8 mM ATP, pH 8.3,

and white lead phosphate precipitates were documented by scanning.

High-resolution oxygraphy

Oxygen consumption by cybrid cells (0.75 mg protein/ml) was determined at 30 °C in a KCl medium (80 mM KCl, 10 mM Tris/HCl, 3 mM $MgCl_2$, 1 mM EDTA and 5 mM potassium phosphate, pH 7.4) as described previously [16], using Oxygraph-2k (Oroboros). Cells were permeabilized by 0.05 g of digitonin/g of protein. Respiration was measured with 10 mM succinate in the presence of 2.5 μM rotenone and 25 μM Ap5A (P^1,P^5-di(adenosine-5′)pentaphosphate), then 1.25 mM ADP was added. ADP-stimulated respiration was inhibited after 6 min with 1 μM oligomycin and after 2 min, 0.1 μM FCCP (carbonyl cyanide *p*-trifluoromethoxyphenylhydrazone) was added. Activity of COX was measured with 5 mM ascorbate and 1 mM TMPD (*N,N,N′,N′*-tetramethyl-*p*-phenylenediamine) in the presence of 1 mg/ml antimycin A and was corrected for substrate autoxidation insensitive to 0.33 mM KCN. Oxygen consumption was expressed in pmol of oxygen/s/mg of protein.

Mitochondrial membrane potential $\Delta\psi_m$ measurements

$\Delta\psi_m$ was measured with TPP^+ (tetraphenylphosphonium)-selective electrode in 1 ml of KCl medium as described in [16]. Cells (2 mg of protein/ml) were permeabilized with digitonin (0.04 g/g of protein) and the following substrates and inhibitors were used: 10 mM succinate, 10 mM glutamate, 3 mM malate, 1.5 mM ADP, 1 μM oligomycin and 1 μM FCCP. The membrane potential was plotted as pTPP, i.e. negative decimal logarithm of TPP^+ concentration.

ATP synthesis

During respiration measurements, 10 μl samples were collected from the oxygraphic chamber (before and 6 min after ADP addition) and immediately mixed with the same volume of 100 % DMSO. ATP content was then determined in DMSO-quenched samples by a luciferin–luciferase reaction [17]. Bioluminescence was measured in the medium containing 25 mM tricine, 5 mM $MgSO_4$, 0.1 mM EDTA, 1 mM dithiothreitol, 0.6 mM luciferin (Promega) and 6×10^7 luciferase units/ml luciferase (Promega), pH 7.8, using 1250 Luminometer (BioOrbit). Calibration curve was measured in the range 0–10 pmol of ATP. ATP production was expressed in nmol of ATP/min/mg of protein.

Ethics

The present study was carried out in accordance with the Declaration of Helsinki of the World Medical Association and was approved by the Committee of Medical Ethics of Institute of Physiology Academy of Sciences of the Czech Republic. Informed consent from the parents of the patients was obtained.

RESULTS

Cybrids with mtDNA 9205delTA mutation

The cybrid cell lines used in the present study were derived from the fibroblasts of two patients (P1 and P2) with the 9205delTA mutation (Figure 1A) and included cybrid clones of varying mutation heteroplasmy. To estimate the relationship between biochemical consequences and the 9205delTA mutation load we used wild-type mtDNA homoplasmic control cybrids, several clones of 9205delTA heteroplasmic cybrids with the content of

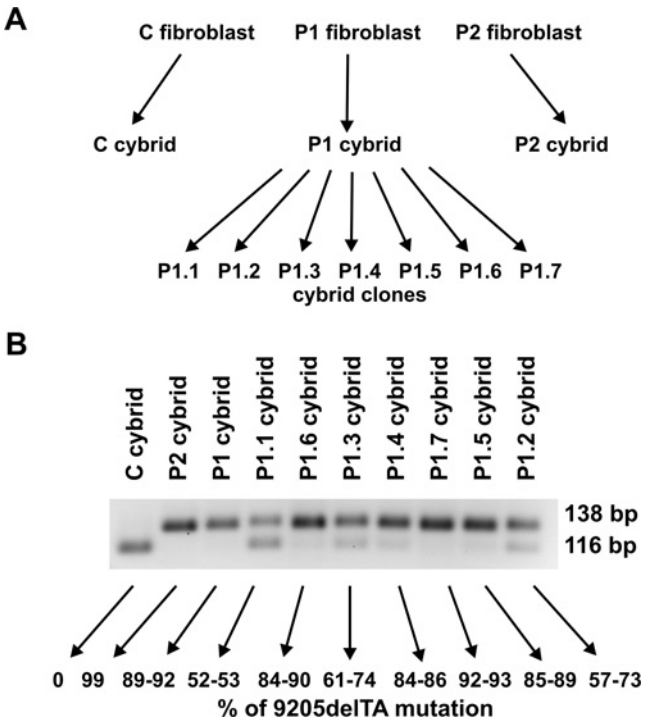

Figure 1 Cybrid cell lines used in the study

(**A**) Fibroblasts from two patients with the mtDNA 9205delTA microdeletion and from a control were enucleated and then fused with mtDNA-less (ρ^0) 143B TK^- osteosarcoma cells to produce transmitochondrial cybrid cell lines. (**B**) Mutation load in cybrid clones and subclones was analysed by restriction analysis with *Nsi*I of nt 9183–9329 mtDNA PCR products and was calculated from the amounts of 138 bp and 116 bp fragments corresponding to the mutated and wild-type mtDNA, respectively.

9205delTA mtDNA ranging between 52 and 92 % (derived from P1 fibroblasts) and 9205delTA cybrids with >99 % of mutated mtDNA (derived from P2 fibroblasts).

Throughout the course of the studies, individual cybrid cell lines maintained a stable heteroplasmy level, which was routinely checked by restriction analysis of PCR products and was expressed as a percentage of the mutated mtDNA relative to the total mtDNA (Figure 1B).

Changes in mitochondrial content and composition of ATP synthase and cytochrome *c* oxidase subunits in 9205delTA homoplasmic cells

Previous analysis of fibroblasts from the P2 patient demonstrated a very strong reduction in subunit F_o-a content [7]. The reduced content of COX subunits Cox1, Cox4 and Cox6c as well as altered maturation of Cox3 mRNA further indicated that the 9205delTA mutation may also disrupt the synthesis of subunit Cox3. To verify this assumption, we analysed cell homogenates and isolated mitochondria from control and 9205delTA homoplasmic cybrids by SDS-PAGE and Western blot (WB) (Figure 2A) using antibodies against several subunits of ATP synthase and COX. To quantify their specific content, the signals of individual subunits were normalized to those of porin and expressed as a percentage of control (Figure 2B).

The subunit F_o-a content was strongly reduced in 9205delTA homoplasmic cybrid cells; only a very low amount of F_o-a could be detected in isolated mitochondria. In contrast, F_1-α and F_1-β subunits of the catalytic part were present in near-normal levels

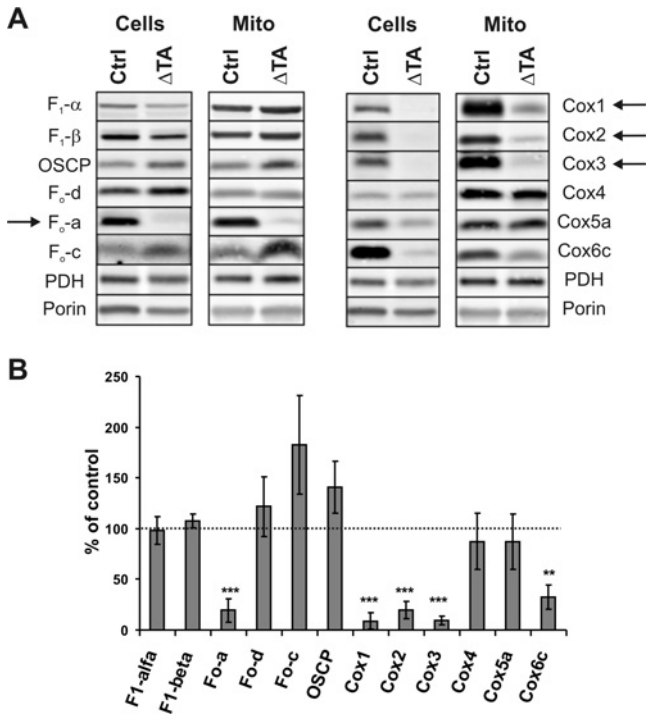

Figure 2 Specific content of ATP synthase and cytochrome *c* oxidase subunits in control and 9205delTA cybrid cells and isolated mitochondria

(**A**) Protein aliquots of cell homogenate (Cells, 15 μg) and isolated mitochondria (Mito, 10 μg) from control (Ctrl) and 9205delTA homoplasmic (ΔTA) cybrids were analysed by SDS-PAGE and WB with antibodies against indicated subunits. (**B**) Specific content of each subunit in 9205delTA samples was normalized for the signal of porin and expressed as a percentage of the content in the control. Data are the means $\pm$ S.E.M. for five experiments. $^{***}P < 0.001$, $^{**}P < 0.01$ (Student's *t* test).

in both cell homogenates and isolated mitochondria. Similarly, a normal or even increased content was found in the case of several subunits of F_o membrane part (F_o-d, OSCP and F_o-c; Figure 2B). Thus, with the exception of subunit F_o-a which was reduced to less than 20 %, all other ATP synthase subunits were present in normal or increased levels in homoplasmic 9205delTA cybrids when compared with the control cybrids.

The analysis of Cox3 clearly showed that the content of this subunit was strongly reduced due to the 9205delTA mutation. Interestingly, all mitochondrially encoded COX subunits (Cox1, Cox2 and Cox3) were similarly decreased in whole cells and isolated mitochondria (Figure 2A) and their respective content in 9205delTA homoplasmic cybrids was 8–20 % of the control (Figure 2B). Nuclear-encoded subunits were less affected and their content varied – Cox4 was almost normal in whole cells and isolated mitochondria, Cox6c was decreased to ~40 % of control in both samples, and Cox5a was decreased in the whole cells but not in isolated mitochondria (Figure 2A).

Changes in the assembled complexes of ATP synthase and cytochrome *c* oxidase in 9205delTA homoplasmic cells

Further, we were interested how the primary lack of F_o-a and Cox3 alters the properties of the assembled ATP synthase and COX. Mitochondria from the control and homoplasmic 9205delTA cybrids were solubilized by DDM or digitonin, resolved by BNE and visualized by WB using subunit-specific antibodies.

As shown in Figures 3A and 3B, in DDM-solubilized mitochondrial proteins of control cells, practically all F_1-β was recovered in ATP synthase monomer (complex V, cV) of approximately 600 kDa and a small amount, less than 10 %, was present in subcomplexes of 460 and 350 kDa. In 9205delTA cybrids, the pattern detected by anti-F_1-β antibody was completely different and revealed a strongly reduced amount of ATP synthase monomer (cV) but a high content of smaller sub-assemblies. The largest one, cV*, was approximately 60 kDa smaller than the cV monomer. Judging from the presence of subunits F_o-c and F_o-a, this could represent an almost complete cV without subunit F_o-a and possibly some other small subunit(s) (Figure 3A). This cV* was present in a similar amount as cV in 9205delTA cybrids but was completely absent from control cells. The majority of F_1-β was present in the three other, smaller, subcomplexes with the largest one being also the most abundant. None of those subcomplexes contained the F_o-a subunit. As similar subcomplexes were repeatedly described in *MT-ATP6* patients and ρ° cells [18–21], one may predict their composition. The 460 kDa subcomplex is thus expected to contain F_1 with the ring of F_o-c subunits (c-ring) and the inhibitory factor IF_1 (F_1IF_1c); the 380 kDa subcomplex corresponds to F_1IF_1, and the 350 kDa subcomplex represents F_1 alone. Judging from the F_1-β signal the relative content of these forms was 16:23:46:8:7 % for F_1:F_1IF_1:F_1IF_1c:cV*:cV, respectively. Importantly, the total amount of DDM-solubilized F_1-β signal, and thus of various cV assembly intermediates, in 9205delTA cybrids was the same or even higher than in control cells. The increase in DDM concentration from 2 g/g of protein to 4 g/g of protein did not affect the observed pattern of ATP synthase assembly forms (Figure 3A).

While it was previously proposed that ATP synthase subcomplexes observed in cells with *MT-ATP6* mutations do represent the breakdown products of assembled ATP synthase with mutated F_o-a [19], their formation may also be an artefact of the stringent conditions during BNE separation as was observed in ρ° cells [22]. Therefore, we used hrCNE1 to analyse ATP synthase assembly in 9205delTA cells. As shown in Figure 3C, when the DDM-solubilized proteins were resolved by hrCNE1, predominantly a single form of 9205delTA ATP synthase was present with a molecular mass of about 540 kDa that corresponded to the cV* detected on BNE. In-gel ATPase activity and WB analysis showed that this complex contains F_o subunits F_o-c and F_o-d but not F_o-a. A similar incomplete ATP synthase complex was described in ρ° cells, lacking both subunits F_o-a and A6L, with the mass around 550 kDa [22]. When the dye Coomassie Blue G was added to the 9205delTA sample before hrCNE1 (Figure 3C), the complex cV* broke down to the same 460 kDa and 350 kDa subcomplexes demonstrated in Figure 3A. Their composition detected by 2D analysis is shown in detail in Figure 3D. These experiments thus provide clear evidence supporting the view that mammalian ATP synthase can assemble even without the F_o-a subunit, but that the complex is unstable and dissociates easily.

When COX was analysed by BNE (Figures 4A and 4B) in control mitochondria solubilized by DDM (1 g/g protein), Cox1- and Cox4-specific antibodies detected most of the signal in the form of COX monomer (respiratory chain complex IV, cIV). A small amount was also present in higher structures – as COX dimer (cIV_2) and a supercomplex of two copies of complexes III and one copy of COX ($cIII_2cIV$), which was also detected by the antibody against cIII subunit Core2 (not shown). A small amount of both a 180 kDa subcomplex, which appears to represent the COX assembly intermediate S3, and free Cox1 subunit was also present. At a higher DDM concentration (4 g/g of protein), less supercomplex and cIV_2 but more S3 could be seen. In 9205delTA cybrid mitochondria (Figures 4A and 4B), we found no cIV_2 and strong reduction in other forms of COX compared with the control – $cIII_2cIV$, cIV and S3 were similarly decreased to 14 %,

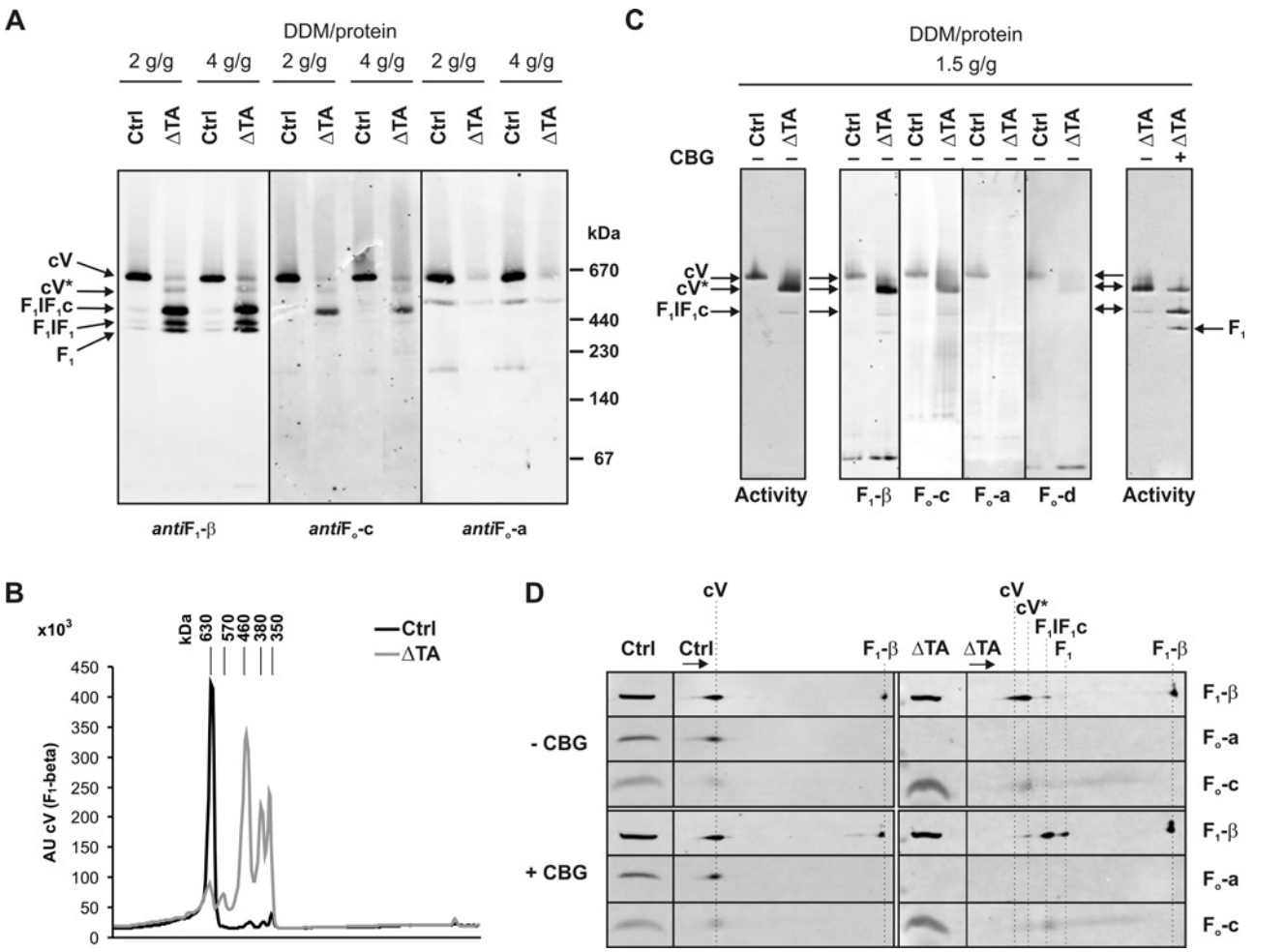

Figure 3 BNE analysis of ATP synthase complex in control and 9205delTA cybrid mitochondria

(**A**) Isolated mitochondria from control (Ctrl) and 9205delTA homoplasmic (ΔTA) cybrids were solubilized with indicated concentrations of *n*-dodecyl-β-D-maltoside (DDM) and analysed by BNE and WB using antibodies against indicated ATP synthase subunits. cV – ATP synthase complex; cV* – ATP synthase complex lacking subunit F_o-a; F_1IF_{1c} – subcomplex of F_1 with c-ring and IF_1 inhibitory factor; F_1IF_1 – subcomplex F_1 with IF_1; F_1 – F_1 alone. In (**B**) quantitative distribution of F_1-β subunit in samples solubilized at 4 g of DDM/g of protein is shown. (**C** and **D**) Mitochondrial membranes were solubilised with 1.5 g of DDM and samples with or without Coomassie Blue G dye (CBG) were analysed by hrCNE1 and 2D hrCNE1/SDS-PAGE. (**C**) ATPase activity staining and WB analysis of the hrCNE1 first dimension. (**D**) WB analysis of the hrCNE1/SDS PAGE second dimension. Aliquots of 15 μg of DDM-solubilized proteins were used.

20 % and 37 %, respectively. In contrast, the amount of free Cox1 subunit was comparable between 9205delTA and control cybrids suggesting that the early biogenesis of COX is not affected. Given the decrease in assembled enzyme, free Cox1 represented 55 % of the total Cox1 signal in 9205delTA cybrids and only 17 % in controls. Digitonin solubilization and subsequent BNE analysis achieves better resolution of supramolecular COX forms such as S2 intermediate of ∼100–140 kDa. While S2 is specifically increased in cells with COX deficiency due to *SURF1* mutations [23], Figure 4B clearly shows that this is not the case with 9205delTA cybrids.

9205delTA heteroplasmy-dependent variation in the subunit F_o-a and Cox3 content

It can be expected that the primary effect of the 9205delTA mutation is impaired synthesis of subunits F_o-a and Cox3, which leads to the formation of defective and unstable ATP synthase complex and decreased content of the fully assembled COX. To estimate how the subunit F_o-a content varies with the mutation load, we analysed several cybrid cell lines for the content of F_o-a (Figure 5A). The protein level of subunit F_o-a in 9205delTA cybrid cells did not change, until the heteroplasmy reached ∼90 %. When the mutation load exceeded this threshold, the F_o-a content progressively declined towards homoplasmy.

When we performed analogous analyses of the effect of 9205delTA mutation on the amount of Cox3 subunit (Figure 5B), again a pronounced threshold dependence could be observed. The normal amount of Cox3 subunit was present up to ∼90 % heteroplasmy, followed by a steep decrease in Cox3 content afterwards. Altogether, the contents of F_o-a and Cox3 were decreased 5 times and 10 times, respectively, in the homoplasmic cybrid cell line.

9205delTA heteroplasmy-dependent changes in the mitochondrial energetic function

9205delTA mutation affects both ATP synthase and COX, yet the functional outcome seems to be different. As shown in Figure 6, the mutation strongly affects both the generation of mitochondrial membrane potential by substrate oxidation and its utilization for ATP synthesis. In homoplasmic 9205delTA cybrids,

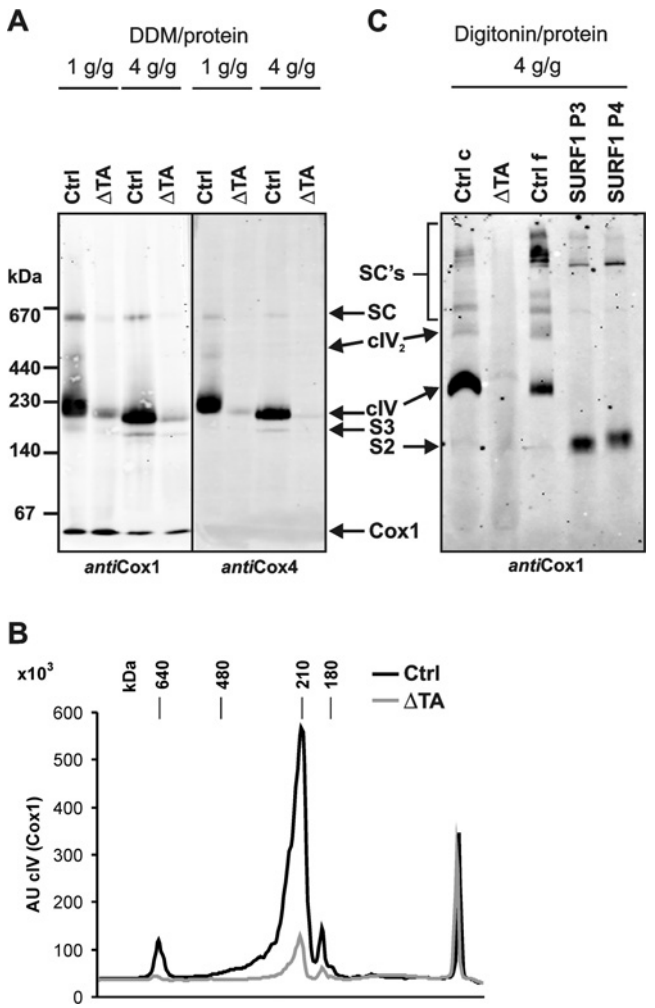

Figure 4 BNE analysis of cytochrome *c* oxidase complex in control and 9205delTA cybrid mitochondria

Isolated mitochondria of control (Ctrl) and 9205delTA homoplasmic (ΔTA) cybrids and of control (Ctrl f) and SURF1 patient (P3 and P4) fibroblasts were solubilized with given concentrations of (**A**) *n*-dodecyl-β-D-maltoside (DDM) or (**C**) digitonin, and analysed by BNE and WB using antibodies to indicated subunits of cytochrome *c* oxidase. SC's – COX supercomplexes, SC – $cIII_2cIV$ supercomplex of COX with two complexes III, cIV_2 – COX dimer, cIV – COX monomer, S3 and S2 – COX assembly intermediates. In (**B**) quantitative distribution of Cox1 subunit in samples solubilized at 4 g of DDM/g of protein is shown. Aliquots of 20 μg of DDM-solubilized proteins were used in (**A**). In (**C**) digitonin-solubilized proteins were loaded as follows: 20 μg of control cybrids and 30 μg of ΔTA cybrids, 10 μg of control fibroblasts and 30 μg of the SURF1 patient fibroblasts (P3 and P4).

the mitochondrial membrane potential $\Delta\psi_m$, expressed relatively to state 3-FCCP, was very low at state 2 and state 4 (3.1-times and 3.6-times lower in 9205delTA compared with the control cybrids, respectively). This clearly shows that the low content of COX drastically decreases the overall H^+-pumping activity of the respiratory chain. Only a minor decrease in state 2 $\Delta\psi_m$ was observed after the addition of ADP (state 3-ADP), the effect of which was oligomycin-sensitive. In accordance, the respiration in 9205delTA cybrids was only negligibly stimulated by ADP and the rate of respiration at state 3-ADP as well as at state 3-FCCP was very low. The both types of measurements excluded the possibility that alterations in ATP synthase structure would induce an enhanced proton leak.

In further experiments, we used cybrid cell lines with a varying 9205delTA mutation load and investigated how the mutation load affects the function of mitochondrial OXPHOS. We performed combined analysis of respiration by oxygraphic measurements of digitonin-permeabilized cells and of ATP production by estimating the ATP content in the course of coupled respiration with succinate as substrate. The rate of ADP-stimulated oxygen consumption was determined as the oligomycin-sensitive respiration in the presence of an excess of ADP (1.25 mM). Samples were collected during respiration measurements and content of the generated ATP was analysed by a coupled luciferase assay. In the same experiment, we also determined the activity of COX as the KCN-sensitive respiration induced by ascorbate + TMPD in the presence of antimycin A. In 9205delTA cybrid cell lines, both the oligomycin-sensitive ADP-stimulated respiration (Figure 7A) and ATP production (Figure 7B) were maintained at the control levels up to circa 90 % heteroplasmy. Both parameters decreased rapidly beyond this threshold. As shown in Figure 7C, COX activity displayed an analogous dependence on the mutation load. In 9205delTA homoplasmic cell line, the ADP-stimulated oligomycin-sensitive respiration, ATP production and COX activity were reduced to 10 %, 27 % and 16 % of the control values, respectively.

Altogether, these attempts to correlate the OXPHOS function, COX and ATP synthase activities as well as the primary changes in the F_o-a and Cox3 subunits with the 9205delTA mutation load revealed a highly similar threshold dependence. This implies that the energetic function of the mitochondrial OXPHOS could be proportionally related to the available quantity of these subunits. Figure 8 demonstrates that this was indeed the case as a near-linear relationship was observed between the content of the F_o-a and Cox3 subunits and the measured functional parameters: ADP-stimulated respiration, ATP synthesis and COX activity.

DISCUSSION

In the present study, we investigated a unique model of mitochondrial dysfunction based on selective down-regulation of biosynthesis of two OXPHOS subunits encoded by the mtDNA *MT-ATP6* and *MT-CO3* genes due to the altered processing and maturation of their mRNAs, caused by the mtDNA 9205delTA microdeletion.

The 9205delTA mutation has so far been found in only two cases that differed markedly in biochemical and clinical phenotypes, although both showed a nearly homoplasmic mutation load [3,7]. This could suggest the involvement of a nuclear-encoded factor that would take part in posttranscriptional regulation of F_o-a/Atp6 biosynthesis and thus modulate the presentation of homoplasmic mutation [7]. However, it is relatively difficult to rule out that in the "homoplasmic" cases, there are not trace amounts of wild-type mtDNA present. Indeed, after extended cultivation and numerous passages of fibroblasts from P1 (with a milder presentation) the presence of increased and detectable level of wild-type mtDNA became apparent. This suggests that at least P1 was not 100 % homoplasmic for the 9205delTA mutation. The distinct phenotypic presentation of the two cases thus could results from differences in the mutation load with a critical threshold for disease manifestation present at a very high heteroplasmy level. To unravel the biochemical consequences of the mtDNA 9205delTA microdeletion, we prepared a panel of cybrid cell lines with variable heteroplasmy ranging from 52 % to 100 % and investigated the structure and function of ATP synthase and COX at different heteroplasmy levels.

The first important finding of these studies was that the homoplasmic mtDNA 9205delTA microdeletion leads to down-regulation of the content of both F_o-a and Cox3 subunits to less than 20 % and 10 %, respectively, relative to the control. The

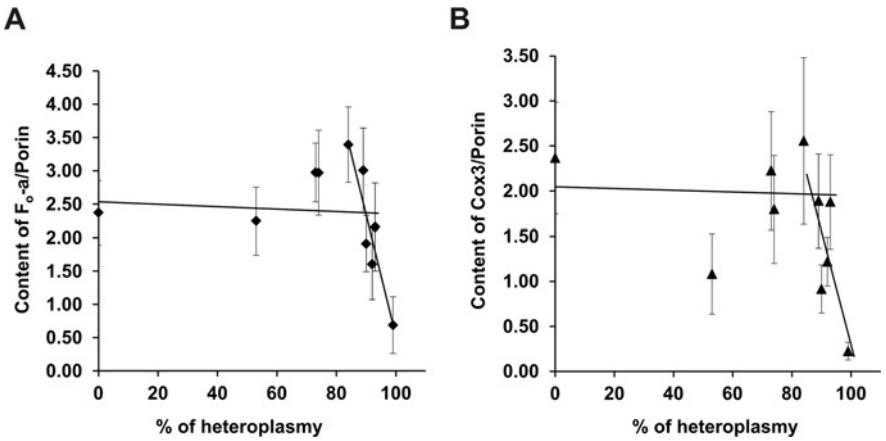

Figure 5 Dependence of subunit F_o-a and Cox3 content on the 9205delTA mutation load

Specific content of (**A**) F_o-a and (**B**) Cox3 subunits was determined in mitochondria of control and 9205delTA cybrid clones by SDS-PAGE and WB, normalized to the content of porin and plotted against the 9205delTA mutation load expressed as a percentage. Data are the means ± S.E.M. for three experiments.

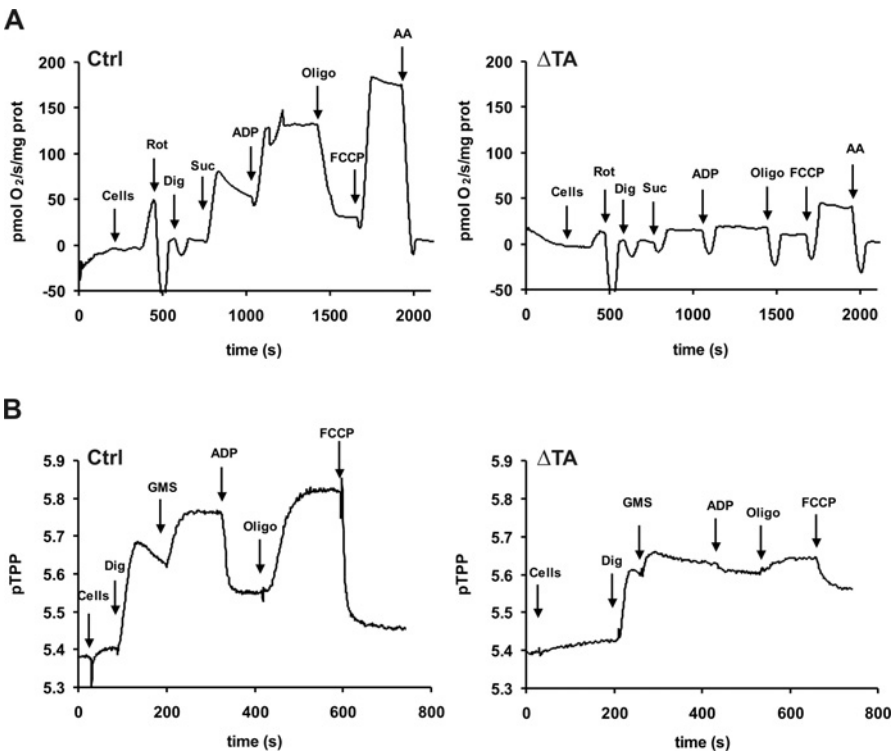

Figure 6 Respiration and mitochondrial membrane potential analysis in control and 9205delTA homoplasmic cybrid mitochondria

(**A**) Respiration and (**B**) TPP^+ measurement of $\Delta\psi_m$ were performed in control (Ctrl) and 9205delTA homoplasmic (ΔTA) cybrids permeabilized with digitonin (Dig) using glutamate (G), malate (M), succinate (Suc, S), ADP, oligomycin (Oligo), FCCP and antimycin A (AA) as indicated.

previously observed insufficient maturation of the *MT-ATP6* and *MT-CO3* mRNAs originating from the polycistronic primary transcript (*MT-ATP8*/*MT-ATP6*/*MT-CO3*) [7] thus decreases the efficacy of their translation to a very low level. Here we show that all the successive changes in the biogenesis and function of OXPHOS complexes cIV and cV are caused by the lack of these two proteins.

The manifestation of the 9205delTA microdeletion in the cybrid cell lines displayed a non-linear dependence on the mutation load and exerted a threshold effect at about 90 % heteroplasmy. This dependence was observed at several levels – the content of subunits F_o-a and Cox3, the content and activity of COX, as well as OXPHOS function measured as coupled respiration and ATP synthesis. Apparently, the non-linear threshold character of the dependence of structural-functional consequences of the 9205delTA mutation originates at the gene–protein level, due to post-transcriptional events affecting the amount of translated subunits F_o-a and Cox3. The 9205delTA microdeletion thus behaves similarly to missense mutations of *MT-ATP6* although the underlying mechanism is mRNA processing and maturation.

From the bioenergetics point of view, it is difficult to conclude which enzyme deficiency is more critical for the disease progression. There was no real difference in threshold effects

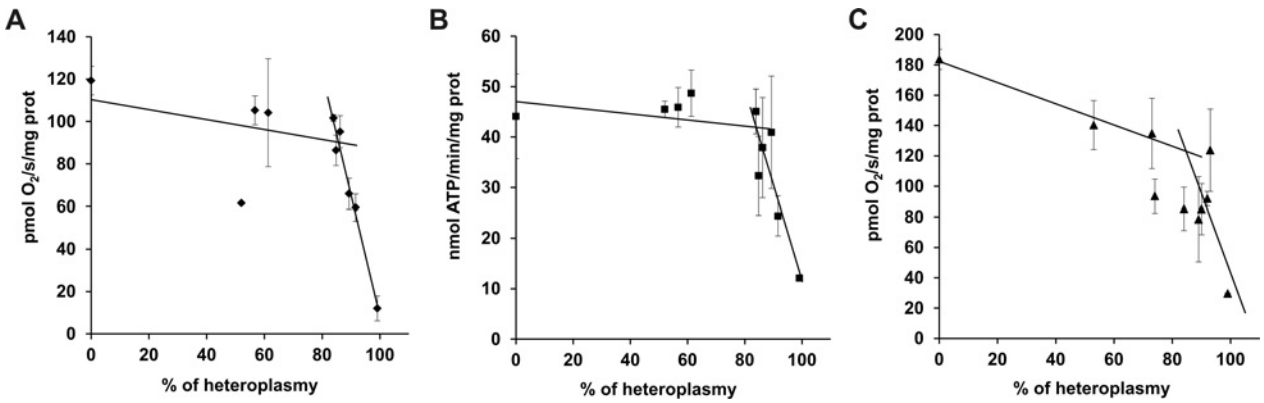

Figure 7 Dependence of ADP-stimulated respiration and ATP synthase and cytochrome *c* oxidase activities on the 9205delTA mutation load

In cybrid cells permeabilized with digitonin, (**A**) ADP-stimulated, oligomycin-sensitive respiration with succinate was measured by oxygraphy, (**B**) ATP production was measured by luciferase assay and (**C**) cytochrome *c* oxidase activity was measured as antimycin A + TMPD + ascorbate oxygen consumption sensitive to KCN. All three parameters were expressed per mg of protein and plotted against the 9205delTA mutation load expressed as a percentage. Data are the means ± S.E.M. for three experiments.

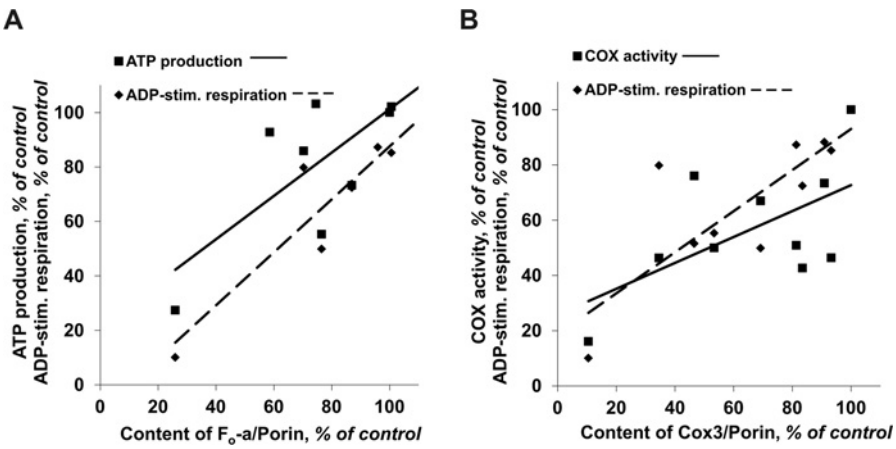

Figure 8 Correlations among 9205delTA-dependent variables

ADP-stimulated respiration, ATP synthesis and cytochrome *c* oxidase activity were plotted against the content of (**A**) F_o-a or (**B**) Cox3 subunits, as indicated, using data from Figures 5 and 7. All values are expressed as a percentage of control.

of COX activity, ADP-stimulated respiration and ATP synthesis. However, the measurements of mitochondrial membrane potential indicated that respiration-dependent proton translocation is severely affected by 9205delTA homoplasmy despite the fact that about 15–20 % of assembled COX and COX activity was preserved. This would imply that the deficiency of COX might be primary and more critical for the overall mitochondrial energy provision.

Our analysis of subunits and assembly forms of cIV and cV revealed, in accordance with our previous studies [7], that for COX, the lack of Cox3 limits the amount of the matured enzyme, but not its structure, while in the case of ATP synthase it is the quality of the enzyme, which is changed – lack of F_o-a results in the production of incomplete, labile and non-functional enzyme.

COX consists of 13 subunits. The three largest mtDNA-encoded Cox1, Cox2 and Cox3 form the catalytic core, the ten small regulatory subunits (Cox4, Cox5a, Cox5b, Cox6a, Cox6b, Cox6c, Cox7a, Cox7b, Cox7c and Cox8) are encoded in the nuclear genome. COX assembly is a stepwise process, which proceeds through several intermediates (S1–S4) [24]. Cox1 represents the first intermediate S1 which progresses to Cox1–Cox4–Cox5a sub-assembly. Subsequently, Cox2 joins this intermediate S2. The process continues with the formation of intermediate S3 after the addition of Cox3 and most of the other remaining subunits. The COX holoenzyme formation (S4) is then completed by the addition of Cox7a/b and Cox6a to S3 [24–27].

At least 14 different heteroplasmic and/or homoplasmic mutations in the *MT-CO3* gene have been reported (www.mitomap.org); and in most cases the decrease in COX activity associates with the defect in COX biogenesis. The clinical outcomes are variable, from optic neuropathies, through Alzheimer's disease, rhabdomyolysis, mitochondrial encephalopathies and myopathies with lactic acidosis, to Leigh or Leigh-like syndromes (LS, LLS). Analysis of affected families in accordance with the studies of the cybrid cell lines revealed that the severity of several *MT-CO3* mutations is heteroplasmy-dependent [28–31]. Interestingly, an improvement in clinical presentation in the case of the 9379G>A mutation was connected with a pronounced decrease in the mutation load [32].

As with many other mtDNA-encoded proteins, most of the *MT-CO3* mutations are single base pair transitions that change highly conserved amino acid residues. Predominantly, they are proposed to affect the interaction of Cox3 with Cox1, or they create a premature stop codon [33,34]. Another type of mutation

is a single base pair insertion or deletion [35,36] leading to the synthesis of truncated Cox3 protein. In addition, a 15-bp deletion, 9480del15, that removes five amino acids (two of them highly conserved) in the third transmembrane region of Cox3 protein was described [29]. This caused pronounced down-regulation of Cox3 steady state levels, similar to the frameshift mutation 9537insC leading to the incomplete Cox3 protein of only 110 amino acids [36]. In 9480del15 cells, Cox3 was translated but was highly unstable. In 9537insC cybrids, the mature *MT-CO3* mRNA was present but was not translated, while in our case of 9205delTA, the low Cox3 content was due to the altered splicing and maturation of the *MT-CO3* transcript. These Cox3-lacking cell lines displayed a pronounced decrease in the content of Cox1 and Cox2 but not of Cox4. No change in Cox5a was found in 9537insC and our 9205delTA cybrids (Figure 2) or in 9952G>A muscle [33] while Cox6c subunit content was significantly reduced in 9205delTA cybrids (Figure 2) and 9952G>A muscle. When Tiranti et al. [36] investigated COX assembly intermediates in 9537insC cybrids, they found the majority of Cox1 in S1 (free Cox1), but significant amounts of Cox1 were also associated with Cox2-containing intermediates depicted as S3 and S2a, both larger than canonical S2. In 9205delTA assembly intermediates (Figure 4), we also found most Cox1 as S1 and little as S3, but there was no indication of S2a, which appears to be specific for 9537insC cells and may reflect the presence of low levels of truncated Cox3. However, we have not observed any accumulated S2 in 9205delTA cells either (Figure 4), which may indicate that these intermediates are quickly degraded, if the COX biogenesis is stalled between S2 and S3. The relative accumulation of free small subunits Cox4 and Cox5a which we observed in our model (Figure 2) was repeatedly described also in other types of COX deficiencies, e.g. *SURF1* or *SCO1* mutations [37], and stems from their relative resistance to degradation.

ATP synthase complex is composed of 16 different subunits organized into membrane-extrinsic F_1 catalytic part (F_1-α, F_1-β, F_1-γ, F_1-δ and F_1-ε subunits) and membrane-embedded F_o part (F_o-a, F_o-c, F_o-e, F_o-f, F_o-g, A6L, F_o-b, F_o-d, F_6 and OSCP) that are connected by two stalks [38]. Small regulatory subunit IF_1 binds to F_1 at low pH and prevents the enzyme from undergoing a switch to hydrolytic mode and ATP hydrolysis. The formation of ATP synthase from individual subunits is a stepwise procedure, expected to proceed via assembly of several modules, starting with an independent formation of F_1 and oligomer of F_o-c subunits [39,40]. Afterwards the F_1 is attached to the membrane-embedded c-ring and the subunits of peripheral arm and of the membranous subcomplex are added. In the last stage the enzyme structure is completed by incorporation of the two mtDNA-encoded subunits, F_o-a and A6L [22].

Over 20 mutations in the mtDNA *MT-ATP6* gene have been reported, all of them single base pair missense mutations. They have been associated with variable brain, heart and muscle disorders, but also with autism, multiple sclerosis, optic neuropathy and diabetes in combination with other mtDNA mutations (www.mitomap.org). The most common are 8993 T>G and T>C mutations manifesting as early-onset maternally inherited Leigh syndrome (MILS) or milder neurogenic muscle weakness, ataxia, and retinitis pigmentosa (NARP) [41–43]. T>G mutations are clinically and biochemically more deleterious, T>C transitions are less frequent and rather late-onset. Similar features were described for the second most common transitions at nt 9176, T>G and T>C associated with LS or familial bilateral striatal necrosis [44,45]. The 9176T>C mutation was also found in the patients with Charcot-Marie-Tooth hereditary neuropathy [46] or the late-onset hereditary spastic paraplegia [47]. Other rare *MT-ATP6* mutations (9185T>C, 9191T>C, 8851T>C, 8989G>C, 8839G>C, 8597T>C) present as LS, LLS, NARP or cardiomyopathy [48–54].

Distinct phenotypes of different *MT-ATP6* mutations are related to the mutation load, but with variable relationships between heteroplasmy and phenotypic presentation. The asymptomatic family members often have a mutation load lower than the affected patients; however, the implicated threshold mutation level for the disease manifestation varies. The best example of phenotypic dependence on the mutation load represents 8993T>G transition – the severity of the disease increases with the mutation load and a milder NARP manifests at lower heteroplasmy (around 70 %) than early-onset devastating MILS (around 90 %). In some cases the severity of symptoms in 8993 patients was found to be heteroplasmy-dependent but without a distinct threshold level for the disease manifestation [55–57] or even with a linear correlation between the mutation load and biochemical parameters [58]. As discussed above, the biochemical defects and the severity of the 9205delTA disease appear to be also heteroplasmy-dependent and point to a steep decline in mitochondrial energy provision above the threshold close to mutation homoplasmy. Interestingly, the healthy mother of the second patient had 85 % heteroplasmy in the blood and 92 % heteroplasmy in fibroblasts [7]. Considering the results obtained in the cybrid cells, the threshold of 9205delTA mutation occurs above 90 % heteroplasmy.

The pathogenicity of *MT-ATP6* mutations is usually given by decreased synthesis of ATP due to defective translocation of the protons across the membrane in 9176T>G mutation [59], or by inefficient coupling between proton translocation and synthesis of ATP in the 8993T>G, 8993T>C, 9035T>C, 9176T>C and 8839G>C mutations [53,57–61]. In the 8993T>C, 9035T>C and 9176T>C mutations, the ATP synthesis is not that severely affected and increased production of ROS (reactive oxygen species) can also contribute to the proposed pathogenic mechanism [47,57,60]. In the 9205delTA mutation, severe reduction in the production of ATP is given by the lack of subunit F_o-a, making the F_o proton channel unable to translocate protons as the reduction in ATP synthesis is accompanied with decreased ADP-stimulated respiration and almost no effect of ADP on mitochondrial membrane potential.

From the structural point of view, the insufficient production of F_o-a subunit resulted in the formation of several BNE-resolved F_1-containing complexes which were smaller than ATP synthase monomer. On the other hand the total amount of various intermediates from F_1 up was normal or even increased. The size of these subcomplexes (460, 380 and 350 kDa), their relative abundance and involvement of F_o subunits closely resembled such complexes found in cells with *MT-ATP6* mutations, ρ° cells, cells upon mtDNA depletion or inhibition of mitochondrial protein synthesis [18,19,21,62–65], where they represent breakdown products of fully assembled ATP synthase complex rather than assembly intermediates. As demonstrated by our hrCNE1 analysis, ATP synthase devoid of subunit F_o-a had a size only ~60 kDa smaller than the control enzyme and was detected as the only form of the 9205delTA enzyme when Coomassie Blue G was omitted. Our data thus provide clear evidence that, in the absence of F_o-a, the almost complete F_1F_o-ATP synthase complex can be quantitatively formed.

F_o-a-deficient cells represent a valuable model for a better understanding of the assembly of mitochondrial ATP synthase structure as well as its function. F_o-a/Atp6 has been implicated as the last subunit incorporating into the enzyme complex during biosynthesis of both the eukaryotic and the prokaryotic enzyme. Our data suggest that ATP synthase lacking F_o-a is assembled and incorporated into the membrane. This is evident from the hrCNE1 experiments, where we could resolve fully assembled (albeit

without F_o-a) enzyme. However, this complex becomes unstable and dissociates when exposed to Coomassie Blue G. After the dye binds to the proteins, it introduces negative charge which apparently breaks down some fragile inter-subunit interactions which keep the F_1c rotor structure connected with the external stalk of the enzyme in the absence of F_o-a. After Coomassie Blue G binding, the major form of F_o-a-deficient enzyme had molecular mass of approximately 460 kDa and contained F_1 subunits and subunit F_o-c, but not subunits F_o-d and OSCP.

The F_o-a-deficient ATP synthase was unable to synthesize ATP but did not leak the protons as both the respiration and mitochondrial membrane potential were affected by FCCP. When an analogous model of bacterial ATP synthase lacking subunit F_o-a was investigated [66], the enzyme complex was found to be rather stable. It could be isolated upon solubilization with Triton X-100 and deoxycholate, incorporated into liposomes and the isolated F_o lacking F_o-a could be reconstituted with F_1. The bacterial enzyme lacking F_o-a was also not proton leaky and, as expected, unable to synthesize ATP as the proton channel was inactive. The absence of F_o-a in the bacterial enzyme further decreased/prevented ATP-hydrolytic activity, indicating that altered F_o structure, possibly the anomalous interaction between c-ring subunits and subunits F_o-b, prevented the rotor rotation. In contrast, the F_o-a-deficient 9205delTA enzyme retained its hydrolytic activity [7], suggesting that c-ring rotation was possible and not hampered, possibly reflecting differences in structure between bacterial and mammalian mitochondrial F_o.

AUTHOR CONTRIBUTION

Josef Houštěk and Kateřina Hejzlarová conceived and designed the experiments. Vilma Kaplanová and Kateřina Hejzlarová prepared cybrid cell lines and analysed mtDNA. Kateřina Hejzlarová and Nikola Kovářová performed electrophoretic experiments, Kateřina Hejzlarová, Pavel Ješina, Hana Nůsková and Zdeněk Drahota performed oxygraphic and spectrophotometric measurements. Kateřina Hejzlarová, Sara Seneca, Tomáš Mráček and Josef Houštěk analysed the data and wrote the paper.

ACKNOWLEDGEMENTS

We acknowledge helpful comments on the manuscript by Professor R.N. Lightowlers and Professor Z.M. Chrzanowska-Lightowlers before submission.

FUNDING

This work was supported by the Grant Agency of the Czech Republic [grant numbers GAP303/11/0970, GAP303/12/1363 and GB14-36804G] and Ministry of Education, Youth and Sports of the Czech Republic [grant number LL1204, RVO:67985823].

REFERENCES

1 DiMauro, S. (2007) Mitochondrial DNA medicine. Biosci. Rep. **27**, 5–9 CrossRef PubMed
2 Ruiz-Pesini, E., Lott, M.T., Procaccio, V., Poole, J.C., Brandon, M.C., Mishmar, D., Yi, C., Kreuziger, J., Baldi, P. and Wallace, D.C. (2007) An enhanced MITOMAP with a global mtDNA mutational phylogeny. Nucleic Acids Res **35**, D823–D828 CrossRef PubMed
3 Seneca, S., Abramowicz, M., Lissens, W., Muller, M.F., Vamos, E. and de Meirleir, L. (1996) A mitochondrial DNA microdeletion in a newborn girl with transient lactic acidosis. J. Inherit. Metab. Dis. **19**, 115–118 CrossRef PubMed
4 Temperley, R.J., Seneca, S.H., Tonska, K., Bartnik, E., Bindoff, L.A., Lightowlers, R.N. and Chrzanowska-Lightowlers, Z.M. (2003) Investigation of a pathogenic mtDNA microdeletion reveals a translation-dependent deadenylation decay pathway in human mitochondria. Hum. Mol. Genet. **12**, 2341–2348 CrossRef PubMed
5 Chrzanowska-Lightowlers, Z.M., Temperley, R.J., Smith, P.M., Seneca, S.H. and Lightowlers, R.N. (2004) Functional polypeptides can be synthesized from human mitochondrial transcripts lacking termination codons. Biochem. J. **377**, 725–731 CrossRef PubMed
6 Fornuskova, D., Tesarova, M., Hansikova, H. and Zeman, J. (2003) New mtDNA mutation 9204delTA in a family with mitochondrial encephalopathy and ATP synthase defect. Cas. Lek. Cesk. **142**, 313
7 Jesina, P., Tesarova, M., Fornuskova, D., Vojtiskova, A., Pecina, P., Kaplanova, V., Hansikova, H., Zeman, J. and Houstek, J. (2004) Diminished synthesis of subunit a (ATP6) and altered function of ATP synthase and cytochrome c oxidase due to the mtDNA 2 bp microdeletion of TA at positions 9205 and 9206. Biochem. J. **383**, 561–571 CrossRef PubMed
8 Rossignol, R., Faustin, B., Rocher, C., Malgat, M., Mazat, J.P. and Letellier, T. (2003) Mitochondrial threshold effects. Biochem. J. **370**, 751–762 CrossRef PubMed
9 Tiranti, V., Munaro, M., Sandona, D., Lamantea, E., Rimoldi, M., DiDonato, S., Bisson, R. and Zeviani, M. (1995) Nuclear DNA origin of cytochrome c oxidase deficiency in Leigh's syndrome: genetic evidence based on patient's-derived rho degrees transformants. Hum. Mol. Genet. **4**, 2017–2023 CrossRef PubMed
10 Bentlage, H.A., Wendel, U., Schagger, H., ter Laak, H.J., Janssen, A.J. and Trijbels, J.M. (1996) Lethal infantile mitochondrial disease with isolated complex I deficiency in fibroblasts but with combined complex I and IV deficiencies in muscle. Neurology **47**, 243–248 CrossRef PubMed
11 Wittig, I., Braun, H.P. and Schagger, H. (2006) Blue native PAGE. Nat. Protoc. **1**, 418–428 CrossRef PubMed
12 Schagger, H. and von Jagow, G. (1987) Tricine-sodium dodecyl sulfate-polyacrylamide gel electrophoresis for the separation of proteins in the range from 1 to 100 kDa. Anal. Biochem. **166**, 368–379 CrossRef PubMed
13 Schagger, H. and von Jagow, G. (1991) Blue native electrophoresis for isolation of membrane protein complexes in enzymatically active form. Anal. Biochem. **199**, 223–231 CrossRef PubMed
14 Wittig, I., Karas, M. and Schagger, H. (2007) High resolution clear native electrophoresis for in-gel functional assays and fluorescence studies of membrane protein complexes. Mol. Cell. Proteomics **6**, 1215–1225 CrossRef PubMed
15 Wittig, I., Carrozzo, R., Santorelli, F.M. and Schagger, H. (2007) Functional assays in high-resolution clear native gels to quantify mitochondrial complexes in human biopsies and cell lines. Electrophoresis **28**, 3811–3820 CrossRef PubMed
16 Havlickova, V., Kaplanova, V., Nuskova, H., Drahota, Z. and Houstek, J. (2010) Knockdown of F1 epsilon subunit decreases mitochondrial content of ATP synthase and leads to accumulation of subunit c. Biochim. Biophys. Acta **1797**, 1124–1129 CrossRef PubMed
17 Ouhabi, R., Boue-Grabot, M. and Mazat, J.P. (1998) Mitochondrial ATP synthesis in permeabilized cells: assessment of the ATP/O values *in situ*. Anal. Biochem. **263**, 169–175 CrossRef PubMed
18 Carrozzo, R., Wittig, I., Santorelli, F.M., Bertini, E., Hofmann, S., Brandt, U. and Schagger, H. (2006) Subcomplexes of human ATP synthase mark mitochondrial biosynthesis disorders. Ann. Neurol. **59**, 265–275 CrossRef PubMed
19 Smet, J., Seneca, S., De Paepe, B., Meulemans, A., Verhelst, H., Leroy, J., De Meirleir, L., Lissens, W. and Van Coster, R. (2009) Subcomplexes of mitochondrial complex V reveal mutations in mitochondrial DNA. Electrophoresis **30**, 3565–3572 CrossRef PubMed
20 Wittig, I., Carrozzo, R., Santorelli, F.M. and Schagger, H. (2006) Supercomplexes and subcomplexes of mitochondrial oxidative phosphorylation. Biochim. Biophys. Acta **1757**, 1066–1072 CrossRef PubMed
21 Houstek, J., Klement, P., Hermanska, J., Houstkova, H., Hansikova, H., Van den Bogert, C. and Zeman, J. (1995) Altered properties of mitochondrial ATP-synthase in patients with a T–>G mutation in the ATPase 6 (subunit a) gene at position 8993 of mtDNA. Biochim. Biophys. Acta **1271**, 349–357 CrossRef PubMed
22 Wittig, I., Meyer, B., Heide, H., Steger, M., Bleier, L., Wumaier, Z., Karas, M. and Schagger, H. (2010) Assembly and oligomerization of human ATP synthase lacking mitochondrial subunits a and A6L. Biochim. Biophys. Acta **1797**, 1004–1011 CrossRef PubMed
23 Kovarova, N., Cizkova Vrbacka, A., Pecina, P., Stranecky, V., Pronicka, E., Kmoch, S. and Houstek, J. (2012) Adaptation of respiratory chain biogenesis to cytochrome c oxidase deficiency caused by SURF1 gene mutations. Biochim. Biophys. Acta **1822**, 1114–1124 CrossRef PubMed
24 Nijtmans, L.G., Taanman, J.W., Muijsers, A.O., Speijer, D. and Van den Bogert, C. (1998) Assembly of cytochrome-c oxidase in cultured human cells. Eur. J. Biochem. **254**, 389–394 CrossRef PubMed
25 Tiranti, V., Galimberti, C., Nijtmans, L., Bovolenta, S., Perini, M.P. and Zeviani, M. (1999) Characterization of SURF-1 expression and Surf-1p function in normal and disease conditions. Hum. Mol. Genet. **8**, 2533–2540 CrossRef PubMed
26 Stiburek, L., Hansikova, H., Tesarova, M., Cerna, L. and Zeman, J. (2006) Biogenesis of eukaryotic cytochrome c oxidase. Physiol. Res. **55** (Suppl 2), S27–S41 PubMed
27 Fornuskova, D., Stiburek, L., Wenchich, L., Vinsova, K., Hansikova, H. and Zeman, J. (2010) Novel insights into the assembly and function of human nuclear-encoded cytochrome c oxidase subunits 4, 5a, 6a, 7a and 7b. Biochem. J. **428**, 363–374 CrossRef PubMed
28 Mkaouar-Rebai, E., Ellouze, E., Chamkha, I., Kammoun, F., Triki, C. and Fakhfakh, F. (2010) Molecular-clinical correlation in a family with a novel heteroplasmic Leigh syndrome missense mutation in the mitochondrial cytochrome c oxidase III gene. J. Child Neurol. **26**, 12–20 CrossRef PubMed

29 Hoffbuhr, K.C., Davidson, E., Filiano, B.A., Davidson, M., Kennaway, N.G. and King, M.P. (2000) A pathogenic 15-base pair deletion in mitochondrial DNA-encoded cytochrome c oxidase subunit III results in the absence of functional cytochrome c oxidase. J. Biol. Chem. **275**, 13994–14003 CrossRef PubMed

30 Manfredi, G., Schon, E.A., Moraes, C.T., Bonilla, E., Berry, G.T., Sladky, J.T. and DiMauro, S. (1995) A new mutation associated with MELAS is located in a mitochondrial DNA polypeptide-coding gene. Neuromuscul. Disord. **5**, 391–398 CrossRef PubMed

31 Bortot, B., Barbi, E., Biffi, S., Angelini, C., Faleschini, E., Severini, G.M. and Carrozzi, M. (2009) Two novel cosegregating mutations in tRNAMet and COX III, in a patient with exercise intolerance and autoimmune polyendocrinopathy. Mitochondrion **9**, 123–129 CrossRef PubMed

32 Horvath, R., Lochmuller, H., Hoeltzenbein, M., Muller-Hocker, J., Schoser, B.G., Pongratz, D. and Jaksch, M. (2004) Spontaneous recovery of a childhood onset mitochondrial myopathy caused by a stop mutation in the mitochondrial cytochrome c oxidase III gene. J. Med. Genet. **41**, e75 CrossRef PubMed

33 Hanna, M.G., Nelson, I.P., Rahman, S., Lane, R.J., Land, J., Heales, S., Cooper, M.J., Schapira, A.H., Morgan-Hughes, J.A. and Wood, N.W. (1998) Cytochrome c oxidase deficiency associated with the first stop-codon point mutation in human mtDNA. Am. J. Hum. Genet. **63**, 29–36 CrossRef PubMed

34 Horvath, R., Scharfe, C., Hoeltzenbein, M., Do, B.H., Schroder, C., Warzok, R., Vogelgesang, S., Lochmuller, H., Muller-Hocker, J., Gerbitz, K.D. et al. (2002) Childhood onset mitochondrial myopathy and lactic acidosis caused by a stop mutation in the mitochondrial cytochrome c oxidase III gene. J. Med. Genet. **39**, 812–816 CrossRef PubMed

35 Marotta, R., Chin, J., Kirby, D.M., Chiotis, M., Cook, M. and Collins, S.J. (2011) Novel single base pair COX III subunit deletion of mitochondrial DNA associated with rhabdomyolysis. J. Clin. Neurosci. **18**, 290–292 CrossRef PubMed

36 Tiranti, V., Corona, P., Greco, M., Taanman, J.W., Carrara, F., Lamantea, E., Nijtmans, L., Uziel, G. and Zeviani, M. (2000) A novel frameshift mutation of the mtDNA COIII gene leads to impaired assembly of cytochrome c oxidase in a patient affected by Leigh-like syndrome. Hum. Mol. Genet. **9**, 2733–2742 CrossRef PubMed

37 Stiburek, L., Vesela, K., Hansikova, H., Pecina, P., Tesarova, M., Cerna, L., Houstek, J. and Zeman, J. (2005) Tissue-specific cytochrome c oxidase assembly defects due to mutations in SCO2 and SURF1. Biochem. J. **392**, 625–632 CrossRef PubMed

38 Walker, J.E. (2013) The ATP synthase: the understood, the uncertain and the unknown. Biochem. Soc. Trans. **41**, 1–16 CrossRef PubMed

39 Ackerman, S.H. and Tzagoloff, A. (2005) Function, structure, and biogenesis of mitochondrial ATP synthase. Prog. Nucleic Acid Res. Mol. Biol. **80**, 95–133 CrossRef PubMed

40 Rak, M., Gokova, S. and Tzagoloff, A. (2011) Modular assembly of yeast mitochondrial ATP synthase. EMBO J. **30**, 920–930 CrossRef PubMed

41 Holt, I.J., Harding, A.E., Petty, R.K. and Morgan-Hughes, J.A. (1990) A new mitochondrial disease associated with mitochondrial DNA heteroplasmy. Am. J. Hum. Genet. **46**, 428–433 PubMed

42 Vazquez-Memije, M.E., Shanske, S., Santorelli, F.M., Kranz-Eble, P., De Vivo, D.C. and DiMauro, S. (1998) Comparative biochemical studies of ATPases in cells from patients with the T8993G or T8993C mitochondrial DNA mutations. J. Inherit. Metab. Dis. **21**, 829–836 CrossRef PubMed

43 Morava, E., Rodenburg, R.J., Hol, F., de Vries, M., Janssen, A., van den Heuvel, L., Nijtmans, L. and Smeitink, J. (2006) Clinical and biochemical characteristics in patients with a high mutant load of the mitochondrial T8993G/C mutations. Am. J. Med. Genet. A **140**, 863–868 CrossRef PubMed

44 Thyagarajan, D., Shanske, S., Vazquez-Memije, M., De Vivo, D. and DiMauro, S. (1995) A novel mitochondrial ATPase 6 point mutation in familial bilateral striatal necrosis. Ann. Neurol. **38**, 468–472 CrossRef PubMed

45 Carrozzo, R., Tessa, A., Vazquez-Memije, M.E., Piemonte, F., Patrono, C., Malandrini, A., Dionisi-Vici, C., Vilarinho, L., Villanova, M., Schagger, H. et al. (2001) The T9176G mtDNA mutation severely affects ATP production and results in Leigh syndrome. Neurology **56**, 687–690 CrossRef PubMed

46 Synofzik, M., Schicks, J., Wilhelm, C., Bornemann, A. and Schols, L. (2012) Charcot-Marie-Tooth hereditary neuropathy due to a mitochondrial ATP6 mutation. Eur. J. Neurol. **19**, e114–e116 CrossRef PubMed

47 Verny, C., Guegen, N., Desquiret, V., Chevrollier, A., Prundean, A., Dubas, F., Cassereau, J., Ferre, M., Amati-Bonneau, P., Bonneau, D. et al. (2011) Hereditary spastic paraplegia-like disorder due to a mitochondrial ATP6 gene point mutation. Mitochondrion **11**, 70–75 CrossRef PubMed

48 Moslemi, A.R., Darin, N., Tulinius, M., Oldfors, A. and Holme, E. (2005) Two new mutations in the MTATP6 gene associated with Leigh syndrome. Neuropediatrics **36**, 314–318 CrossRef PubMed

49 Castagna, A.E., Addis, J., McInnes, R.R., Clarke, J.T., Ashby, P., Blaser, S. and Robinson, B.H. (2007) Late onset Leigh syndrome and ataxia due to a T to C mutation at bp 9,185 of mitochondrial DNA. Am. J. Med. Genet. A **143A**, 808–816 CrossRef PubMed

50 Honzik, T., Tesarova, M., Vinsova, K., Hansikova, H., Magner, M., Kratochvilova, H., Zamecnik, J., Zeman, J. and Jesina, P. (2013) Different laboratory and muscle biopsy findings in a family with an m.8851T>C mutation in the mitochondrial MTATP6 gene. Mol. Genet. Metab. **108**, 102–105 CrossRef PubMed

51 De Meirleir, L., Seneca, S., Lissens, W., Schoentjes, E. and Desprechins, B. (1995) Bilateral striatal necrosis with a novel point mutation in the mitochondrial ATPase 6 gene. Pediatr. Neurol. **13**, 242–246 CrossRef PubMed

52 Duno, M., Wibrand, F., Baggesen, K., Rosenberg, T., Kjaer, N. and Frederiksen, A.L. (2013) A novel mitochondrial mutation m.8989G>C associated with neuropathy, ataxia, retinitis pigmentosa – the NARP syndrome. Gene **515**, 372–375 CrossRef PubMed

53 Blanco-Grau, A., Bonaventura-Ibars, I., Coll-Canti, J., Melia, M.J., Martinez, R., Martinez-Gallo, M., Andreu, A.L., Pinos, T. and Garcia-Arumi, E. (2013) Identification and biochemical characterization of the novel mutation m.8839G>C in the mitochondrial ATP6 gene associated with NARP syndrome. Genes Brain Behav. **12**, 812–820 CrossRef PubMed

54 Tsai, J.D., Liu, C.S., Tsao, T.F. and Sheu, J.N. (2012) A novel mitochondrial DNA 8597T>C mutation of Leigh syndrome: report of one case. Pediatr. Neonatol. **53**, 60–62 CrossRef PubMed

55 Carelli, V., Baracca, A., Barogi, S., Pallotti, F., Valentino, M.L., Montagna, P., Zeviani, M., Pini, A., Lenaz, G., Baruzzi, A. and Solaini, G. (2002) Biochemical-clinical correlation in patients with different loads of the mitochondrial DNA T8993G mutation. Arch. Neurol. **59**, 264–270 CrossRef PubMed

56 Puddu, P., Barboni, P., Mantovani, V., Montagna, P., Cerullo, A., Bragliani, M., Molinotti, C. and Caramazza, R. (1993) Retinitis pigmentosa, ataxia, and mental retardation associated with mitochondrial DNA mutation in an Italian family. Br. J. Ophthalmol. **77**, 84–88 CrossRef PubMed

57 Baracca, A., Sgarbi, G., Mattiazzi, M., Casalena, G., Pagnotta, E., Valentino, M.L., Moggio, M., Lenaz, G., Carelli, V. and Solaini, G. (2007) Biochemical phenotypes associated with the mitochondrial ATP6 gene mutations at nt8993. Biochim. Biophys. Acta **1767**, 913–919 CrossRef PubMed

58 Sgarbi, G., Baracca, A., Lenaz, G., Valentino, L.M., Carelli, V. and Solaini, G. (2006) Inefficient coupling between proton transport and ATP synthesis may be the pathogenic mechanism for NARP and Leigh syndrome resulting from the T8993G mutation in mtDNA. Biochem. J. **395**, 493–500 CrossRef PubMed

59 Vazquez-Memije, M.E., Rizza, T., Meschini, M.C., Nesti, C., Santorelli, F.M. and Carrozzo, R. (2009) Cellular and functional analysis of four mutations located in the mitochondrial ATPase6 gene. J. Cell. Biochem. **106**, 878–886 CrossRef PubMed

60 Sikorska, M., Sandhu, J.K., Simon, D.K., Pathiraja, V., Sodja, C., Li, Y., Ribecco-Lutkiewicz, M., Lanthier, P., Borowy-Borowski, H., Upton, A., Raha, S. et al. (2009) Identification of ataxia-associated mtDNA mutations (m.4052T>C and m.9035T>C) and evaluation of their pathogenicity in transmitochondrial cybrids. Muscle Nerve **40**, 381–394 CrossRef PubMed

61 Pallotti, F., Baracca, A., Hernandez-Rosa, E., Walker, W.F., Solaini, G., Lenaz, G., Melzi D'Eril, G.V., Dimauro, S., Schon, E.A. and Davidson, M.M. (2004) Biochemical analysis of respiratory function in cybrid cell lines harbouring mitochondrial DNA mutations. Biochem. J. **384**, 287–293 CrossRef PubMed

62 Nijtmans, L.G., Klement, P., Houstek, J. and van den Bogert, C. (1995) Assembly of mitochondrial ATP synthase in cultured human cells: implications for mitochondrial diseases. Biochim. Biophys. Acta **1272**, 190–198 CrossRef PubMed

63 Buchet, K. and Godinot, C. (1998) Functional F1-ATPase essential in maintaining growth and membrane potential of human mitochondrial DNA-depleted rho degrees cells. J. Biol. Chem. **273**, 22983–22989 CrossRef PubMed

64 Nijtmans, L.G., Henderson, N.S., Attardi, G. and Holt, I.J. (2001) Impaired ATP synthase assembly associated with a mutation in the human ATP synthase subunit 6 gene. J. Biol. Chem. **276**, 6755–6762 CrossRef PubMed

65 Cortes-Hernandez, P., Vazquez-Memije, M.E. and Garcia, J.J. (2007) ATP6 homoplasmic mutations inhibit and destabilize the human F1F0-ATP synthase without preventing enzyme assembly and oligomerization. J. Biol. Chem. **282**, 1051–1058 CrossRef PubMed

66 Ono, S., Sone, N., Yoshida, M. and Suzuki, T. (2004) ATP synthase that lacks F0a-subunit: isolation, properties, and indication of F0b2-subunits as an anchor rail of a rotating c-ring. J. Biol. Chem. **279**, 33409–33412 CrossRef PubMed

Received 3 December 2014/12 January 2015; accepted 15 January 2015
Published as BJ Immediate Publication 15 January 2015, doi:10.1042/BJ20141462

OPEN ACCESS Freely available online

PLOS ONE

High Molecular Weight Forms of Mammalian Respiratory Chain Complex II

Nikola Kovářová[1☯], Tomáš Mráček[1☯], Hana Nůsková[1], Eliška Holzerová[1], Marek Vrbacký[1], Petr Pecina[1], Kateřina Hejzlarová[1], Katarína Kľučková[2], Jakub Rohlena[2], Jiri Neuzil[2,3], Josef Houštěk[1*]

1 Department of Bioenergetics, Institute of Physiology Academy of Sciences of the Czech Republic, Prague, Czech Republic, **2** Laboratory of Molecular Therapy, Institute of Biotechnology Academy of Sciences of the Czech Republic, Prague, Czech Republic, **3** Apoptosis Research Group, School of Medical Science and Griffith Health Institute, Griffith University, Southport, Queensland, Australia

Abstract

Mitochondrial respiratory chain is organised into supramolecular structures that can be preserved in mild detergent solubilisates and resolved by native electrophoretic systems. Supercomplexes of respiratory complexes I, III and IV as well as multimeric forms of ATP synthase are well established. However, the involvement of complex II, linking respiratory chain with tricarboxylic acid cycle, in mitochondrial supercomplexes is questionable. Here we show that digitonin-solubilised complex II quantitatively forms high molecular weight structures (CII_{hmw}) that can be resolved by clear native electrophoresis. CII_{hmw} structures are enzymatically active and differ in electrophoretic mobility between tissues (500 – over 1000 kDa) and cultured cells (400–670 kDa). While their formation is unaffected by isolated defects in other respiratory chain complexes, they are destabilised in mtDNA-depleted, rho0 cells. Molecular interactions responsible for the assembly of CII_{hmw} are rather weak with the complexes being more stable in tissues than in cultured cells. While electrophoretic studies and immunoprecipitation experiments of CII_{hmw} do not indicate specific interactions with the respiratory chain complexes I, III or IV or enzymes of the tricarboxylic acid cycle, they point out to a specific interaction between CII and ATP synthase.

Citation: Kovářová N, Mráček T, Nůsková H, Holzerová E, Vrbacký M, et al. (2013) High Molecular Weight Forms of Mammalian Respiratory Chain Complex II. PLoS ONE 8(8): e71869. doi:10.1371/journal.pone.0071869

Editor: Nagendra Yadava, UMASS-Amherst/Tufts University School of Medicine, United States of America

Received May 14, 2013; **Accepted** July 10, 2013; **Published** August 13, 2013

Funding: This work was supported by the Grant Agency of the Czech Republic (P303/10/P227, P301/10/1937), Ministry of Education, Youth and Sports of the Czech Republic (ERC CZ LL1204 and RVO: 67985823) and Ministry of Health of the Czech Republic (NT12370-5). The funders had no role in study design, data collection and analysis, decision to publish, or preparation of the manuscript.

Competing interests: The authors have declared that no competing interests exist.

* E-mail: houstek@biomed.cas.cz

☯ These authors contributed equally to this work.

Introduction

The mitochondrial oxidative phosphorylation system (OXPHOS) is the main source of energy in mammals. This metabolic pathway is localised in the inner mitochondrial membrane (IMM) and includes the respiratory chain complexes I, II, III and IV (CI, CII, CIII, CIV), ATP synthase (complex V, CV), plus the mobile electron transporters coenzyme Q (CoQ) and cytochrome *c*. Energy released by oxidation of NADH and $FADH_2$ is utilised for proton transport across the membrane to establish proton gradient. The resulting electrochemical potential ($\Delta\mu_H^+$) is then utilised as a driving force for phosphorylation of ADP by ATP synthase.

CII (succinate: ubiquinone oxidoreductase; EC 1.3.5.1), catalyses electron transfer from succinate (via $FADH_2$) to CoQ and thus represents important crossroads of cellular metabolism, interconnecting the tricarboxylic acid (TCA) cycle and the respiratory chain [1]. It consists of 4 nuclear encoded subunits. The hydrophilic head of CII is formed by the SDHA subunit with covalently bound FAD and the SDHB subunit, which contains three Fe–S centres. The SDHC and SDHD subunits form the hydrophobic membrane anchor and are the site of cytochrome *b* binding [2].

Mutations in genes coding for any of the CII subunits are associated with severe neuroendocrine tumours such as paraganglioma and phaeochromocytoma [3–5] as well as other tumour types, including gastrointestinal stromal tumours [6] or renal tumours [7]. Conversely, the CII subunits also function as tumour suppressors and represent one of the potential molecular targets of anti-cancer drugs [8], whose mechanisms of action could lead to apoptosis of cancer cells through the inhibition of CII and a consequent metabolic collapse.

In comparison with other respiratory chain complexes, the assembly of CII has not yet been fully characterised. Up to now, two evolutionarily conserved assembly factors for CII have been described; SDHAF1 was discovered as disease-

causing gene in a case of infantile leukoencephalopathy presenting with a decrease in the CII content and activity [9]. The LYR motif in the protein structure suggests its role in the metabolism of the Fe–S centres [10]. The second assembly factor, SDH5, is a soluble mitochondrial matrix protein, which is most likely required for insertion of FAD into the SDHA subunit [11].

Recent studies indicate that the organisation of the OXPHOS complexes in the inner mitochondrial membrane (IMM) is characterised by non-stochastic protein–protein interactions. Individual complexes specifically interact with each other to create supramolecular structures referred to as supercomplexes (SCs). SCs behave as individual functional units, enabling substrate channelling [12]; more effective electron transport should prevent electron leak and reactive oxygen species generation [13]. Besides the kinetic advantage, SCs stabilise OXPHOS complexes and help to establish the IMM ultrastructure [14].

To date, the presence of CII in SCs is still a matter of debate. In yeast and mammalian mitochondria, the interaction of CI, III, IV and V within different types of SCs has been proven using native electrophoretic techniques in combination with mild detergents and/or the Coomassie Blue G (CBG) dye [15,16]. However, the presence of CII in such structures has only been reported by Acín-Peréz et al. [17], who described the existence of a large respirasome comprising all OXPHOS complexes including CII in mammalian cells. On the other hand, CII has been detected as a structural component of the mitochondrial ATP-sensitive K^+ channel (mitoK_{ATP}) [18]. Such structures do indeed represent higher molecular forms of CII, but their structural and physiological importance remains to be investigated.

CII as the only membrane bound component of the TCA cycle could also form complexes with other TCA cycle proteins, e.g. with its functional neighbours fumarase and succinyl CoA lyase. Different studies indicate the existence of a TCA cycle metabolon and possible supramolecular organisation of various parts of the TCA cycle [19,20], but these may be significantly more labile than the well described respiratory chain SCs.

In the present study we demonstrate the existence of high molecular weight forms of CII (CII_{hmw}), i.e. SCs containing CII, using mitochondrial membrane solubilisation with mild non-ionic detergents followed by electrophoretic analysis. These complexes are rather labile, and the presence of n-dodecyl-β-D-maltoside or CBG during the electrophoretic separation causes their dissociation to individual units. CII_{hmw} structures differ in their electrophoretic migration between mammalian cells and tissues, and their formation depends on the presence of the functional respiratory chain. Our experiments also clearly indicate the association of CII with CV.

Materials and Methods

Cell lines

The following cell lines were used in experiments: control human fibroblasts and fibroblasts from patients with isolated deficiency of CI (an unknown mutation), CIV (the *SURF1* mutation, described in [21,22]), CV (the *TMEM70* mutation described in [23]), human rho0 (ρ^0) cells (mtDNA-depleted 143B TK^- osteosarcoma cells [24]), human embryonic kidney cells HEK293, primary mouse (derived from the C57/Bl6 strain) and rat (derived from the SHR strain) fibroblasts. All cell lines were grown in the high-glucose DMEM medium (Lonza) supplemented with 10% (v/v) foetal bovine serum (Sigma) at 37 °C in 5% CO_2 atmosphere. Cells were harvested using 0.05% trypsin and 0.02% EDTA and stored as pellets at -80 °C.

Isolation of cell membranes and mitochondria from cells and tissues

Mitochondria from cultured cells were isolated after cell disruption by hypotonic shock as described [25]. In some experiments, membrane fractions from fibroblasts were prepared as described [26]. Human heart mitochondria and mitochondria from rat heart, liver and brown adipose tissues were isolated according to established procedures [27]. The protein concentration was measured by the Bradford method (BioRad).

Ethical aspects

All work involving human samples was carried out in accordance with the Declaration of Helsinki of the World Medical Association and was approved by the Ethics Committee of the Institute of Physiology, Academy of Sciences of the Czech Republic v.v.i. The written informed consent was obtained from patients or patients' parents.

All animal tissues were obtained on the basis of approval by the Expert Committee for Work with Animals of the Institute of Physiology, Academy of Sciences of the Czech Republic v.v.i. (Permit Number: 165/2010) and animal work was in accordance with the EU Directive 2010/63/EU for animal experiments.

Electrophoresis and western blot analysis

Isolated membranes or mitochondria were solubilised with digitonin (Sigma, 4 g/g protein) in an imidazole buffer (2 mM aminohexanoic acid, 1 mM EDTA, 50 mM NaCl, 50 mM imidazole, pH 7.0) for 15 min at 0 °C and centrifuged for 20 min at 20 000 *g* [26]. Samples were prepared by adding 5% (v/v) glycerol and 0.005% (v/v) Ponceau S dye for clear native and high resolution clear native electrophoresis (CNE, hrCNE3), or 5% (v/v) glycerol and CBG dye (Serva Blue G 250, 1:8 ratio (w/w) to digitonin) for blue native electrophoresis (BNE). Separation of mitochondrial proteins was performed using CNE, BNE [26] and hrCNE3 [28] on 6–15% polyacrylamide gradient gels using the Mini-Protean apparatus (BioRad). For 2D separation by CNE/SDS PAGE, the gel after CNE was cut into stripes that were incubated in 1% SDS and 1% 2-mercaptoethanol for 1 h and then subjected to SDS PAGE on a 10% slab gel [29]. In case of 2D separation by CNE/CNE_{CBG}, gel stripes after CNE were incubated in 3% CBG in the CNE cathode buffer for 1 h and then subjected to CNE on 6–15% gradient gels.

For western blot immunodetection, the separated proteins were transferred to a PVDF membrane (Immobilon-P, Millipore) by semi-dry electrotransfer. The membranes were blocked with 5% (w/v) non-fat dried milk in TBS (150 mM NaCl, 10 mM Tris,

pH 7.5) for 1 h and incubated overnight at 4 °C with specific primary antibodies diluted in TBST (TBS with 0.1% Tween-20). Monoclonal or polyclonal primary antibodies to the following enzymes of OXPHOS or TCA cycle were used: SDHA (ab14715, Abcam), SDHB (ab14714, Abcam), Core1 (ab110252, Abcam), NDUFA9 (ab14713, Abcam), Cox4 (ab14744, ab110261, Abcam), citrate synthase (ab129095, Abcam), isocitrate dehydrogenase (α subunit, ab58641, Abcam), aconitase 2 (ab110321, Abcam), α subunit of CV [30], fumarase (M01, Abnova), succinyl-CoA synthetase (α subunit, 5557, Cell Signaling Technology) and malate dehydrogenase (8610, Cell Signaling Technology). The detection of the signals was performed with the secondary Alexa Fluor 680-labelled antibody (Life Technologies) using the Odyssey fluorescence scanner (LI-COR).

Enzyme in-gel activity staining

In-gel activity assays were performed after separation of the respiratory complexes using CNE. For CIV in-gel activity staining, we used a recently described protocol [21]. The in-gel activity assay of the CV ATP hydrolytic activity was performed as described [28]. The activity of CII was detected using the modified succinate: nitroblue tetrazolium reductase assay [28]. Briefly, gel slices from CNE were incubated for 1 h (for tissues) or overnight (for cells) at room temperature in the dark in the staining solution (200 mM Tris, pH 7.4), 10 mM EDTA, 1 mg/mL nitroblue tetrazolium, 80 μM phenazine methosulfate, 2 mM KCN, 1.5 μg/mL rotenone and 30 mM succinate).

Immunoprecipitation

For co-immunoprecipitation analysis we used a rabbit polyclonal antibody against the F_1 part of ATP synthase (reacting with the ATP synthase subunits α, γ, and predominantly β, generated in our laboratory) or a mouse monoclonal antibody against the SDHA subunit of CII (ab14715, Abcam). The antibodies were immobilised on CNBr-activated agarose matrix (Sigma). Agarose beads with the bound antibody were equilibrated in PBS (140 mM NaCl, 5 mM KCl, 8 mM Na_2HPO_4, 1.5 mM KH $_2PO_4$, pH 7.2 -7.3) supplemented with 0.2% protease inhibitor cocktail (PIC, Sigma). For storage at 4 °C, they were dissolved in PBS+PIC supplemented with 0.025% thimerosal (Sigma). Solubilisation of rat heart mitochondria and human fibroblasts was performed with digitonin (2 g/g protein) in PBS+PIC. The solubilisates were mixed with the antibody-conjugated agarose beads and diluted with PBS+PIC supplemented with the same digitonin concentration as for sample solubilisation. The mixture was incubated overnight at 4 °C on a rotating mixer. The beads were then washed three times with PBS+PIC+digitonin (the same concentration as for sample solubilisation), PBS+PIC +digitonin (ten times diluted), and finally with PBS+PIC. All the washing steps included incubation for 5 min at 4 °C on a rotating mixer and centrifugation at 1000 *g* for 1 min at room temperature. The pelleted beads were combined with a small volume of the 2x SDS sample lysis buffer and incubated at 65 °C for 15 min. After a brief centrifugation, the supernatant with the released co-immunoprecipitated proteins was subjected to SDS PAGE and western blot analysis using specific antibodies (described in section 2.4.).

Results

High molecular weight forms of CII

The mammalian CII consists of four subunits, SDHA, SDHB, SDHC and SDHD, with the approximate molecular weight (MW) of 70, 30, 18 and 17 kDa, respectively. Digitonin-solubilised CII from mitochondria of human fibroblasts was resolved by BNE (in the presence of CBG) or hrCNE3 (in the presence of n-dodecyl-β-D-maltoside and deoxycholic acid in the cathode buffer) as a CII monomer of the expected mass of approximately 140 kDa (Figure 1A, B) which represented most of the CII signal. In addition, weaker bands smaller than 140 kDa and at approximately 200 kDa were also present; these could be CII sub-complexes and CII hetero-oligomers. When milder conditions of separation were applied using CNE, a completely different pattern of the CII signal was obtained, indicating the presence of its higher molecular weight forms (CII_{hmw}). As revealed by immunodetection with the SDHA antibody, the signal of CII was almost completely localised within the region of 400–670 kDa (Figure 1A). Similarly, the SDHB antibody (Figure 1B) or in-gel staining of CII (SDH) activity (Figure 1C) confirmed the presence of CII in the 400–670 kDa region. This was further demonstrated by 2D CNE/SDS PAGE analysis of the cells (Figure 2A), where the distributions of SDHA and SDHB in the second dimension gel indicate that the CII_{hmw} forms represent a complete and active CII, in accord with the profiles of CII activity in CNE. For comparison, we also analysed the CII profile in mitochondria isolated from rat heart and obtained similar results, except for the size of tissue CII_{hmw} on CNE gels, which increased to 500 – over 1000 kDa when detected either with the SDHA or SDHB antibodies (Figure 1D, E) or by the in-gel SDH activity staining (Figure 1F). This was also confirmed by 2D analysis (Figure 2B).

Further, we analysed the distribution profiles of other OXPHOS complexes on 2D blots with subunit-specific antibodies in an attempt to determine potential CII interaction partners within CII_{hmw}. As expected, a substantially different migration pattern was found in the case of CI (NDUFA9) while some CIII (Core1) signal overlapped with CII in heart, but not in fibroblasts (Figure 2A, B). The signal of CIV (Cox4) partially overlapped with that of CII_{hmw} (SDHA, SDHB), as shown by the distribution profiles below the western blot images. A similar overlap with the CII_{hmw} signal was found for CV (the α subunit), in particular in the case of fibroblasts (Figure 2A). This may reflect a coincidental co-migration of respective complexes because of the imprecise electrophoretic mobility inherent to the CNE system in the first dimension [31], but it can also indicate a possibility that CII_{hmw} include SCs of CII with CIII, CIV or CV.

CII_{hmw} differ between tissues and cells

When CNE analysis of digitonin-solubilised proteins was performed using fibroblasts and different immortalised/ malignant human or rodent cell lines (Figure 3A), an analogous

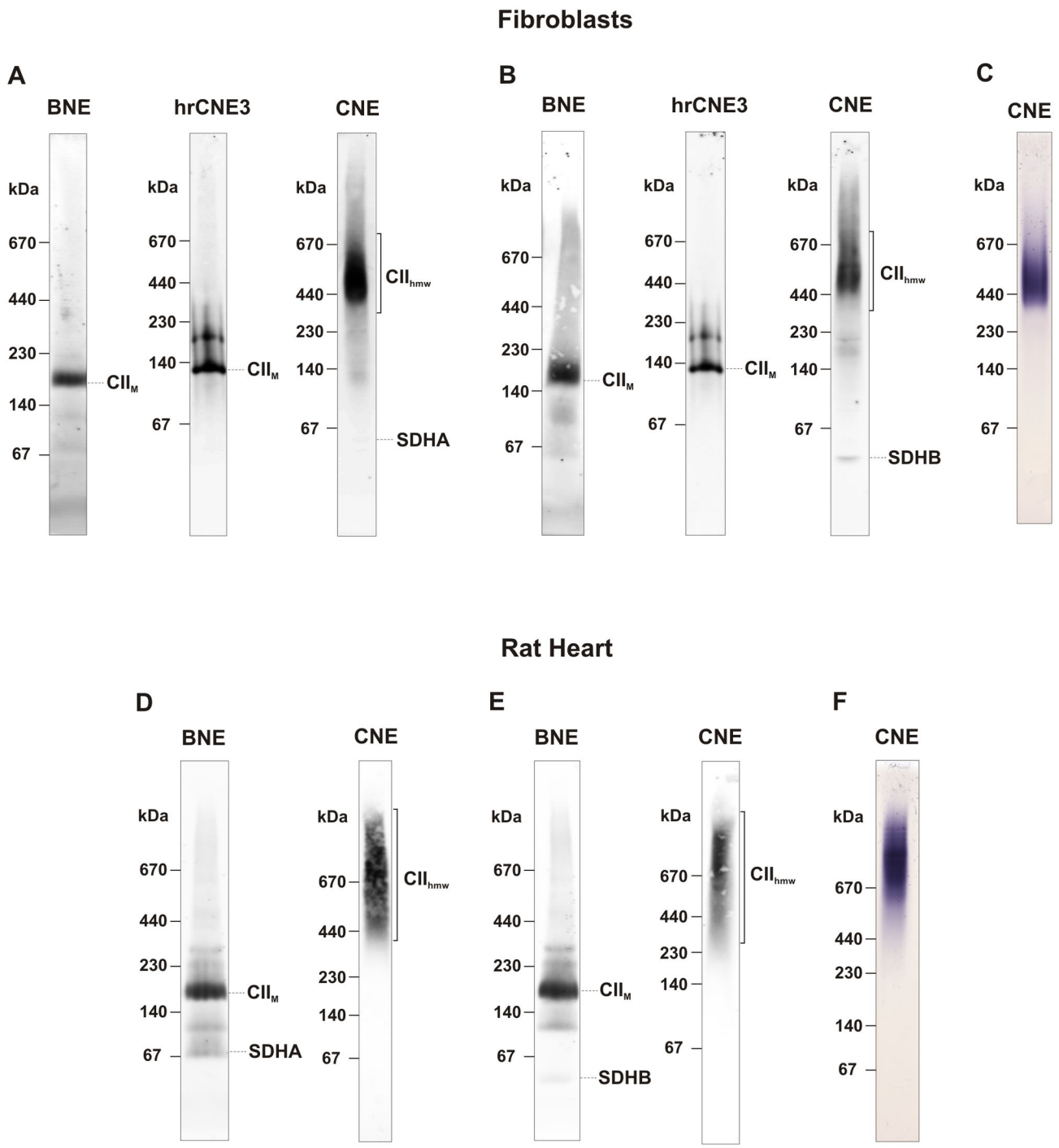

Figure 1. Higher molecular weight forms of complex II. Mitochondrial membrane proteins from control fibroblasts and rat heart were solubilised with digitonin (4 g/g protein), and 20 µg protein aliquots were separated using BNE, hrCNE3 and CNE. CII was immunodetected with the SDHA antibody (A, D) and SDHB antibody (B, E). In-gel activity staining of CII was performed in CNE gels (C, F). Migrations of higher molecular weight forms of CII (CII_{hmw}), CII monomer (CII_M), SDHA and SDHB subunits of CII are marked. The images are representative of three independent experiments.

doi: 10.1371/journal.pone.0071869.g001

CII_{hmw} pattern was obtained in all human, mouse and rat cells, indicating that most of CII is present as CII_{hmw}. Similarly, CII_{hmw} was found as a predominant form of CII in mitochondria of different human and rodent tissues (Figure 3B), suggesting that

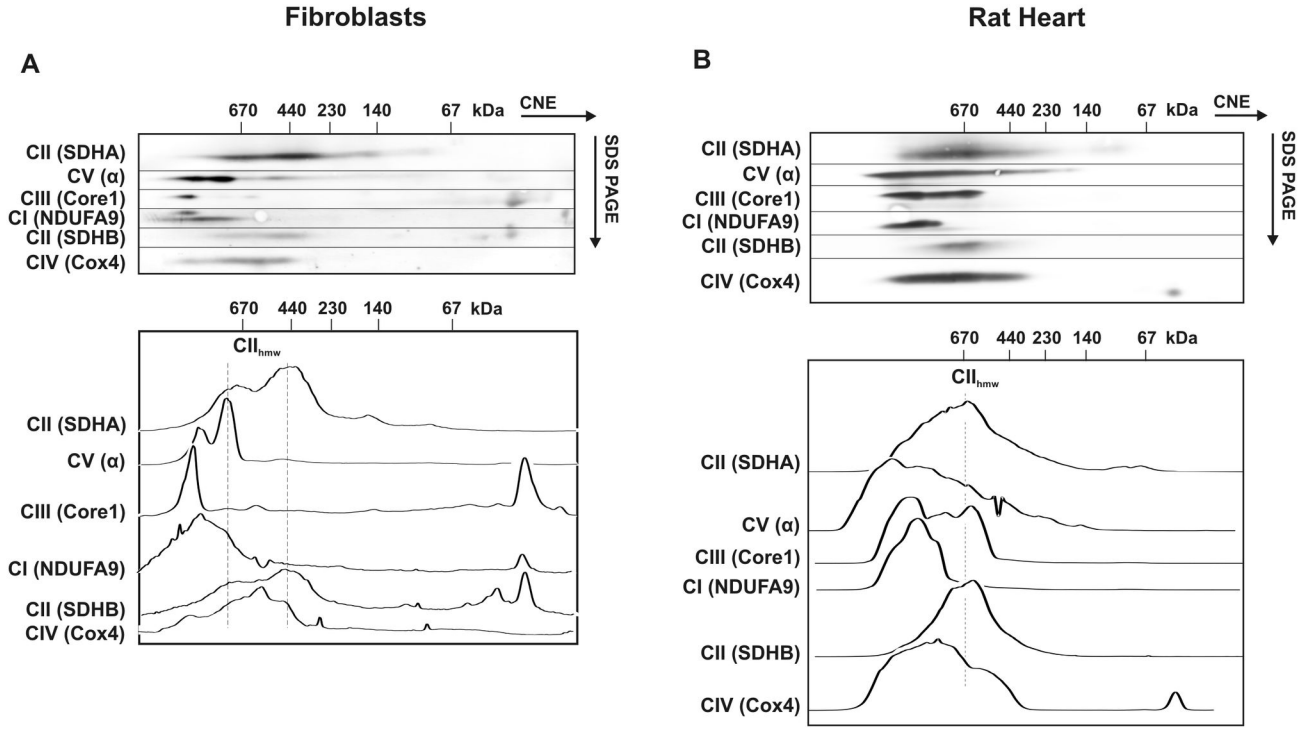

Figure 2. CNE/SDS PAGE analysis of OXPHOS proteins. Digitonin-solubilised proteins from human fibroblasts (A) and rat heart (B) mitochondria were separated by CNE in the first dimension (40 µg protein load) and by SDS PAGE in the second dimension. Subunits of the respiratory chain CI (NDUFA9), CII (SDHA, SDHB), CIII (Core1), CIV (Cox4) and CV (α) were immunodetected using specific antibodies. The dashed vertical lines in the distribution profiles below the western blots depict the main area of higher molecular weight forms of complex II (CII$_{hmw}$).

doi: 10.1371/journal.pone.0071869.g002

high molecular forms of CII are a universal property of mammalian respiratory chain. Nevertheless, the mobility of CII$_{hmw}$ in tissues was considerably different in comparison with cell lines. As shown in Figure 3B the main signal of the SDHA antibody in tissues was detected above 670 kDa, in the MW range of larger respiratory SCs (SDHB displayed an analogous distribution pattern, not shown). This was also observed on 2D CNE/SDS PAGE western blots (Figure 2B), where the signal of the CII SDHA and SDHB subunits was shifted to a higher MW. In contrast, other OXPHOS complexes were distributed comparably with the cultured cells (Figure 2A). Therefore, we performed in-gel activity staining of CII in CNE gels to confirm the detected antibody signals in the cells and tissues. Figure 3C, D reveals that CII$_{hmw}$ complexes were catalytically active and, indeed, differed between cells and tissues. In parallel, we performed in-gel CIV and CV activity staining to further analyse a possible co-migration or interaction with CII. In the case of cells, the dominant CIV activity signal could be ascribed to the CIV dimer (CIV$_D$) (Figure 3C), in the position corresponding to some of CII$_{hmw}$. The higher active CIV SCs did not co-migrate with the CII signal. Thus, the size of CII$_{hmw}$ in the cells more likely points to a mere co-migration of CII homo-/hetero-oligomers with CIV$_D$, rather than to a genuine specific interaction between the OXPHOS complexes.

Interestingly, the CIV activity signals were shifted to the higher MW in tissues and overlapped with the activity signal of CII$_{hmw}$ (see Figure 3D). The interaction of CII with CIV or other OXPHOS complexes in the MW range > 1 MDa thus cannot be excluded. The differences in the size of CII$_{hmw}$ when comparing cells and tissues could suggest the existence of two major functional forms of CII SCs. In cells, they may be present largely as CII homo-oligomers, while in tissues, CII may possibly form SCs with other OXPHOS complexes. In-gel activity of monomeric and homo-oligomeric CV did indicate co-migration or interaction with CII$_{hmw}$ in tissues but not in cells (Figure 3C, D).

CII$_{hmw}$ formation depends on other respiratory chain complexes

To learn more about possible interactions with other OXPHOS complexes, we performed CNE analysis of digitonin-solubilised mitochondria of human fibroblasts harbouring different types of OXPHOS defects that affect one or more respiratory chain complexes. We found that the selective deficiency of CIV (due to a *SURF1* mutation, Figure 4B) or CV (due to a *TMEM70* mutation, Figure 4C) did not affect the presence of CII$_{hmw}$ (Figure 4A). Similarly, the selective deficiency of CI (an unknown mutation) was without any effect

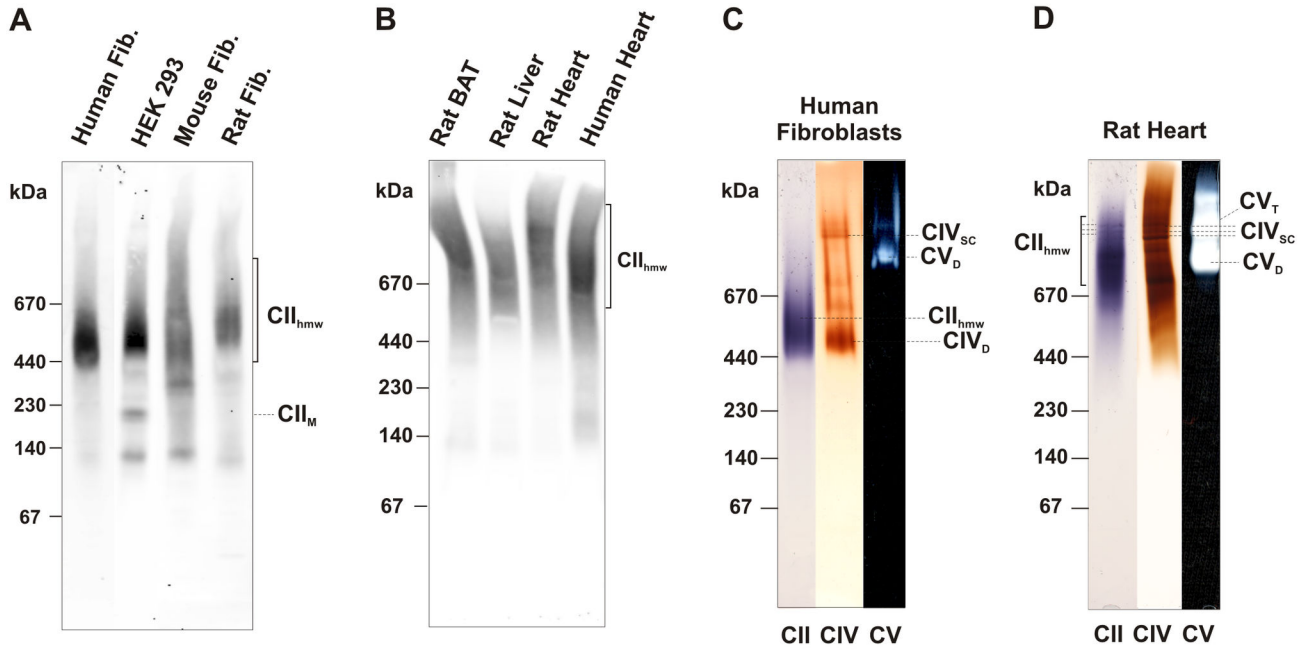

Figure 3. Comparison of CII$_{hmw}$ in cells and tissues by western blot and in-gel activity staining. Mitochondria from different human and rodent cells (A) and tissues (B) were solubilised with digitonin (4 g/g protein) and 20 µg protein aliquots were separated using CNE. CII was immunodetected with the SDHA antibody. The activities of CII (violet), CIV (brown) and CV (white) in CNE gels (protein load 50 µg for cells and 40 µg for tissues) are shown in human fibroblasts (C) and rat heart (D). The positions of higher molecular weight forms of CII (CII$_{hmw}$), CII monomer (CII$_M$), CIV dimer (CIV$_D$) and its supercomplexes (CIV$_{SC}$), CV dimer (CV$_D$) and tetramer (CV$_T$) are indicated in the figure. Rat BAT, rat brown adipose tissue.

doi: 10.1371/journal.pone.0071869.g003

on the CII$_{hmw}$ pattern. However, we obtained a different pattern in ρ^0 cells with depletion of mtDNA and thus lack of functional complexes I, III, IV and V [24]. Here, most of the CII$_{hmw}$ signal disappeared and CII was present as unassembled subunits or monomer. This demonstrates the requirement of fully assembled CII monomer for subsequent CII$_{hmw}$ formation, and also its dependence on the preserved integrity of a fully functional respiratory chain (Figure 4A).

CII$_{hmw}$ stability depends on very weak protein–protein interactions

The fact that CII$_{hmw}$ are retained in CNE gels but dissociate in BNE gels (Figure 1) points to their rather labile nature. To analyse these interactions in more detail, we used CNE as before but with the CBG dye added to the sample (Figure 5A). In this experiment, CII$_{hmw}$ dissociated into monomeric CII due to the presence of CBG, while other respiratory chain SCs (CIV shown as an example) remained unaffected, apart from the fact that they were better focused due to the negative charge introduced by CBG. We therefore performed 2D CNE/CNE$_{CBG}$ electrophoresis using CBG to treat the gel slice after the CNE separation in the first dimension (Figure 5 B–F). As shown by western blots with the antibodies to SDHA and SDHB, all CII$_{hmw}$ dissociated into CII monomers after exposure to CBG, that can bind to proteins due to its negative charge and thus interfered with weak non-covalent interactions. The main signal of CII from the first dimension can again be observed within the MW range of 400–670 kDa. On the contrary, the SCs of CI+III+IV were practically unaffected by CBG treatment (Figure 5E). Interestingly, the addition of CBG also partially affected oligomers of CV, which dissociated to lower molecular weight forms corresponding to the CV monomer and the F_1 sub-complex (Figure 5F).

To follow the potential differences between cultured cells and tissues, we examined the stability of CII$_{hmw}$ from rat heart mitochondria in the presence of CBG. While we detected a complete breakdown of CII$_{hmw}$ in the CNE gel after the addition of CBG to the sample (Figure 6A), most of the CII$_{hmw}$ was unaffected under 2D CNE/CNE$_{CBG}$ conditions. Based on good reproducibility of the experiments, we can conclude that CII$_{hmw}$ do have higher MW and are more stable in tissues than in cultured cells. This may indicate that CII has different interaction partners in tissues and cultured cells, and CII$_{hmw}$ thus ultimately represents several structurally and functionally different SCs. As in cultured cells, CIV and its SCs were unaffected (Figure 6A, 6D), while CV partially dissociated from its higher forms to the monomeric and the F_1 sub-complex forms (Figure 6E). The sensitivity of CII and CV to CBG indicates a similar type of mild interactions responsible for the formation of their respective higher molecular weight complexes.

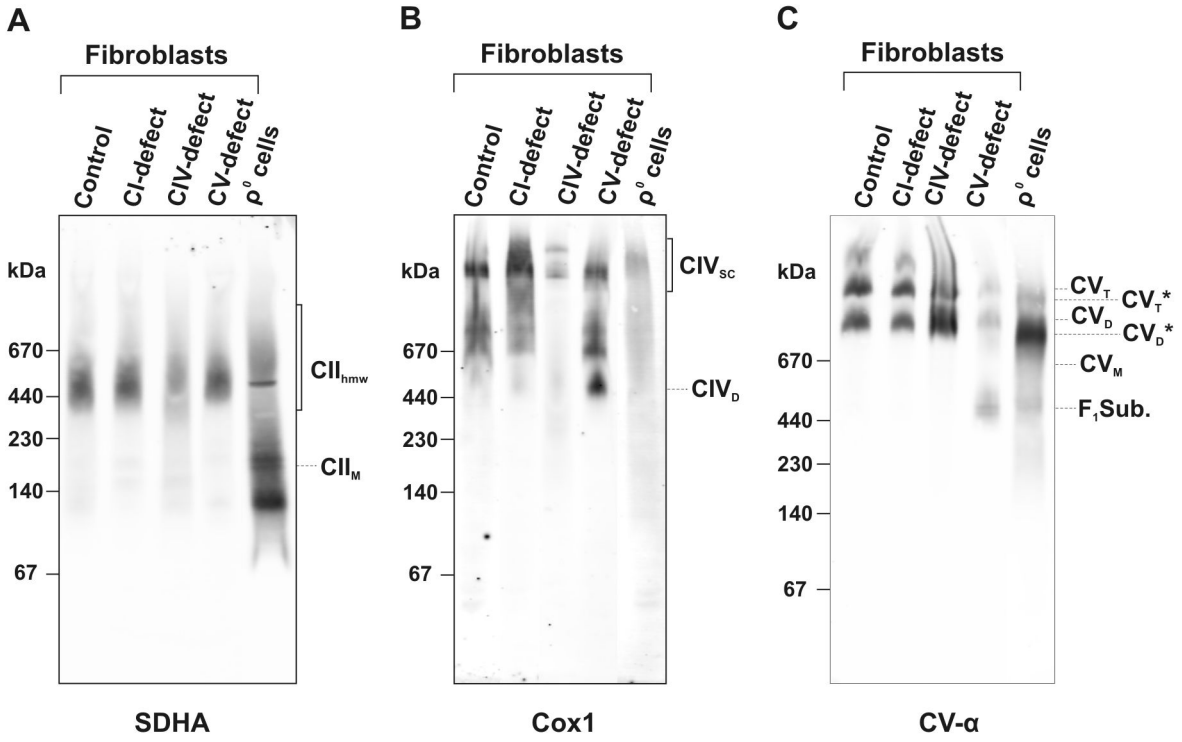

Figure 4. Presence of CII$_{hmw}$ in human fibroblasts with different types of OXPHOS defects and ρ⁰ cells. Digitonin-solubilised mitochondrial complexes were analysed by CNE (20 µg protein load) and immunodetected using antibodies to individual subunits: (A) CII, SDHA; (B) CIV, Cox1; (C) CV, α subunit. Positions of the CII monomer (CII$_M$), high molecular weight forms of CII (CII$_{hmw}$), CIV dimer (CIV$_D$), supercomplexes of CIV (CIV$_{SC}$), F_1 subcomplex of CV (F_1Sub.), the monomer, dimer and tetramer of CV (CV$_M$, CV$_D$ and CV$_T$), and the dimer and tetramer of CV lacking the mtDNA-coded subunits (CV$_D$* and CV$_T$*) are marked.
doi: 10.1371/journal.pone.0071869.g004

CII co-immunoprecipitates with CV

To investigate possible interactions between CII and CV by a different approach, we immunoprecipitated CV from rat heart mitochondria (Figure 7A) using a highly specific rabbit polyclonal antibody (CV–F_1) to CV subunits α, β and γ. The antibody immobilised to agarose beads immunoprecipitated whole CV, as evidenced by the presence of both F_1 (α and γ) and F_o (a) subunits. The immunoprecipitate was free of CI, CIII and CIV subunits, but it contained a significant amount of the SDHA subunit of CII. Similarly, SDHA was co-immunoprecipitated using CV-F_1 antibody and solubilised fibroblasts (Figure 7B). In a cross-experiment, we immunoprecipitated CII from heart mitochondria using a highly specific monoclonal antibody against SDHA. The resulting immunoprecipitate contained CII as well as the whole CV as revealed by the presence of subunits from F_1 and F_o parts of CV (Figure 7A). In contrast, it was free of CI, CIII and CIV. Again, CV was also co-immunoprecipitated using SDHA antibody and solubilised fibroblasts (Figure 7B). As none of the commercially available antibodies against SDHC and SDHD we tested were reasonably specific, we cannot confirm the presence of fully assembled CII in the precipitate. In principle, it is possible that only the two hydrophilic subunits SDHA and SDHB are present in the SC with CV. Notwithstanding, this result is compatible with recent data showing the presence of CII as well as CV in the mitoK$_{ATP}$ channel complex, whose size was found to be approximately 940 kDa, similarly to CII$_{hmw}$ forms observed in tissues.

CII does not form SC with TCA cycle enzymes

CII can also potentially interact with components of the TCA cycle. We therefore used CNE to separate digitonin-solubilised (4 g/g) rat heart mitochondria and subsequently analysed the lysate by western blotting for the presence and distribution pattern of individual TCA cycle enzymes, which were then compared with the distribution of CII. We observed high molecular weight form complexes of fumarase and succinyl-CoA synthetase in the region above 670 kDa (Figure 8A). Although they dissociated into lower molecular forms after the addition of CBG, as was the case for CII (Figure 8B), the CNE migration pattern for both fumarase and succinyl-CoA synthetase was slightly different from that of CII, which does not support the existence of their direct interaction. Other digitonin-solubilised TCA cycle enzymes did not show any co-migration with CII on the CNE gels (not shown).

To check for the potential associations between CII and other TCA cycle enzymes, we immunoprecipitated CII from rat heart mitochondria using the monoclonal antibody against the

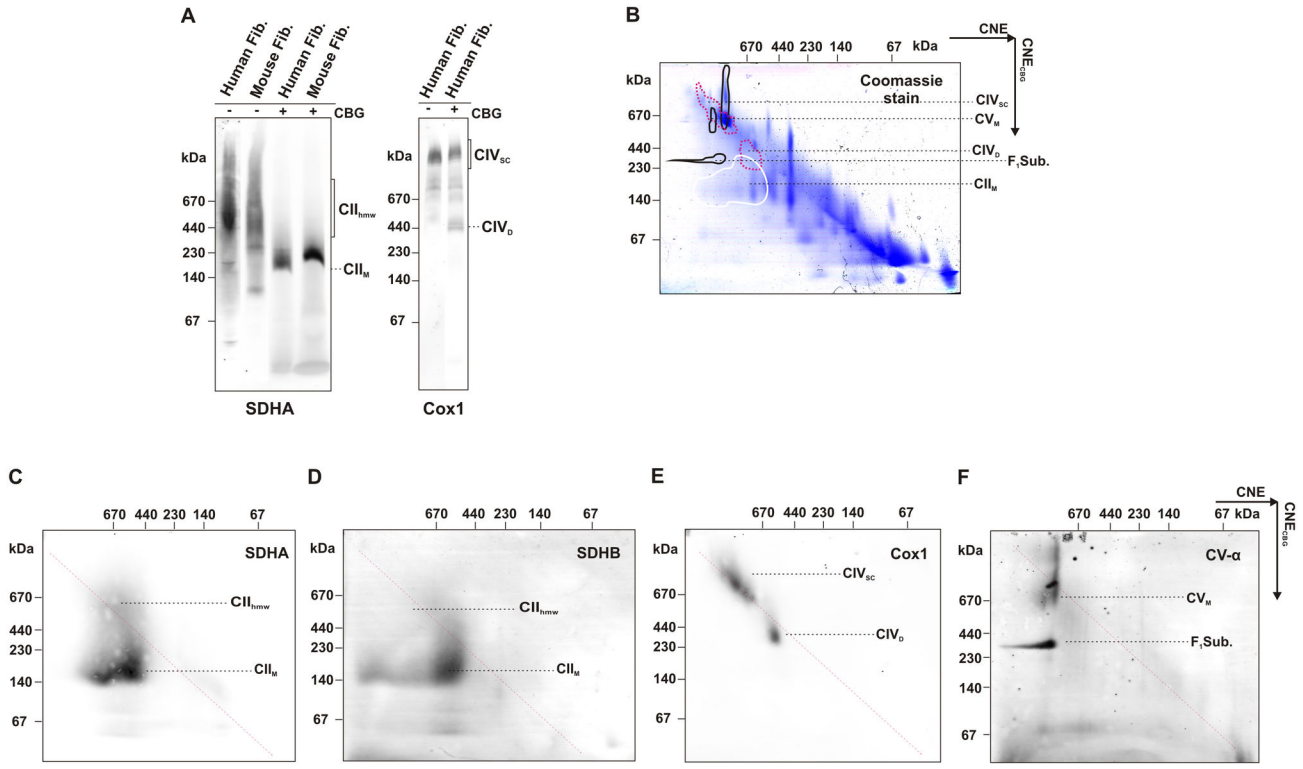

Figure 5. Low stability of CII_{hmw} in fibroblasts. (A) Digitonin-solubilised (4 g/g protein; 20 µg protein load) mitochondrial proteins from control human fibroblasts or control mouse fibroblasts were resolved by CNE with (+) or without (-) CBG. (B–F) Two-dimensional CNE/CNE_{CBG} analysis of mitochondrial proteins from control fibroblasts (50 µg protein load). After separation of mitochondrial proteins with CNE, the gel slices were incubated in CBG and subjected to CNE in the second dimension. One gel was stained in Coomassie blue stain and identical duplicate gel was used for western blot. The positions of individual OXPHOS complexes are highlighted on the stained gel (B) according to their immunodetection: full white line, CII monomer (CII_M); dashed red line, CIV dimer (CIV_D) and supercomplexes of CIV (CIV_{SC}); full black line, F_1 subcomplex of CV (F_1Sub.) and monomer of CV (CV_M) based on the signals of SDHA (C), SDHB (D), Cox1 (E) and CV-α (F) subunits.

doi: 10.1371/journal.pone.0071869.g005

SDHA subunit as above. The resulting immunoprecipitated CII contained no other TCA cycle enzymes, namely α-ketoglutarate dehydrogenase (subunit E1), aconitase, fumarase, citrate synthase, isocitrate dehydrogenase (subunit α), succinyl-CoA synthetase (subunit α) or malate dehydrogenase (Figure 8B).

Discussion

The key finding of this study is the discovery of CII propensity to form higher molecular structures (CII_{hmw}) in the IMM. We demonstrated that under sufficiently mild conditions, CII associates into CII_{hmw} forms in both mammalian cultured cells and tissues. As the representative cell line/tissue we used human fibroblasts and rat heart, and we have clearly shown that CII_{hmw} are present regardless of the species (rat, mouse, human), tissue type (heart, liver, brown adipose tissue) or the origin of the cell line (fibroblasts, kidney cells). As such, CII_{hmw} can be found in mitochondria with a wide range of content of the respiratory chain complexes. The interactions responsible for CII_{hmw} formation must be rather weak as the supramolecular structures are not retained under the conditions of the commonly used native electrophoretic techniques, such as BNE or hrCNE [26,28], where either negatively charged CBG or additional detergents are present and, presumably, disrupt the weak interactions responsible for CII_{hmw} formation. Thus, these complexes can only be visualised using the CNE electrophoretic system, where proteins migrate according to their intrinsic charge routinely lost by the charged dyes or detergents used to introduce the net charge to the protein micelles formed during the solubilisation of the membrane. Despite the lower resolution of CNE in comparison with other native electrophoretic systems [31], we have shown that CII_{hmw} forms differ in their apparent molecular mass between tissues (500 – over 1000 kDa) and cultured cells (400–670 kDa). The reasons for this difference are not immediately obvious. Possibly, this may be the effect of detergent (i.e. digitonin) and its concentrations used for solubilisation of proteins from the IMM. Apart from the critical micellar concentration [32], the ratio of the detergent and the protein can also dictate the outcome of

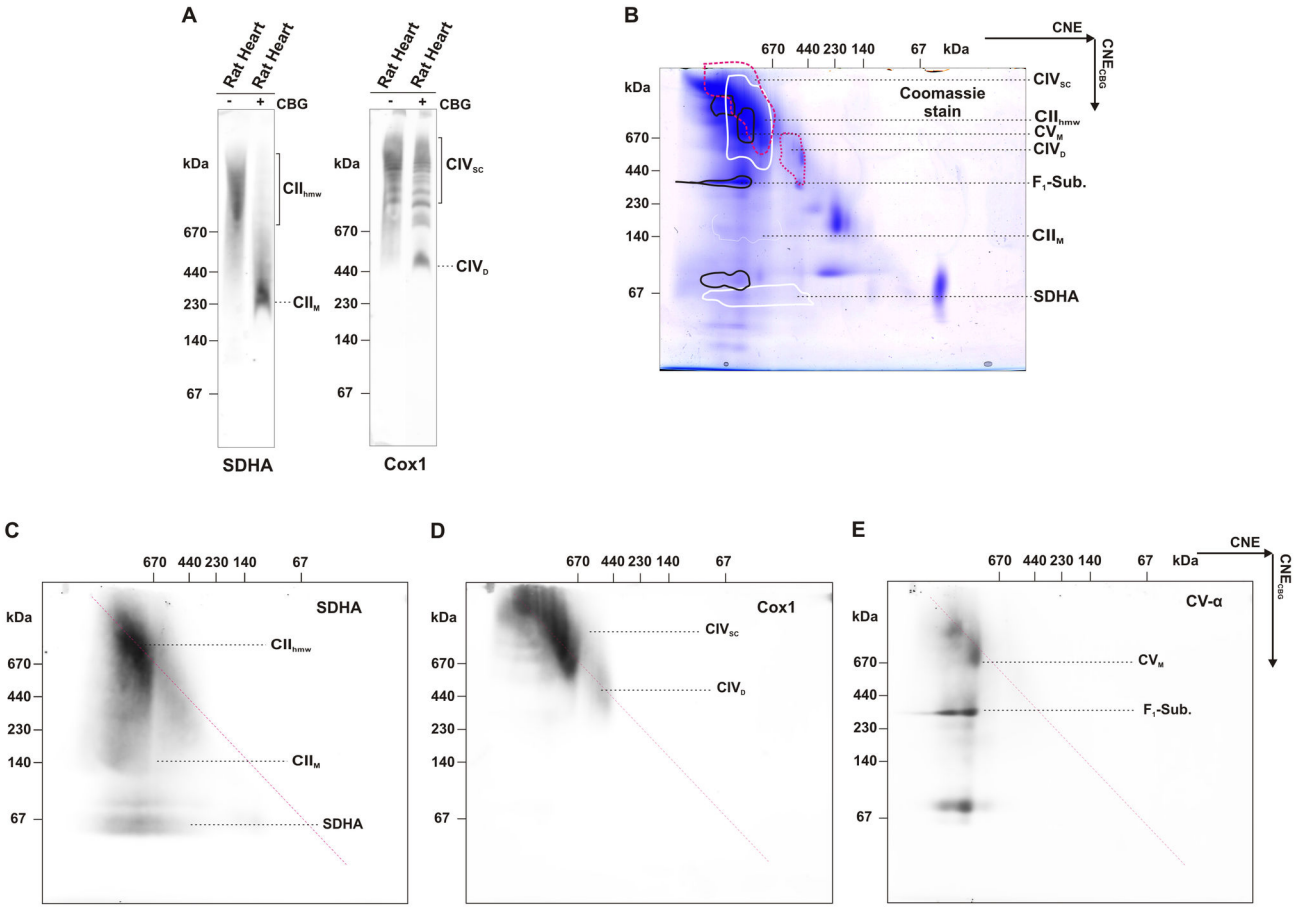

Figure 6. Low stability of CII_{hmw} in rat heart. (A) Digitonin-solubilised (4 g/g protein, 20 µg protein load) mitochondrial proteins from rat heart mitochondria were resolved by CNE with (+) or without (-) CBG. (B–F) Two-dimensional CNE/CNE_{CBG} analysis of mitochondrial proteins from rat heart (40 µg protein load). After separation of mitochondrial proteins with CNE, the gel slices were incubated in CBG and subjected to CNE in the second dimension. One gel was stained in Coomassie blue stain and identical duplicate gel was used for western blot. The positions of individual OXPHOS complexes are highlighted on the stained gel (B) according to their immunodetection: full white line, CII monomer (CII_M), high molecular weight forms of CII (CII_{hmw}), and the SDHA subunit of CII; dashed red line, CIV dimer (CIV_D) and supercomplexes of CIV (CIV_{SC}); full black line, F_1 subcomplex of CV (F_1Sub.) and monomer of CV (CV_M) based on the signals of SDHA (C), Cox1 (D), and CV-α (E) subunits.

doi: 10.1371/journal.pone.0071869.g006

the solubilisation process. As tissues display higher density of mitochondria than cultured cells, the use of the same detergent/protein ratio for both may yield different results when resolving the mitochondrial SCs. Another possible reason for the different mobility of CII_{hmw} from the two sources could be a different phospholipid composition of the IMM between cells and tissues, although the recent work indicates similarities in the relative abundance of mitochondrial phospholipids in tissues and cultured cells [33,34]. Ultimately, this difference may simply reflect a higher number of OXPHOS complexes in the IMM [33,35] and different energetic demands of tissues when compared with cells that lead to a higher probability of CII uptake into larger structures in the tissue mitochondria. Importantly, the observed differences between cells and tissues in CII_{hmw} size and stability as well as their dependence on mtDNA depletion, support the view that they reflect biological properties of complex II and do not represent an artefact of CNE electrophoresis.

When assessing the stability of CII_{hmw} complexes, we detected the CII_{hmw} as the dominant structural form of CII in digitonin solubilisates under the CNE separation conditions. The presence of either detergents (n-dodecyl-β-D-maltoside, deoxycholic acid) or CBG in the running buffer, i.e. conditions usually used to achieve better separation and resolution in the hrCNE and BNE electrophoretic systems, readily dissociated CII_{hmw} in both cells and tissues to CII monomers and individual subunits. Even the very low CBG concentration added to the sample (0.02%, 50-fold less than used in BNE samples) was sufficient for the complete CII_{hmw} dissociation. Similarly, incubation of the CNE gel slice with separated CII_{hmw} in a CBG solution also caused a partial dissociation of the CII_{hmw} structures, mainly in cultured cells. The addition of CBG to the

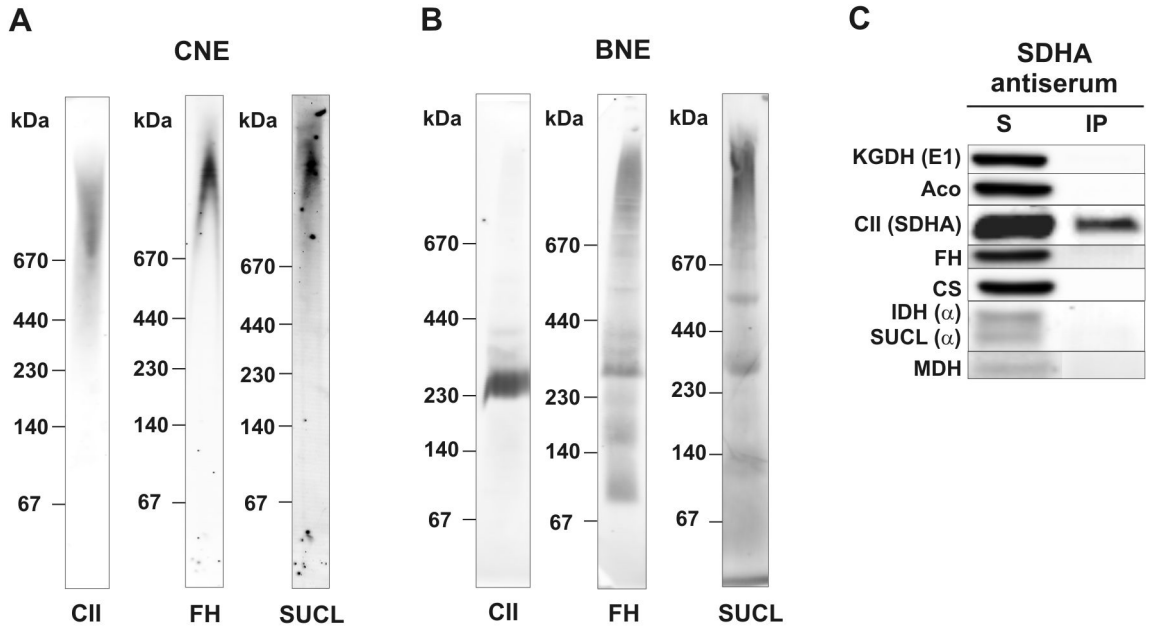

Figure 8. CII does not associate with other components of TCA cycle. (A) Mitochondrial membrane proteins from rat heart were solubilised with digitonin (4 g/g protein) and 20 µg protein aliquots separated using CNE. SDHA subunit of CII (CII), fumarase (FH) and subunit α of succinyl-CoA synthetase (SUCL) were detected with specific antibodies. (B) After digitonin solubilisation of mitochondria from rat heart, CII was immunoprecipitated with anti-SDHA antibody (SDHA antiserum). Proteins in the immunoprecipitate (IP) and solubilisate (S) were separated by SDS PAGE and analysed for the presence of individual components of the TCA cycle: α-ketoglutarate dehydrogenase subunit E1, KGDH (E1); aconitase, Aco; CII, SDHA; fumarase, FH; citrate synthase, CS; isocitrate dehydrogenase subunit α, IDH (α); succinyl-CoA synthetase (subunit α), SUCL (α); malate dehydrogenase, MDH.

doi: 10.1371/journal.pone.0071869.g008

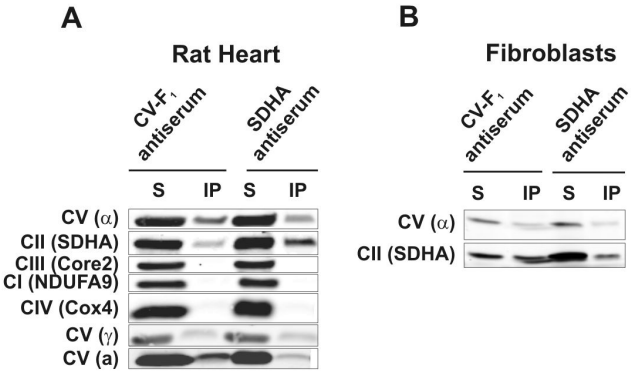

Figure 7. CII and CV co-immunoprecipitates. After digitonin solubilisation of mitochondria from the rat heart (A) and human fibroblasts (B), CV was immunoprecipitated with antibodies to its F_1 part and CII with anti-SDHA. Proteins in the immunoprecipitate (IP) and solubilisate (S) were separated by SDS PAGE and individual subunits of OXPHOS complexes detected as indicated with antibodies to CI, NDUFA9; CII, SDHA; CIII, Core2; CIV, Cox4; CV, α, γ, a.

doi: 10.1371/journal.pone.0071869.g007

sample/solution induces a dissociation effect by binding of the dye to proteins surface and introduction of a negative charge that can affect intermolecular interactions. Apparently, this process is more effective in solution than in the gel slice.

To understand the CII_{hmw} function, it is important to define CII interaction partners in CII_{hmw}. The most obvious candidates would be other OXPHOS complexes, but the putative presence of CII in the SCs with other OXPHOS complexes is still a matter of discussion. For example, single particle electron microscopy and X-ray imaging structural studies seem to contradict such idea [36,37]. These methods did not reveal the presence of CII in any type of SCs. It should be noted, though, that due to its relatively small size, CII may simply be below the detection limit of these techniques. Similarly, studies of the assembly kinetics of the CI+CIII+CIV SC did not reveal any participation of CII in this process [38]. On the other hand, at least some immunocapture and electrophoretic experiments demonstrated the existence of a large respirasome comprising respiratory chain complexes, including CII, as well as mobile electron carriers [17]. We therefore attempted to find any indication of the interaction between CII and other OXPHOS complexes. CNE analysis and in-gel activity staining in CNE gels pointed to a possible interaction with CIV or CV, but due to the low resolution of protein bands in the CNE gels it is hard to interpret this as genuine interactions. In the MW range 400–

670 kDa where CII_{hmw} are found in the cells, many other protein complexes and small SCs migrate. It is more likely that CII_{hmw} represents CII oligomers co-migrating with CV or CIV_D, as incorporation of CII into other complexes migrating in this range would require a shift in the electrophoretic mobility of the resulting SCs towards MW greater by at least 140 kDa, i.e. the molecular weight of the CII monomer. On the other hand, CII_{hmw} in the tissues with size over 1 MDa may represent CII as a part of OXPHOS SCs.

In another attempt to detect specific OXPHOS interacting partner(s) for CII, we studied cell lines with both isolated and combined deficiencies of OXPHOS complexes. With one of the interaction partners missing, the CII_{hmw} signal would be decreased or undetectable in the respective cell line. Such interdependency is well described for canonical OXPHOS SCs [12,17,38]. However, in our experiments, the levels and position of CII_{hmw} appear to be unchanged in cells with isolated defects of CI, CIV or CV, presenting additional evidence that no stable interaction is formed between CII and other OXPHOS complexes. On the other hand, when we analysed ρ^0 cells lacking mtDNA, unassembled subunits predominated over the CII monomer, and the CII_{hmw} structures were almost absent. The absence of the mtDNA-encoded subunits impedes the assembly and function of OXPHOS in ρ^0 cells [39]. Because CII is entirely encoded by the nuclear DNA, it was considered to be unchanged, but a recent study by Mueller et al. [40] reports a decreased level of CII with its activity reduced to 12%. Although the synthesis of the nuclear encoded subunits is unaffected in ρ^0 cells, mitochondrial protein import is disturbed as a consequence of decreased levels of ATP and the Tim44 protein, an essential effector of mitochondrial protein import [41]. Our experiments suggest that the CII and CII_{hmw} assembly depends on fully active mitochondria and the OXPHOS complexes of the IMM.

Immunoprecipitation was another independent approach we used to detect possible CII interaction partners. Here we identified CV as a plausible interaction partner of CII both in cultured cells and tissues. Generally, immunoprecipitation is more sensitive and selective than electrophoresis and can reveal rather weak interactions. Based on our experiments, we can conclude that CII, at least partially, co-immunoprecipitates with CV, constituting possibly a part of the $mitoK_{ATP}$ channel described in recent studies. Although the role for CII in $mitoK_{ATP}$ remains elusive, it was shown that SDH inhibitors modulate the channel activity and subsequently the process of ischemic preconditioning [18,42]. Only 0.4% of the CII present in mitochondria is necessary to activate the $mitoK_{ATP}$ and the inhibition of such a small portion of CII has no effect on the overall CII activity in OXPHOS [43]. The interaction of CII with CV is also not in conflict with our results with ρ^0 cells, as CV is assembled in ρ^0 cells, except for the two mtDNA-encoded subunits, ATP6 and ATP8 [44]. Such form of CV (lacking the two subunits) is sufficient for the survival of ρ^0 cells as it can hydrolyse ATP produced by glycolysis and allow for the maintenance of the transmembrane H^+ gradient by the electrogenic exchange of ATP for ADP by adenine nucleotide translocator [45,46].

An attractive proposal may be that CII may interact with other proteins from the TCA cycle, forming an organised multi-enzyme cluster. As the only membrane bound component of the TCA metabolism, CII would represent an anchor for the docking of TCA metabolism to the IMM into the spatial proximity of OXPHOS, in accordance with the known association of soluble TCA cycle enzymes with the mitochondrial membrane [47]. The existence of the metabolon composed of at least several TCA cycle proteins has been suggested [47,48]. However, most of the evidence points to the interactions of malate dehydrogenase, citrate synthase and, potentially, aconitase [19,20]. To date, no interaction involving CII has been demonstrated. Native electrophoretic systems represent a plausible model to study such interactions; although they involve solubilisation of membrane proteins by detergents, the solubilisates of whole mitochondria contain also matrix proteins. Naturally, any such interactions may be disrupted during the analysis. Here, crosslinking may help to capture such interactions in the future studies. Despite the fact that we did not identify any interacting partners for CII among the tested TCA cycle proteins, this deserves additional work as such interactions would appear functionally plausible.

It is possible that interactions of CII other than the one detected with CV do exist, and that such interactions may not even necessarily involve the whole of CII. For example, Gebert et al. [49] have published that the Sdh3 subunit of yeast CII (SDHC in mammals) has a dual function in mitochondria. It acts as a structural and functional subunit of CII and also plays a role in the biogenesis and assembly of the TIM22 complex via a direct interaction between Sdh3 and Tim18. Therefore, we cannot exclude that other CII subunits would have specific functions outside of the OXPHOS system. Notwithstanding these potential interactions of CII, our data lead to the conclusion that CII does form high molecular weight assemblies, but these structures are unlikely to represent traditional respiratory supercomplexes with CI, CIII and CIV as proposed previously by Acin-Perez et al. [17]. At least, some of these interactions are complexes with CV where CII plays a role as a regulatory component of $mitoK_{ATP}$ channel [42]. To summarise, our findings are consistent with the emerging notion that the individual OXPHOS complexes, or they subunits, have a role that may go beyond direct involvement in the mitochondrial bioenergetics.

Author Contributions

Conceived and designed the experiments: NK TM HN JN JH. Performed the experiments: NK TM HN EH. Analyzed the data: NK TM HN EH MV PP JH. Contributed reagents/materials/ analysis tools: KH KK JR. Wrote the manuscript: NK TM PP JN JH.

References

1. Cecchini G (2003) Function and structure of complex II of the respiratory chain. Annu Rev Biochem 72: 77-109. doi:10.1146/annurev.biochem.72.121801.161700. PubMed: 14527321.
2. Sun F, Huo X, Zhai YJ, Wang AJ, Xu JX et al. (2005) Crystal structure of mitochondrial respiratory membrane protein complex II. Cell 121: 1043-1057. doi:10.1016/j.cell.2005.05.025. PubMed: 15989954.
3. Brière JJ, Favier J, El Ghouzzi V, Djouadi F, Bénit P et al. (2005) Succinate dehydrogenase deficiency in human. Cell Mol Life Sci 62: 2317-2324. doi:10.1007/s00018-005-5237-6. PubMed: 16143825.
4. Bardella C, Pollard PJ, Tomlinson I (2011) SDH mutations in cancer. Biochim Biophys Acta 1807: 1432-1443. doi:10.1016/j.bbabio.2011.07.003. PubMed: 21771581.
5. Burnichon N, Brière JJ, Libé R, Vescovo L, Rivière J et al. (2010) SDHA is a tumor suppressor gene causing paraganglioma. Hum Mol Genet 19: 3011-3020. doi:10.1093/hmg/ddq206. PubMed: 20484225.
6. Perry CG, Young WF Jr, McWhinney SR, Bei T, Stergiopoulos S et al. (2006) Functioning paraganglioma and gastrointestinal stromal tumor of the jejunum in three women: syndrome or coincidence. Am J Surg Pathol 30: 42-49. doi:10.1097/01.pas.0000178087.69394.9f. PubMed: 16330941.
7. Ricketts C, Woodward ER, Killick P, Morris MR, Astuti D et al. (2008) Germline SDHB mutations and familial renal cell carcinoma. J Natl Cancer Inst 100: 1260-1262. doi:10.1093/jnci/djn254. PubMed: 18728283.
8. Kluckova K, Bezawork-Geleta A, Rohlena J, Dong L, Neuzil J (2013) Mitochondrial complex II, a novel target for anti-cancer agents. Biochim Biophys Acta 1827: 552-564. doi:10.1016/j.bbabio.2012.10.015. PubMed: 23142170.
9. Ghezzi D, Goffrini P, Uziel G, Horvath R, Klopstock T et al. (2009) SDHAF1, encoding a LYR complex-II specific assembly factor, is mutated in SDH-defective infantile leukoencephalopathy. Nat Genet 41: 654-656. doi:10.1038/ng.378. PubMed: 19465911.
10. Shi YB, Ghosh MC, Tong WH, Rouault TA (2009) Human ISD11 is essential for both iron-sulfur cluster assembly and maintenance of normal cellular iron homeostasis. Hum Mol Genet 18: 3014-3025. doi:10.1093/hmg/ddp239. PubMed: 19454487.
11. Hao HX, Khalimonchuk O, Schraders M, Dephoure N, Bayley JP et al. (2009) SDH5, a gene required for flavination of succinate dehydrogenase, is mutated in paraganglioma. Science 325: 1139-1142. doi:10.1126/science.1175689. PubMed: 19628817.
12. Bianchi C, Genova ML, Parenti Castelli G, Lenaz G (2004) The mitochondrial respiratory chain is partially organized in a supercomplex assembly: kinetic evidence using flux control analysis. J Biol Chem 279: 36562-36569. doi:10.1074/jbc.M405135200. PubMed: 15205457.
13. Shibata N, Kobayashi M (2008) The role for oxidative stress in neurodegenerative diseases. Brain Nerve 60: 157-170. PubMed: 18306664.
14. Strauss M, Hofhaus G, Schröder RR, Kühlbrandt W (2008) Dimer ribbons of ATP synthase shape the inner mitochondrial membrane. EMBO J 27: 1154-1160. doi:10.1038/emboj.2008.35. PubMed: 18323778.
15. Schägger H, Pfeiffer K (2000) Supercomplexes in the respiratory chains of yeast and mammalian mitochondria. EMBO J 19: 1777-1783. doi:10.1093/emboj/19.8.1777. PubMed: 10775262.
16. Wittig I, Schägger H (2009) Native electrophoretic techniques to identify protein-protein interactions. Proteomics 9: 5214-5223. doi:10.1002/pmic.200900151. PubMed: 19834896.
17. Acín-Pérez R, Fernández-Silva P, Peleato ML, Pérez-Martos A, Enriquez JA (2008) Respiratory active mitochondrial supercomplexes. Mol Cell 32: 529-539. doi:10.1016/j.molcel.2008.10.021. PubMed: 19026783.
18. Ardehali H, Chen Z, Ko Y, Mejía-Alvarez R, Marbán E (2004) Multiprotein complex containing succinate dehydrogenase confers mitochondrial ATP-sensitive K+ channel activity. Proc Natl Acad Sci U S A 101: 11880-11885. doi:10.1073/pnas.0401703101. PubMed: 15284438.
19. Meyer FM, Gerwig J, Hammer E, Herzberg C, Commichau FM et al. (2011) Physical interactions between tricarboxylic acid cycle enzymes in Bacillus subtilis: evidence for a metabolon. Metab Eng 13: 18-27. doi:10.1016/j.ymben.2010.10.001. PubMed: 20933603.
20. Vélot C, Mixon MB, Teige M, Srere PA (1997) Model of a quinary structure between Krebs TCA cycle enzymes: a model for the metabolon. Biochemistry 36: 14271-14276. doi:10.1021/bi972011j. PubMed: 9400365.
21. Kovářová N, Cížková Vrbacká A, Pecina P, Stránecký V, Pronicka E et al. (2012) Adaptation of respiratory chain biogenesis to cytochrome c oxidase deficiency caused by SURF1 gene mutations. Biochim Biophys Acta 1822: 1114-1124. doi:10.1016/j.bbadis.2012.03.007. PubMed: 22465034.
22. Piekutowska-Abramczuk D, Magner M, Popowska E, Pronicki M, Karczmarewicz E et al. (2009) SURF1 missense mutations promote a mild Leigh phenotype. Clin Genet 76: 195-204. doi:10.1111/j.1399-0004.2009.01195.x. PubMed: 19780766.
23. Honzík T, Tesarová M, Mayr JA, Hansíková H, Jesina P et al. (2010) Mitochondrial encephalocardio-myopathy with early neonatal onset due to TMEM70 mutation. Arch Dis Child 95: 296-301. doi:10.1136/adc.2009.168096. PubMed: 20335238.
24. King MP, Attardi G (1996) Isolation of human cell lines lacking mitochondrial DNA. Methods Enzymol 264: 304-313. doi:10.1016/S0076-6879(96)64029-4. PubMed: 8965704.
25. Bentlage HA, Wendel U, Schägger H, ter Laak HJ, Janssen AJ et al. (1996) Lethal infantile mitochondrial disease with isolated complex I deficiency in fibroblasts but with combined complex I and IV deficiencies in muscle. Neurology 47: 243-248. doi:10.1212/WNL.47.1.243. PubMed: 8710086.
26. Wittig I, Braun HP, Schägger H (2006) Blue native PAGE. Nat Protoc 1: 418-428. doi:10.1038/nprot.2006.62. PubMed: 17406264.
27. Mrácek T, Pecinová A, Vrbacký M, Drahota Z, Houstek J (2009) High efficiency of ROS production by glycerophosphate dehydrogenase in mammalian mitochondria. Arch Biochem Biophys 481: 30-36. doi:10.1016/j.abb.2008.10.011. PubMed: 18952046.
28. Wittig I, Karas M, Schägger H (2007) High resolution clear native electrophoresis for in-gel functional assays and fluorescence studies of membrane protein complexes. Mol Cell Proteomics 6: 1215-1225. doi:10.1074/mcp.M700076-MCP200. PubMed: 17426019.
29. Schägger H, von Jagow G (1987) Tricine-sodium dodecyl sulfate-polyacrylamide gel electrophoresis for the separation of proteins in the range from 1 to 100 kDa. Anal Biochem 166: 368-379. doi:10.1016/0003-2697(87)90587-2. PubMed: 2449095.
30. Moradi-Ameli M, Godinot C (1983) Characterization of monoclonal antibodies against mitochondrial F1-ATPase. Proc Natl Acad Sci U S A 80: 6167-6171. doi:10.1073/pnas.80.20.6167. PubMed: 6194526.
31. Wittig I, Schägger H (2005) Advantages and limitations of clear-native PAGE. Proteomics 5: 4338-4346. doi:10.1002/pmic.200500081. PubMed: 16220535.
32. Ko YH, Delannoy M, Hullihen J, Chiu W, Pedersen PL (2003) Mitochondrial ATP synthasome. Cristae-enriched membranes and a multiwell detergent screening assay yield dispersed single complexes containing the ATP synthase and carriers for Pi and ADP/ATP. J Biol Chem 278: 12305-12309. doi:10.1074/jbc.C200703200. PubMed: 12560333.
33. Lenaz G, Genova ML (2012) Supramolecular organisation of the mitochondrial respiratory chain: a new challenge for the mechanism and control of oxidative phosphorylation. Adv Exp Med Biol 748: 107-144. doi:10.1007/978-1-4614-3573-0_5. PubMed: 22729856.
34. Rosca M, Minkler P, Hoppel CL (2011) Cardiac mitochondria in heart failure: normal cardiolipin profile and increased threonine phosphorylation of complex IV. Biochim Biophys Acta 1807: 1373-1382. doi:10.1016/j.bbabio.2011.02.003. PubMed: 21320465.
35. Benard G, Faustin B, Passerieux E, Galinier A, Rocher C et al. (2006) Physiological diversity of mitochondrial oxidative phosphorylation. Am J Physiol Cell Physiol 291: C1172-C1182. doi:10.1152/ajpcell.00195.2006. PubMed: 16807301.
36. Dudkina NV, Eubel H, Keegstra W, Boekema EJ, Braun HP (2005) Structure of a mitochondrial supercomplex formed by respiratory-chain complexes I and III. Proc Natl Acad Sci U S A 102: 3225-3229. doi:10.1073/pnas.0408870102. PubMed: 15713802.
37. Schäfer E, Seelert H, Reifschneider NH, Krause F, Dencher NA et al. (2006) Architecture of active mammalian respiratory chain supercomplexes. J Biol Chem 281: 15370-15375. doi:10.1074/jbc.M513525200. PubMed: 16551638.
38. Moreno-Lastres D, Fontanesi F, García-Consuegra I, Martín MA, Arenas J et al. (2012) Mitochondrial complex I plays an essential role in human respirasome assembly. Cell Metab 15: 324-335. doi:10.1016/j.cmet.2012.01.015. PubMed: 22342700.
39. Chevallet M, Lescuyer P, Diemer H, van Dorsselaer A, Leize-Wagner E et al. (2006) Alterations of the mitochondrial proteome caused by the absence of mitochondrial DNA: A proteomic view. Electrophoresis 27: 1574-1583. doi:10.1002/elps.200500704. PubMed: 16548050.
40. Mueller EE, Mayr JA, Zimmermann FA, Feichtinger RG, Stanger O et al. (2012) Reduction of nuclear encoded enzymes of mitochondrial energy metabolism in cells devoid of mitochondrial DNA. Biochem Biophys Res Commun 417: 1052-1057. doi:10.1016/j.bbrc.2011.12.093. PubMed: 22222373.

41. Mercy L, Pauw Ad, Payen L, Tejerina S, Houbion A et al. (2005) Mitochondrial biogenesis in mtDNA-depleted cells involves a Ca2+-dependent pathway and a reduced mitochondrial protein import. FEBS J 272: 5031-5055. doi:10.1111/j.1742-4658.2005.04913.x. PubMed: 16176275.
42. Wojtovich AP, Smith CO, Haynes CM, Nehrke KW, Brookes PS (2013) Physiological consequences of complex II inhibition for aging, disease, and the mKATP channel. Biochim Biophys Acta 1827: 598-611. doi: 10.1016/j.bbabio.2012.12.007. PubMed: 23291191.
43. Wojtovich AP, Nehrke KW, Brookes PS (2010) The mitochondrial complex II and ATP-sensitive potassium channel interaction: quantitation of the channel in heart mitochondria. Acta Biochim Pol 57: 431-434. PubMed: 21103454.
44. Carrozzo R, Wittig I, Santorelli FM, Bertini E, Hofmann S et al. (2006) Subcomplexes of human ATP synthase mark mitochondrial biosynthesis disorders. Ann Neurol 59: 265-275. doi:10.1002/ana. 20729. PubMed: 16365880.
45. Buchet K, Godinot C (1998) Functional F1-ATPase essential in maintaining growth and membrane potential of human mitochondrial DNA-depleted rho degrees cells. J Biol Chem 273: 22983-22989. doi: 10.1074/jbc.273.36.22983. PubMed: 9722521.
46. García JJ, Ogilvie I, Robinson BH, Capaldi RA (2000) Structure, functioning, and assembly of the ATP synthase in cells from patients with the T8993G mitochondrial DNA mutation. Comparison with the enzyme in Rho(0) cells completely lacking mtdna. J Biol Chem 275: 11075-11081. doi:10.1074/jbc.275.15.11075. PubMed: 10753912.
47. Robinson JB Jr, Inman L, Sumegi B, Srere PA (1987) Further characterization of the Krebs tricarboxylic acid cycle metabolon. J Biol Chem 262: 1786-1790. PubMed: 2433288.
48. Haggie PM, Verkman AS (2002) Diffusion of tricarboxylic acid cycle enzymes in the mitochondrial matrix in vivo. Evidence for restricted mobility of a multienzyme complex. J Biol Chem 277: 40782-40788. doi:10.1074/jbc.M207456200. PubMed: 12198136.
49. Gebert N, Gebert M, Oeljeklaus S, von der Malsburg K, Stroud DA et al. (2011) Dual function of Sdh3 in the respiratory chain and TIM22 protein translocase of the mitochondrial inner membrane. Mol Cell 44: 811-818. doi:10.1016/j.molcel.2011.09.025. PubMed: 22152483.

Biochimica et Biophysica Acta 1837 (2014) 98–111

Contents lists available at ScienceDirect

Biochimica et Biophysica Acta

journal homepage: www.elsevier.com/locate/bbabio

ROS generation and multiple forms of mammalian mitochondrial glycerol-3-phosphate dehydrogenase

Tomáš Mráček, Eliška Holzerová, Zdeněk Drahota, Nikola Kovářová, Marek Vrbacký, Pavel Ješina, Josef Houštěk *

Institute of Physiology Academy of Sciences of the Czech Republic v.v.i., Vídeňská 1083, 14220 Prague 4, Czech Republic

ARTICLE INFO

Article history:
Received 1 March 2013
Received in revised form 20 August 2013
Accepted 25 August 2013
Available online 30 August 2013

Keywords:
Mitochondrial glycerol-3-phosphate dehydrogenase
E.C. 1.1.5.3
ROS production
Supercomplex
In-gel ROS detection

ABSTRACT

Overproduction of reactive oxygen species (ROS) has been implicated in a range of pathologies. Mitochondrial flavin dehydrogenases glycerol-3-phosphate dehydrogenase (mGPDH) and succinate dehydrogenase (SDH) represent important ROS source, but the mechanism of electron leak is still poorly understood. To investigate the ROS production by the isolated dehydrogenases, we used brown adipose tissue mitochondria solubilized by digitonin as a model. Enzyme activity measurements and hydrogen peroxide production studies by Amplex Red fluorescence, and luminol luminescence in combination with oxygraphy revealed flavin as the most likely source of electron leak in SDH under in vivo conditions, while we propose coenzyme Q as the site of ROS production in the case of mGPDH. Distinct mechanism of ROS production by the two dehydrogenases is also apparent from induction of ROS generation by ferricyanide which is unique for mGPDH. Furthermore, using native electrophoretic systems, we demonstrated that mGPDH associates into homooligomers as well as high molecular weight supercomplexes, which represent native forms of mGPDH in the membrane. By this approach, we also directly demonstrated that isolated mGPDH itself as well as its supramolecular assemblies are all capable of ROS production.

1. Introduction

Reactive oxygen species (ROS) are produced by all eukaryotic cells and the predominant source in most of them is mitochondrial respiration [1]. ROS have been implicated to be instrumental in many pathological processes, ranging from oxidative phosphorylation (OXPHOS) dysfunction to chronic neurodegenerative diseases and cancer. In addition and partially in contrary to this detrimental role, ROS have also been proposed to function as signaling and regulatory factors in various metabolic processes [2].

Mitochondrial respiratory chain contains many components that may leak electrons. Since the pivotal experiments of Britton Chance [3,4], two major superoxide producing sites in mitochondria have been established: respiratory chain complex I (NADH:ubiquinone oxidoreductase) [5] and complex III (ubiquinol:cytochrome *c* oxidoreductase) [6]. In addition, several other components of mitochondrial respiratory chain have been proposed as potential sources of ROS. To date, at least four additional sites of superoxide production in mammalian mitochondria have been described. These sites include dihydrolipoamide dehydrogenase (component of α-ketoglutarate dehydrogenase and pyruvate dehydrogenase) [7,8], electron transferring flavoprotein (ETF):Q oxidoreductase [9,10], succinate dehydrogenase (SDH, complex II) [11], and mitochondrial glycerol-3-phosphate dehydrogenase (mGPDH) [12,13].

All of these enzymes are flavin dependent dehydrogenases functioning either in tricarboxylic acid metabolism or supplying electrons to coenzyme Q (CoQ) in the respiratory chain. mGPDH and SDH seem to play prominent roles in ROS production. Several studies have shown mGPDH to be a potent ROS producer both in mammalian and insect mitochondria [12,14]. Levels of ROS production from mGPDH can be very high, even comparable with the levels of ROS from Q_o site of complex III when inhibited with antimycin A (AA), i.e. the most potent ROS source in mitochondria [15]. Furthermore, a significant glycerol-3-phosphate (GP)-dependent ROS production has been found even in mitochondria from tissues with low mGPDH content. Here the amount of ROS produced per unit of mGPDH enzyme activity tends to be extremely high [16], although a significant portion of these ROS originates from flavin site of complex II [17]. mGPDH can therefore be a potentially important ROS source even in typically aerobic tissues with negligible enzyme content such as the heart [16].

On the contrary, SDH was considered to be well protected against electron leak and SDH associated ROS production was only linked to pathologies, where mutations in SDH subunits lead to defective

Abbreviations: AA, antimycin A; BAT, brown adipose tissue; CoQ, coenzyme Q; DCPIP, 2,6-dichlorophenolindophenol; FeCN, ferricyanide, potassium hexacyanoferrate(III); GP, sn-glycerol-3-phosphate; mGPDH, mitochondrial FAD-dependent glycerol-3-phosphate dehydrogenase; HAR, hexaammineruthenium(III) chloride; HQNO, 2-n-heptyl-4-hydroxyquinoline N-oxide; HRP, horseradish peroxidase; MXT, myxothiazol; OXPHOS, oxidative phosphorylation; ROS, reactive oxygen species; SDH, succinate dehydrogenase

* Corresponding author. Tel.: +420 241 062 434; fax: +420 241 062 149.
E-mail address: houstek@biomed.cas.cz (J. Houštěk).

0005-2728/$ – see front matter © 2013 Elsevier B.V. All rights reserved.
http://dx.doi.org/10.1016/j.bbabio.2013.08.007

coordination of prosthetic groups and subsequent leak of electrons [18]. However, it has been demonstrated very recently, that also SDH can produce significant amounts of ROS when levels of available succinate are low. Here flavin was implicated as the ROS source — under low succinate concentrations, flavin site is not fully occupied by the substrate and may therefore be accessible to oxygen, allowing electron leak and superoxide formation [11]. In vivo steady state concentrations of succinate have been reported to be approximately 0.5 mM in the tissues [19] or even in the micromolar range for cells in tissue culture [20,21]. Such mode of ROS production by SDH may therefore be a significant contributor to the overall cellular ROS levels.

Despite these recent advances in understanding of flavin dehydrogenases dependent ROS production, detailed molecular mechanism of electron leak is still missing and may differ between individual enzymes. For example the mechanism of ROS production by mGPDH has been shown to be in many respects different from ROS production at other sites of the respiratory chain: (i) mGPDH has a simple structure and is localized on the outer side of the inner mitochondrial membrane but despite that, ROS are produced equally to both sides of the membrane [14]; (ii) it displays unique and specific activation of electron leak by ferricyanide [12,15,22]; (iii) its expression is highly tissue dependent and mGPDH may be a significant contributor to overall ROS production in glycolytic tissues [13]. All this stresses out the importance to further characterize pathways leading to electron leak in flavin dehydrogenases.

Over the last couple of years our understanding of inner mitochondrial membrane organization changed significantly as theory of respiratory chain supercomplexes gained traction. OXPHOS supercomplexes were proposed to play several roles — apart from facilitation of their biogenesis, supercomplex organization should improve substrate channeling between individual complexes and thus reduce the chance of electron leak and ROS production. So far, such type of association has clearly been documented only for complex I, but given the potential for electron leak from SDH and mGPDH their protection by streamlining the electron transport by association into supercomplex would make thermodynamic sense. However, so far there are only limited data on supramolecular organization of these enzymes. For example, in bacteria it is documented that SDH forms trimers, which are the active conformation [23] but no data on association with other OXPHOS complexes are available. In case of mGPDH, in yeast it has been shown that several mitochondrial dehydrogenases including mGPDH analog Gut2p associate into supramolecular complex but again without clear further association with downstream OXPHOS complexes [24].

In this study we focused on mGPDH and SDH and their ability to support ROS formation at different sites of respiratory chain. We used mild detergent digitonin to solubilize mitochondrial membranes into individual complexes and supercomplexes of respiratory chain enzymes as a tool for elucidating their role in ROS production. Mild detergent solubilization also allowed us to study native organization of these dehydrogenases in the inner mitochondrial membrane and formation of higher molecular weight complexes.

2. Material and methods

2.1. Isolation of mitochondria and solubilization

For experiments we used interscapular brown adipose tissue (BAT) of one to three weeks old Wistar rats kept at room temperature and 12 h/12 h light/dark cycle on a standard diet and water supply ad libitum. All animal works were approved by the institutional ethics committee and were in accordance with the EU Directive 2010/63/EU for animal experiments. Mitochondria were isolated in STE medium (250 mM sucrose, 10 mM Tris–HCl, 1 mM EDTA, pH 7.4) supplemented with BSA (10 mg.mL^{-1}) by differential centrifugation [25] and frozen at −80 °C. Subsequently frozen–thawed mitochondria were used in experiments. Membrane proteins were solubilized in KCl based medium (120 mM KCl, 3 mM HEPES, 5 mM KH_2PO_4, 3 mM $MgSO_4$, 1 mM EGTA, pH 7.2) with varying amount of digitonin (1 to 8 w/w ratio detergent/protein) for 10 min on ice and separated into supernatant and sediment fraction by centrifugation 20 min at 20,000 *g*.

2.2. Enzyme activity assays

Activities of SDH and mGPDH were determined spectrophotometrically either as CoQ_1 (monitored at 275 nm, $\varepsilon_{275} = 13.6$ mM^{-1}.cm^{-1}), 2,6-dichlorophenolindophenol (DCPIP, monitored at 610 nm, $\varepsilon_{610} = 20.1$ mM^{-1}.cm^{-1}) or cytochrome *c* oxidoreductases (monitored at 550 nm, $\varepsilon_{550} = 19.6$ mM^{-1}.cm^{-1}). The assay medium contained 50 mM KCl, 10 mM Tris–HCl, 1 mM EDTA, 1 mg.mL^{-1} BSA, 1 mM KCN, pH 7.4 and 25 μM CoQ_1, 10 mM 2,6-dichlorophenolindophenol (DCPIP) or 50 μM cytochrome *c* respectively. The reaction was started by adding 10 mM sn-glycerol -3-phosphate (GP) or succinate and changes of absorbance were monitored at 30 °C. Enzyme activities were expressed as nmol.min^{-1}.mg^{-1} protein.

2.3. Fluorometric detection of hydrogen peroxide production

Hydrogen peroxide production was determined fluorometrically by measuring oxidation of Amplex Red coupled to the enzymatic reduction of H_2O_2 by horseradish peroxidase (HRP). Fluorescence of the Amplex Red oxidation product was measured at 37 °C using Tecan Infinite M200 multiwell fluorometer. Excitation/emission wavelengths were 544 nm (bandwidth 15 nm)/590 nm (bandwidth 30 nm). The assay was performed with 15 μg of mitochondrial protein per mL in KCl based medium (120 mM KCl, 3 mM HEPES, 5 mM KH_2PO_4, 3 mM $MgSO_4$, 1 mM EGTA, pH 7.2) supplemented either with 10 mM succinate or 10 mM GP. Amplex Red was used at the final concentration of 50 μM with HRP at 1 U.mL^{-1}. Where indicated, 1 μg.mL^{-1} antimycin A (AA) or 12 μM CoQ_1 was added. Fluorescence signal from the well containing all substrates and inhibitors, but not mitochondria, was subtracted as background for every experimental condition used. Thus any non-enzymatic effect of inhibitors on apparent ROS production was eliminated. Signal was calibrated using H_2O_2 at the final concentration of 0–5 μM and H_2O_2 stock concentration was routinely checked by measuring its absorption at 240 nm.

2.4. ROS production in gel slices

Proteins in solubilizates were separated by hrCN3-PAGE [26] on 4–13% gradient gels. Individual lanes were excised and washed 3 × 10 min in KCl based medium (120 mM KCl, 3 mM HEPES, 5 mM KH_2PO_4, 3 mM $MgSO_4$, 1 mM EGTA, pH 7.2) to remove salts used in electrophoresis buffers. Subsequently, each lane was cut to 1 mm long slices by custom made cutter. Individual slices (circa 1 × 1 × 6 mm) were transferred into separate wells of 96 well plate and ROS production was detected by Amplex Red dye using the same conditions as for solubilized mitochondria (see above). Four measurements were done for each well (Tecan reader always uses only part of the well area for fluorescence detection) to ensure that presence of gel slice did not cause inhomogeneity and average was used in calculations. In-well SD was within 10%, which was the same as with mitochondria or solubilizates. As we do not know exact protein content in each slice, values were only expressed as pmol H_2O_2.min^{-1}.

2.5. Luminescence detection of hydrogen peroxide production

ROS production was also measured as luminescence, principally as described earlier [27]. Tecan Infinite M200 in luminescence mode was used to detect signal. Measurements were performed at 37 °C in 0.1 mL of KCl based medium, as in Amplex Red assay (120 mM KCl, 3 mM HEPES, 5 mM KH_2PO_4, 3 mM $MgSO_4$, 1 mM EGTA, pH 7.2) containing 1 μM myxothiazol (MXT), 1 mM luminol (5-amino-2,3-dihydro-1,4-

phtalazinedione) and 2.5 U.mL^{-1} HRP. 10 μg of solubilizate (digitonin 2 g/g) protein was used per well. Assay was performed on per well basis — the reaction was started by 10 mM GP or succinate, after 60 s 500 μM ferricyanide (potassium hexacyanoferrate(III); FeCN) was added. Other conditions are specified in Results and Legends to figures. Luminescence was recorded in 0.5 s intervals for further 60 s. The luminescence peak reached maximum values in the first second after FeCN injection and declined subsequently. For evaluation of peroxide production the maximum value (peak) was used. This value was proportional to integral luminescence intensity over the whole 60 second period. Each trace represents average value of quadruplicate measurement done in series. A calibration with hydrogen peroxide was routinely performed to check for the linearity of response.

2.6. Western blotting

Proteins in solubilizates were analyzed by BN-PAGE and hrCN3-PAGE [26,28] on 4–13% separating gels using the Mini-Protean III apparatus (BioRad). For two-dimensional electrophoresis, gel slices from the 1st dimension were incubated in 1% SDS and 1% mercaptoethanol for 1 h and then subjected to SDS-PAGE on 10% gels [29]. Proteins were transferred from gels to PVDF-membranes (Immobilon-P, Millipore) using semidry electrotransfer (BioRad). The membranes were blocked with 5% non-fat dried milk in TBST (150 mM NaCl, 10 mM Tris, 0.1% Tween-20, pH 7.5) for 1 h and incubated for 2 h with the specific primary antibodies diluted in TBST. Monoclonal antibodies to SDHA and Blue Native OXPHOS Complexes Detection Kit (containing monoclonal antibodies to NDUFA9, SDHA, Core2, Cox4, α-subunit of complex V) were obtained from Abcam; rabbit polyclonal antibody to mGPDH was custom prepared [30]. Membranes were then incubated for 1 h with corresponding secondary fluorescent antibodies — IRDye 680- or 800-conjugated goat anti-mouse IgG (Invitrogen) or goat anti-rabbit IgG (Rockland). Detection of proteins was performed using Odyssey fluorescence scanner. The quantification of signals was carried out in Aida Image Analyzer program version 3.21.

2.7. In-gel activity staining of mGPDH

Activity staining of mGPDH in native gels was performed according to a modified protocol originally described in [31]. Gel slices were stained using solution of 5 mM Tris–HCl (pH 7.4), 3 mM $MgCl_2$, 0.88 mM menadione, 1.2 mM NitroBlue Tetrazolium, 1.5 μM rotenone, 2 μM KCN and 10 mM glycerol-3-phosphate for 1 h. Subsequently gels were denatured in 50% methanol/10% acetic acid for 15 min, fixed in 10% acetic acid for 10 min and scanned on flatbed scanner.

2.8. Polarographic detection of oxygen consumption

Oxygen consumption was measured at 30 °C as described before [12] using Oxygraph-2k (Oroboros, Austria). Measurements were performed in 2 mL of KCl medium (80 mM KCl, 10 mM Tris–HCl, 3 mM $MgCl_2$, 1 mM EDTA, 5 mM K-Pi, pH 7.4) using 50–100 μg protein.mL^{-1} of digitonin solubilized mitochondria. For measurements, 10 mM GP, 125 μM hexaammineruthenium(III)chloride (HAR), 62.5 μM FeCN, 16 μM CoQ_1, and 1 μM MXT were used. The oxygen consumption was expressed in pmol oxygen.s^{-1}.mg^{-1} protein.

3. Results

3.1. Solubilization of mitochondrial membrane with digitonin affects mGPDH and SDH enzyme activities by CoQ depletion

Solubilization of mitochondrial membrane using mild nonionic detergents represents established approach to obtain respiratory chain enzymes in a range of different forms, from monomers to supercomplexes depending on the type and concentration of the detergent used. To study mGPDH and SDH in a soluble state, BAT mitochondria were solubilized with increasing concentrations of digitonin (1–8 g/g protein) and the solubilized (supernatant) and the residual non-soluble (sediment) fractions were separated by the centrifugation (20,000 *g*, 20 min). The average amounts of the protein recovered in supernatants after solubilization were 51.5, 70.4, 82.8, 81.9 and 64.5% of the original mitochondrial protein at 1, 2, 4, 6 and 8 g digitonin/g protein, respectively. The composition of the fractions was analyzed by SDS-PAGE and WB. As shown in Supplementary Fig. 1, specific content of respiratory chain complexes was quantified using subunit specific antibodies. Within the range of detergent concentrations used, the relative content of respiratory chain complexes, including SDH and mGPDH was maintained at levels similar to the original mitochondria. To assess the effect of solubilization on these dehydrogenases, we compared the specific activities (activities expressed per mg of protein in each sample) of mGPDH and SDH in the whole, frozen thawed mitochondria and in detergent solubilized mitochondrial proteins, i.e. at conditions when the dehydrogenases as well as the whole OXPHOS are assembled in the membrane versus the conditions when the membrane structure and interaction with mobile carriers and other respiratory chain complexes are disrupted by membrane solubilization. We followed the sole activity of mGPDH and SDH using DCPIP or CoQ (DH:DCPIP, DH:Q) as the acceptor as well as the combined activity of dehydrogenase and complex III (GCCR, SCCR). Solubilization of mitochondria by digitonin caused pronounced decline of GCCR and SCCR activity with increasing detergent concentration (Fig. 1). However, samples solubilized with digitonin 1 g/g protein still retained up to 10 and 27% of GCCR and SCCR activity in the soluble fraction respectively i.e. indicating presence of functional respiratory patches composed of at least dehydrogenase and complex III under these mild conditions, while electron transport to cytochrome *c* was completely abolished at higher digitonin concentrations.

Observed decrease in the sole activities of both solubilized dehydrogenases (acceptors DCPIP or CoQ) that declined with increasing detergent concentration, was much less pronounced and occurred at higher detergent/protein ratios than was the case for GCCR or SCCR. When comparing two acceptors for isolated dehydrogenase activity, we observed faster decline of DH:DCPIP than DH:Q activity, which was even more pronounced in SDH than in mGPDH. As DCPIP does not take electrons directly from the dehydrogenases, but takes them preferentially via CoQ pool [32], this suggested that CoQ_9 is effectively depleted from the dehydrogenase containing micelles during digitonin solubilization. Therefore, we tested effect of exogenous CoQ_1 supplementation. Addition of exogenous CoQ_1 to digitonin 2 g/g protein solubilizates significantly increased measured activities for both dehydrogenases. The activating effect was much more pronounced in SDH (>20-fold increase) than in mGPDH (2-fold increase) (Fig. 2), in accordance with much higher decline and almost complete loss of succinate:DCPIP activities in the digitonin solubilizates. This translated to approximately 5-fold higher specific activity of SDH compared to that of mGPDH. On the one hand, this difference points to a significant inactivation of mGPDH during solubilization by nonionic detergents, a general problem previously observed in mGPDH isolation and purification [33]. On the other hand, it indicates that bound CoQ is more easily and efficiently lost from SDH than mGPDH, in accordance with minute content of CoQ observed in isolated SDH [34].

3.2. ROS production by digitonin solubilized mGPDH and SDH responds differently to external CoQ

To characterize ROS production by solubilized mGPDH and SDH, we measured GP- and succinate-induced hydrogen peroxide production at 10 mM substrate concentration following oxidation of 50 μM Amplex Red in the presence of added peroxidase (1 U.mL^{-1}). When dehydrogenase-dependent ROS production was analyzed as succinate-induced ROS production in mitochondria (Fig. 3B, "0" digitonin values), it showed very low basal levels (50 pmol H_2O_2.min^{-1}.mg^{-1} protein)

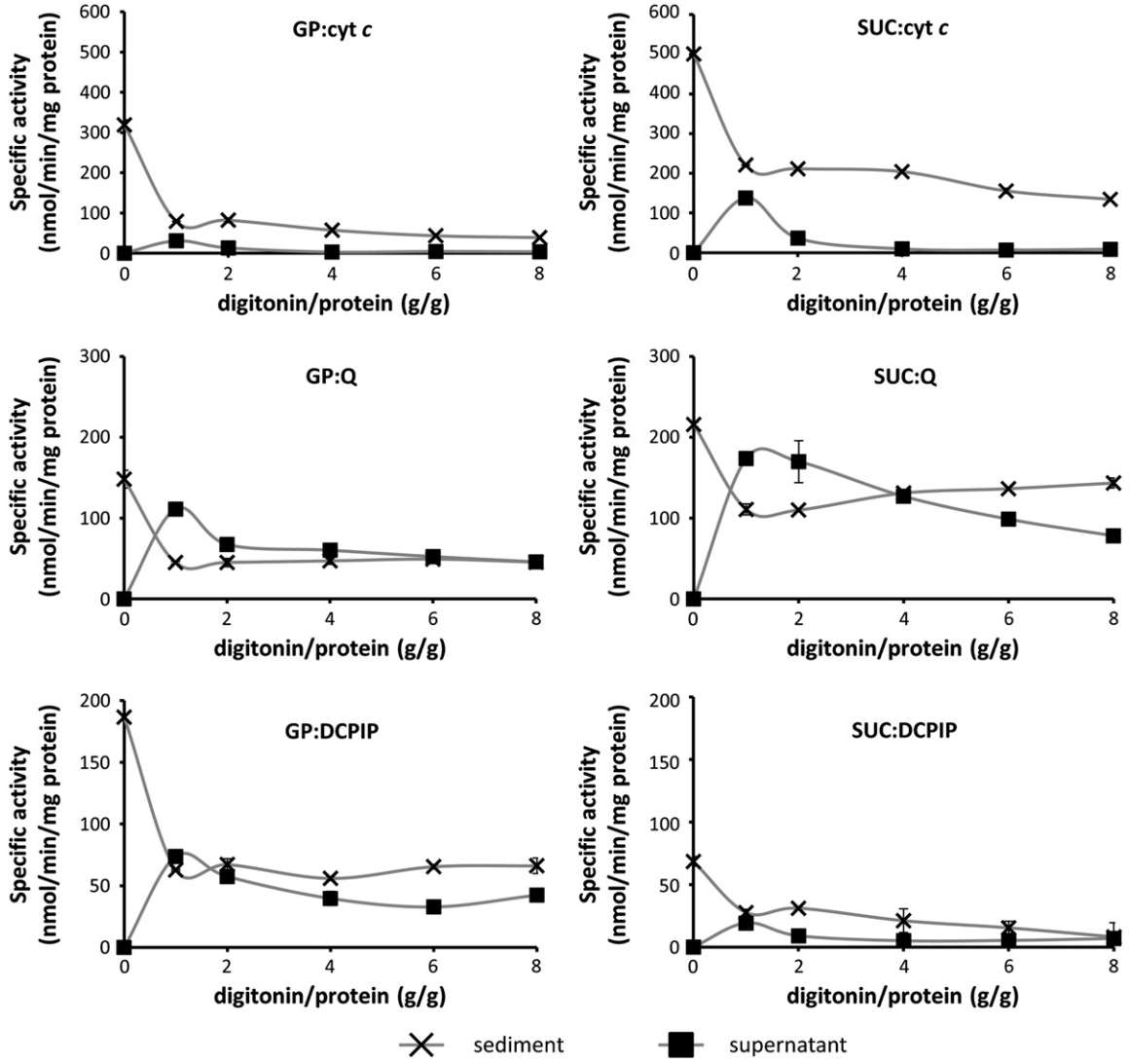

Fig. 1. Enzyme activities in digitonin-solubilized BAT mitochondria. Mitochondria were solubilized with increasing amounts of digitonin (1, 2, 4, 6, 8 g/g protein). SDH and mGPDH enzyme activities were detected both in supernatants and sediments (20,000 *g*) after solubilization. Activities were determined as CoQ_1 reductase (GP:Q, succinate:Q) or DCPIP reductase (GP:DCPIP, succinate:DCPIP), i.e. isolated dehydrogenase activity or as cytochrome *c* reductase (GP:cyt *c*, succinate:cyt *c*), i.e. combined activity of dehydrogenase and complex III, referring about intactness of electron transport chain in respective sample. Activities are expressed per mg protein of solubilizates (digitonin 1–8 g/g protein) or mitochondria (digitonin 0). Results are mean ± SD from 2 to 4 replicates.

but strong, more than 5-fold activation by myxothiazol (MXT). This effect of MXT on SDH-dependent ROS generation rapidly declined in solubilized enzyme with increasing digitonin concentration, analogically to SCCR and succinate:DCPIP activity (Fig. 1). In the case of mGPDH-dependent ROS production, the basal mitochondrial ROS production was higher (140 pmol $H_2O_2.min^{-1}.mg^{-1}$ protein) (Fig. 3A) and MXT displayed similar activation in whole mitochondria. But, in a sharp contrast to SDH, solubilization of the inner mitochondrial membrane led to the pronounced increase in basal mGPDH-dependent ROS production at increasing digitonin concentrations. Despite higher SCCR than GCCR activities in isolated mitochondria (see "0" digitonin values for supernatants in Fig. 1), mGPDH-dependent ROS production in fully solubilized mitochondrial membranes (digitonin 4–8 g/g protein) was >15 fold higher than SDH-dependent ROS production.

It has been recently reported, that SDH may be a significant ROS producer under low succinate concentrations [11]. We therefore determined the levels of ROS production with 0.4 mM succinate as well. As seen in Fig. 3C, the pattern of SDH-dependent ROS generation was rather different under these conditions. As in the case of 10 mM succinate, basal ROS production in mitochondria was low with 0.4 mM succinate and it was strongly increased by blockade of complex III by MXT. To the contrary, basal ROS production with 0.4 mM succinate concentration was strongly stimulated by detergent solubilization, steadily increasing up to the highest digitonin concentration used, similarly as was the case for mGPDH-dependent ROS production. With all substrates used, no activation effect of MXT was observed in solubilizates with digitonin 4–8 g/g protein respectively, indicating that at these detergent concentrations dehydrogenases do not communicate directly with complex III and the observed ROS production originates solely from the respective dehydrogenases. These data are in general agreement with dehydrogenase:cyt *c* enzyme activities measured in Fig. 1. It should also be noted that the actual absolute levels of ROS production with 0.4 mM succinate are underestimated, as SDH is known to be inhibited by oxaloacetate [35,36] and 0.4 mM succinate is not sufficient to displace oxaloacetate from the active site of the enzyme. As can be seen from Supplementary Fig. 2, approximately 50–60% of SDH in our preparations was in inactive state. While with 10 mM succinate, this inhibition is released and whole bulk of the enzyme contributes to the ROS production, for 0.4 mM succinate the inactivated portion of SDH does not contribute to the measured ROS production. However, this does not have effect on the relative changes in ROS production due to solubilization or inhibitor action.

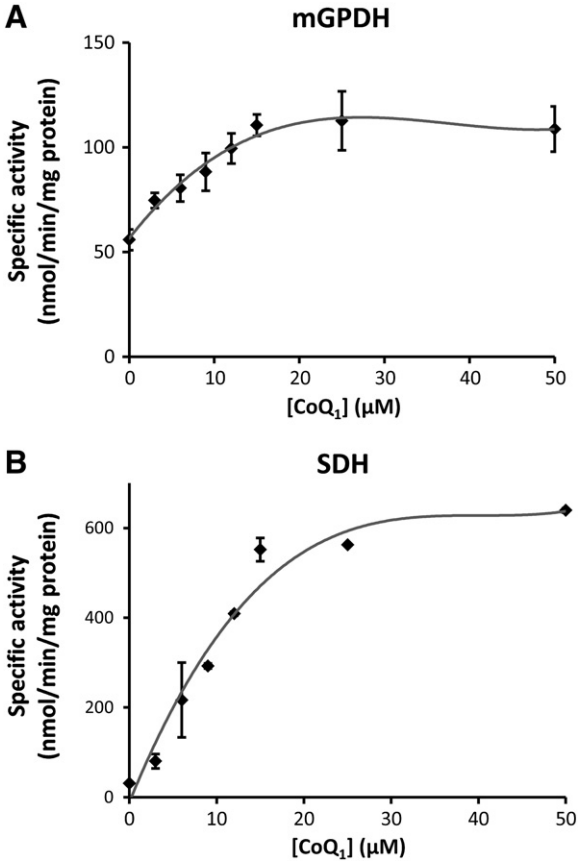

Fig. 2. Activation of digitonin-solubilized dehydrogenases by CoQ. Effect of CoQ_1 addition on mGPDH (A) and SDH (B) enzyme activities measured as dehydrogenase:DCPIP reductases was studied in BAT mitochondria solubilized with digitonin (2 g/g protein 20,000 *g* supernatants). 0 to 50 μM CoQ_1 was added to the cuvette and enzyme activity was measured. Results are mean ± SEM from 3 to 5 measurements.

Recent work of Brand's group [11] suggested significant portion of mGPDH-dependent ROS to originate from SDH due to reverse flow of electrons. This is possibly of lower importance in frozen thawed mitochondria used in our experiments, but as shown in Supplementary Fig. 3, in frozen mitochondria supplied with GP, there is still significant SDH-dependent portion of ROS under the conditions with MXT present (compare values with MXT vs. MXT + atpenin A5). However, this part of ROS production is completely abolished in solubilized mitochondria, where dehydrogenases cannot communicate directly via CoQ pool (Supplementary Fig. 3).

As mGPDH and SDH are supposed to differ in their ability to bind CoQ, we decided to analyze effect of exogenous CoQ_1 on the measured ROS production (data in Fig. 3D–F and in the redrawn form in Fig. 4 to emphasize differences between membrane-bound and solubilized dehydrogenases). Addition of oxidized CoQ_1 to isolated mitochondria had prooxidant effect for all three substrates tested: GP (Fig. 4A), succinate 10 mM (Fig. 4B) and succinate 0.4 mM (Fig. 4C). This prooxidant behavior of CoQ_1 was fully retained after addition of complex III inhibitor — MXT, while the absolute values of ROS production after MXT addition rose as in the absence of CoQ_1 (Fig. 4A–C). The effects of CoQ_1 and MXT were thus simply additive, probably reflecting the increase in available CoQ pool size. This behavior changed, when fully solubilized complexes (digitonin 6 g/g protein) were studied. Here CoQ_1 had strong antioxidant effect on ROS production with GP (Fig. 4D) and 0.4 mM succinate (Fig. 4F), while it still acted as prooxidant in case of 10 mM succinate (Fig. 4E). Addition of MXT alone to solubilized mitochondria did not influence basal ROS production, but it abolished antioxidant effect of CoQ_1 on GP and 0.4 mM succinate (Fig. 4D–F). In the case of 0.4 mM succinate, CoQ_1 and MXT led to even more pronounced ROS production than observed at basal levels (726 ± 31 vs. 266 ± 22 pmol.min^{-1}.mg^{-1}), representing the highest ROS production observed in solubilized mitochondria (Fig. 4E). Thus the ability to reoxidate soluble CoQ_1 on complex III (which is still present in the solubilizate, albeit not in the same respiratory supercomplex as flavin dehydrogenases) seems to be essential for its antioxidant effect on ROS production supported by GP and 0.4 mM succinate. Overall picture of pro-/anti-oxidant effects was the same when AA was used as complex III inhibitor. However, absolute ROS production with AA was higher given the fact, that ROS are under these conditions produced at the level of complex III as well (data not shown). Presumably loss of endogenous CoQ_9 facilitates electron leak from mGPDH, supporting the view that Q-binding site is the locus of electron leak. In case of SDH analogous mechanism seems to operate at low substrate concentration, probably reflecting the direct effect of CoQ on SDH activity [37], even though the substrate binding site was proposed to generate ROS at these conditions [11].

3.3. Electron leak induction by single electron acceptors

In further experiments we followed ROS production induced by single electron acceptor potassium ferricyanide (FeCN). Here, ROS production can be detected as a burst of oxygen consumption due to the formation of hydrogen peroxide under the conditions, when respiratory chain is blocked at the level of complex III (with AA or MXT) or complex IV (with KCN). This phenomenon has been demonstrated in mitochondria with GP but not with succinate used as a substrate [12]. Presumably, FeCN accepts one electron from mGPDH and the second electron leaks to oxygen, forming superoxide ($O_2^{\bullet-}$) which is subsequently dismutated to hydrogen peroxide. The net effect manifests as oxygen consumption, which can be abolished by the presence of catalase that induces decomposition of hydrogen peroxide to water and oxygen (not shown and [12]).

As shown in Fig. 5A, the FeCN-induced oxygen consumption by mGPDH is fully retained after solubilization with digitonin (2 g/g protein). Similarly to whole mitochondria [12], it is completely prevented by addition of CoQ_1 (Fig. 5A) or by addition of another one-electron acceptor, hexaammineruthenium(III) chloride (HAR) (Fig. 5B). Electron leak due to one electron transfer to FeCN can therefore be disturbed by other electron acceptors interacting with mGPDH, presumably downstream of the flavin site. Complex II inhibitor atpenin A5 did not influence GP-dependent, FeCN-induced electron leak (Fig. 5C), indicating that the leak occurs directly on mGPDH and not indirectly via electron backflow towards SDH. As in mitochondria, no FeCN-induced ROS production can be observed in digitonin (2 g/g protein) solubilizates with 10 mM succinate (not shown). However, as SDH was shown to produce ROS at much higher rate with low succinate concentrations, we tested FeCN effect with 0.4 mM succinate. Nevertheless, neither here there was any observable induction by FeCN of oxygen consumption due to electron leak (Fig. 5D). Leak of electrons from flavin in SDH may also be facilitated by blockade of CoQ binding site by atpenin A5. Here FeCN would allow for the electrons to be channeled away immediately upstream of atpenin binding site but neither the addition of atpenin induced FeCN-mediated leak with 0.4 mM succinate (Fig. 5D). To make sure that atpenin A5 acts as a specific SDH inhibitor even for solubilized enzymes, we followed the effect of atpenin A5 on mGPDH and SDH activities (Supplementary Fig. 4A–C). As can be seen, atpenin A5 did not inhibit mGPDH when measured either as Q, DCPIP or FeCN reductase, but fully inhibited succinate:Q and succinate:DCPIP activity and only partially abrogated succinate:FeCN activity, which is in agreement with atpenin A5's role as specific SDH inhibitor acting at CoQ binding site. This points to a major difference between mGPDH and SDH in the mechanism of electron leak and ROS generation.

Broad absorption spectrum of FeCN interferes with the fluorescent detection of oxidized Amplex Red, but FeCN-induced ROS production

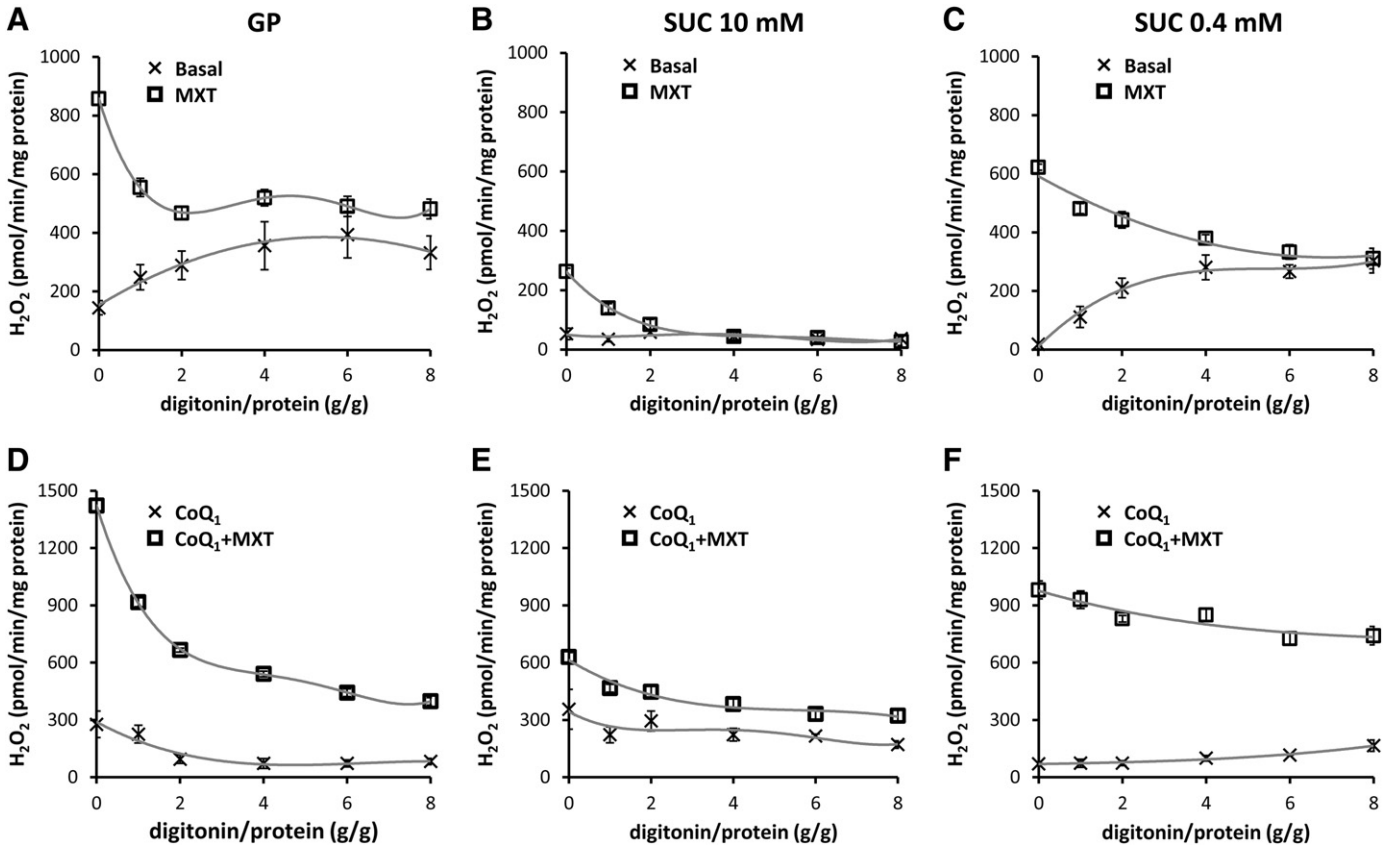

Fig. 3. Reactive oxygen species production in digitonin-solubilized BAT mitochondria. Mitochondria were solubilized with increasing amounts of digitonin (1, 2, 4, 6, 8 g/g protein) and ROS were detected as hydrogen peroxide production measured fluorometrically following oxidation of Amplex Red (50 μM) in the presence of HRP (1 $U.mL^{-1}$) in mitochondria (0 digitonin values) and 20,000 *g* supernatants after digitonin solubilization. 10 mM glycerol-3-phosphate (GP), 10 mM succinate (SUC 10 mM) or 0.4 mM succinate (SUC 0.4 mM) was used as substrate respectively. Titration curves are for basal ROS production without inhibitor (Basal), in the presence of 1 μM myxothiazol (MXT), 12 μM CoQ_1 (CoQ_1) or 12 μM CoQ_1 plus 1 μM myxothiazol (CoQ1 + MXT). Note that effect of myxothiazol, inhibitor of complex III, on ROS production can only be observed in mitochondria and at low digitonin/protein ratios, when intact electron transfer pathway between dehydrogenase and complex III exists. Results are mean ± SD from 3 to 6 replicates.

can also be detected by luminometry [12]. Here, HRP mediated luminol oxidation causes luminescence flash and is detected. As can be seen in Fig. 6A, FeCN can induce GP-dependent electron leak in digitonin 2 g/g protein solubilizates, while there is no observable electron leak with HAR under the same conditions. HAR also partially inhibits FeCN-induced electron leak (Fig. 6B and D), both when added after the FeCN (Fig. 6B) or when prior present in the medium (Fig. 6D). These data are in accordance with the analogous measurements of oxygen consumption (Fig. 5B). We cannot confirm that HAR accepts electron directly from the dehydrogenase, as HAR redox state cannot be detected spectrophotometrically. Nevertheless, from Supplementary Fig. 4D it is obvious, that HAR can positively influence apparent rate of FeCN reduction in spectrophotometric activity assay, indicating that HAR can facilitate electron transfer to FeCN, possibly as an intermediate electron carrier. Further, we wanted to confirm that mGPDH electron leak really occurs on the dehydrogenase itself. Fig. 6C demonstrates significant FeCN-induced ROS production in digitonin 2 g/g protein solubilizates with GP as a substrate in the presence of 1 μM rotenone, 1 μM MXT, 1 $mg.mL^{-1}$ AA, 1 μM atpenin A5 and 10 mM malonate, it is at conditions when all other possible sites of electron leak have been blocked by their respective inhibitors. Maximum luminescence peak in the presence of all inhibitors was only marginally changed compared to basal conditions, thus demonstrating that in overall ROS production the primary source of FeCN-mediated electron leak has to be mGPDH. There was also no significant ROS production when sn-glycerol-2-phosphate, a glycerol-3-phosphate stereoisomer that is not oxidized by mGPDH was used as a substrate (Fig. 6C, dashed line), further confirming that FeCN-induced electron leak only occurs when GP is oxidized on mGPDH and electrons are supplied into the enzyme.

All these experiments point towards CoQ binding site of mGPDH as the most likely source of the electron leak. To our knowledge, there is no specific inhibitor of CoQ site on mGPDH. We therefore tested effect of 2-n-heptyl-4-hydroxyquinoline N-oxide (HQNO), generalized competitive inhibitor, which binds to CoQ sites of various enzymes [38]. As shown in Fig. 7, in fully solubilized mitochondria (digitonin 6 g/g protein) blockade of mGPDH with 10 μM HQNO significantly decreases GP-dependent ROS production, while it has no effect on succinate-dependent ROS production, further implying that CoQ binding site is the source of electron leak on mGPDH.

3.4. mGPDH supercomplexes

Previous studies on isolation of mammalian mGPDH repeatedly observed a "holoenzyme" of 250–300 kDa consisting of only 75 kDa mGPDH protein suggesting oligomerization of this rather hydrophobic dehydrogenase. To search for different forms of the two dehydrogenases we analyzed digitonin solubilizates of mitochondrial membranes by means of native BN-PAGE and hrCN3-PAGE [26,28]. For detection we used WB with specific antibodies and in-gel activity staining (Fig. 8). We found mGPDH to be present in several homooligomeric forms, presumably as dimer, trimer and tetramer, as well as in high molecular mass supercomplex (SC) of more than 1000 kDa of yet unknown composition. The SC quantity was higher in hrCN3-PAGE judged both by WB (Fig. 8B) and in-gel activity (Fig. 8C), than in BN-PAGE (Fig. 8A) where

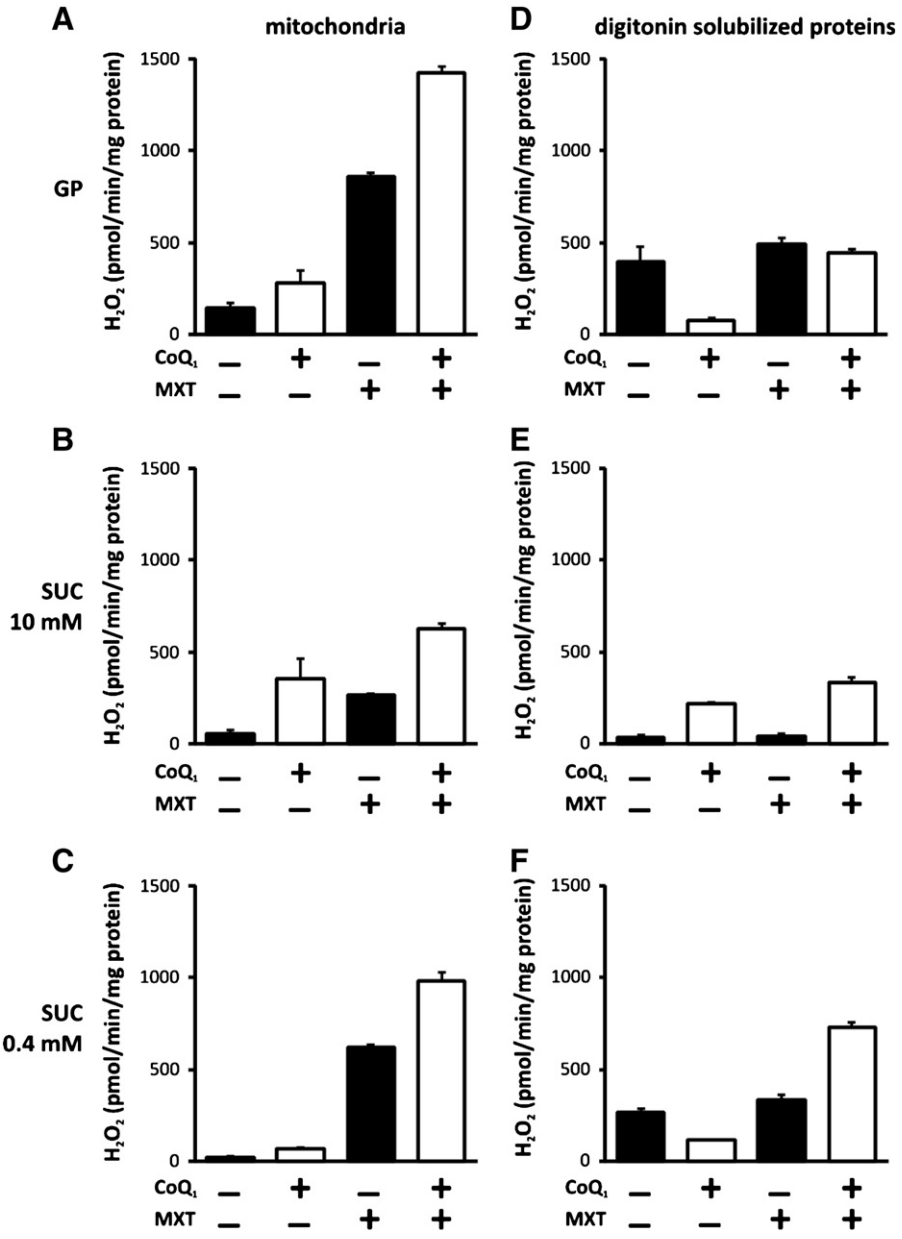

Fig. 4. Intactness of respiratory chain and CoQ influence ROS production. Data from Fig. 3 were redrawn to better document effect of decoupling dehydrogenase from complex III by solubilization on ROS production and its influence by CoQ_1. ROS production was detected in BAT mitochondria or 20,000 *g* digitonin solubilizates (6 g/g protein) with 10 mM glycerol-3-phosphate (GP), 10 mM succinate (SUC 10 mM) or 0.4 mM succinate (SUC 0.4 mM) respectively. Where indicated 1 μM myxothiazol (MXT) or 12 μM CoQ_1 (CoQ_1) was added into the assay. Results are mean ± SD from 3 to 6 replicates.

SC appeared as significantly fainter band and where monomer of mGPDH was observed as well. This indicates that this complex is labile and dissociates by the change of electrostatic interactions caused by the addition of Coomassie Blue dye. The content of mGPDH SC apparently declined with increasing concentration of digitonin and in turn, the contents of dimer and trimer increased correspondingly (Fig. 8C). In terms of the relative contribution of individual forms, dimer seems to be the most prominent form of mGPDH. Quantification of western signal gave the following relative values (dimer content set as 100%) for supercomplex:tetramer:trimer:dimer:monomer — 50:14:40:100:5 using hrCN3-PAGE and 25:17:51:100:42 using BN-PAGE and digitonin 2 g/g solubilizates. In the case of SDH only a 140 kDa monomer was found (not shown specifically but see western signal in Fig. 10).

To find out possible cross-reactions with other respiratory chain complexes we performed 2D electrophoretic analysis with the digitonin (2 g/g protein) solubilizates resolved by hrCN3-PAGE in the first dimension and by SDS-PAGE in the second. As seen in Fig. 9, individual forms of mGPDH were well resolved and even two distinct spots of mGPDH SC of >1 MDa could be seen (Fig. 9A), but none of them associated with signal of complex I, complex III or complex IV (Fig. 9B) i.e. OXPHOS complexes, which may share common electron transfer pathway with mGPDH and would therefore make kinetic sense. The putative mGPDH supercomplexes were smaller/larger than canonical respiratory chain SCs as can clearly be seen from the overlay of densitometric traces in Fig. 9C. As for the low molecular weight forms of mGPDH and their co-migration with the signal of other RC complexes, the patterns observed did not indicate association of mGPDH with assembled monomeric forms of respiratory chain complexes. Overlapping signals of mGPDH and SDH at 140 kDa apparently represent separate SDH monomers and mGPDH dimers because putative SDH–mGPDH heterodimer would have to have molecular weight of at least 210 kDa. With the antibody to Core2 subunit a significant signal was observed

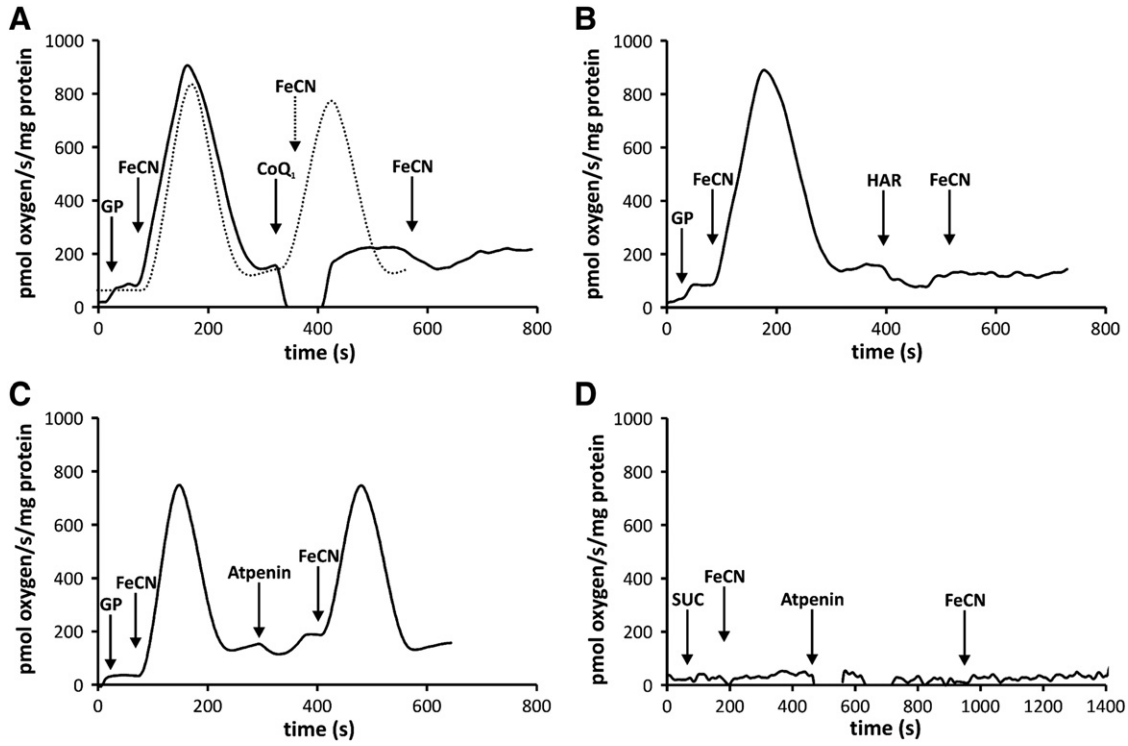

Fig. 5. Polarographic detection of ferricyanide-induced ROS production. ROS production was detected as ferricyanide (FeCN)-activated myxothiazol-insensitive oxygen uptake by digitonin solubilized BAT mitochondria (20,000 *g*, 2 g/g protein). (A,B) Coenzyme Q and hexaamine ruthenium (HAR) inhibit FeCN-induced ROS production by solubilized mGPDH determined as oxygen consumption with 10 mM glycerol-3-phosphate. At time intervals indicated in the graph, FeCN was added at a concentration of 62.5 μM. Addition of 16 μM CoQ_1 (A) or 125 μM HAR (B) completely abrogated FeCN-induced ROS production peak. Dotted line in (A) represents control trace with two subsequent additions of FeCN. (C) Addition of atpenin A5, inhibitor of SDH Q site does not have effect on GP-dependent, FeCN-induced ROS production. (D) FeCN induced ROS production is specific for mGPDH as there is no measurable myxothiazol-independent FeCN-induced ROS production if 0.4 mM succinate is used as substrate, and neither it is induced by the addition of atpenin A5. In each case representative measurement obtained independently with 2–5 different solubilizate preparations is shown.

in the region of 67 to 230 kDa but its profile was also different from that of mGPDH and most likely represents free Core2 subunit and assembly intermediates of complex III.

3.5. ROS production by the isolated enzyme

With the aim to analyze the ability to generate ROS by different soluble forms of mGPDH and SDH we set to develop protocol for in gel ROS measurements. Using this approach we were able to identify ROS production which co-localized with the WB signal detected by antibodies against mGPDH or SDH respectively (Fig. 10). ROS production was apparent in both dehydrogenases when soluble CoQ analog CoQ_1 was present, however, much higher intensity of ROS signal was again associated with mGPDH although the activity of mGPDH was 4-fold lower than that of SDH in the digitonin 2 g/g protein solubilizates used (see Fig. 2). ROS was thus detected in putative homooligomers as well as supercomplex form of mGPDH. In the absence of exogenous CoQ_1 only the signal of mGPDH-dependent ROS production was observed, mainly at mGPDH mono- and homooligomers. SDH ROS production without CoQ_1 was not observed with 0.4 mM succinate either (not shown), implicating that the isolated mGPDH but not SDH can generate ROS due to electron leak when supplied with the substrate only.

4. Discussion

In this paper we set to study ROS production by two flavin dehydrogenases of the mitochondrial respiratory chain — SDH and mGPDH in the system of frozen–thawed mitochondria solubilized with mild detergent digitonin. Solubilization of mitochondrial membranes with mild detergents is well established both for enzyme isolation and for the analysis of respiratory chain enzyme interactions in the membrane. Naturally, even this approach has its drawbacks. Solubilization may influence enzyme behavior as it is documented that enzyme activities of both SDH and especially mGPDH are affected by the lipid composition of the surrounding membrane. But on the other hand, it represents convenient option how to study dehydrogenases in isolation and dissect the portion of ROS production associated with enzymes themselves. It is well known that other complexes do contribute to overall ROS production from flavin dehydrogenases. This applies both for downstream complex III and for the upstream complex I or even complex II, which can be source of ROS through reverse electron transport from mGPDH. Solubilized enzymes thus offer unique opportunity to define *bona fide* sites of ROS production and to help with explanation of the mechanism of electron leak.

4.1. Solubilization and enzyme activities

As an experimental setup we chose to solubilize BAT mitochondria with increasing concentrations of digitonin and subsequently to fractionate them by centrifugation at 20,000 *g* for 20 min. This type of solubilization is widely used for the study of respiratory supercomplexes and has been shown to separate multiprotein complexes of up to 10 MDa [28,39]. To characterize conditions of solubilization we have first studied enzymatic activities in both solubilizates and sediments after solubilization. From these studies we can conclude that: (i) Only part of the mitochondrial proteins gets solubilized by detergent treatment (51–66% depending on digitonin concentration). Portion remains in the sediment and this does not change significantly by increasing detergent concentrations. (ii) Both mGPDH and SDH are partially inactivated by solubilization. As can be calculated from protein recoveries, at the highest digitonin concentration used (8 g/g protein), 53% of the protein was recovered in supernatant, but only 25.5% of GP:Q and 29.8% of succinate:Q activities

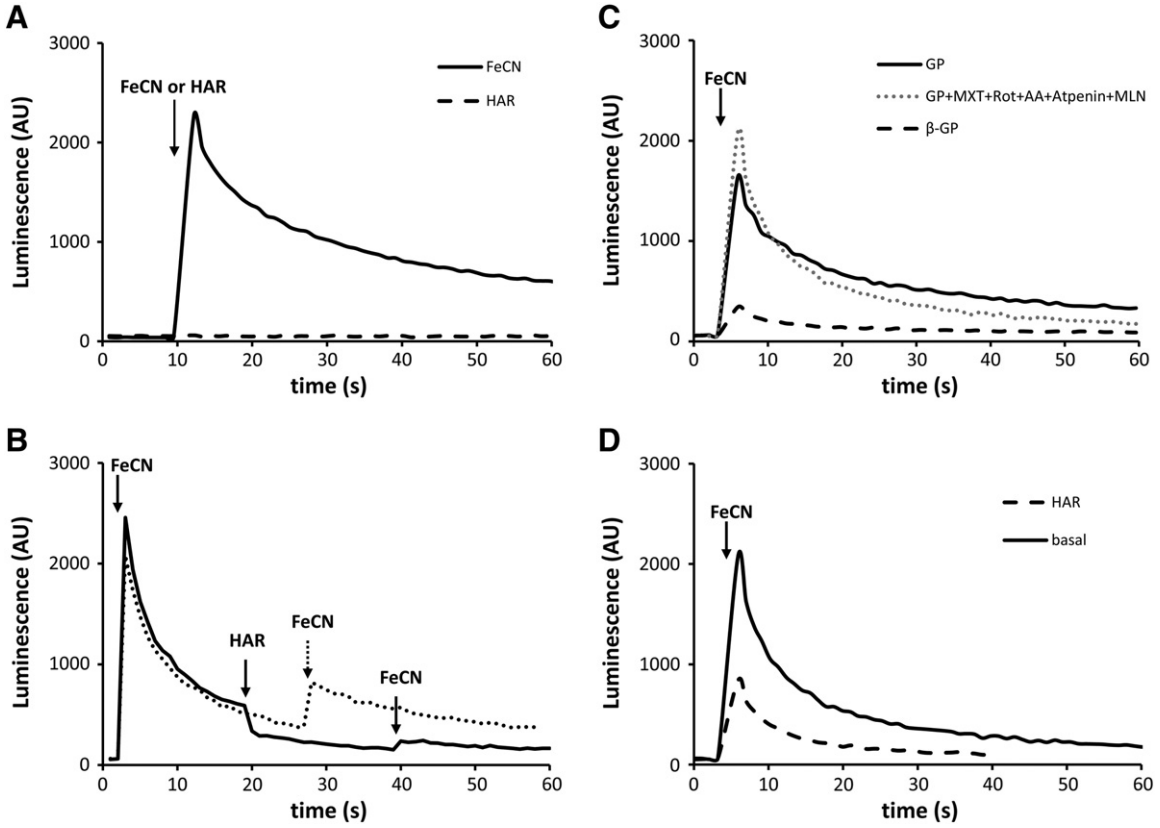

Fig. 6. Luminescence detection of ferricyanide-induced ROS production. ROS were detected as luminescence peak caused by the oxidation of luminol (1 mM) catalyzed by the HRP (2.5 U.mL^{-1}). ROS production was induced by FeCN (500 μM) or hexaamine ruthenium (HAR, 125 μM). 20,000 *g* solubilizates (digitonin 2 g/g protein) oxidizing 10 mM glycerol-3-phosphate were used. (A) While ferricyanide (FeCN, solid line) induces ROS production, hexaamine ruthenium (HAR, dashed line) cannot induce electron leak under identical conditions (n = 6). (B) HAR partially abrogates FeCN-induced ROS production if added sequentially to the same sample — solid line (n = 3). Dotted line represents control trace with two sequential additions of FeCN. (C) FeCN electron leak is mGPDH specific — does not depend on other complexes of respiratory chain. Solid line — control trace; dotted line — trace in the presence 1 μM rotenone (Rot), 1 μM myxothiazol (MXT), 1 mg.mL^{-1} antimycin A (AA), 1 μM atpenin A5, 10 mM malonate (MLN). It also cannot be induced when 10 mM non-oxidizable sn-glycerol-2-phosphate (β-GP) is used as a substrate — dashed line (n = 2). (D) HAR in the medium attenuates FeCN-induced ROS production. Solid line — no HAR present in the medium, dashed line — 125 μM HAR added to the incubation medium before measurement (n = 3). In each case representative measurement is shown and number of independent replicates from different solubilizate preparations is indicated as (n).

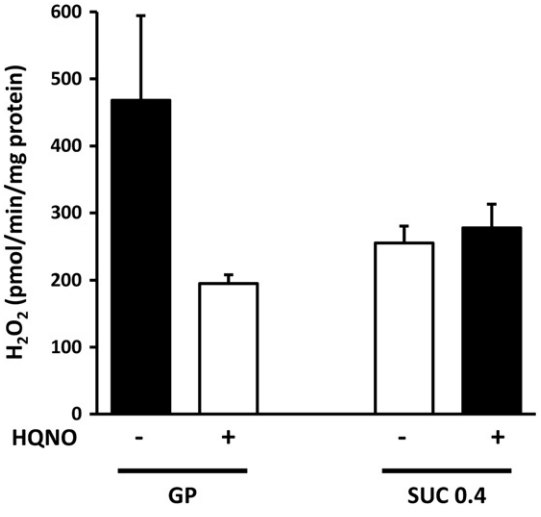

Fig. 7. HQNO inhibits GP-dependent ROS production. Hydrogen peroxide production was measured fluorometrically as oxidation of Amplex Red (50 μM) in the presence of HRP (1 U.mL^{-1}) in 20,000 *g* supernatants after solubilization of BAT mitochondria with digitonin (4 g/g protein). Either 10 mM glycerol-3-phosphate (GP) or 0.4 mM succinate (SUC 0.4) was used as substrates. Where indicated 10 μM 2-n-Heptyl-4-hydroxyquinoline N-oxide (HQNO) was used. Results are mean ± SD from 2 replicates.

were recovered. However, this inactivation is a well documented phenomenon, especially for mGPDH [33]. (iii) CoQ seems to be lost during solubilization, apparently more so in the case of SDH. This may be an indirect measure of enzyme affinity towards CoQ. Interestingly, low CoQ recovery during SDH purification has already been described [34]. In that study, SCCR activity could be reestablished by the addition of purified complex I, which retains CoQ during purification and thus served as CoQ source in the final preparation. In this context, the presence of CoQ observed in supercomplexes respiring on succinate [40] may not represent its direct association with SDH. (iv) At low digitonin concentration (1 g/g) we have observed the presence of patches of respiratory chain in the solubilizates, that contained at least flavin dehydrogenase (SDH, mGPDH) and complex III, as reported by the DH:cyt c activity. But based only on these measurements, they cannot be directly declared as respiratory supercomplexes. Furthermore, their content is low and above digitonin 4 g/g protein dehydrogenases become separated as individual entities without connection with the rest of OXPHOS. Apart from dehydrogenases and complex III, it is not clear, what are these complexes composed of (see below).

4.2. ROS production in solubilized mitochondria

In order to characterize ROS production by mGPDH and SDH we chose BAT mitochondria, that contain high (near equimolar) levels of both dehydrogenases [41]. Recently, several papers explored ROS production by flavin dehydrogenases, focusing on potential in vivo sources

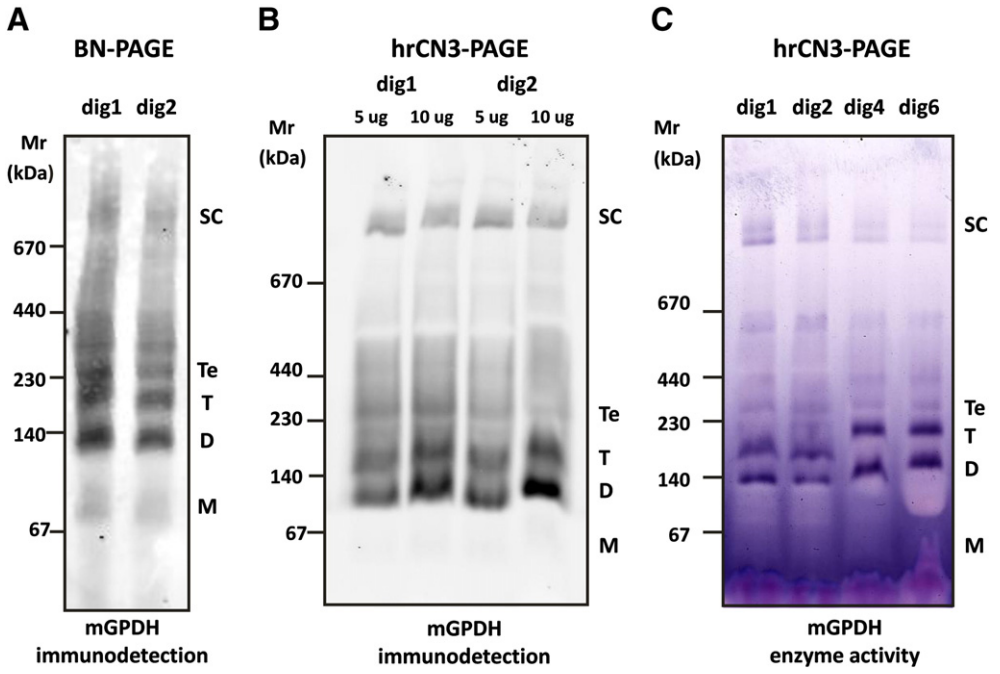

Fig. 8. Association of mGPDH into oligomeric complexes. BAT mitochondria were solubilized with different amounts of digitonin (dig) — 1, 2, 4 or 6 g/g protein. Solubilized proteins were separated using either BN-PAGE (A) or hrCN3-PAGE (B, C) native electrophoretic system (gel gradient 4–13%). (A, B) Western blot detection of mGPDH protein with specific antibody; (C) histochemical detection of mGPDH enzymatic activity using nitroblue tetrazolium as electron acceptor. mGPDH can be observed as faint monomer (M) band and in higher molecular mass complexes, presumably representing homodimer (D), homotrimer (T) homotetramer (Te) and high molecular mass supercomplex (SC) of unknown composition. Monomer was only visible, when BN-PAGE was used.

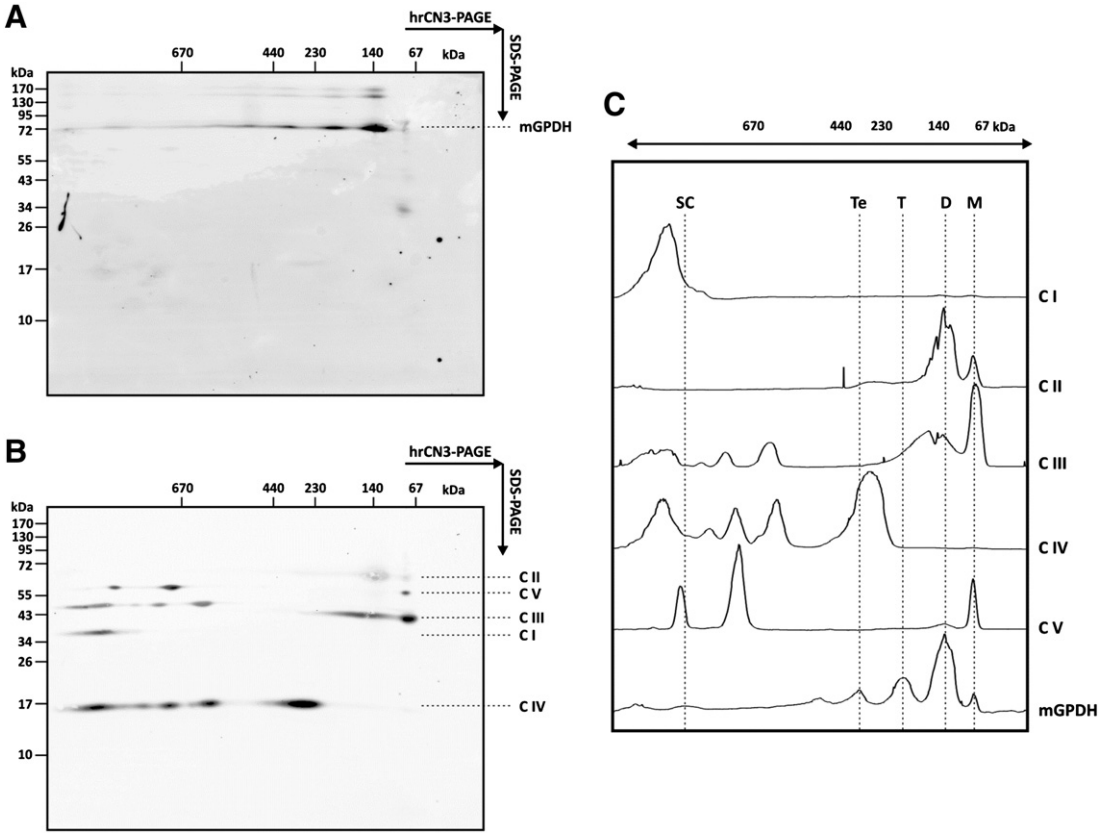

Fig. 9. 2D electrophoretic analysis of the association between mGPDH and OXPHOS complexes. Digitonin-solubilized mitochondrial proteins (2 g/g protein) were analyzed by two-dimensional hrCN3-PAGE/SDS-PAGE. After the first dimension separation by hrCN3-PAGE (50 μg protein), gel strip was treated with mercaptoethanol/SDS solution and SDS-PAGE was used in the second dimension followed by western blot analysis. (A) Detection of mGPDH protein. (B) Detection of OXPHOS subunits for individual respiratory chain complexes I–V: CI (NDUFA9), CII (SDHA), CIII (Core2), CIV (Cox4) and CV (α). (C) Profiles for 2D signal patterns of respective complexes. Position of mGPDH monomers (M), dimers (D), trimers (T), tetramers (Te) or supercomplexes (SC) is indicated.

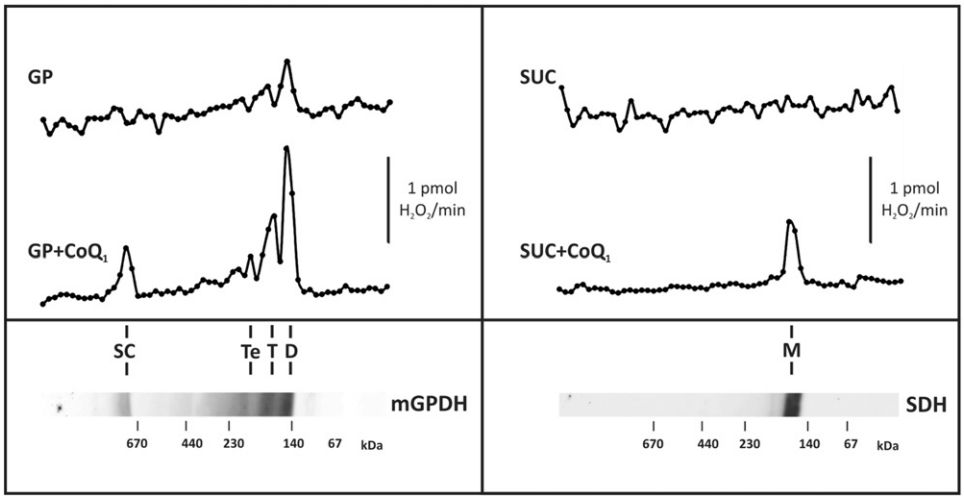

Fig. 10. Reactive oxygen species production by isolated enzyme. BAT mitochondria were solubilized with digitonin (2 g/g protein) and separated on hrCN3-PAGE. Part of the gel was used for western blot detection of mGPDH and SDH with specific antibodies (bottom panels). Gel strips were cut into 1 mm thick slices and those were used for fluorometric detection of ROS production with Amplex Red and HRP in the presence of substrate only (GP, SUC) or substrate and 12 μM CoQ_1 (GP + CoQ_1, SUC + CoQ_1). Representative traces from experiments performed on 3–6 independent preparations are shown; points on the curves represent actual measurements of ROS production in individual gel slices. M indicates monomer of SDH D, T, Te and SC indicate dimer, trimer, tetramer and supercomplex forms of mGPDH.

of ROS with succinate or GP as substrates [11,17,42]. While this analysis is important as well, due to the fact, that total in vivo ROS production with respective substrate will occur on several places in the OXPHOS, it may not provide an insight detailed enough to see into the mechanism on respective enzymes themselves. As our work focuses on solubilized mitochondria, we also chose to use frozen–thawed mitochondria as a control. Here we do not observe backflow towards complex I, which contributes to overall measured ROS levels [43].

Our data confirmed previous observations that SDH with saturating concentration of succinate (10 mM), produces very low quantities of ROS itself and most of the observed production happens on complex III [15]. Such ROS production diminishes after solubilization of the enzyme and points to low importance of electron leak from SDH under these conditions. More important are the observations with low succinate concentration (0.4 mM) and with GP. In both cases, the leak of electrons (ROS production) from respective dehydrogenase increases with increasing digitonin concentration. This clearly demonstrates that if electrons cannot be transferred further down the respiratory chain, both dehydrogenases tend to leak them towards O_2. As the dehydrogenases are fully soluble under high digitonin concentrations, it also demonstrates that such leak occurs on the respective enzymes themselves. In the case of SDH, this confirms recent observation made with the use of SDH inhibitor atpenin A5 [11,44]. As our system does not use inhibitors, it can serve as a further confirmation, that such ROS production really occurs on SDH and is not an artifact due to the presence of atpenin A5.

4.3. Effect of coenzyme Q

Because CoQ appeared to be depleted from solubilizates, we decided to check the effect of the addition of the soluble analog CoQ_1 on ROS production. For these experiments we used oxidized CoQ_1. While it was generally a pro-oxidant in mitochondrial preparations, it acted as an antioxidant in solubilized mitochondria with GP and 0.4 mM succinate. It most likely shows that reestablishment of electron flux by soluble CoQ_1 decreases pressure for electron leak from either mGPDH or SDH. As the antioxidant effect was abolished by MXT, it is clear that reoxidation of CoQ_1 on complex III is vital for its antioxidant role. Rather interesting is the strong prooxidant effect of reduced CoQ_1 (in the presence of MXT) with 0.4 mM succinate as substrate, because FAD should be the proposed site of electron leak here [11]. However, it has been shown that SDH activity is strongly regulated by the reduction state of CoQ pool and is highest with CoQ pool fully reduced [36]. Increase in the observed ROS production may therefore be also the effect of increased SDH enzymatic activity.

We further studied the potential of Q site as the source of electron leak by the use of one electron acceptors FeCN and HAR. The ability of ferricyanide to induce electron leak from mGPDH is well established [12,22]. Here we show that it is fully retained in solubilized mitochondria. Importantly, it cannot be inhibited by SDH inhibitor atpenin A5 or by complete inhibition of all other OXPHOS complexes but mGPDH. On the other hand, addition of the other single electron acceptor HAR (previously used in studies of complex I [45,46]) or CoQ abolishes the ability of FeCN to induce the leak of electrons. We do not have direct evidence of interaction sites for FeCN and HAR in case of mGPDH. In complex I, it was demonstrated, that FeCN displays ping–pong bi–bi kinetics [47], while HAR has ordered reaction mechanism [45]. It was interpreted so that FeCN interacts with FMN from the side of NADH binding cleft and HAR accepts electrons downstream of FMN. It is likely that FeCN interacts directly with FAD in mGPDH as well. mGPDH was proposed to have ping–pong reaction mechanism for GP reduction, analogously to the bacterial homolog GlpD [13,48]. FeCN would thus take one electron from $FADH_2$, producing flavin semiquinone, the actual source of ROS under these conditions. Most plausible explanation for the inhibitory effect of CoQ_1 and HAR on FeCN-induced electron leak is that they react downstream of FeCN reduction site (similarly to complex I) and channel electrons away from flavin semiquinone.

FeCN effect on SDH ROS production has not been demonstrated yet, despite the fact that SDH effectively transfers electrons to FeCN [49]. Here we show that neither solubilization, nor low succinate concentration or presence of atpenin A5 can induce FeCN-facilitated electron leak from SDH. It is rather surprising especially at low succinate concentrations, as it was suggested that incomplete substrate site occupancy is the prerequisite for ROS formation on SDH [11]. Empty substrate binding cleft with flavin semiquinone would represent rather likely place for one electron FeCN reduction, thus inducing electron leak, but this did not occur. All these demonstrate that transfer of electrons must be different between FAD and Q in both enzymes, with potential for channeling electrons away by single electron acceptor in the case of mGPDH.

Most direct evidence for CoQ site as the place of electron leak comes from experiments with HQNO. This generalized competitive inhibitor,

which binds to CoQ sites of various enzymes [38] has been found to bind also to bacterial mGPDH analog GlpD [48]. As the CoQ binding site is relatively conserved between GlpD and mGPDH, it is therefore conceivable to expect that it can interact with mGPDH as well. Interpretation of HQNO effect on GP-dependent ROS production is difficult in frozen thawed mitochondria, where inhibition of other CoQ sites in the respiratory chain, such as Q_o site of complex III, adds too much complexity. On the other hand, in fully solubilized mitochondria used in our experiment, its effect on GP-dependent ROS production should be specific for mGPDH only.

4.4. Mechanism of mGPDH dependent ROS production

This brings us to the question what is the exact mechanism of ROS production by mGPDH. Given its simple structure and most probable absence of FeS center, only the semiquinones formed at flavin or Q sites can be sources of electron leak. As discussed earlier, in SDH flavin has been proposed as the place of electron leak [11]. However, this does not seem to be the case with mGPDH. For this type of leak to occur in SDH, it is necessary that succinate concentrations are low and the substrate cleft displays only partial occupancy, thus allowing access of molecular oxygen to the flavin semiquinone intermediate formed and subsequent formation of superoxide. For mGPDH, ROS production increases linearly with increasing GP concentration at least to 40 mM, well past the Km for GP (2.9 mM) [43], which contradicts such possibility. Q site, or rather the CoQ semiquinone formed here, is therefore the most plausible source of electron leak on mGPDH. This is supported by our observations in this paper regarding interaction between CoQ and mGPDH as well as several lines of evidence in the literature.

(i) Structural evidence comes from the bacterial mGPDH analog GlpD, as there is no crystal structure available for the mammalian enzyme yet. However, the sequence is relatively well conserved between these proteins, as is the CoQ binding site. CoQ docking in GlpD occurs in the planar region oriented towards the lipid bilayer, which is analogous fold with another monotopic mitochondrial dehydrogenase — ETF:Q oxidase, which has also been shown to produce ROS [9,10,50]. On the contrary, SDH has a deep pocket with two binding sites for CoQ, which may represent natural protection against electron leak by the stabilization of ubisemiquinone radical formed during CoQ reduction [51,52]. Such stabilization seems to be essential in minimizing of the electron leak, as mutations in CoQ binding site of SDHC subunit were shown to increase ROS production [53].

(ii) It is also likely, that FAD semiquinone is only short lived and not present in the absence of GP in the substrate binding pocket. Yeh et al. proposed that it is most likely that catalysis occurs by ping–pong mechanism [48], meaning that fully reduced $FADH_2$ is produced by the oxidation of GP to dihydroxyacetone phosphate, which subsequently dissociates from the substrate binding pocket. Transfer of electrons to CoQ should then be concerted two electron process, but insufficient stabilization of semiquinone and its dissociation from the enzyme would result in electron leak. Analogous situation occurs in the presence of FeCN, where transfer of one electron from $FADH_2$ to FeCN leads to the formation of flavin semiquinone and formation of superoxide [12].

(iii) Another indirect evidence for CoQ as the source of electron leak in mGPDH comes from the observations of Brand's group, that superoxide is produced equally on both sides of the mitochondrial inner membrane [14,17]. FAD binding site is oriented towards intermembrane space and electrons leaking from this site would presumably be produced mostly towards intermembrane space as well.

4.5. mGPDH supercomplexes

Mitochondrial inner membrane is dense with average distance between protein complexes calculated to be only a few nanometers [54]. It is therefore not surprising that protein–protein interactions may occur. Their non-stochastic nature has been shown for example in the organization of oxidative phosphorylation apparatus. Here the theory of respiratory supercomplexes is widely accepted with individual OXPHOS complexes organized into higher molecular structures [40,55]. Among others it has been suggested that supercomplexes allow channeling of substrates between individual complexes and thus decrease the possibility of electron leak towards molecular oxygen and ROS production [56]. However, of the dehydrogenases communicating with CoQ pool, only complex I now represents an established part of OXPHOS supercomplex. Data on flavin dehydrogenases are scarcer and more controversial. They are absent in single particle electron microscopy studies of OXPHOS supercomplexes [57,58], but given their relatively small size they may simply be under the resolution limit of this technique. Neither kinetic studies of substrate channeling seem to support the presence of SDH in any supercomplex with complex III [56]. On the other hand at least some of the electrophoretic studies do detect SDH signal in high molecular weight complexes and could isolate other OXPHOS complexes by immunocapture via SDH antibody [40]. The same study also described respiratory competence of supercomplexes using succinate as substrate. There is also some support for mGPDH involvement in supercomplexes coming from yeast, where the mGPDH homolog Gut2p associates into “dehydrogenasome”, i.e. complex of several dehydrogenases supplying electrons to coenzyme Q [24].

It has also been clear since the early isolation experiments that mGPDH forms higher molecular weight aggregates, most likely due to its high hydrophobicity. During the purification by gel filtration the native mGPDH “holoenzyme” migrated at a molecular weight of approximately 250–300 kDa. As no other protein could be detected in this fraction, such complexes were considered to be homooligomeric aggregates [33].

Indeed, these homooligomeric structures were observed under native electrophoretic conditions of digitonin-solubilized BAT mitochondria. We were unsuccessful in determining any other interaction partners in these bands by crosslinking experiments and only mGPDH–mGPDH crosslinks were observed (not shown). It is therefore quite plausible that such homooligomers do represent native in vivo organization. It should also be noted that crystals of the bacterial mGPDH homolog GlpD also detect the native conformation to be a dimer and such dimerization seems to be determined by large hydrophobic areas present on the surface of the protein not buried into the membrane [48]. However, this does not explain the molecular nature of the observed approximately 1 MDa mGPDH supercomplex. Its partial dissociation after Coomassie dye addition points more towards weak electrostatic interactions than to hydrophobic interface which is likely in the homooligomers. As it does not co-migrate with OXPHOS complexes on 2D gels, it most likely does not represent “OXPHOS supercomplex” in the traditional sense. Our experiments also indicate that ROS production by the supercomplex form of the enzyme is broadly in par with the relative content of individual forms of mGPDH. Therefore such structure does not seem to be any better in channeling electrons towards complex III and thus preventing ROS production. We do not know molecular nature of this complex yet, but one speculation based on yeast gut2p may be, that such complex represents association of several flavin dehydrogenases such as mGPDH and ETF:Q oxidoreductase.

4.6. Isolated mGPDH as an ROS producer

Last, we have also demonstrated, that both isolated mGPDH and SDH are capable of ROS production. While mGPDH can do so in the absence of exogenous CoQ, SDH can produce ROS only, if exogenous CoQ was present. This is presumably in agreement with our observations that SDH is preferentially depleted of CoQ during solubilization. It has been demonstrated, that partially purified mGPDH did produce FeCN-dependent ROS [12]. However, this is the first direct confirmation, that both dehydrogenases can be independent sources of ROS and this does not occur only indirectly on other OXPHOS complexes. We have

also demonstrated that all native forms of mGPDH — homooligomers as well as its supercomplex form do produce ROS. It would be interesting to judge, whether association on mGPDH into supercomplex structures reduces ROS production. Although majority of ROS were produced by lower molecular forms it is difficult to make such conclusions. ROS detection in gel is merely semiquantitative and thus it is hard to correlate its intensity with the native western signal.

Taken together, in this paper we studied mechanisms of ROS production by two mitochondrial flavin dehydrogenases mGPDH and SDH. While we confirmed flavin as the most likely source of electron leak in SDH, we propose coenzyme Q as the site of ROS production in the case of mGPDH. Furthermore, using native electrophoretic systems, we demonstrated that mGPDH associates into homooligomers as well as high molecular weight supercomplexes, which represent native forms of mGPDH in the membrane. In the end, we also demonstrated that isolated mGPDH itself as well as its supramolecular assemblies are all capable of ROS production.

Supplementary data to this article can be found online at http://dx.doi.org/10.1016/j.bbabio.2013.08.007.

Acknowledgements

This work was supported by Grant Agency of the Czech Republic (P303/10/P227), Ministry of Education, Youth and Sports of the Czech Republic (ERC CZ LL1204 and RVO 67985823) and Grant Agency of the Charles University (750213).

References

[1] B. Halliwell, J. Gutteridge, Free Radicals in Biology and Medicine, Third ed. Oxford University Press, Oxford, 1999.
[2] S.G. Rhee, Cell signaling. H_2O_2, a necessary evil for cell signaling, Science 312 (2006) 1882–1883.
[3] A. Boveris, N. Oshino, B. Chance, The cellular production of hydrogen peroxide, Biochem. J. 128 (1972) 617–630.
[4] G. Loschen, L. Flohe, B. Chance, Respiratory chain linked H(2)O(2) production in pigeon heart mitochondria, FEBS Lett. 18 (1971) 261–264.
[5] E. Cadenas, K.J. Davies, Mitochondrial free radical generation, oxidative stress, and aging, Free Radic. Biol. Med. 29 (2000) 222–230.
[6] Q. Chen, E.J. Vazquez, S. Moghaddas, C.L. Hoppel, E.J. Lesnefsky, Production of reactive oxygen species by mitochondria: central role of complex III, J. Biol. Chem. 278 (2003) 36027–36031.
[7] A.V. Kareyeva, V.G. Grivennikova, G. Cecchini, A.D. Vinogradov, Molecular identification of the enzyme responsible for the mitochondrial NADH-supported ammonium-dependent hydrogen peroxide production, FEBS Lett. 585 (2011) 385–389.
[8] L. Tretter, V. Adam-Vizi, Generation of reactive oxygen species in the reaction catalyzed by alpha-ketoglutarate dehydrogenase, J. Neurosci. 24 (2004) 7771–7778.
[9] E.L. Seifert, C. Estey, J.Y. Xuan, M.E. Harper, Electron transport chain-dependent and -independent mechanisms of mitochondrial H_2O_2 emission during long-chain fatty acid oxidation, J. Biol. Chem. 285 (2010) 5748–5758.
[10] P. Schonfeld, L. Wojtczak, Brown adipose tissue mitochondria oxidizing fatty acids generate high levels of reactive oxygen species irrespective of the uncoupling protein-1 activity state, Biochim. Biophys. Acta 1817 (2012) 410–418.
[11] C.L. Quinlan, A.L. Orr, I.V. Perevoshchikova, J.R. Treberg, B.A. Ackrell, M.D. Brand, Mitochondrial complex II can generate reactive oxygen species at high rates in both the forward and reverse reactions, J. Biol. Chem. 287 (2012) 27255–27264.
[12] Z. Drahota, S.K. Chowdhury, D. Floryk, T. Mracek, J. Wilhelm, H. Rauchova, G. Lenaz, J. Houstek, Glycerophosphate-dependent hydrogen peroxide production by brown adipose tissue mitochondria and its activation by ferricyanide, J. Bioenerg. Biomembr. 34 (2002) 105–113.
[13] T. Mracek, Z. Drahota, J. Houstek, The function and the role of the mitochondrial glycerol-3-phosphate dehydrogenase in mammalian tissues, Biochim. Biophys. Acta 1827 (2013) 401–410.
[14] S. Miwa, M.D. Brand, The topology of superoxide production by complex III and glycerol 3-phosphate dehydrogenase in *Drosophila* mitochondria, Biochim. Biophys. Acta 1709 (2005) 214–219.
[15] M. Vrbacky, Z. Drahota, T. Mracek, A. Vojtiskova, P. Jesina, P. Stopka, J. Houstek, Respiratory chain components involved in the glycerophosphate dehydrogenase-dependent ROS production by brown adipose tissue mitochondria, Biochim. Biophys. Acta 1767 (2007) 989–997.
[16] T. Mracek, A. Pecinova, M. Vrbacky, Z. Drahota, J. Houstek, High efficiency of ROS production by glycerophosphate dehydrogenase in mammalian mitochondria, Arch. Biochem. Biophys. 481 (2009) 30–36.
[17] A.L. Orr, C.L. Quinlan, I.V. Perevoshchikova, M.D. Brand, A refined analysis of superoxide production by mitochondrial sn-glycerol 3-phosphate dehydrogenase, J. Biol. Chem. 287 (2012) 42921–42935.
[18] F. Sun, X. Huo, Y. Zhai, A. Wang, J. Xu, D. Su, M. Bartlam, Z. Rao, Crystal structure of mitochondrial respiratory membrane protein complex II, Cell 121 (2005) 1043–1057.
[19] F.L. Muller, Y. Liu, M.A. Abdul-Ghani, M.S. Lustgarten, A. Bhattacharya, Y.C. Jang, H. Van Remmen, High rates of superoxide production in skeletal-muscle mitochondria respiring on both complex I- and complex II-linked substrates, Biochem. J. 409 (2008) 491–499.
[20] M.A. Selak, S.M. Armour, E.D. MacKenzie, H. Boulahbel, D.G. Watson, K.D. Mansfield, Y. Pan, M.C. Simon, C.B. Thompson, E. Gottlieb, Succinate links TCA cycle dysfunction to oncogenesis by inhibiting HIF-alpha prolyl hydroxylase, Cancer Cell 7 (2005) 77–85.
[21] M. Jain, R. Nilsson, S. Sharma, N. Madhusudhan, T. Kitami, A.L. Souza, R. Kafri, M.W. Kirschner, C.B. Clish, V.K. Mootha, Metabolite profiling identifies a key role for glycine in rapid cancer cell proliferation, Science 336 (2012) 1040–1044.
[22] Z. Drahota, H. Rauchova, P. Jesina, A. Vojtiskova, J. Houstek, Glycerophosphate-dependent peroxide production by brown fat mitochondria from newborn rats, Gen. Physiol. Biophys. 22 (2003) 93–102.
[23] P.M. Sousa, S.T. Silva, B.L. Hood, N. Charro, J.N. Carita, F. Vaz, D. Penque, T.P. Conrads, A.M. Melo, Supramolecular organizations in the aerobic respiratory chain of *Escherichia coli*, Biochimie 93 (2011) 418–425.
[24] X. Grandier-Vazeille, K. Bathany, S. Chaignepain, N. Camougrand, S. Manon, J.M. Schmitter, Yeast mitochondrial dehydrogenases are associated in a supramolecular complex, Biochemistry 40 (2001) 9758–9769.
[25] B. Cannon, O. Lindberg, Mitochondria from brown adipose tissue: isolation and properties, Methods Enzymol. 55 (1979) 65–78.
[26] I. Wittig, M. Karas, H. Schagger, High resolution clear native electrophoresis for in-gel functional assays and fluorescence studies of membrane protein complexes, Mol Cell Proteomics 6 (2007) 1215–1225.
[27] J. Wilhelm, V. Vilim, Variables in xanthine oxidase-initiated luminol chemiluminescence: implications for chemiluminescence measurements in biological systems, Anal. Biochem. 158 (1986) 201–210.
[28] I. Wittig, H.P. Braun, H. Schagger, Blue native PAGE, Nat. Protoc. 1 (2006) 418–428.
[29] H. Schagger, G. von Jagow, Tricine-sodium dodecyl sulfate-polyacrylamide gel electrophoresis for the separation of proteins in the range from 1 to 100 kDa, Anal. Biochem. 166 (1987) 368–379.
[30] T. Mracek, P. Jesina, P. Krivakova, R. Bolehovska, Z. Cervinkova, Z. Drahota, J. Houstek, Time-course of hormonal induction of mitochondrial glycerophosphate dehydrogenase biogenesis in rat liver, Biochim. Biophys. Acta 1726 (2005) 217–223.
[31] W.M. Frederiks, F. Marx, G.L. Myagkaya, A histochemical study of changes in mitochondrial enzyme activities of rat liver after ischemia in vitro, Virchows Arch B Cell Pathol Incl Mol Pathol 51 (1986) 321–329.
[32] L. Yu, C.A. Yu, Quantitative resolution of succinate–cytochrome c reductase into succinate–ubiquinone and ubiquinol–cytochrome c reductases, J. Biol. Chem. 257 (1982) 2016–2021.
[33] I.R. Cottingham, C.I. Ragan, Purification and properties of L-3-glycerophosphate dehydrogenase from pig brain mitochondria, Biochem. J. 192 (1980) 9–18.
[34] Y. Hatefi, A.G. Haavik, L.R. Fowler, D.E. Griffiths, Studies on the electron transfer system. XLII. Reconstitution of the electron transfer system, J. Biol. Chem. 237 (1962) 2661–2669.
[35] B.A. Ackrell, E.B. Kearney, T.P. Singer, Mammalian succinate dehydrogenase, Methods Enzymol. 53 (1978) 466–483.
[36] M. Gutman, E.B. Kearney, T.P. Singer, Control of succinate dehydrogenase in mitochondria, Biochemistry 10 (1971) 4763–4770.
[37] M. Gutman, E.B. Kearney, T.P. Singer, Regulation of succinate dehydrogenase activity by reduced coenzymes Q10, Biochemistry 10 (1971) 2726–2733.
[38] M. Kogut, J.W. Lightbown, Selective inhibition by 2-heptyl-4-hydroxyquinoline N-oxide of certain oxidation-reduction reactions, Biochem. J. 84 (1962) 368–382.
[39] V. Strecker, Z. Wumaier, I. Wittig, H. Schagger, Large pore gels to separate mega protein complexes larger than 10 MDa by blue native electrophoresis: isolation of putative respiratory strings or patches, Proteomics 10 (2010) 3379–3387.
[40] R. Acin-Perez, P. Fernandez-Silva, M.L. Peleato, A. Perez-Martos, J.A. Enriquez, Respiratory active mitochondrial supercomplexes, Mol Cell 32 (2008) 529–539.
[41] J. Houstek, B. Cannon, O. Lindberg, Gylcerol-3-phosphate shuttle and its function in intermediary metabolism of hamster brown-adipose tissue, Eur. J. Biochem. 54 (1975) 11–18.
[42] L. Tretter, V. Adam-Vizi, High Ca^{2+} load promotes hydrogen peroxide generation via activation of alpha-glycerophosphate dehydrogenase in brain mitochondria, Free Radic. Biol. Med. 53 (2012) 2119–2130.
[43] L. Tretter, K. Takacs, V. Hegedus, V. Adam-Vizi, Characteristics of alpha-glycerophosphate-evoked H_2O_2 generation in brain mitochondria, J. Neurochem. 100 (2007) 650–663.
[44] I. Siebels, S. Drose, Q-site inhibitor induced ROS production of mitochondrial complex II is attenuated by TCA cycle dicarboxylates, Biochim. Biophys. Acta 1827 (2013) 1156–1164.
[45] V.D. Sled, A.D. Vinogradov, Kinetics of the mitochondrial NADH-ubiquinone oxidoreductase interaction with hexammineruthenium(III), Biochim. Biophys. Acta 1141 (1993) 262–268.
[46] A.D. Vinogradov, NADH/NAD+ interaction with NADH: ubiquinone oxidoreductase (complex I), Biochim. Biophys. Acta 1777 (2008) 729–734.
[47] G. Dooijewaard, E.C. Slater, Steady-state kinetics of high molecular weight (type-I) NADH dehydrogenase, Biochim. Biophys. Acta 440 (1976) 1–15.
[48] J.I. Yeh, U. Chinte, S. Du, Structure of glycerol-3-phosphate dehydrogenase, an essential monotopic membrane enzyme involved in respiration and metabolism, Proc. Natl. Acad. Sci. U. S. A. 105 (2008) 3280–3285.
[49] A.D. Vinogradov, E.V. Gavrikova, V.G. Goloveshkina, A new ferricyanide reactive site in soluble succinate dehydrogenase, Biochem. Biophys. Res. Commun. 65 (1975) 1264–1269.

[50] J. Zhang, F.E. Frerman, J.J. Kim, Structure of electron transfer flavoprotein-ubiquinone oxidoreductase and electron transfer to the mitochondrial ubiquinone pool, Proc. Natl. Acad. Sci. U. S. A. 103 (2006) 16212–16217.
[51] R. Horsefield, V. Yankovskaya, G. Sexton, W. Whittingham, K. Shiomi, S. Omura, B. Byrne, G. Cecchini, S. Iwata, Structural and computational analysis of the quinone-binding site of complex II (succinate-ubiquinone oxidoreductase): a mechanism of electron transfer and proton conduction during ubiquinone reduction, J. Biol. Chem. 281 (2006) 7309–7316.
[52] C.A. Yu, S. Nagaoka, L. Yu, T.E. King, Evidence for the existence of a ubiquinone protein and its radical in the cytochromes b and c1 region in the mitochondrial electron transport chain, Biochem. Biophys. Res. Commun. 82 (1978) 1070–1078.
[53] B.G. Slane, N. Aykin-Burns, B.J. Smith, A.L. Kalen, P.C. Goswami, F.E. Domann, D.R. Spitz, Mutation of succinate dehydrogenase subunit C results in increased O2.-, oxidative stress, and genomic instability, Cancer Res. 66 (2006) 7615–7620.
[54] G. Lenaz, M.L. Genova, Structure and organization of mitochondrial respiratory complexes: a new understanding of an old subject, Antioxid Redox Signal 12 (2010) 961–1008.
[55] H. Schagger, Respiratory chain supercomplexes of mitochondria and bacteria, Biochim. Biophys. Acta 1555 (2002) 154–159.
[56] G. Lenaz, M.L. Genova, Supramolecular organisation of the mitochondrial respiratory chain: a new challenge for the mechanism and control of oxidative phosphorylation, Adv Exp Med Biol 748 (2012) 107–144.
[57] N.V. Dudkina, M. Kudryashev, H. Stahlberg, E.J. Boekema, Interaction of complexes I, III, and IV within the bovine respirasome by single particle cryoelectron tomography, Proc Natl Acad Sci U S A 108 (2011) 15196–15200.
[58] N.V. Dudkina, H. Eubel, W. Keegstra, E.J. Boekema, H.P. Braun, Structure of a mitochondrial supercomplex formed by respiratory-chain complexes I and III, Proc. Natl. Acad. Sci. U. S. A. 102 (2005) 3225–3229.

Supplementary data related to research article "ROS generation and multiple forms of mammalian mitochondrial glycerol-3-phosphate dehydrogenase".

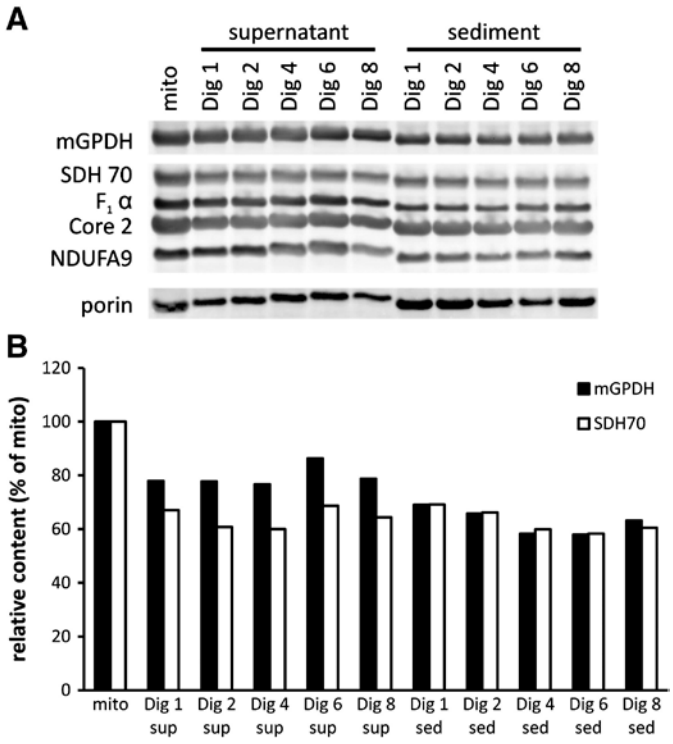

Supplementary Fig. 1.

Protein composition of digitonin solubilizates. Mitochondria and digitonin-solubilized mitochondrial proteins (1–8 g/g protein) were analyzed on SDS-PAGE followed by western blot analysis. Equal amount (15 μg of protein) was loaded into each slot. (A) Detection of protein content with respective antibodies: mGPDH, SDH (SDH70 subunit), $F_1\alpha$ (CV), Core2 (CIII), NDUFA9 (CI) and porin (marker of outer membrane). (B) Relative distribution of mGPDH and SDH into individual fractions. Whole mitochondria are considered as 100%.

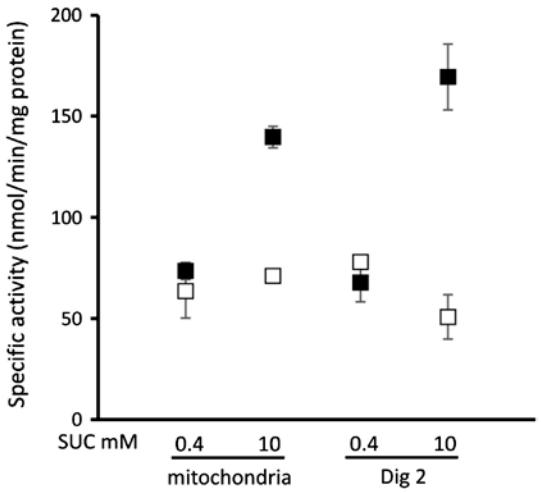

Supplementary Fig. 2.

Inhibition status of SDH. Mitochondria or digitonin (2 g/g protein) solubilizates were incubated with indicated succinate concentration at 0 °C (open symbols) or 37 °C (closed symbols) for 5 min to allow for displacement of oxaloacetate and enzyme activation at 37 °C. Following the incubation, enzyme activity was determined at 15 °C as DCPIP:reductase in the presence of 20 μM CoQ_1 and 10 mM succinate. At 15 °C, succinate cannot displace the inhibitory oxaloacetate and thus the measured value serves as a proxy for inhibitory state in the original incubation.

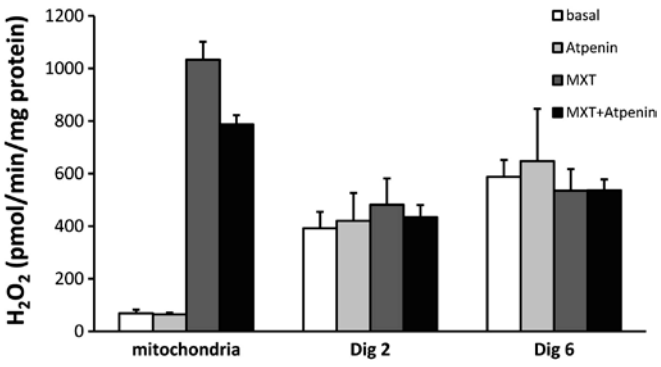

Supplementary Fig. 3.

GP-dependent ROS production on mGPDH and SDH. Hydrogen peroxide production was measured fluorometrically as oxidation of Amplex Red (50 μM) in the presence of HRP (1 $U.mL^{-1}$) either in original mitochondria (mitochondria) or in 20,000 *g* supernatants after solubilization with digitonin 2 or 6 g/g of protein (Dig2 or Dig6 respectively) with 10 mM

glycerol-3-phosphate used as a substrate. Where indicated 1 μM atpenin A5, 1 μg.mL^{-1} myxothiazol (MXT) or the combination of both was used. Results are mean ± SD from 3 replicates.

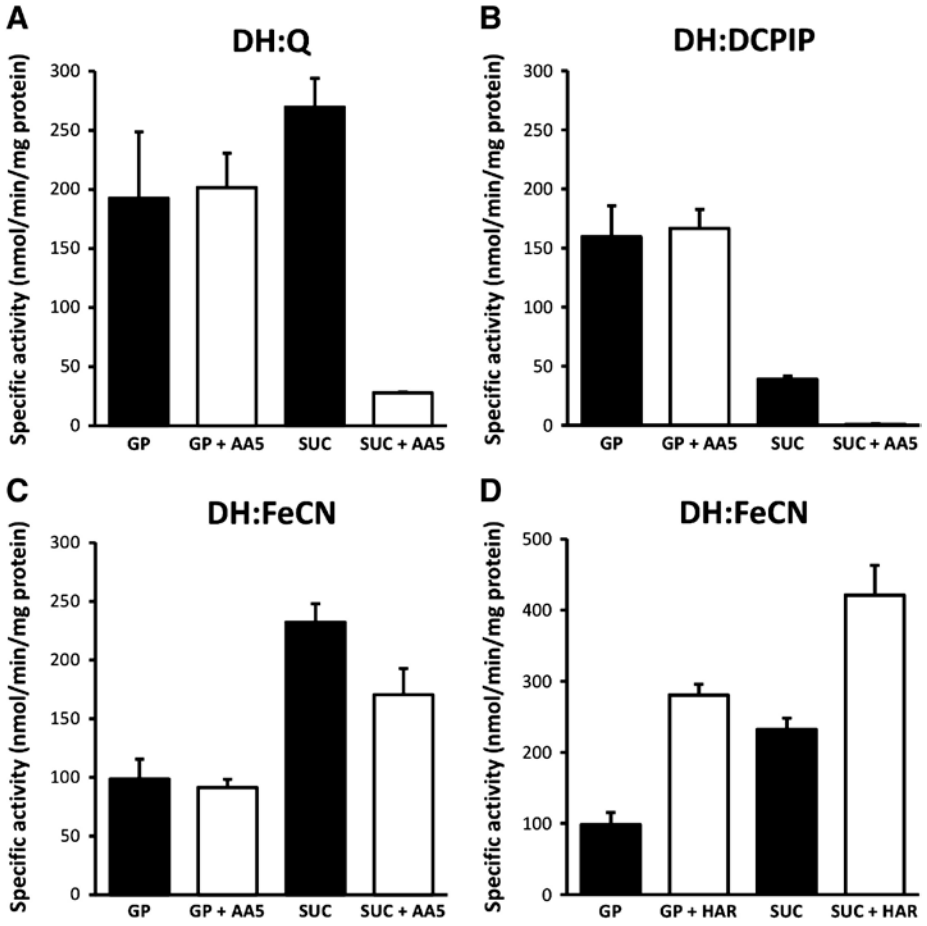

Supplementary Fig. 4.

Effect of atpenin A5 and HAR on activities of the dehydrogenases. BAT mitochondria were solubilized with digitonin (2 g/g protein). Enzyme activities were determined as CoQ_1 reductase (A), DCPIP reductase (B) of FeCN reductase (C, D) with 10 mM glycerol-3-phosphate (GP) or 10 mM succinate (SUC). Effect of established SDH inhibitor atpenin A5 (1 μM) was examined on all respective combinations of substrates and electron acceptors (white bars, A–C). Effect of another single electron acceptor HAR on apparent FeCN reductase activity was determined in (D). Black bars — FeCN reductase activity with respective substrate, white bars — analogous activity in the presence of 125 μM HAR. Results are mean ± SD from 2 to 3 replicates.